Optimizing Offshore Cable Operations

A study Identifying, Quantifying and Implementing Limiting Motions for Cable Lay Operations

MSc Thesis

Final version, June 2021

F.J. Diepenmaat

DEME OFFSHORE

TU Delft

Optimizing Offshore Cable Operations

A study Identifying, Quantifying and Implementing Limiting Motions for Cable Lay Operations

by

F.J. Diepenmaat

to obtain the degree of
Master of Science in Offshore & Dredging Engineering
at the Delft University of Technology,
to be defended publicly on Wednesday June 9^{th}, 2021 at 14:00 PM.

Student number:	4296842
Email address:	Frank.diepenmaat@gmail.com

Graduation trajectory:	June 2020 - June 2021	
Thesis committee:		
Dr. ir. S.A. Miedema	TU Delft	Chair & Daily supervisor
Dr. ir. P. Naaijen	TU Delft	2^{nd} Supervisor
Ir W. van den Bos	TU Delft	3^{rd} Supervisor
Ir. J. Willems	DEME Offshore NL	Daily supervisor

This thesis is confidential and cannot be made public until June 9^{th}, 2023.

An electronic version of this thesis is available at `http://repository.tudelft.nl/`.

TU Delft
Delft University of Technology

DEME
Dredging, Environmental & Marine Engineering

Abstract

Offshore contractors use special cable laying vessels (CLV's) in order to install subsea power cables, which transport offshore generated energy. Workability studies are performed to evaluate whether operations can be performed or not. These workability studies are subsequently a combination between operability assessments (performed in OrcaFlex months prior to operation) and forecasted weather windows. During the operability assessment, eventually limiting sea states are defined which are expressed in significant wave height H_s, wave peak period (T_p) and incident wave angle relative to the vessel heading (α). If the forecasted weather windows exceed the predefined limiting sea states, operations cannot be executed. These current workability assessments are based on 1D JONSWAP spectra.

This thesis contains an exploratory study of implementing a motion-based forecasting (MBF) method into workability studies, based on 2D wave spectra. This is done by focusing on the motions at the chute of the CLV, as this is where the subsea power cable leaves the CLV. Before MBF can be implemented, however, at first a specific limiting motion predictor needs to be identified that covers the cables integrity limits. Furthermore, this limiting motion needs to be quantified as well in order to compare this essentially composed new cable limit with MBF predicted chute motions.

Subsequently, all cable integrity criteria need to be converted into this limiting motion to preserve the subsea power cables integrity. For normal cable lay operations, eventually all mechanical properties and cable limits are covered by three main cable integrity criteria. These are minimum bending radius (MBR), minimum bottom tension (BT) and maximum top tension (TT). By means of modelling a lot of various environmental loading conditions, the research described in this thesis shows that the chute z velocity is eventually indicated as a proper limiting motion predictor. Out of all investigated chute motions, chute z velocity (which represents the vertical velocity of the chute) shows the best correlations with the aforementioned cable integrity criteria.

To determine workability by implementing motion based forecasting, this limiting chute z velocity needs to be quantified. The chute z velocity needs to account for all three main cable integrity limits, hence these limits are essentially converted into one single chute z velocity limit (which is essentially a new introduced cable limit). To quantify this limiting chute z velocity not the entire relation is of interest, but only the range close to breaching the cable integrity limits. Therefore, a percentile line method is introduced which is constructed on the $90^{th}_{percentile}$ values per bin. Based on this research, it was found that binwidths must not exceed values of $0.5m/s$ to obtain robust results. However, no minimum amount of data points per bin was established as this varied for all assessed subsea power cables.

Finally, workability studies of the current 1D JONSWAP (based on a single $H_s - T_p$ sea state) method was compared to a 2D superimposed JONSWAP accounting for both swell and wind wave contributions. This comparison indicates that when determining workability based on more detailed 2D spectra, the workability study provides more smoothed results. This means, the higher chute z velocity peaks from the 1D total sea state are downscaled when simulating a 2D spectrum, whereas the lower chute z velocity peaks from the 1D total sea state are upscaled when implementing a 2D spectrum. The obtained motion-based chute z velocity forecasts indicate that optimization is possible by splitting the total sea states into both swell and sea waves contributions and accounting for wave spreading.

Preface

During my studies I have always been intrigued by the offshore industry, especially the renewable energy sector. The fact that there is so much engineering going on at sea with turbine magnitudes that are hard to imagine fascinates me. For this final research I decided to dive into the offshore power cable laying business. DEME Offshore NL gave me the opportunity to perform my MSc thesis at their NL office in Breda. As I was about to start my graduation trajectory the world was surprised with the rapid spread of the Coronavirus. This meant offices where closed and working from home became the new standard of 2020 and 2021. Hence I performed almost my entire work on this thesis from my student room in Delft and later from my apartment in Zeist.

First of all I would like to express my gratitude to all members of my graduation committee for their support and guidance. Getting on the right track and sticking on this came with its challenges. Therefore I would like to thank Dr. ir. Sape Miedema and Dr. ir. Peter Naaijen for the interesting (online) meetings and academic supervision. Besides, I would like to thank ir. Wouter van den Bos for his guidance and feedback in the last stages of my graduation trajectory. At last I want to thank my daily supervisor from DEME ir. Joost Willems for his continuous enthusiasm and motivation. Our weekly (online) meetings every wednesday afternoon provided me with clever insights and new energy to continue my work.

Secondly, I would like to thank DEME Offshore NL for giving me the opportunity to execute my thesis research within their international oriented offshore company. I was looking for a major offshore contractor to collaborate for my thesis and DEME gave me the opportunity. Although I wasn't able to nose around in the office due to the Covid-19 pandemic, I did get a much better feeling for the contractors side regarding offshore projects. Moreover, I would like to thank the entire offshore cable laying team in general, it was a pleasant team to be part of.

At last I would like to thank my family and friends. My family has always supported me throughout my studies and decisions I made during the past seven years. Besides, they have always encouraged me to develop myself and do not give up easily. Furthermore, I would like to thank my friends. In Enschede I left a bunch of good friends, and during my Masters in Delft I made some new ones. The one thing all have common is that without all of them I never would be where I am now. Last but definitely not least I would like to thank my girlfriend, Nena, for her never ending optimism and enthusiasm.

At the moment of writing, I'm almost finished with my thesis hence about to close my educational life's chapter and open the next. I am looking forward to this next chapter in life and start an international career within the offshore business. I very much enjoyed working on my thesis. I hope you enjoy reading it and it will provide you with new information, ideas and/or insights.

Frank Johan Diepenmaat
Zeist, June 2021

Abbreviations and nomenclature

Please note that only abbreviations and nomenclature from the main Thesis are summarized. Hence additional abbreviations and nomenclature mentioned introduces in the Appendices is not summarized below.

Abbreviations

Abbreviation	Description	Unit
1D	1 Dimensional	[-]
2D	2 Dimensional	[-]
3D	3 Dimensional	
AC	Alternating current	[v]
BR	Bending radius	[m]
BT	Bottom tension	[kN]
CI	Confidence interval	[-]
CLV	Cable laying vessel	[-]
COG	Centre fo gravity	[-]
CPS	Cable protection system	[-]
DC	Direct current	[v]
DEME	Dredging, Environmental and Marine Engineering	[-]
DOF	Degree of freedom	[-]
DP	Dynamic positioning	[-]
EoM	Equation of motion	[-]
EU	European union	[-]
FEM	Finite element model	[-]
FFT	Fast fourier transfor	[-]
HVAC	High voltage alternating current	[-]
HVDC	High voltage direct current	[-]
IEA	International energy agency	[-]
JIP	Joint industry project	[-]
JONSWAP	Joint north sea wave project	[-]
LMM	Lumped mass method	[-]
MBF	Motion-based forecasting	[-]
MBR	Minimum bending radius	[m]
MPM	Most probable maximum	[-]
O&G	Oil & Gas	[-]
WTG	Wind turbine generator	[-]
OWF	Offshore wind farm	[-]
PDF	Probability-density function	[-]
PE	Polyehtylene	[-]
MM	Pierson-Moskowitz	[-]
QTF	Quadratic transfer function	[-]
RAO	Response amplitude operator	[-]
ROV	Remote operated vehicle	[-]
RQ	Research question	[-]
SWP	Side wall pressure	[kN/m]
TDP	Touchdown point	[-]
TT	Top tension	[kN]
VIV	Vortex induced vibrations	[-]
XLPE	Cross-linked polyethylene	[-]

Nomenclature

Symbol	Description	Unit
a	Added mass matrix	[kg]
A	Exponential LMS fitting parameter	[-]
A	Area	[m^2]
a_b	Acceleration of structure relative to earth	[m/s^2]
b	Damping coefficient matrix	[-]
B	Exponential LMS fitting parameter	[-]
c	Restoring coefficients matrix	[-]
C	Exponential LMS fitting parameter	[-]
C_a	Added mass coefficient regarding structure	[-]
C_d	Drag block coefficient	[-]
C_m	Inertial block coefficient	[-]
d	Water depth	[m]
$D(\theta)$	directional spreading function	[rad]
D_d	Drag block coefficient	[-]
$Duration$	Total time duration	[s]
$E(z)$	Expectation operator	[-]
E	Certain scaling factor	[-]
E_{energy}	Total wave energy	[m^2/Hz]
$E_{variance}$	Variance density	[m^2/Hz]
f	Wave frequency	[Hz]
f_m	Wave peak frequency	[Hz]
F_0	Static bottom tension	[kN]
F	Total force on structure per unit length	[kN/m]
F_I	Inertial force contribution per unit length	[kN/m]
F_D	Drag force contribution per unit length	[kN/m]
$\hat{F}(\omega)$	Wave force	[kN]
$Frac$	Corresponding fractional part	[-]
g	Gravitational acceleration constant	9.81 [m/s^2]
H_s	Significant wave height	[*m*]
$Index_{low}$	The value in the composed array on the determined percentile index in rounded off to the lowest possible integer	[#]
$Index_{high}$	The value on the determined percentile index rounded off to the highest possible integer	[#]
k	Wave number	[rad/m]
l	Layback	[m]
m	Submerged weight of subsea power cable	[kg/m]
m	Mass matrix	[kg]
n	Number of waves in duration	[#]
N	Total amount of data points	[#]
$Percentile_{value}$	The final percentile value	[-]
$q^{th}_{percentile}$	The to be investigated percentile	[%]
R^2	Regression coefficient	[-]
S	Total wave spectrum	[m^2s]
$S(\omega,\theta)$	Function for the entire directional wave spectrum	[m^2s]
$S(\omega)$	wave spectrum	[m^2s/rad]
SS_{xx}	Sum of squares of the x variable	[-]
SS_{yy}	Sum of squares of the y variable	[-]
SS^2_{xy}	Corrected sum of products x and y	[-]
t	Time	[s]
T_p	Wave peak period	[*s*]
T_z	Zero up-crossing wave period	[s]
U_{wind}	Wind velocity	[m/s]
v_f	Fluid velocity relative to earth	[m/s]
v_r	Fluid velocity relative to structure	[m/s]
x	Total cable catenary length	[m]
z	Height above mean sea level	[m]
$\hat{z_a}$	Heave amplitude	[m]

Greek	Description	Unit
α	Incoming wave direction relative to the vessel	[*deg*]
α	Dimensionless catenary parameter	[-]
α	Dimensionless JONSWAP shape factor	0.0081
α_f	Fluid acceleration relative to earth	[m/s^2]
Δt	OrcaFlex time step	[s]
Δ	Displaced fluid mass	[kN]
η	Surface elevation	[m]
γ	Peak enhancement factor	[-]
μ	Mean value	[m]
ω	Wave frequency	[Hz]
ρ_s	Sea water density	1,025 [kg/m^3]
ρ	Fluid density	[kg/m^3]
$\rho(\tau)$	Autocorrelation factor	[-]
σ	Dimensionless pea-width parameter	$\sigma_1 = 0.07$ & $\sigma_2 = 0.07$
σ	Standard deviation	[m]
σ^2	Sea surface elevation variance	[m^2]
τ	Time lag	[s]
ξ_a	Wave amplitude	[m]
ζ_1	Surge-direction	[*m/m*]
ζ_2	Sway-direction	[*m/m*]
ζ_3	Heave-direction	[*m/m*]
ζ_4	Roll-direction	[*rad/m*]
ζ_5	Pitch-direction	[*rad/m*]
ζ_6	Yaw-direction	[*rad/m*]

Contents

List of Figures xiii

List of Tables xvii

1 Introduction 1
- 1.1 Report outline . . . 1
- 1.2 Global energy mix . . . 1
- 1.3 Offshore energy and subsea power cables . . . 2
- 1.4 Operability and workability . . . 3
- 1.5 DEME Offshore NL . . . 4

2 Problem statement 5
- 2.1 Research motivation . . . 5
- 2.2 Objectives . . . 7
- 2.3 Research questions . . . 8
- 2.4 Scope and boundaries . . . 8
- 2.5 Approach . . . 9

3 Subsea power cables and installation 11
- 3.1 Subsea power cables . . . 11
- 3.2 Cable failure . . . 14
- 3.3 Cable properties . . . 17
- 3.4 Cable laying vessel and onboard installation equipment . . . 19
- 3.5 Offshore cable operations . . . 22
- 3.6 Conclusions . . . 24

4 Offshore environment and OrcaFlex modelling 25
- 4.1 Offshore environment . . . 25
- 4.2 Motions . . . 29
- 4.3 OrcaFlex software . . . 32
- 4.4 Subsea power cable modelling . . . 35
- 4.5 Multi system dynamics . . . 36
- 4.6 Final OrcaFlex model set up . . . 38

5 Limiting motion analysis 41
- 5.1 Subsea power cable data . . . 41
- 5.2 Initial local chute motion analysis . . . 42
- 5.3 Line of best fit . . . 43
- 5.4 Test cases . . . 44
- 5.5 Results . . . 46
- 5.6 Verification and validation . . . 48
- 5.7 Conclusions . . . 52

6 Motion quantification method 53
- 6.1 Percentile method . . . 53
- 6.2 Results . . . 55
- 6.3 Verification and validation . . . 59
- 6.4 Conclusions . . . 63

7 Motion-based forecasting **65**
7.1 Wave spreading . . . 65
7.2 Weather forecasts . . . 66
7.3 Motion forecast model . . . 68
7.4 Results . . . 69
7.5 Conclusions . . . 70

8 Discussion **71**
8.1 Subsea power cables and cable integrity . . . 71
8.2 OrcaFlex modelling . . . 71
8.3 Identification analysis . . . 72
8.4 Quantification method . . . 72
8.5 Motion-based forecasting . . . 73

9 Conclusions and recommendations **75**
9.1 Conclusions . . . 75
9.2 Recommendations . . . 77

Bibliography **79**

A Appendix - Problem statement **83**
A.1 Offshore software packages . . . 83
A.2 Methodology overview . . . 84

B Appendix - OrcaFlex modelling **85**
B.1 DEME's Living Stone CLV . . . 85
B.2 Wave theory . . . 87
B.3 Compose motions in direction of cable departure direction . . . 89
B.4 Lumped mass method . . . 91
B.5 Fourier transform . . . 93
B.6 QTF's . . . 94

C Appendix - Investigated subsea power cable properties **95**
C.1 Typical 3*300mm2 HVAC inter-array cable 1 . . . 95
C.2 Typical 3*300mm2 HVAC inter-array cable 2 . . . 98
C.3 Typical 3*1800 mm2 HVAC export cable 1 . . . 100
C.4 Typical 1*1300 mm2 HVDC export cable 2 . . . 101

D Appendix - Limiting motion identification **103**
D.1 Initial analysis results . . . 104
D.2 Least Mean Square methods . . . 107
D.3 Test cases control cables . . . 109
D.4 Results all cables, BR, BT and TT . . . 111
D.5 Normal lay configuration verification results . . . 124
D.6 Another vessel verification results . . . 129
D.7 Examine extreme minimum or extreme maximum motions . . . 131

E Appendix - Limiting motion quantification **135**
E.1 Interesting ranges . . . 135
E.2 Quantification graphs typical export cable 1 . . . 136
E.3 Amount of seeds and binwidth sensitivity . . . 166

List of Figures

1.1 World electricity generation by power station type [14] . . . 2
1.2 Current workability calculation flowchart [18, 49] . . . 3

2.1 Global subsea cable installation and vessel demand, 2013-2022 [22] . . . 5
2.2 Overview of approach, methods and data separated per research question . . . 10

3.1 Example of grid connection [61] . . . 11
3.2 Examples of AC and DC cables . . . 12
3.3 AC cables versus DC cables [61] . . . 12
3.4 Common subsea power cable cross-sections [49] . . . 13
3.5 Failure... . . . 15
3.6 Unwinded helical structure, birdcaging [46] . . . 16
3.7 Typical SN-curve for subsea power cables [29] . . . 17
3.8 Helical cable structure [29] . . . 18
3.9 Nonlinear bending stiffness . . . 18
3.10 Typical CLV layout and photograph of Living Stone CLV . . . 20
3.11 Onboard equipment Living Stone CLV (photo taken from DEME archive) . . . 21
3.12 Typical S-Lay configuration [53] (adjusted) . . . 22
3.13 Cable laying vessel, chute movement [49] . . . 23

4.1 Time scale differentiating between wave types [24] . . . 26
4.2 Fetch and wind-wave energy transfer [24] . . . 26
4.3 Wave superposition [24] . . . 27
4.4 Regular and irregular wave fields and accompanying wave spectra [24] . . . 29
4.5 Vessel motions from COG [1, 49] . . . 30
4.6 Local chute motions (adjusted screenshot taken from OrcaFlex) . . . 31
4.7 Illustration of motions in cable departure direction (CLV sideview) . . . 31
4.8 OrcaFlex directions and heading conventions, azimuth projection, all angles are in degrees [31] (adjusted) . . . 33
4.9 OrcaFlex JONSWAP example for seed number 12345 ($H_s = 4m$, $T_p = 10s$) . . . 34
4.10 Autocorrelation and overall sea elevation examples for seed number 12345 ($H_s = 4m$, $T_p = 10s$ & $\alpha = 180^o$) . . . 34
4.11 Visualization OrcaFlex line models [31] . . . 36
4.12 OrcaFlex base cases shallow (top) and deep water (bottom) . . . 39

5.1 Initial chute motion analysis base case (OrcaFlex screenshot) . . . 42
5.2 Initial motion analysis - All chute x/y/z motions w.r.t. - Bending radius . . . 43
5.3 Overfitting, proper fitting and underfitting [5] . . . 44
5.4 OrcaFlex typical inter-array cable 1 base cases for shallow water (top) and deep water (bottom) . . . 45
5.5 Regression coefficient results typical inter-array cable 1 w.r.t. MBR in shallow water ($30m$) 46
5.6 Regression coefficient results typical inter-array cable 1 w.r.t. MBR in deep water ($30m$) 47

6.1 Quantification graphs w.r.t. MBR limit - Typical export cable 1 - Shallow water ($30m$) - All binwidths for 5 seeds data . . . 56
6.2 Quantification graphs w.r.t. BT limit - Typical export cable 1 - Shallow water ($30m$) - All binwidths for 5 seeds data . . . 57

7.1 Combine 1D wave spectrum with directional wave spreading (cosine approximation) to obtain a 2D wave spectrum [24, 31, 33] . . . 66

7.2 Real weather forecast information April 2^{nd} to April 8^{th} . . . 67
7.3 Differences 1D JONSWAP and superimposed 2D JONSWAP . . . 68
7.4 3-hour MPM chute z velocity response forecast . . . 69

A.1 Research methodology overview . . . 84

B.1 Technical drawing DP3 cable installation & multipurpose vessel 'Living Stone' [50] . . . 85
B.2 Orbital particle velocity profiles in deep, intermediate and shallow water [24] . . . 87
B.3 Illustration of motions in cable departure direction (CLV sideview) . . . 89
B.4 Chute z motions versus chute cable motions in extreme deep water (1000m) . . . 90

C.1 Typical inter-array cable 1 cross section and listed components [-] . . . 95
C.2 Non-linear bending stiffness typical inter-array cable 1 [-] . . . 96
C.3 Minimum bending radius versus working load typical inter-array cable 1 [-] . . . 97
C.4 Typical inter-array cable 2 cross section [-] . . . 98
C.5 Typical export cable 1 [-] . . . 100
C.6 typical export cable 2 cross section [-] . . . 101

D.1 Initial motion analysis, all chute z motions w.r.t. cable integrity criteria . . . 104
D.2 Initial motion analysis, all chute x motions w.r.t. cable integrity criteria . . . 105
D.3 Initial motion analysis, all chute y motions w.r.t. cable integrity criteria . . . 106
D.4 Typical inter-array cable 1 at 30m water depth, MBR regression analysis . . . 111
D.5 Typical inter-array cable 1 at 30m water depth, BT regression analysis . . . 112
D.6 Typical inter-array cable 1 at 30m water depth, TT regression analysis . . . 112
D.7 Typical inter-array cable 2 at 30m water depth, MBR regression analysis . . . 113
D.8 Typical inter-array cable 2 at 30m water depth, BT regression analysis . . . 113
D.9 Typical inter-array cable 2 at 30m water depth, TT regression analysis . . . 114
D.10 Typical export cable 1 at 30m water depth, MBR regression analysis . . . 114
D.11 Typical export cable 1 at 30m water depth, BT regression analysis . . . 115
D.12 Typical export cable 1 at 30m water depth, TT regression analysis . . . 115
D.13 Typical export cable 2 at 30m water depth, MBR regression analysis . . . 116
D.14 Typical export cable 2 at 30m water depth, BT regression analysis . . . 116
D.15 Typical export cable 2 at 30m water depth, TT regression analysis . . . 117
D.16 Typical inter-array cable 1 at 150m water depth, MBR regression analysis . . . 117
D.17 Typical inter-array cable 1 at 150m water depth, BT regression analysis . . . 118
D.18 Typical inter-array cable 1 at 150m water depth, TT regression analysis . . . 118
D.19 Typical inter-array cable 2 at 150m water depth, MBR regression analysis . . . 119
D.20 Typical inter-array cable 2 at 150m water depth, BT regression analysis . . . 119
D.21 Typical inter-array cable 2 at 150m water depth, TT regression analysis . . . 120
D.22 Typical export cable 1 at 150m water depth, MBR regression analysis . . . 120
D.23 Typical export cable 1 at 150m water depth, BT regression analysis . . . 121
D.24 Typical export cable 1 at 150m water depth, TT regression analysis . . . 121
D.25 Typical export cable 2 at 150m water depth, MBR regression analysis . . . 122
D.26 Typical export cable 2 at 150m water depth, BT regression analysis . . . 123
D.27 Typical export cable 2 at 150m water depth, TT regression analysis . . . 123
D.28 Typical inter-array cable 1 at 30m water depth with a static bottom tension of 2kN, MBR regression analysis . . . 124
D.29 Typical inter-array cable 1 at 30m water depth with a static bottom tension of 10kN, MBR regression analysis . . . 125
D.30 Typical inter-array cable 1 at 30m water depth with a static bottom tension of 20kN, MBR regression analysis . . . 125
D.31 Typical inter-array cable 1 at 30m water depth with a static bottom tension of 2kN, BT regression analysis . . . 126
D.32 Typical inter-array cable 1 at 30m water depth with a static bottom tension of 10kN, BT regression analysis . . . 126
D.33 Typical inter-array cable 1 at 30m water depth with a static bottom tension of 20kN, BT regression analysis . . . 127

D.34 Typical inter-array cable 1 at 30m water depth with a static bottom tension of 2kN, TT regression analysis . . . 127
D.35 Typical inter-array cable 1 at 30m water depth with a static bottom tension of 10kN, TT regression analysis . . . 128
D.36 Typical inter-array cable 1 at 30m water depth with a static bottom tension of 20kN, TT regression analysis . . . 128
D.37 Typical inter-array cable 1 at 30m water depth with a static bottom tension of 5kN, BR regression analysis, another vessel . . . 129
D.38 Typical inter-array cable 1 at 30m water depth with a static bottom tension of 5kN, BT regression analysis, another vessel . . . 130
D.39 Typical inter-array cable 1 at 30m water depth with a static bottom tension of 5kN, TT regression analysis, another vessel . . . 130
D.40 Absolute minimum motions against maximum motions inter array cable 1 in 30m water depth . . . 131
D.41 Absolute minimum motions against maximum motions inter array cable 1 in 150m water depth . . . 132
D.42 Absolute minimum motions against maximum motions export cable 1 in 30m water depth 132
D.43 Absolute minimum motions against maximum motions export cable 1 in 150m water depth133

E.1 Quantification graphs typical export cable 1 in shallow water ($30m$), 1 seed number, binwidth of $1m/s$ . . . 136
E.2 Quantification graphs typical export cable 1 in shallow water ($30m$), 1 seed number, binwidth of $0.5m/s$ . . . 137
E.3 Quantification graphs typical export cable 1 in shallow water ($30m$), 1 seed number, binwidth of $0.25m/s$ . . . 138
E.4 Quantification graphs typical export cable 1 in shallow water ($30m$), 2 seed numbers, binwidth of $1m/s$ . . . 139
E.5 Quantification graphs typical export cable 1 in shallow water ($30m$), 2 seed numbers, binwidth of $0.5m/s$ . . . 140
E.6 Quantification graphs typical export cable 1 in shallow water ($30m$), 2 seed numbers, binwidth of $0.25m/s$ . . . 141
E.7 Quantification graphs typical export cable 1 in shallow water ($30m$), 3 seed numbers, binwidth of $1m/s$ . . . 142
E.8 Quantification graphs typical export cable 1 in shallow water ($30m$), 3 seed numbers, binwidth of $0.5m/s$ . . . 143
E.9 Quantification graphs typical export cable 1 in shallow water ($30m$), 3 seed numbers, binwidth of $0.25m/s$ . . . 144
E.10 Quantification graphs typical export cable 1 in shallow water ($30m$), 4 seed numbers, binwidth of $1m/s$ . . . 145
E.11 Quantification graphs typical export cable 1 in shallow water ($30m$), 4 seed numbers, binwidth of $0.5m/s$ . . . 146
E.12 Quantification graphs typical export cable 1 in shallow water ($30m$), 4 seed numbers, binwidth of $0.25m/s$ . . . 147
E.13 Quantification graphs typical export cable 1 in shallow water ($30m$), 5 seed numbers, binwidth of $1m/s$ . . . 148
E.14 Quantification graphs typical export cable 1 in shallow water ($30m$), 5 seed numbers, binwidth of $0.5m/s$ . . . 149
E.15 Quantification graphs typical export cable 1 in shallow water ($30m$), 5 seed numbers, binwidth of $0.25m/s$ . . . 150
E.16 Quantification graphs typical export cable 1 in deep water ($150m$), 1 seed number, binwidth of $1m/s$ . . . 151
E.17 Quantification graphs typical export cable 1 in deep water ($150m$), 1 seed number, binwidth of $0.5m/s$ . . . 152
E.18 Quantification graphs typical export cable 1 in deep water ($150m$), 1 seed number, binwidth of $0.25m/s$ . . . 153

E.19 Quantification graphs typical export cable 1 in deep water ($150m$), 2 seed numbers, binwidth of $1m/s$ . . . 154
E.20 Quantification graphs typical export cable 1 in deep water ($150m$), 2 seed numbers, binwidth of $0.5m/s$ . . . 155
E.21 Quantification graphs typical export cable 1 in deep water ($150m$), 2 seed numbers, binwidth of $0.25m/s$ . . . 156
E.22 Quantification graphs typical export cable 1 in deep water ($150m$), 3 seed numbers, binwidth of $1m/s$ . . . 157
E.23 Quantification graphs typical export cable 1 in deep water ($150m$), 3 seed numbers, binwidth of $0.5m/s$ . . . 158
E.24 Quantification graphs typical export cable 1 in deep water ($150m$), 3 seed numbers, binwidth of $0.25m/s$ . . . 159
E.25 Quantification graphs typical export cable 1 in deep water ($150m$), 4 seed numbers, binwidth of $1m/s$ . . . 160
E.26 Quantification graphs typical export cable 1 in deep water ($150m$), 4 seed numbers, binwidth of $0.5m/s$ . . . 161
E.27 Quantification graphs typical export cable 1 in deep water ($150m$), 4 seed numbers, binwidth of $0.25m/s$ . . . 162
E.28 Quantification graphs typical export cable 1 in deep water ($150m$), 5 seed numbers, binwidth of $1m/s$ . . . 163
E.29 Quantification graphs typical export cable 1 in deep water ($150m$), 5 seed numbers, binwidth of $0.5m/s$ . . . 164
E.30 Quantification graphs typical export cable 1 in deep water ($150m$), 5 seed numbers, binwidth of $0.25m/s$ . . . 165

List of Tables

4.1 6 DOF right-handed vessel system [31] . . . 30
4.2 All local chute motions . . . 31

5.1 Summary of modelled subsea power cable mechanical properties . . . 41
5.2 Summary of modelled subsea power cable integrity limits . . . 41
5.3 Static report - Initial 6 DOF motion analysis . . . 42
5.4 Static report - Typical inter-array cable 1, shallow water $30m$ . . . 46
5.5 Static report - Typical inter-array cable 1, deep water $150m$ . . . 46
5.6 Typical inter-array cable 1 - All regression coefficient (R^2) results - Shallow water ($30m$) 48
5.7 Typical inter-array cable 1 - All regression coefficient (R^2) results - Deep water ($150m$) . 48
5.8 Static report - Typical inter-array cable 1, static bottom tension 2kN . . . 49
5.9 Static report - Typical inter-array cable 1, static bottom tension 5kN . . . 49
5.10 Static report - Typical inter-array cable 1, static bottom tension 10kN . . . 49
5.11 Static report - Typical inter-array cable 1, static bottom tension 20kN . . . 49
5.12 Various static bottom tensions - Inter-array cable 1 regression coefficient results - Shallow water ($30m$) . . . 49
5.13 Typical inter-array cable 1 - All regression coefficient (R^2) results - Shallow water ($30m$) - Other CLV . . . 50
5.14 Regression coefficient results - Typical inter-array cables 1 and 2 - Shallow water ($30m$) 51
5.15 Regression coefficient results - Typical export cables 1 and 2 - Shallow water ($30m$) . . 51
5.16 Regression coefficient results - Typical inter-array cables 1 and 2 - Deep water ($150m$) . 51
5.17 Regression coefficient results - Typical export cables 1 and 2 - Deep water ($150m$) . . . 51

6.1 Chute z velocities [m/s] for typical export cable 1 in shallow water ($30m$) and deep water ($150m$) . . . 58
6.2 Results quantification method limiting chute z velocity [m/s] typical inter-array cables in shallow water . . . 59
6.3 Results quantification method limiting chute z velocity [m/s] typical export cables in shallow water . . . 60
6.4 Results quantification method limiting chute z velocity [m/s] typical inter-array cables in deep water . . . 61
6.5 Results quantification method limiting chute z velocity [m/s] typical export cables in deep water . . . 62

B.1 Most important Living Stone characteristics [21] . . . 86
B.2 Static report - Extreme deep water case to verify chute cable motion composition (1000m) 89

C.1 Cable limits typical inter-array cable 1 [-] . . . 95
C.2 Mechanical performance parameters typical inter-array cable 1 [-] . . . 96
C.3 Typical inter-array cable 2 cable components [-] . . . 98
C.4 Typical inter-array cable 2 dimensional characteristics [-] . . . 98
C.5 Typical inter-array cable 2 limits [-] . . . 98
C.6 Typical inter-array cable 2 mechanical performance parameters [-] . . . 99
C.7 Typical export cable 1 cable components [-] . . . 100
C.8 Typical export cable 1 limits [-] . . . 100
C.9 Typical export cable 1 mechanical performance parameters [-] . . . 100
C.10 Typical export cable 2 components [-] . . . 101
C.11 Typical export cable 2 limits [-] . . . 101
C.12 Typical export cable 2 mechanical performance parameters [-] . . . 101

D.1 Static report - Typical inter-array cable 2, water depth of $30m$ 109
D.2 Static report - Typical inter-array cable 2, water depth of $150m$ 109
D.3 Static report - Typical export cable 1, water depth of $30m$ 109
D.4 Static report - Typical export cable 1, water depth of $150m$ 109
D.5 Static report - Typical export cable 2, water depth of $30m$ 110
D.6 Static report - Typical export cable 2, water depth of $150m$ 110

E.1 Binwidth sensitivity analysis inter-array cable 1, shallow water 166
E.2 Seeds sensitivity analysis inter-array cable 1, shallow water 166
E.3 Binwidth sensitivity analysis inter-array cable 2, shallow water 166
E.4 Seeds sensitivity analysis inter-array cable 2, shallow water 167
E.5 Binwidth sensitivity analysis export cable 1, shallow water 167
E.6 Seeds sensitivity analysis export cable 1, shallow water 167
E.7 Binwidth sensitivity analysis export cable 2, shallow water 168
E.8 Seeds sensitivity analysis export cable 2, shallow water 168
E.9 Binwidth sensitivity analysis inter-array cable 1, deep water 168
E.10 Seeds sensitivity analysis inter-array cable 1, deep water 169
E.11 Binwidth sensitivity analysis inter-array cable 2, deep water 169
E.12 Seeds sensitivity analysis inter-array cable 2, deep water 169
E.13 Binwidth sensitivity analysis export cable 1, deep water 170
E.14 Seeds sensitivity analysis export cable 1, deep water 170
E.15 Binwidth sensitivity analysis export cable 2, deep water 170
E.16 Seeds sensitivity analysis export cable 2, deep water 171

1 Introduction

In this chapter, the topic of subsea power cables is introduced by first elaborating on the growing energy demand and incorporation of renewable energies (such as offshore wind) within the energy mix. Narrowing down, the need for subsea power cables is explained and workability regarding offshore cable operations is discussed. At last, DEME Offshore NL is briefly introduced as this was the mentoring company during this thesis.

1.1. Report outline

Chapter 1 contains a general introduction to this thesis, containing the global energy demand, offshore wind, the growing need for subsea power cables, offshore workability and an introduction to supervising company DEME Offshore NL. In ***Chapter 2*** the problem statement is provided containing research motivation, overall thesis objectives, research questions, scope, boundaries and approach. Subsea power cables, criteria in order to preserve cable integrity and subsea power cable lay operations are described in ***Chapter 3***. The offshore environment and how this environment is modelled using OrcaFlex software is explained in ***Chapter 4***. An analysis to identify which motion is limiting during a normal subsea power cable lay procedure is performed in ***Chapter 5***, and in ***Chapter 6*** a quantification method for these specific limiting motions is set up and tested. Finally, the obtained limiting motions are combined with a motion-based forecasting (MBF) method in ***Chapter 7***. A discussion and final conclusions are enclosed in ***Chapter 8*** and ***Chapter 9*** respectively.

1.2. Global energy mix

The energy industry has been rising globally ever since electricity was invented and especially in the past few years demands have increased significantly. The International Energy Agency (IEA) has done research regarding energy increase, and until 2040 the energy demand is estimated to increase by 1% each year [2]. At the moment, various companies have found their way into the energy industry and (partly) together they are working on an energy mix in order to supply future generations. Obviously each company has a different vision regarding this energy mix and opinions differ on the best approaches and techniques, especially since carbon emissions need to decrease drastically in order to comply with targets described in the Paris Agreement regarding global warming. However, both the industry and politicians agree that a global combination of multiple energy production procedures is the key to provide enough energy capacity for the future.

The oil and gas (O&G) industry has dominated for decades, but currently renewable energy resources are being investigated. These renewable energy sources are especially interesting because of CO_2 reduction and limitations regarding global warming as presented in the Paris Agreement. This Paris Agreement is an European agreement to combat climate change together, by accelerating and intensifying required actions and investments in order to decrease carbon emissions and create a sustainable low carbon future [2, 9].

The precise goal defined in the 2015 Paris Agreement is to limit the rise of the global mean temperature to $2°C$ by 2100 with a probability of 66% (although the aim is a temperature rise of $1.5°C$). In order to reach this limit of 2°C by 2100, all nations that signed the agreement strive for a combined

decrease in carbon energy intensity by 85% and a total emission budget of $790 Gigatonnes\ CO_2$ from 2015 to 2100. [9, 14, 27]

1.3. Offshore energy and subsea power cables

Ever since the steam engine was invented, physicist and researchers have been looking for new innovative possibilities to generate electricity. Now that the earth is getting warmer each year and global warming is a real issue on the political agenda, renewable energies have gained broad support from both governments as citizens worldwide.

1.3.1. Offshore renewable energies

At the moment 14% of the electricity demand in the European Union (EU) is generated by renewable energy techniques (wind and solar), of which 2% is offshore and 12% is onshore [8]. Studies show that around 2030 the global energy increase of the past century will slow down and reach a plateau. Therefore, this is a good starting point to penetrate renewable energy sources into the energy mix. The past few years wind and solar energy have rapidly gained in their share and even accounted for more than half of the added energy capacity. It is expected that the renewable energy capacity will almost double from 2020 to 2050, meaning a share increase from 19% to 34% [34].

In Figure 1.1 the global electricity generation per type of energy source is illustrated over a period of $70 years$ (from 1980 to 2050). This graph is taken from an energy transition outlook presented by DNV-GL in 2019. From Figure 1.1 it is clear that indeed renewable energy techniques such as offshore/onshore wind and solar panels are expected to increase rapidly in shares. Besides, this graph gives a clear idea of how the total energy demand has roughly tripled from $8 PWh/yr$ back in 1980 to $27 PWh/yr$ in 2020. Moreover, it is expected that this increase will continue the following years to even $58 PWh/yr$ in 2050.

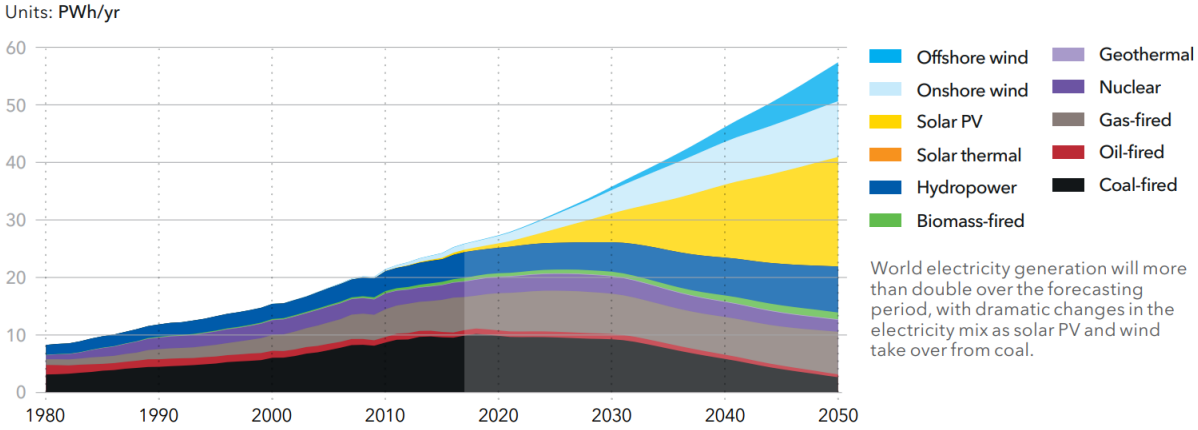

Figure 1.1: World electricity generation by power station type [14]

Onshore wind currently has the most capacity regarding renewable energy, but offshore wind is gaining share fast. At sea, wind speeds are higher and the wind direction is more consistent. Besides, turbines built offshore are larger than onshore thus offshore wind turbine generators (OWTG) generate more electricity in a more efficient way. In 2019 operations started to built the largest offshore wind farm (OWF) near the coast of Yorkshire in the UK. When completed, the farm called ”Hornsea” will contain 174 OWTG’s which together produce $1200 MW$, enough to supply roughly $1 million$ households in the UK [25]. However, OWTGs also come with some challenges since the offshore environment is harsher than onshore and in addition the generated power needs to be transported both over sea as over land. In order to transport the generated offshore energy to shore, subsea power cables are used.

1.3.2. Subsea power cables

Subsea power cables are totally different than onshore power cables transporting electricity via electricity pylons. Subsea power cables are installed using cable laying vessels (CLV’s), and are connected to the OWTG itself and a power station that can be located offshore (e.g. a manifold) or an onshore power station depending on the distance to shore.

The cable laying process is a delicate process since power cables are highly vulnerable and offshore conditions varying continuously in due to environmental loading such as wind, waves and currents. There are a lot of different variables and factors which have to be accounted for, both regarding the cable itself and the operating CLV. Cables are easily damaged and the integrity of the cables is of paramount importance. If there is an issue, repairing or replacing the cable takes up a lot of time and is expensive.

Often, a damaged cable is only discovered when the cable laying procedure is finished. This means that in order to repair the cable, a repair operation is required. Firstly, the subsea cable protection (rocks or trenched) need to be removed, then the cable needs to be lifted up or specialized divers are required. Altogether, if the cable must be repaired or adjusted this will lead to severe delays with respect to the projects delivery date. Moreover, this delay often leads to an overrun in costs as well. Therefore, it would be beneficial for all involved parties to prevent or reduce unnecessary cable damages.

1.4. Operability and workability

In order to decide whether and when CLV's can operate (or not) workability studies are performed. Workability is an enclosing term covering the total amount of time offshore operations can be executed during a project. In other words, the total time that the actual sea state is within the limits of the predefined limiting sea state. In the case of cable laying, limiting sea states are defined by a combination of H_s (significant wave height), T_p (wave peak period) and α (incoming wave direction relative to the vessel). This method is widely applied throughout the entire offshore industry.

Workability studies are based on the combination of two underlying components; *operability calculations* and *weather windows*. In Figure 1.2 a flowchart is attached in which the current method is briefly explained using underlying steps. It is important to maintain operability and workability as separate terms as they have a different meaning. The definitions are given below.

- **Operability**
  Determine limiting sea states CLV's can operate or not
- **Workability**
  Connect operability to real time weather data to obtain the actual time a certain CLV can operate

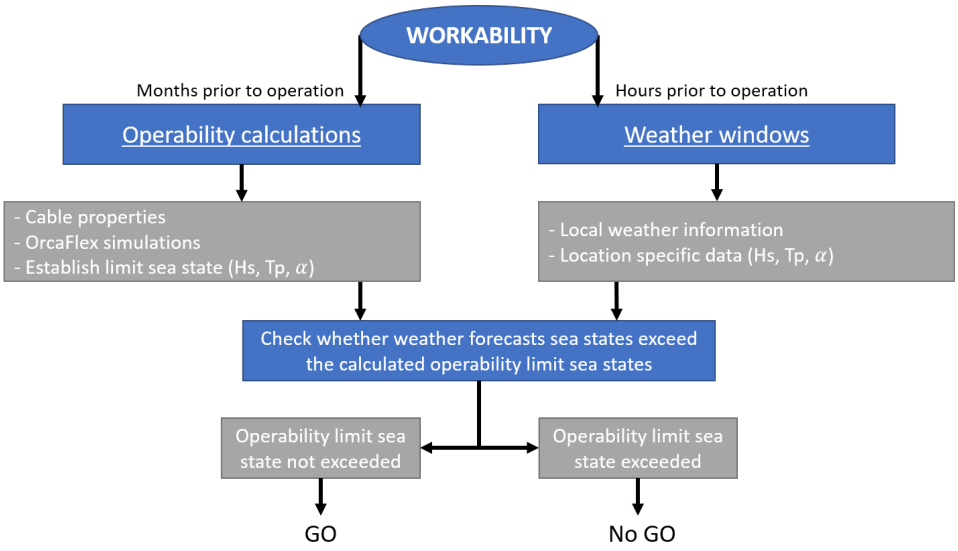

Figure 1.2: Current workability calculation flowchart [18, 49]

1.4.1. Operability calculation

The first component that has to be investigated is operability. The purpose of operability calculations is to determine in which environmental conditions (e.g. specific information regarding wind, waves and current) a certain vessel can operate offshore. Thus, in the end limiting sea states are defined.

Operability studies are vessel dependent, and highly influenced by response amplitude operators (RAO's) and quadratic transfer functions (QTF's). Besides, these calculations can both be performed in time- and frequency domain (as extensively explained in chapter 4).

The current operability method is based on specific cable properties as provided by cable manufacturers. An analysis is performed using OrcaFlex software, a leading software package developed especially for the offshore industry covering dynamic analysis of offshore marine systems such as cables, risers and anchor-systems (in Appendix A section A.1 an overview of several offshore software packages is enclosed). These OrcaFlex analyses are performed based on time-domain calculations as modelling subsea power cables is a nonlinear process. As input variables, besides the specific cable properties, OrcaFlex requires information regarding environmental conditions such as H_s, T_p and α. Since a time-domain analysis is applied, a time step (Δt) needs to be chosen to perform the calculations. If applicable, special information regarding the seabed, currents etc. can also be incorporated within the OrcaFlex model as well.

Performing time-domain simulations in OrcaFlex takes a lot of time. Depending on the chosen time step, type of available computer and amount of simulation cases (all different H_s T_p and α combinations) the duration can vary between a couple of hours to even multiple days. All steps are clearly described in DNV-GL codes, and are based upon 3-hour JONSWAP (joint north sea wave project) spectra calculations. Consequently, using a lot of varying variables, sea states are simulated and eventually a limit sea state is defined consisting of $H_s - T_p$ combinations for multiple incident wave directions relative to the vessel (α). These limiting sea states are provide a CLV's operability in a so called operability table. In general, α is taken from $0deg$ to $360deg$ in steps of $30deg$.

1.4.2. Weather forecasts

The second component that is required to perform a workability assessments are weather forecasts. In the operability calculation, in the end limit sea states are defined. This means that accurate daily weather data is required in order to compare the actual sea state with the predefined limiting sea states to see whether it is possible to operate ot not.

These weather forecasts are purchased via specialized third party companies. Such weather forecasting companies can provide accurate and location specific wave forecasts. These forecasts also consist of $H_s - T_p$ combinations, and if applicable directions these waves originate from. Besides the purchased weather forecast data, sometimes an additional wave buoy is used in order to verify the predicted weather conditions. Not every OWF has the possession of such a wave buoy, and therefore weather forecasts are always bought.

1.4.3. Workability

Considering workability, there are a lot of different variables that have to be accounted for. Currently, combining the calculated operability with the bought weather forecasts provides enough information to make a decision whether offshore operations are possible or not. However, the calculation is quite conservative and there are multiple simplifications as described in subsection 2.1.1.

1.5. DEME Offshore NL

DEME group is a global aggregation of international offshore oriented companies that merged in 1991. However, the roots of those companies go back to the 19^{th} century. DEME stands for '*Dredging, Environmental and Marine Engineering*'. The main focus is on dredging, land reclamation, offshore infrastructure, offshore logistics and other offshore services. Originally DEME was a dredging company, but over the years they have developed themselves broader into the offshore industry and also infrastructural projects. [20]

DEME Offshore is an offshore contractor founded in 2019 as the result of a merger, that provides services in the offshore O&G and renewable energy industry. Regarding the O&G sector, DEME Offshore focuses on landfalls, rock placement, heavy lift and decommissioning work. Within the renewable energy sector, DEME Offshore has three main specialities covered over three offices. In Denmark, the focus is on WTG's and in Belgium the main line of work is aimed at foundations. DEME Offshore NL, located in Breda, focuses mainly on subsea aspects such as subsea power cable installation, umbilical installation and trenching operations. This thesis was conducted at the Research & Development (R&D) department of DEME Offshore NL, at the international subsea power cable installation team explicitly.

2

Problem statement

In this chapter the problem statement is presented. At first, specific research motivation is provided and the objectives are composed. Next, the research questions of this study are presented. In the fourth section the scope and boundaries of this research are given. At last, the approach throughout this thesis is addressed.

2.1. Research motivation

The offshore industry is a cost intensive industry, especially since installation and maintenance operations executed offshore are expensive. A typical rate for offshore vessels depends on their size and capability, but roughly most CLV's costs vary from $€50k$ to $€100k$ per day [18] (the most expensive CLV's can be hired with rates of up to $1million$ euros per day). Therefore, offshore workability plays a significant role in both costs and time of the cable laying processes when constructing OWF's. Since, the higher the workability, the less days a contractor needs to complete the job leading to lower installation costs.

The demand in subsea power cables is expected to increase with 17% in the period from 2018 to 2022, illustrating a total growth of 71% compared to the period of 2013-2017 [22]. This increasing subsea power cable demand is visualized in Figure 2.1.

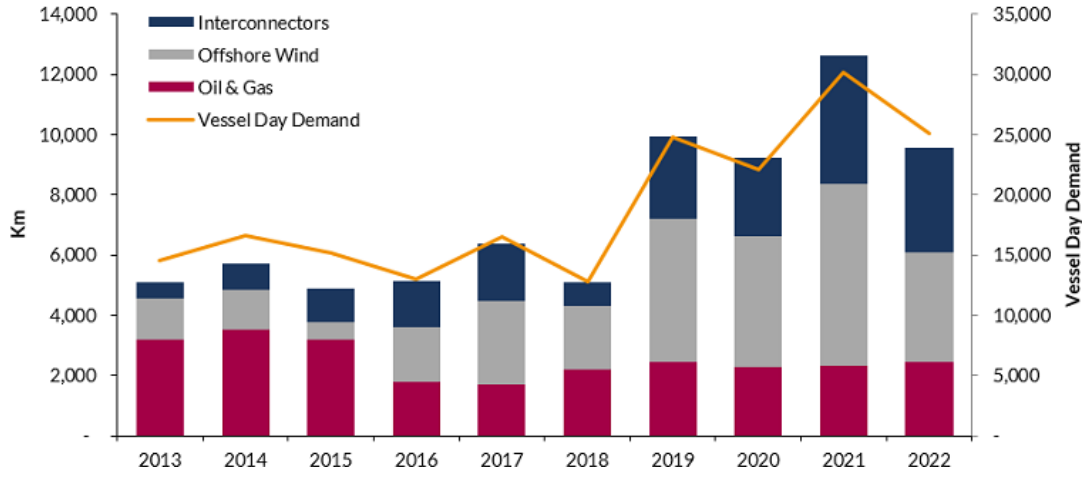

Figure 2.1: Global subsea cable installation and vessel demand, 2013-2022 [22]

From Figure 2.1 it is clear that both the total length of installed subsea power cable for offshore wind and interconnectors has increased significantly from 2013-2017 compared to 2019-2022. This increase is also observed when taking a look at the vessel day demand. This increasing demand shows that more and more vessels are required for offshore operations. Besides, Figure 2.1 also clearly indicates the decrease in the O&G sector. [11, 22].

Optimizing workability is a hot topic in the offshore industry, since renewable energies are booming and the demand for subsea power cables keeps increasing. This increase in subsea power cable demand opens doors for both cable manufacturers and offshore contractors. Offshore contractors strive for installing these cables as efficient (quick and cheap, whilst preserving quality and safety at all times) as possible so that they can execute as many projects to maximize their profit.

The current method to determine workability, however, does contain certain limitations and disadvantages. These are enlightened in the next section.

2.1.1. Limitations current workability method

Firstly, the operability calculations (time-domain OrcaFlex simulations) are time consuming and demand a lot of computational power. Hence these calculations are performed onshore in offices, where special computers are accessible, instead of offshore where the actual operations take place. This means the communication between staff onshore and offshore needs to be perfectly aligned and all documentation needs to be very clear.

Furthermore, the current approach is somewhat conservative because there is no room for anticipation regarding which CLV to use as workability studies are vessel dependent. Before starting operability calculations months prior to the actual operations, it is not always known which CLV is available. So, if for whatever reason the modelled CLV is unavailable, last minute vessel changes mean the entire operability study needs to be redone to come up with the correct limiting sea states accompanying the substituting CLV.

A third aspect is that currently only one loading condition is investigated. This loading condition is taken such that this is the worst loading condition that can occur (further referred to as worst-scenario). In reality, multiple loading conditions can occur, and by modelling only the worst-case all other loading conditions are covered as well. The reason for only simulating this one worst-scenario is clarity for the offshore crew. If several loading conditions would have been modelled, this would result into multiple operability reports. Hence the offshore crew needs to check continuously which loading condition should be persisted and whether the right report is followed. This could easily lead to confusion and mistakes. This simplification, however, does indicate that there is some room for innovation as the workability is indeed in some cases somewhat conservative.

Another limitation of the current workability method is that wave spreading is not accounted for. When defining limiting sea states during the operability assessment, the incident wave angles relative to the vessel are modelled such that these originate from one single direction, resulting from a 1D JONSWAP spectrum. In reality, however, waves never originate from only one direction as for example sea waves and swell can be distinguished (these waves do not necessarily originate from the same direction).

At last there is always some uncertainty and conservatism with respect to weather forecasts. Therefore, DNV-GL codes prescribe the need of alpha factors (essentially safety factors) to counteract these uncertainties. This alpha factor reduces the workability by a certain factor, meaning the closer this alpha factor is to 1, the higher the workability. Since these alpha factors are rather old (last revised in 2016) and regarded as too conservative, DEME Offshore NL is currently part of a joint industry project (JIP) together with some other offshore contractors and DNV-GL itself to reconsider these alpha factors.

2.1.2. Implementing motion-based forecasting

Regarding offshore heavy lift operations, motion-based forecasting (MBF) is widely applied in the industry. In general, there is one main issue why MBF cannot straightforwardly be implemented within subsea power cable operations. During offshore heavy lift operations equipment limits, such as crane and crane cable limitations, are the leading criteria. Thus, these limits are identical for all operations applied with that particular crane and only the load (product) varies. For offshore cable operations, however, not the equipment but the subsea power cables themselves (product) determines the limits as subsea power cables are much more vulnerable than the required equipment. Therefore, applying MBF in offshore cable operations is more difficult since the limits will be different for each installed subsea power cable. Moreover, for every OWF project a custom subsea power cable (both an inter-array and export cable) is designed that meets specific requirements and needs.

Implementing a MBF method into subsea power cable operations would have some significant benefits relative to the current workability method. The main advantage is that MBF takes entire 2-dimensional (2D) weather forecasts into account, hence there is no need to implement a standard

JONSWAP spectrum based on single $H_s - T_p$ combinations. Consequently, wave spreading is instantly accounted for since this is already present in the 2D weather forecasts.

Another advantage of implementing MBF is that the aspect of implementing only worst-case scenarios disappears as well, as all subsea power cable integrity limits are converted into this one limiting motion. To determine the limiting motion, the loading condition actually does not matter because the limit is simply a limit, and how this limit is reached is of less interest. Besides, this means that by implementing MBF the total workability method becomes vessel independent due to the same aforementioned reason.

A last major advantage of this MBF approach is that onboard a vessel MBF calculations can be performed in the frequency-domain instead of the time consuming time-domain. To determine the precise limiting motion and convert this motion into an actual limit, still time-domain need to be performed in OrcaFlex as modelling subsea power cable is a very nonlinear process. When this limit has been established, however, all remaining MBF calculations can be performed in the frequency-domain. This is because the CLV is both larger and heavier than the subsea power cable, thus to determine the vessel motions the subsea power cable does not need to be accounted for in the modelling process.

2.1.3. Thesis topic clarification

Several research has already been conducted regarding the implementation of MBF into offshore cable operations. MO4, for example, have published a brief article in which essentially heave velocity at the chute is indicated as a good predictor for offshore subsea power cable operations [18]. The exact research which led to their conclusion, however, is confidential. Therefore, the main idea behind this thesis is to investigate the possibility of implementing MBF in subsea power cable operations themselves, and subsequently explore what the effect on workability will be when implementing a MBF approach.

First, a specific limiting motion has to be determined, which is basically a link between cable integrity criteria and occurring vessel motions. This limiting motion can hence be regarded as a predictor. This predictor can be combined with MBF since the real-time predicted vessel motions can be compared against this limiting motion predictor, hence the limiting motion becomes the criterion which determines whether it is possible or operate or not. For this method to work, this particular predicting limiting motion needs to be converted into a cable limit, as the cable's integrity is governing. Therefore, a proper method to quantify these occurring limiting motions is required as well.

2.2. Objectives

The purpose of this research topic follows several objectives. However, one main objective can be distinguished. This main objective is formulated as follows:

"Optimizing offshore cable laying workability by operating based on limiting motions in combination with motion-based forecasting"

Optimization of offshore cable operations is something most offshore cable contractors strive for. Moreover, MBF is already widely applied in various other offshore operations, but not so much regarding subsea power cable operations. Within this thesis, the term 'optimized' is interpreted as improving the accuracy of the workability assessment to eventually increase overall workability.
Since the main objective is quite extensive, several sub-objectives for this thesis are listed in the enumeration below.

- Search for a link between cable integrity and maximum vessel motions to
- Gain insight in which motions are limiting during offshore cable operations
- Set up a method in order to convert these limiting motions into specific subsea power cable limit
- Implement an onboard motion-based forecasting method within total workability calculations
- Improve overall accuracy of workability studies and therefore increase CLV workability windows

2.3. Research questions

Taking the research motivation and objectives into account, the main research question is composed. This main research questions is defined as follows:

How is workability of offshore cable installation improved by shifting workability towards limiting motions at the chute instead of the conventional workability method?

Since the main research question is a rather broad and open question, four sub-questions have been formulated as well. These research questions (RQ's) are presented below and by answering each individual sub-question in the end a thorough answer to the main research question can be given.

1. Which mechanical properties and processes determine subsea power cable integrity during offshore cable installation?
2. Which occurring motions at chute level are limiting per cable failure mechanism during the normal cable laying procedure?
3. How can the values of these limiting vessel motions at chute level be quantified?
4. How can the offshore installation workability in practice be improved by implementing motion-based forecasting combined with limiting motions compared to the conventional workability analyses?

2.4. Scope and boundaries

Regarding offshore cable installation there are a lot of variables and degrees of freedom (DOF's) which have to be considered. The scope and accompanying boundaries of this thesis are constructed around the research motivation, objectives, main research question and related sub-questions.

2.4.1. Scope

The first step throughout this thesis is to identify which cable criteria need to be preserved in order to guarantee subsea power cable integrity, hence the cable does not get damaged. Therefore, a literature study regarding subsea power cable mechanical properties and all cable integrity limits is conducted. Besides, literature regarding offshore cable installation procedures has been analysed. By combining cable limits with the forces acting on the cable during installation operations, subsequently cable integrity criteria during subsea cable operations can be established.

Next, an analysis is performed to investigate which vessel motions show the best relations to the predefined cable integrity criteria. In this step the motions are investigated at the chute, since this is where the subsea power cable leaves the CLV. This step is performed using Orcina OrcaFlex software, in which multiple water depths, subsea power cables and normal lay configurations have been assessed.

After the limiting motions have been identified, a method needs to be set up to make a proper quantification of these predefined limiting motions. Hence, all predefined cable integrity limits need to be converted into one single limiting motion cable limit. For this step, the entire relations between chute motions and the cable integrity criteria is not of that much interest anymore, since especially the OrcaFlex cases close around these cable integrity limits are now of interest. In order to obtain more data in these regions close around breaching cable integrity criteria, multiple seed numbers are modelled for these specific cases. By splitting the motions into bins composing a percentile line through these bins, eventually an intersection can be found between the cable integrity limits and the composed percentile line. The limiting motion value accompanying this intersection represents the limiting motion, hence eventually all cable integrity properties are converted into a limiting motion (which is on its own a new introduced cable property).

At last, a brief MBF approach is implemented in order to make a comparison between the current workability assessment and the proposed limiting motion approach. As there were no entire 2D wave spectra available to use as input, a superimposed JONSWAP has been created composed of wind waves and swell contributions. Besides, wave spreading is accounted for within this superimposed wind + swell JONSWAP. This superimposed JONSWAP is compared against the current 1D JONSWAP $H_s - T_p$ combination method without wave spreading by performing a vessel motion analysis in the frequency domain. The resulting chute motions for the indicated limiting motion can hence simply be compared against each other.

2.4.2. Boundaries

There are multiple types of offshore cable operations. Normal cable lay operations are the most common operations, which can either be executed using S-lay or J-lay methods. Besides, both cable ends need to installed by means of a 1^{st} and 2^{nd} end pull in. The majority of the subsea power cable length, however, is installed by means of normal lay. Therefore, for this study only normal lay operations are taken into account. More specialized operations such as pull ins, cable jointing, cable crossings and repair jobs are not considered.

Each subsea power cable is different and no two cables are completely identical. Therefore, four typical subsea power cables are assessed for verification and validation purposes. Furthermore, only cable properties as provided by cable manufacturers themselves are accounted for. Other types of failure modes, such as fatigue and vortex induced vibrations (VIV), are neglected. During cable installation operations the cable endures a high loading only for a very short time, hence fatigue is never of much interest.

Traditionally, vessel motions are measured at a vessels centre of gravity (COG). For this research, however, occurring motions at the chute are investigated. The chute is where the subsea power cable leaves the CLV during cable installation operations. Therefore, the resulting limiting motions are expressed as local chute motions, and not in traditional vessel motions.

For this study cable integrity limits are regarded as governing since subsea power cables are vulnerable products. Hence, it is assumed cable installation equipment will not fail, but the product will. Besides it is assumed the cable limits are independent of each other, hence these limits will not strengthen or weaken each other.

In the offshore environment there are various external loads a vessel and subsea power cable endure. All these loads are environmental, and originate from waves, wind and currents. However, hydrodynamic loading from wind and currents are excluded from this research as their dynamical contribution is substantially lower than contribution coming from wave loading. Moreover, irregular wave fields are studies, since offshore waves in reality are always irregular and not regular.

As aforementioned, alpha factors are implemented in workability studies to correct for uncertainties in weather forecasts. The optimization of these alpha factors, however, is not regarded within this thesis as these are prescribed by DNV-GL rules which offshore contractors simply have to follow. DEME is currently part of a JIP, together with multiple offshore contractors and DNV-GL itself, to have a revision at these alpha factors.

At DEME, Orcina OrcaFlex software is used to model subsea power cable operations. In order to model subsea power cables in OrcaFlex some input variables are required. Besides, the specific cable properties input variables included in this study are the incident wave angle relative to vessel heading (α), significant wave height (H_s), peak period (T_p), layback length (l) and water depth (d). Since the workability assessment is (partly) performed using a time-domain analysis, a time step (Δt) is required as well.

2.5. Approach

To clarify the approach persisted throughout this thesis a flowchart is presented in Figure 2.2. Per sub-question, the applied methods and required data are described.

From Figure 2.2 it is clear multiple software programs and tools will be used. OrcaFlex is the inhouse customary software package to perform subsea cable calculations, and therefore OrcaFlex is also used within this thesis. In section A.1 an overview of several offshore software packages including pros and cons enclosed. Besides, Excel and Python are used as well for fast data pre- and post-processing of OrcaFlex data, creating tables and generating graphs (OrcaFlex software is based on underlying Python code, hence Python was preferred over MatLab).

At first sight it may seem that sub-question 2 (identifying step) and sub-question 3 (quantifying step) are rather related to each other. To some extent, this is indeed true. To identify which motion shows the best relations towards the predefined cable integrity criteria the entire relation is of interest. In order to make a quantification of this limiting motion, however, not the entire relation is of interest but the motion behaviour close to the cables integrity criteria is of particular interest. Therefore, the simulation model and applied method accompanying sub-question 2 needs to be adjusted somewhat for sub-question 3. Moreover, a quantification method is introduced based on the adjusted OrcaFlex model.

Besides this research approach, a methodology overview has been set up as well which is explained in more detail in Appendix A section A.2.

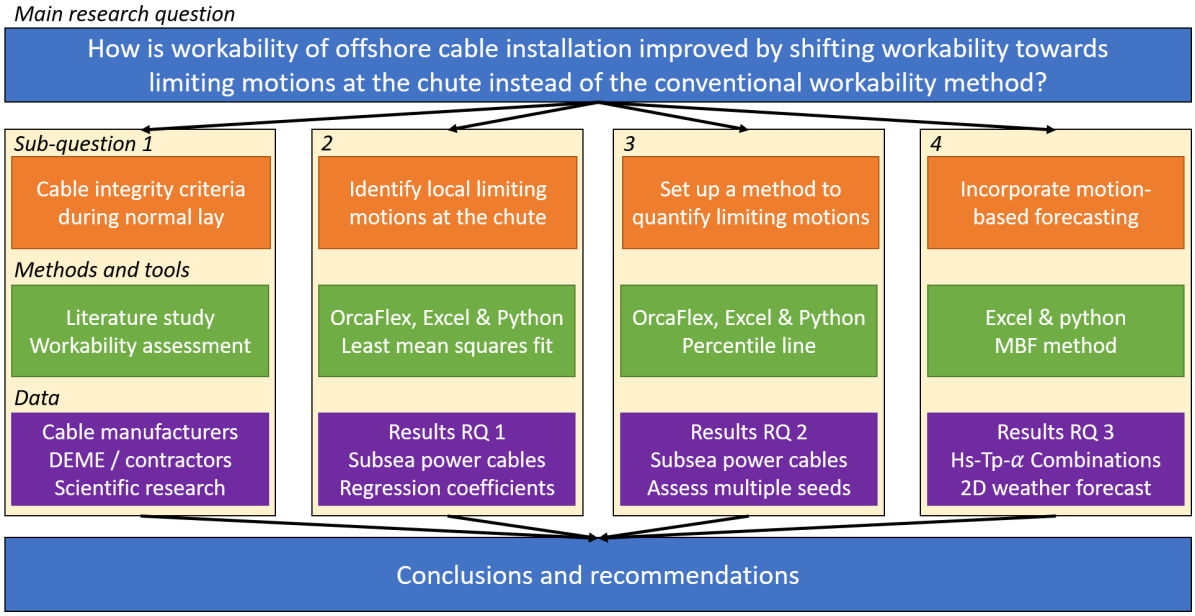

Figure 2.2: Overview of approach, methods and data separated per research question

3

Subsea power cables and installation

In this chapter at first an introduction of subsea power cables is given, followed by a more detailed description of subsea power cables including specific cable properties. Besides, multiple types of cable operations are described and required cable installation equipment is covered. At last, a conclusive set of criteria preserving cable integrity is composed by combining cable integrity properties with cable normal cable lay operations.

3.1. Subsea power cables

Subsea power cables have been undergoing a major transformation in their purpose. Nowadays, subsea power cables are used to export offshore generated electricity to shore, whereas they were formerly used to transport electricity offshore. This has all to do with the changing position of the offshore industry, moving from the somewhat 'conservative' O&G industry towards renewable energy. Especially in the developing offshore wind branch subsea power cables have a crucial role. Cable installation projects have turned into major diverse operations itself and overall the trend is to transport more power over a longer distance [54].

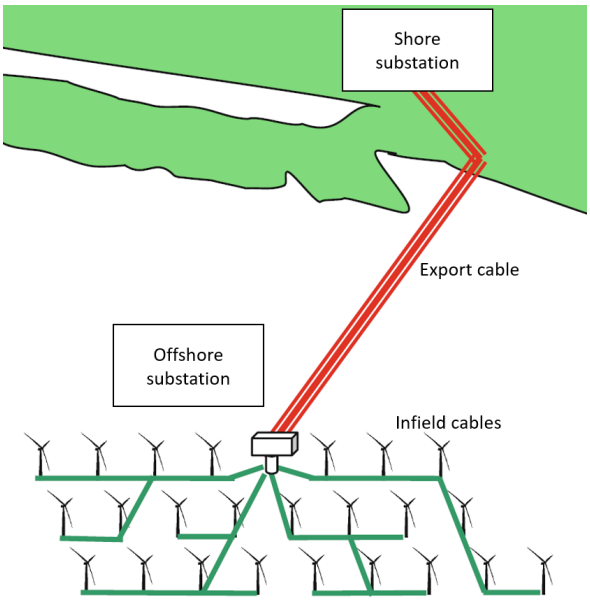

Figure 3.1: Example of grid connection [61]

In order to transfer all energy produced by the OWTG's to shore, all these turbines need to be connected to the electrical power grid. The main elements required in order to connect WTG's to the grid are infield cables, export cables and substations. These substations can either be located offshore, onshore or a combination of the two. Infield cables are used in order to connect the various offshore turbines and structures, whereas the export cable is used in order to connect the offshore structures to the main land. Typical infield cables have voltages of $33kV$ or $66kV$, and export cables in general have voltages ranging from $150kV$ to $320kV$. [49]

An illustrative schematization is shown in Figure 3.1. For each wind farm specific subsea cables are designed in order to comply to specific project needs and requirements. This means no two subsea power cables are completely identical. However, the main idea is obviously identical for all cables, which is to transport energy.

3.1.1. Alternating current and direct current

Besides differences in cable voltages, a general distinction can be made between alternating current (AC) and direct current (DC) cables. The main difference between these two cables is that AC cables have three conductive cores and DC cables consists of only one conductive core, as illustrated in Figure 3.2. These cores are tightly wrapped in protective and insulating materials. The cable composition is further elucidated in subsection 3.1.2.

(a) AC cable [49]

(b) DC cable [29]

Figure 3.2: Examples of AC and DC cables

Other differences between AC and DC cables are linked to costs and energy losses. A DC cable set-up comes with high initial costs since additional AC/DC and DC/AC converters and filters need to be installed. However, DC cables have lower energy losses than AC cables. This means that at a certain point there is a turning point based on the distance the subsea power cable has to cover. Depending on the specific type of cable this turning point is in the range between $50km$ and $100km$. Usually, regarding offshore wind projects inter-array cables are based on AC, whereas the export cables are based on DC. This makes sense since the distance from the OWF to shore is commonly further than cables connecting turbines. However, when a OWF project starts, a special cable is designed to meet the precise requirements and needs. Hence there is no standard, and AC export cables or DC inter-array cables exist as well. [49, 54, 61]

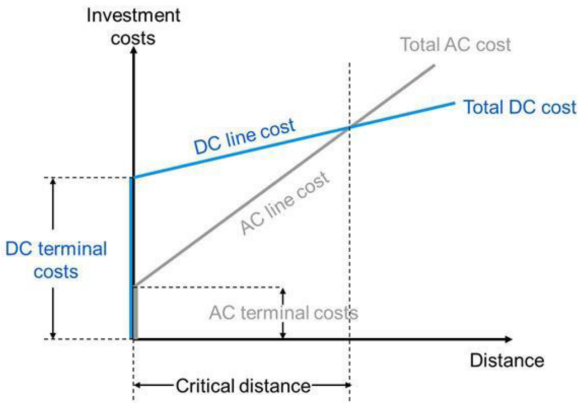

Figure 3.3: AC cables versus DC cables [61]

3.1.2. Cable composition & design elements

From Figure 3.2 it is clear that subsea power cables consists of several layers of various materials. Even though each specific cable is unique, there is consistency in how the cables are composed. Two cross-sections are shown in Figure 3.4 where all different cable elements can be distinguished, for an AC as well as a DC subsea power cable.

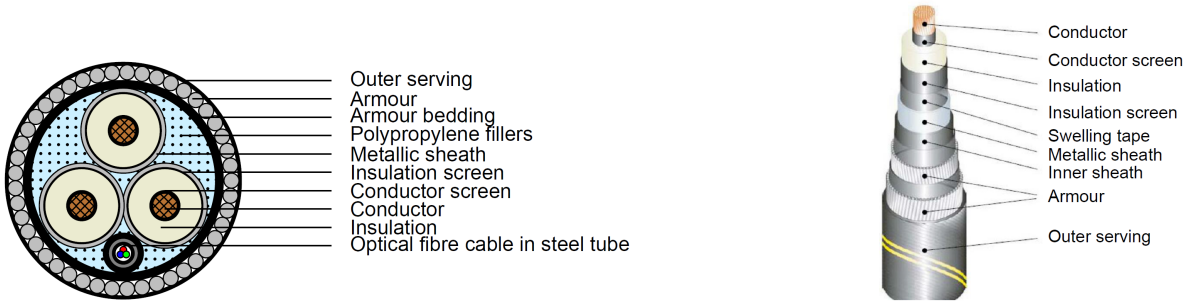

(a) AC cable cross-section

(b) DC cable cross-section

Figure 3.4: Common subsea power cable cross-sections [49]

From Figure 3.4 it can be concluded that AC and DC cables are mostly similar, but there are some differences as well. Essentially, an AC cable comprises of a bundle of three three smaller cores. This means that there are a few extra components required in order to have a tied packed cable [29]. For example, in AC cables polypropylene fillers are required in order to fill up the extra space to form a circular cross-section. Each individual design element is briefly explained in more detail below. [49, 61]

- **Conductor**
  The conductor is the main element of a power cable since this is the part where electricity is actually transported. For subsea power cables the conductors are stranded from helically round wires. The used comprises either out of copper or aluminum. The majority of all subsea cables is produced using copper conductors since less raw material is required, which leads to smaller cross-sections. This holds both for the conductor as for material in the outer layers. Aluminum, however, is cheaper than copper so there are projects where an aluminum core is preferable. It is also possible to combine aluminum and copper, e.g. a copper conductor offshore, and an aluminum conductor onshore. Consequently, there is no superior choice and the decision is project dependent.

- **Insulation system**
  The function of insulation is to provide an effective barrier between extreme potential differences caused by the electrical field. It is of paramount importance that the applied insulative material is completely even and clean. Besides, the insulative material needs to be resistant to aging, able to withstand various temperatures and finally the material needs to be mechanically robust. There are two common insulation materials; polythylene (PE) and cross-linked polyethylene (XLPE). Regarding subsea power cables, XLPE is used most frequently.

- **Semi-conductive screens**
  If insulation material like XLPE would be applied immediately onto the conductor, the dielectric strength of the insulation material would decrease drastically due to grooves, ridges and irregularities. To avoid this reduction, a thin layer of semi-conductive XLPE or special semi-conductive tape is attached on the conductor before applying the entire insulation layer acting like conductor and insulation screens. This thin semi-conductive layer leads to a smooth dielectric surface, thus there are no stress enhancements leading to fewer electrical losses.

- **Metallic sheath**
  Since subsea power cables are vulnerable to water and moisture it is crucial to protect dielectric insulation to water ingression (especially in the offshore environment). Besides, subsea power cables need to be protected against mechanical damages and fatigue. Therefore, subsea cables have a metallic sheath to protect insulation material and the conductor. The metallic sheath can consist of aluminum, copper, lead and other metals. Lead used to be the most widely applied material since it is a relatively heavy metal, which has an advantage regarding cable dynamics. However, lead is also a rather soft metal which is unfavourable with respect to fatigue and mechanical damage. Currently more cable suppliers prefer aluminum or polyethylene sheaths as these protect better against mechanical damages and fatigue. Furthermore, metallic sheaths also protect subsea cables against Teredo (”aggressive” ship worms). These worms live in salt

waters and can do serious harm to subsea cables.
Sometimes, besides a metallic sheath, special water-blocking tape is applied as well.

- **Armoring**
  In order to provide tension stability and mechanical protection of subsea power cables, some type of armor layer is applied. For each individual project this armoring should be designed with respect to tension stability, external threats and protection requirements along the entire cable route. The most widely applied material is stainless steel. Wires of stainless steel are helical wrapped around the power cable. These round wires itself have a diameters varying between $2mm$ to $8mm$ each, and therefore the armoring has a huge impact on cable properties like bending stiffness, tensional stability, torsion balance and even the to be chosen installation method.

- **Outer serving**
  To protect subsea power cables against corrosion outer servings are applied. This outer serving layer also protects the cable against the surrounding environment during loading, laying and potential burying. The most common applied material for this outer layer is polypropylene. In order to even better protect the metallic sheats and armour from corroding, bitumen is also added to the polypropylene mix as well. Modern outer servings are either extruded polymeric, or these layers are constructed from wound yarn layers. Usually, the outer serving has special markings in order to make the subsea cable clearly visible for remote operated vehicles (ROV's).

- **Optical fibres**
  Presently, subsea cables are not only used to transport electricity, but when integrating an extra fibre optic cable within the overall subsea cable data can be transferred as well. This data can consist of temperatures, strain, vibrations, fault detection etc. These optical fibres are tightly wrapped in a tube of stainless steel with a diameter of $0.9mm$ to $4mm$. In single core cables (DC) optical fibres can be accommodated within the armour layers. Regarding three core cables (AC) the optical fibres can be equipped in the interstices between the multiple cores.

3.2. Cable failure

Unfortunately, subsea power cables do not last forever. Failure can occur in multiple phases, either during cable installation or they can wear-out eventually. Besides, there are multiple types of cable failure, such as exceedances in cable limits. All these phases and types of failure are addressed in this section.

3.2.1. Failure phases

Subsea power cables are vulnerable objects and in case of failure of any extent there are numerous serious risks involved. Since the entire operation of subsea cables is a delicate process failure can arise in multiple stages, beginning in the design phase all way to fatigue or end of life.

Obviously the main function of power cables is to transport electricity. These high electricity currents and voltages running through the cables, however, have a huge impact on the overall cable performance. Cables can get overheated or even start arcing, hence the cable will degrade. This can have effects such as layer separation. Over time, layer separation can do disastrous damage. Separated layers might get exposed to electrical loading (not every layer of the cable is designed to withstand these voltage and currents), harsh subsea environments, marine growth or even water penetration. Such events can lead to corrosion, erosion and even further separation of the layers within the cable. Eventually the cable is below proper standards and it either a repair operation is needed, or if the cable is not repairable anymore an entire new cable is required and has to be installed. [51, 52]

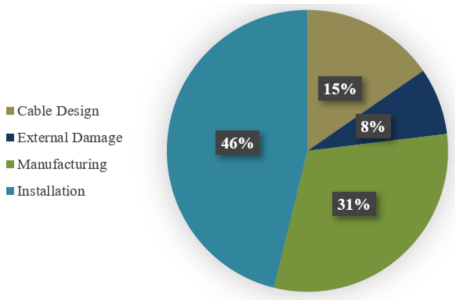

(a) Percentages of main failure modes [52]

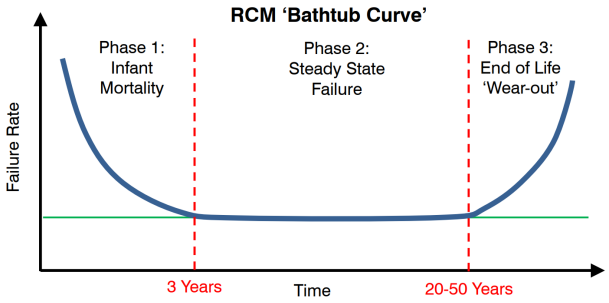

(b) Bathtub curve cable failure [19]

Figure 3.5: Failure...

Cable failure can occur due to four main failure modes: cable design, external damage, manufacturing and installation [52]. These failure modes have been distinguished by determining how failure was initially caused. From Figure 3.5 it can be concluded that especially in subsea power cable manufacturing and during installation failure is most common, 31% and 46% respectively. For the remaining failure modes cable design and external damage these percentages are substantially lower, 15% and 8% respectively.

The subsea power cable manufacturing industry is highly innovative since the demand keeps increasing and the global capacity is increasing as well. Therefore, cable manufacturers strive to design and create the best cables possible, hence reducing the risk of failure. The reliability of the cables is of paramount importance, because repairing a cable leads to an overrun in both costs and time.

The bathtub curve (Figure 3.5) is a graphical representation often used by reliability experts [19, 59]. Within this curve, three main phases are distinguished; infant mortality, steady state and end of life. Each of these phases is briefly explained below.

1. **Infant mortality**
   From Figure 3.5 it can be derived that a large percentage of subsea power cable failure occurs within the first three years after installation. This is due to faults at cable joints and terminations. Besides, incorrect installation operations play an important role as well. [19]

2. **Steady state failure**
   The second phase is referred to as steady state since the failure rate is constant. This state starts around 3 years after cable installation and ends somewhere between 20 to 50 years (depending on the degree of usage, and environmental conditions a particular cable endures).

3. **End of life 'wear-out'**
   When the cable is reaching its end of life after a certain period of usage (roughly 20 to 50 years) the cable starts to fail due to fatigue and the exposure to harsh offshore conditions. The subsea power cable has fulfilled its role, and a new cable needs to be installed. Moreover, a life-cycle of $20 - 50$ years is what cable manufacturers aim for.

3.2.2. Types of failure

In the previous sections, general failure phases and failure mechanisms have been addressed. However, in order to find which criteria are important regarding preserving the integrity of the subsea power cables, a more detailed analysis of what happens within the cable in necessary.

During the cable laying process, subsea power cables are exposed to various forces such as tensional and compressing forces. If these forces are monitored adequately, a lot of cable failure can easily be prevented since cables are damaged if certain cable properties are violated. Besides, during some stages specific tensions or compressions actually need to be maintained, e.g. when performing a post-lay trenching method the bottom tension (BT) needs to be monitored closely.

In order to preserve the subsea power cables integrity, cable manufacturers append cable specific properties to which contractors are obliged to stick to.

Overall, seven causes have been identified which lead to cable failure. These causes are listed, and briefly described, below.

1. **Tension**
   As aforementioned, during some cable laying stages the tension needs to be maintained continuously. Especially when applying a post-lay trenching method it is important to monitor tension, since a static bottom tension of roughly $5kN$ needs to be maintained at all times to successfully complete post-lay trenching operations. If the tension is too low, the trenching method fails, but on the other hand if the tension in the subsea power cable is too high, the cable gets tightened too much round the core. This can lead to cable damage in multiple layers such as the insulation layers, armour and metallic sheaths. Because of the helically wired structure of the power cables, these tensions are converted into a torsional load, which are described directly below.

2. **Torsion**
   Besides tension, there are more contributing factors to torsional loads. Cable twisting and rolling the subsea power cable from the carousel also have contributions to the torsional load. As long as the cable is properly tensioned, the torsional load is not harmful for the cables integrity. However, in case of compression or a tension that is too low, the cable might deform and the entire cable is going to fold into an helical shape. If this helical shape is not decomposed properly (by increasing or reducing the tension) the cable might twist or turn into a loop. As long as the loop does not exceed the cable's minimum bending radius (MBR) this loop itself is not harmful. However, when reducing the tension in order to clear out the loop the cable can start to kink. If the subsea power cable starts to kink, then the cable could be damaged as the MBR might get breached. In addition the inner materials and layers could shear leading to a severely damaged cable.

3. **Compression**
   Overall, compression in subsea power cables is not desired since compressive loads might cause the metallic sheath layers to buckle. Buckling is common occurrence in engineering, and represents a sudden deformation in a structural component under compression. Besides, under compression loads the helical structure of the cable's core can start to unwind itself which is known as birdcaging.

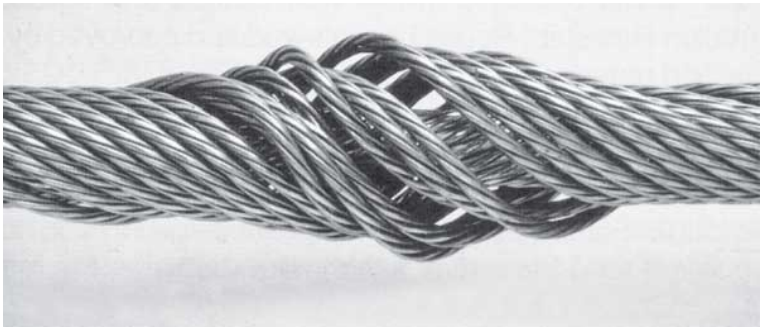

Figure 3.6: Unwinded helical structure, birdcaging [46]

4. **Fatigue**
   Fatigue is a common occurrence in engineering practices. Due to cyclic loading eventually even the strongest materials will fail. Cable manufacturers take fatigue assessments already into account when designing subsea power cables. However, a lot still remains unknown regarding subsea power cable fatigue [29]. Fatigue is often expressed by means of S-N curves, in which a constant cyclic stress is applied to a material to obtain the amount of cycles before the material fails.

   In Figure 3.7 two examples of S-N curves are shown. In the figure, line A represents a S-N-curve that leads towards an endurance limit, hence the material will not fail. On the other hand, line represents a S-N curve which indicates continuous decaying behaviour and the material eventually will fail.

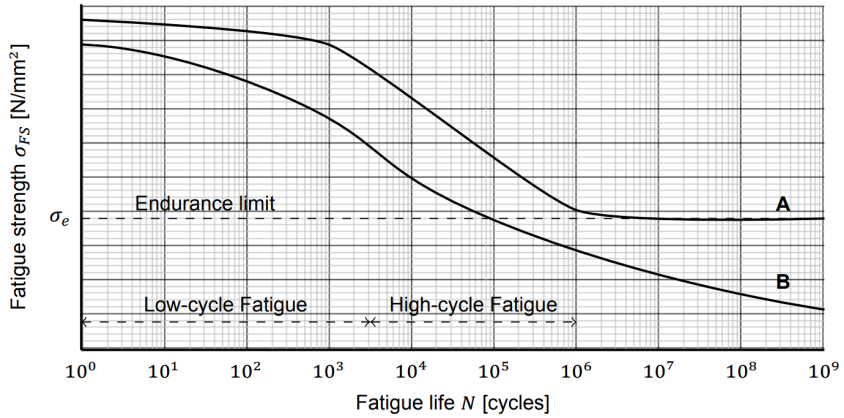

Figure 3.7: Typical SN-curve for subsea power cables [29]

5. **Cable squeezing**
   The Living Stone CLV contains 2 cable carousels which each have a capacity of 5000 tonnes of subsea power cable. This means that even before the cable laying operation starts, the vulnerable power cables are exposed to major gravitational loads due to their own weight, especially the lowest parts on the carousel. These major loads are known as squeezing loads. If the cable undergoes this squeezing load too long or if the load is too high, the subsea power cable is already damaged before it is installed.

6. **Cable crushing**
   After the cable is installed it is exposed to various crushing loads, such as rocks, boulders, anchors, fisher equipment and other dropped or dragged objects. Especially considering the cable over its entire lifetime, all these 'minor' loads add up and eventually might even damage the power cable. Therefore, the maximum side wall pressure (SWP) is introduced, as explained in section 3.3. The SWP is also known as the maximum crushing load.

7. **Cable bending**
   As illustrated in Figure 3.4 subsea power cables consists out of multiple layers, and each layer consists of different materials. All these materials have different properties, hence they all respond differently when a certain load is applied. Moreover, if a certain load is applied one side of the subsea power cable will be tensionally loaded whilst the opposite side will be under compression. Therefore, the cable does not only consists of different materials which ll respond differently, but in addition some parts of the cable will endure tension whilst other endure compression.

   When a subsea power cable is bended in a certain way the first response is always elastic, which means that when the cable is released from the load causing the bend the cable will instantly return to is original (equilibrium) position. In this case, there is no case of permanent (internal) damage or cable deformation. However, all materials will respond differently to the bend. This is due to different stress-strain relations amongst all materials present within a subsea power cable.

   In case of loading the subsea power cable such that the response is not elastic anymore, a certain strain limit is exceeded. This means that the cable does not return to its original (equilibrium) position anymore, and the cable is damaged and deformed. When certain material strains are exceeded, the frictional resistance between the cable's multiple components is reduced and adhesion between those components is reduced. This can lead to slippage of components, which has an effect on the minimum bending stiffness.

   If increasing the bending load even more, the bending radius is reduced. When the cable's bending radius is below the cable's listed MBR the cable is permanently damaged since there are serious forces acting on the cables core and the integrity cannot be preserved sufficiently.

3.3. Cable properties

Now that the cable components have been identified and typical failure modes have been described, the focus of this section is on subsea power cable properties. These properties can be distinguished in

two sub-groups; 1) mechanical cable properties and 2) cable integrity limits. As aforementioned, no two subsea power cables are identical since a project specific cable is designed for each OWF. This means that for each subsea power cable, the cable properties are different as well. Cable manufacturers provide a complete list with all specific properties for each independent subsea power cable. The basic requirements on these lists are explained in the two subsections below. [49, 61]

3.3.1. Mechanical cable properties

Firstly, mechanical properties of subsea power cables are explained. As aforementioned, a lot of the cable components are helically wounded around each other. Due to this helical shape, the cable can withstand hydrodynamic loading since it provides sufficient bending flexibility. This helical geometry is illustrated in Figure 3.8.

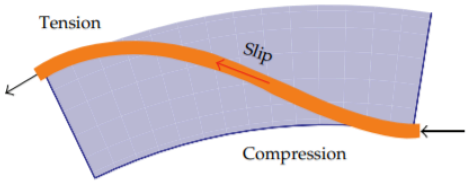

Figure 3.8: Helical cable structure [29]

A list of common mechanical cable properties is provided below. These properties together define a cables shape and design. Differences between subsea inter-array cables and export cables also come forward within the accompanying mechanical properties. Export cables are designed to transport higher voltages, hence energy capacities, hence these cable are often thicker and heavier than inter-array cables. Therefore, subsea export cables usually show stiffer behaviour. Especially bending stiffness is an interesting mechanical cable property, since for subsea power cable bending stiffness is always nonlinear. This nonlinearity is illustrated in Figure 3.9.

- **Cable diameter**
  Subsea power cable outer diameter in [mm]
- **Unit mass in air**
  Subsea power cable weight in air [kg/m]
- **Unit mass in sea water**
  Subsea power cable weight in water [kg/m]
- **Axial stiffness**
  Subsea power cable axial stiffness [MN]
- **Bending stiffness**
  Subsea power cable bending stiffness [kNm^2]
- **Torsional stiffness clockwise**
  Subsea power cable torsional stiffness in clockwise direction [kNm^2/deg]
- **Torsional stiffness counter clockwise**
  Subsea power cable torsional stiffness in counter clockwise direction [kNm^2/deg]

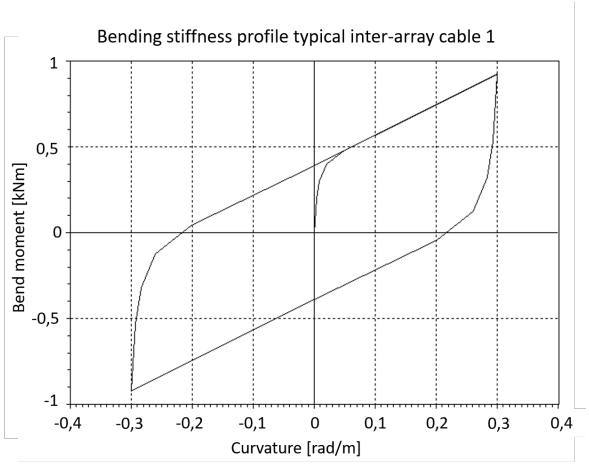

(a) Nonlinear bending stiffness typical inter-array cable 1 (example taken from OrcaFlex)

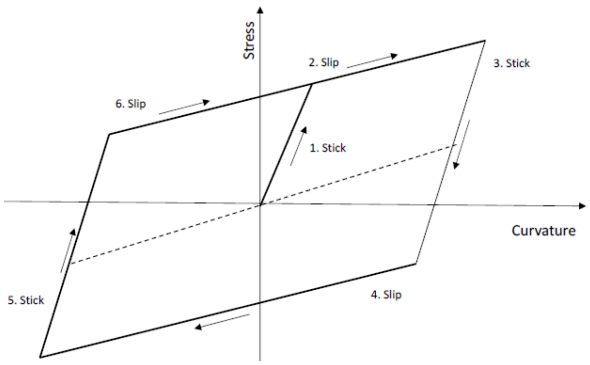

(b) Hysteresis curve for nonlinear bending stiffness explained in terms of stick-slip behaviour [10]

Figure 3.9: Nonlinear bending stiffness

In Figure 3.9a the bending stiffness profile of a typical inter-array cable is presented as modelled in OrcaFlex. It shows that bending stiffness follows a so called hysteresis curve. This hysteresis curve

is illustrated in more detail in Figure 3.9b, in which stick-slip behaviour is addressed in more detail. Stick-slip behaviour occurs between multiple subsea power cable layers. When subjecting the subsea power cable to stresses, for very low curvatures the system is in stick (1). When the curvature increases, eventually a certain friction is overcome causing the slip regime to take over (2). The system is in slip until the curvature (in this case bending direction) is reversed, when the full stick takes over again (3). Following the hysteresis curve, stick-and slip will interchange continuously with each other.

3.3.2. Cable integrity limits

Below a list of cable integrity limits is provided. These cable integrity limits results from the aforementioned mechanical properties. Cable manufactures determine these limits based on inhouse knowledge, experience and tests. In order to preserve a subsea power cables integrity, these limits need to be preserved at all times, hence both during transport, storage and installation. If a limit is breached, the cable either needs to be repaired or in extreme cases an entire new cable needs to be installed.

- **Maximum tensile load**
  The maximum allowable tensile load of the subsea power cable [kN]

- **Maximum compressing load**
  The maximum allowable compression of the subsea power cable [kN]

- **Maximum squeeze load**
  The maximum allowable squeeze load of the subsea power cable [kN/m]

- **Minimum bending radius**
  The minimum allowable bending radius (MBR) of the subsea power cable [m]

- **Side wall pressure**
  The maximum allowable side wall pressure (SWP) of the subsea power cable [kN/m]

- **Minimum bottom tension**
  The minimum bottom tension (BT) at the sea bed [kN] (is actually a negative compression)

- **Maximum top tension**
  The maximum top tension (TT) at the chute [kN]

3.4. Cable laying vessel and onboard installation equipment

In order to install subsea power cables offshore contractors make use of CLV's. These vessels are designed specifically for offshore cable operations. However, since each contractor has its own vessels and because there are multiple installation methods and deck designs there are various vessel options available. A typical CLV layout is illustrated in Figure 3.10, which is based on the 'Living Stone' (more detailed information is enclosed in Appendix B section B.1). The seven main components have been indicated; chute, A-frame, quadrant, tensioner, cable highway, cable storage and winch. Each component is briefly described below.

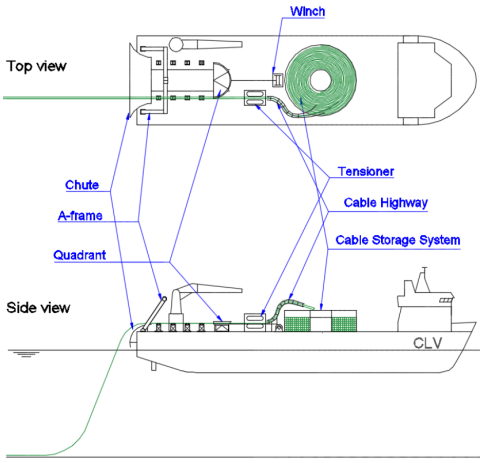

(a) Typical CLV layout [49]

(b) Living Stone CLV on-board equipment (photo taken from DEME archive)

Figure 3.10: Typical CLV layout and photograph of Living Stone CLV

- **Chute**
  The chute is a curved rail where the power cable leaves the vessel. At this point, it is important that both the MBR and SWP of the vessel are not compromised. Besides, it is important to keenly monitor the departure angle since the cable is not supported anymore after having left the chute. If this departure angle is not monitored keenly the cable might start to bend which can damage the cable.

- **A-frame**
  Depending on the type of operation a crane or an A-frame might be required. This is in case of quadrant handling or overboarding of some sort, e.g. cable protection system (CPS) overboarding and clump overboarding. Such overboarding activities need to be carried out using either a crane or an a-frame. Each has its own advantages and disadvantages, although a crane is more versatile. A proper choice can only be made when the exact functional requirements are known.

- **Quadrant**
  The quadrant is a half circle shaped device on guiding rails that is used to safely lower the power cable towards the seabed. By using a quadrant the risk of compromising the MBR is limited during both first as second end pull-in operations. The power cable is guided by the quadrant prior to the pull in operation, and during the operation the quadrant slides over the rails towards the chute. Further on in the process the quadrant is lifted overboard and lowered to the seabed. At the seabed the the quadrant is tripped over so the power cable can safely be deployed. At last the quadrant is lifted to the deck again using a crane of a-frame.
  It is important to keep in mind that quadrant overboarding and tripping are designed for one-way traffic, hence away from or towards the vessel. Furthermore, the quadrant needs to be monitored keenly as the quadrant is lifted and tilted while carrying the cable.

- **Tensioner**
  In order to guide the power cable safely to the seabed, the cable needs to be controlled. This is done by means of a tensioner. The tensioner applies the desired tension value on the cable with the use of friction. The tensioner needs to measure and log at least calibrated tension, paid out distance and speed values. In order to guarantee contingency, a second tensioner could be helpful as back-up.
  There is a close relation between tension in the cable at chute level and the touchdown point (TDP) at the seabed, thus by changing the tension in the cable the TDP can be adjusted. Moreover, installing the tensioner as close to the chute as possible has preference. In this manner the tension on deck can be kept as low as possible.

- **Cable highway**
  To get the power cable from storage towards the tensioner, the cable is guided through the cable

highway. This highway ensures the cables integrity (especially bending radius) is secured during spooling and unspooling activities. The highway needs to work in both ways hence the cable needs to be transported safely during pay-out and pickup. It is important not to push the cable, but only guide the cable by pulling as especially in turns the cable might endure damage. The cable highway is often incorporated with the tensioner, and can either be controlled separately or together. In Figure 3.11 a photo of the cable highway onboard the Living Stone CLV is showed as an illustration.

Figure 3.11: Onboard equipment Living Stone CLV (photo taken from DEME archive)

- **Cable storage**
  Subsea power cable laying routes may reach up to hundreds of kilometers, hence a lot of cable is required. In order to store the cable, several storage systems are available such as a turntable, a carousel, a cable reel and a static tank. Each storage possibility has its own advantages and disadvantages.
  - Turntable → The cable is spooled over a vertical rotating storage basket, meaning each layer is spooled on top of the previous layer
  - Carousel → The cable is spooled over a vertical core layer working from inside outwards. A vertical level winder assures that the cable is spooled evenly spread over the carousel. By means of back tension the cable is prevented from sliding of the carousel.
  - Reel → The cable is spooled using a reel drive system in combination with a horizontal level winder. Thus, in case of multiple short power cables installation each separate cable is stored on its own reel hence can quickly and efficiently be installed.
  - Static tank → The cable is spooled in a vertical fixed basket. In the storage tank the cable is rotated using a turning loading arm and wounded around its own axis. For this method, a large MBR is required and the cable must be able to cope with torsion during storage.
- **Winch**
  To help the power cable move from and towards the storage facility a winch is required. It is important that this winch works fluently whilst both the loading and offloading of the cable. Usually, the winch in incorporated with the cable storage facility and not installed separately.

3.5. Offshore cable operations

Offshore power cable installation projects have a relatively short execution phase but on the contrary a rather long preparation phase. Initial planning can start up to three years prior to the cable laying leaving enough time to prepare the entire operation from legal licenses, marine survey studies and agreements to the detailed installation process [6, 49, 54].

In order to install the entire subsea power cable multiple offshore operations need to be performed and combined. Each technique has its own challenges, specific requirements and needs. To start, the first tip of the cable needs to be installed by performing a 1^{st} end pull-in operation. When the first end of the cable is installed the total required cable length can be installed. This is usually done by means of normal cable laying operations, either S-lay or J-lay. The main difference in that during S lay the cable highway is positioned horizontally, whilst for J-lay the cable highway is positioned vertically. Both S-lay and J-lay have their own advantages and disadvantages. Even though the top tension during S-lay operations is higher, the production rate remains higher as well [23]. Besides, most subsea power cables are not installed in very deep water. Due to the vertical cable highway J-lay is preferable in deep water conditions, since top tension is lower [4]. After the cable has covered the appropriate length, the second cable end can be installed by means of a 2^{nd} end pull-in procedure.

3.5.1. Normal lay operations

Figure 3.12 gives a proper overview of normal subsea power cable laying operations. In this figure, an operating CLV with onboard equipment is shown and the entire process of how a subsea power cable is installed is presented as well (in this case an S-lay operation is shown).

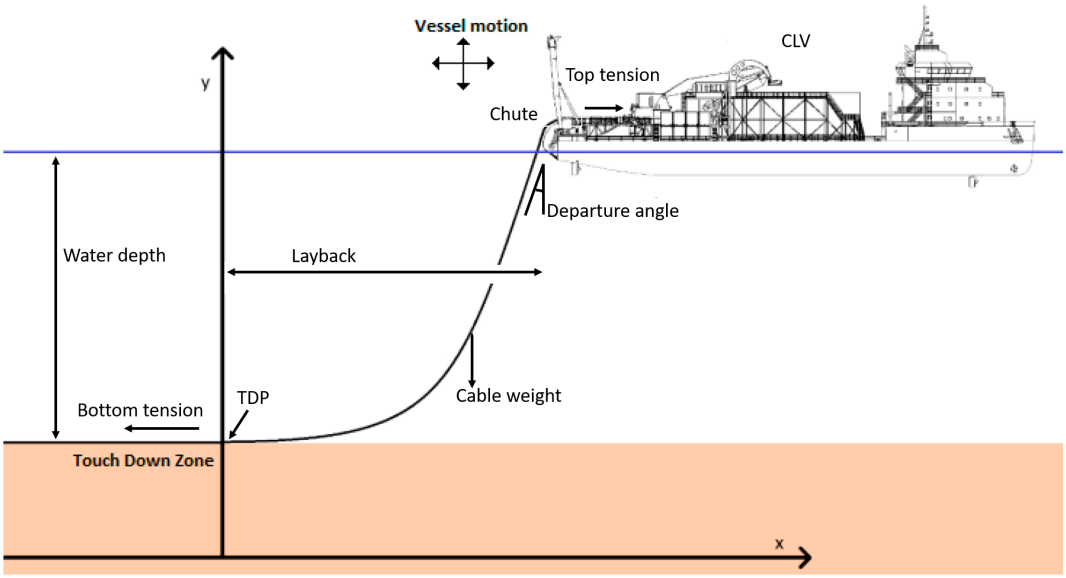

Figure 3.12: Typical S-Lay configuration [53] (adjusted)

In Figure 3.12 a subsea power cable is hanging in the water on a certain water depth. Due to a certain top tension, a certain bottom tension and the cable's own weight the curvature of the cable is formed. This is a common shape of subsea power cables, and often referred to as cable catenary. If top tension is increased, this means that the layback increases as well and curvature in the cable decreases. Hence as a result the bottom tension also increases. Figure 3.12 gives a clear overview of how these parameters influence each other.

Essentially, bottom tension is a negative tension since the force is in the opposite direction as top tension. Therefore, bottom tension limits are negative, and top tension limits are positive.

3.5.2. Cable catenary

In Equation 3.1 the formula for a cable catenary is given, which is based on a hyperbolic cosine function.

$$y = a \cosh \frac{x}{a} \tag{3.1}$$

In which a is a dimensionless catenary parameter calculated by means of Equation 3.2.

$$a = \frac{F_0}{m * g} \tag{3.2}$$

The components in the equations above are briefly explained below.

- a Represents a dimensionless catenary parameter [-]
- x Represents the total cable catenary length [m]
- F_0 Represents static bottom tension [kN]
- m Represents the weight of the submerged subsea power cable in [kg/m]
- g Represents the gravitational acceleration constant [m/s^2] ($9.81 m/s^2$)

Cable catenary shapes, and how these are precisely modelled, are further explained in section 4.4.

3.5.3. Survival mode

Prior to any type of offshore cable operation an extensive workability study is performed, consisting of an operational limit study and weather windows. This means that before any kind of operation a weather assessment is conducted. If the weather is too harsh, the cable installation process is halted. If the operation is halted, the best scenario would be if the CLV can remain on its position and does not have to abandon site since this would mean the cable has to be cut off in order for the CLV to sail away. If the CLV has to remain on its position this is called survival mode. This done by dynamic positioning (DP) systems, which uses thrusters to keep the vessel on its place. The vessel is leaded in the most optimal heading angle, based on the $H_s - T_p$ combination, and the crew can wait out the storm. After a while when the harsh weather is over, the operation can start again. However, remaining on site does mean the cable will continuously be exposed to serious hydrodynamic loading.

3.5.4. Cable integrity limits during normal lay operations

Regarding normal subsea power cable lay operations, in particular the chute, tensioner and cable highway are of interests. This is because a quadrant, A-frame, storage unit and winch are merely tools to assist cable operations, and during installation critical forces occur where the cable leaves the CLV (chute) and the installation process is guided by the tensioner which holds a constant tension in the cable in the cable highway.

During cable installation the operating CLV is sailing forwards, hence the cable is loaded from the carousel with the same speed as the CLV. During this procedure, especially the tensioner plays an important role. In the tensioner, a desired tension is applied on the cable which determines the entire normal lay configuration as the subsea power cable follows a catenary shape.

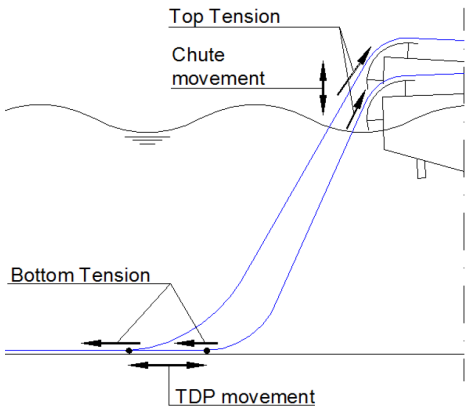

Figure 3.13: Cable laying vessel, chute movement [49]

During normal cable lay operations, the tensioner holds the cable under a constant tension, even though the CLV is moving due to hydrodynamic wave loading. When the chute is moving up- and downwards the top tension, TDP and bottom tension change as illustrated in Figure 3.13. Hence, the chute movement leads to a different cable catenary (normal lay configuration).

Essentially, top tension and bottom tension determine the cable layback behind the vessel, and these two are related to each other. Both maximum allowable top tension (TT) and minimum allowable bottom tension (BT) are indicates as cable integrity criteria during normal cable installation. Since BT is in fact a negative tension (as the direction of the force is opposite to the TT), the BT limit is regarded as a minimum allowable BT. During an upward chute movement, the top tension of the cable increases and the tensioner has to adapt adequately. The desired top tension limit is hence determined by three tension limits, maximum SWP, maximum squeeze load and maximum top tension. Since SWP and

maximum squeeze load are accounted for within the top tension limit, the top tension limit covers all these three tension limits.

Besides upward chute movement, the chute can move downwards as well. When the chute is moving downwards, the cable is compressed to the seabed (at the TDP) causing the cable to bend. Therefore, the minimum bending radius (MBR) of subsea power cables is a indicated as a third cable integrity criteria.

3.6. Conclusions

Taking all mechanical cable properties and failure mechanisms into account, for the normal cable lay operations eventually all cable properties and cable limits are covered by three main cable integrity criteria. These criteria have been listed below. In order to preserve the subsea power cable's integrity, none of the three limits (as provided by cable manufactures) must be exceeded. Note that these limits are independent of each other, hence all three criteria need to be monitored continuously and these do not weaken or strengthen each other.

- **Minimum bending radius [m]**
  The subsea power cable's MBR needs to be closely monitored over the entire cable length from chute to TPD at the seabed. When the chute moves downwards, the cable is compressed to the seabed (at TDP), end therefore the cable starts to bend. This bend can occur over the entire cable length. If the radius gets too small during cable lay operations and the MBR limit is breached, cable layers might shear and water could penetrate and thus damage the cable from the inside. Since there are a lot of differences between subsea power cables regarding specific parameters and characteristics, MBR is especially important regarding inter-array cables as these are commonly more flexible than export cables. Hence, bending stiffness has a lot of influence on MBR as failure criteria.

- **Minimum bottom tension [kN]**
  Bottom tension occurs at the TDP. Since the TDP is the first contact point during cable laying operations between a subsea power cable and the seabed, minimum bottom tension is actually a negative compression but often measured and modelled as a tension. The bottom tension limit is thus prescribed as a negative tension, which may not be exceeded.

- **Maximum top tension [kN**]
  At the chute, where a subsea power cable leaves the CLV, there is a certain top tension. The chute is the last contact point between a CLV and the subsea power cable. This means that at the chute the tension is largest. This tension is referred to as top tension. A low top tension is not harmful, however if the top tension limit is overrun, then the cable might get damaged.

4

Offshore environment and OrcaFlex modelling

This chapter contains information regarding the offshore environment. Besides, Orcina OrcaFlex subsea power cable modelling software is introduced and explained in more detail. At last the specific OrcaFlex model set up within this thesis is described.

4.1. Offshore environment

In the offshore industry structures and equipment have to cope with harsh conditions on a daily basis. All loads these offshore structures have to withstand are environmental. In general there are four types of environmental loading [55].

- **Atmospheric loading**
  Wind
- **Oceanic loading**
  Waves, current & ice
- **Seafloor loading**
  Soil settlement, earthquakes & mudslides
- **Climate loading**
  Chemical & thermal

From all loads listed above especially wave loading plays an important role during cable laying since the dynamical contribution is substantially higher than currents. Wind loading is not that interesting w.r.t cable laying operations, although wind does play an important role in wave generation, wave propagation and the direction from waved originate. Regarding ice loads, researchers have been investigating the idea of major OWF's in the arctic region but at the moment these large OWF's only exist on paper. Hence the vast majority of WTG's is not located near icy conditions. The seabed, however, does have an important role within cable laying operations as subsea power cables are usually trenched or covered with rocks to protect them and guarantee integrity over their lifetime. At last structures have to endure climate loading as well. The topic "climate change" itself has been a frequently appeared subject this century, hence it is evident offshore structures need to cope with extreme temperatures and the changing chemical composition of sea- and rainwater. [24, 55]

4.1.1. Wave types

There are various types of waves. The main distinction between these wave types is based on specific wave frequency and period of vertical motions occurring at the ocean surface, or the specific wave length [24, 39]. A time scale showing all kind of wave types is enclosed in Figure 4.1 below.

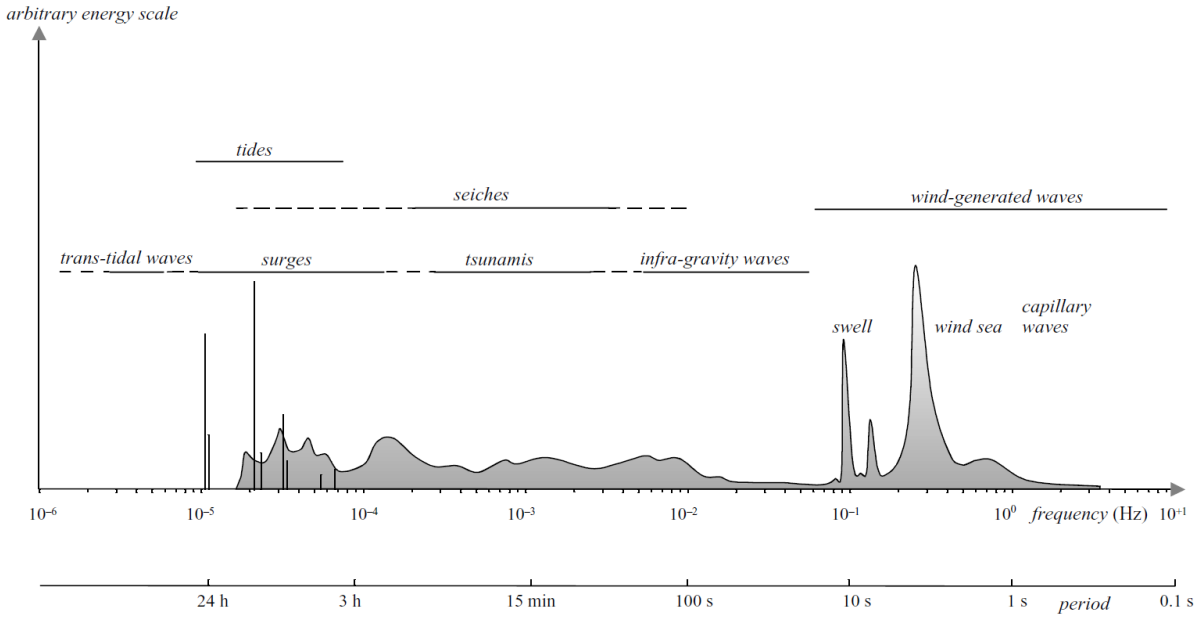

Figure 4.1: Time scale differentiating between wave types [24]

To predict which type of waves will appear in the near future, weather forecasts give an outcome. Out of all wave types illustrated in Figure 4.1, especially swell waves and wind sea waves are of interest as these have the most influences on vessel motions (due to their corresponding wave periods).

Swell waves originate from a further location than sea waves. Therefore, swell is more developed than sea waves which also explains why the swell peak is narrower than the younger wind sea waves.

4.1.2. Wave generation

Waves are generated by storms and develop due to wind blowing over the sea surface. This process is illustrated in Figure 4.2a below. The longer the distance the wind can blow (fetch in [m]), the more energy is transferred from the wind into the waves. Hence, the longer the fetch, the more developed the wave field is which means more and higher waves.

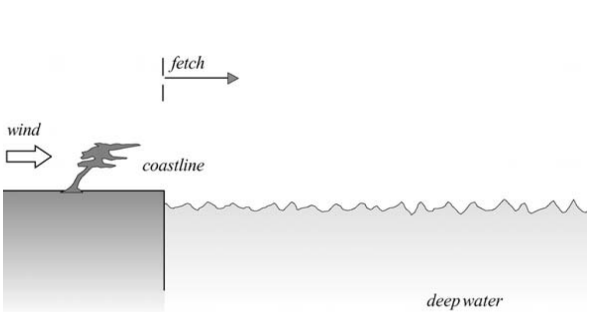

(a) The ideal situation of a constant wind blowing over deep water, perpendicularly off a straight and infinitely long coastline

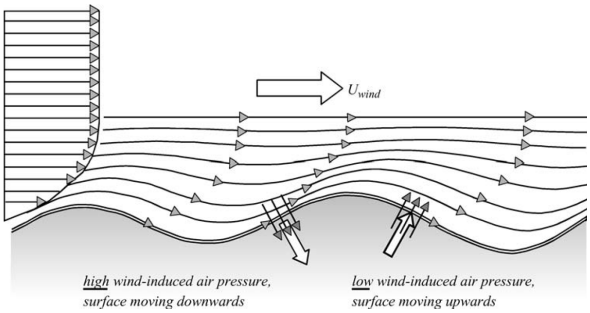

(b) Energy transfer from wind to waves

Figure 4.2: Fetch and wind-wave energy transfer [24]

The process of energy transfer between wind and waves has already been mentioned. This precise transformation is illustrated in Figure 4.2b above. This figure shows a propagating harmonic wave and the wave-induced wave-pressure variation is nicely indicated by means of streamlines.

From Figure 4.2 it is clear that the wind velocity profile (U_{wind} in [m/s]) becomes constant at a certain height above the water level. Just above the water level the wave velocity is increasing following a power law, and especially during this stage energy transfer takes place from wind to waves. At the back of the waves, wind-induced air pressure moves the water surface downwards, while on the front of the waves a low wind-induced air pressure moves the water surface upwards. Due to this downward

and upward movements of the water surface, energy is transferred from wind to waves. Besides, this figure makes clear that the longer the fetch, the longer the wind is able to transfer energy into the waves, hence develop the wave field.

4.1.3. Irregular wave field

Obviously, actual sea waves are never regular since in reality perfect sinusoidal waves do not exist. On the contrary, sea waves are in fact a superposition of multiple single sinusoidal waves. As an example for this superposition let's consider a single point somewhere in the ocean, a so called prediction point (see Figure 4.3. From all different directions, different wave contributions come together in this prediction point. Moreover, all these independent harmonic waves have different periods, amplitudes and phases as well. An illustration of the actual sea surface is provided on the left hand side of Figure 4.3.

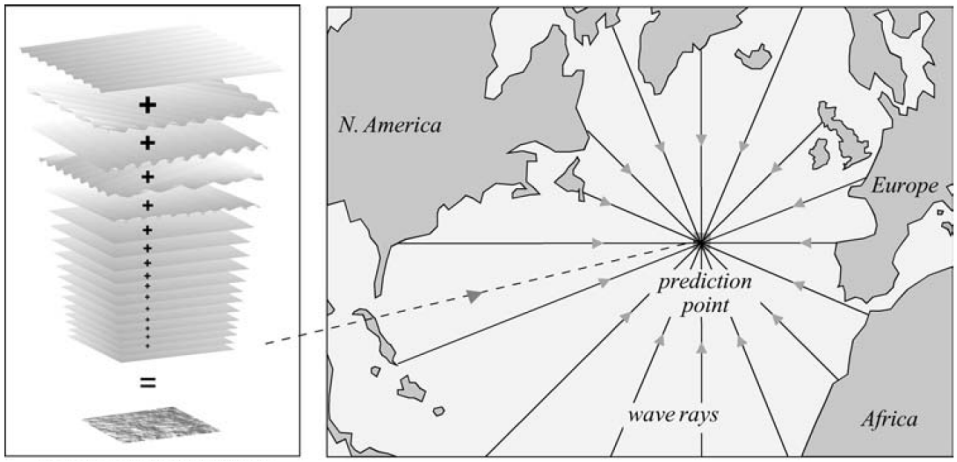

Figure 4.3: Wave superposition [24]

In Appendix B section B.2 wave theory, and applied linear wave statistics are explained in more detail.

4.1.4. Wave spectrum

In 1955 Pierson [28] studied wave spectra, and came with a spectrum that represents a fully developed wave field, the Pierson-Moskowitz (PM) spectrum. In 1968 and 1989 extensive studies where performed based on the PM spectrum in order to create a spectrum that would represent a young developing wave field [35, 36]. Young sea states behave more like groups, hence JONSWAP spectra are relatively narrow compared to PM spectra [24].

Nowadays, the most widely used wave spectrum is a JONSWAP spectrum. This is because in reality, wave fields are almost never fully developed, thus JONSWAP is a better fit as this represents a young sea state. In fact, the formula for a JONSWAP spectrum is very identical to the formula of a PM spectrum. The only difference is that for a JONSWAP spectrum an extra term γ^b is added to the formula. The formula for a JONSWAP formula is presented in Equation 4.1 [24, 26, 36].

$$S(f) = \frac{\alpha g^2}{16\pi^4} f^{-5} \exp\left[-\frac{5}{4}\left(\frac{f}{f_\mathrm{m}}\right)^{-4}\right]\gamma^b \tag{4.1}$$

With

$$b = \exp\left[-\frac{1}{2\sigma^2}\left(\frac{f}{f_\mathrm{m}} - 1\right)^2\right] \tag{4.2}$$

And

$$\sigma = \begin{cases} \sigma_1 & \text{for } f \leq f_\mathrm{m} \\ \sigma_2 & \text{for } f > f_\mathrm{m} \end{cases} \tag{4.3}$$

All components in the equations above are briefly explained below.

- $S(f)$ Represents the total wave spectrum
- α Represents a dimensionless shape factor, generally taken as 0.0081 [38]
- g Represents the gravitational constant ($9.81 m/s^2$)
- f Represents the wave frequency [Hz]
- f_m Represents the wave peak frequency [Hz], and is calculated as $f_m = \frac{2\pi}{T_p}$, in which T_p represents the wave peak period [s]
- σ Represents a dimensionless peak-width parameter which is generally taken as $\sigma_1 = 0.07$ and $\sigma_2 = 0.09$ [3]
- γ Represents peak enhancement factor, which can be calculated based on DNV-GL codes. Alternatively, the dimensionless peak-enhancement factor can be taken as 3.3 [3]

Peak enhancement factor

Gamma (γ) is a dimensionless peak-enhancement factor, which is generally taken as 3.3 [3]. However, the DNV-GL codes also prescribe three equations based on different criteria to calculate a more specific γ factor. These three equations are listed below [13]. In these equations, T_p represents a waves peak period [s] and H_s represents significant wave height [m].

$$For \quad \frac{T_p}{\sqrt{H_s}} \leq 3.6 \qquad \gamma = 5.0 \tag{4.4}$$

$$For \quad 3.6 \leq \frac{T_p}{\sqrt{H_s}} \leq 5.0 \qquad \gamma = \exp\left(5.75 - 1.15\frac{T_p}{\sqrt{H_s}}\right) \tag{4.5}$$

$$For \quad 5.0 \leq \frac{T_p}{\sqrt{H_s}} \qquad \gamma = 1.0 \tag{4.6}$$

Narrow and wide spectra

As aforementioned, waves can be regular and irregular. However, offshore all wave fields are irregular due to superposition of multiple regular waves. This difference between regular and irregular waves can also clearly be visualized by means of wave spectra width. In Figure 4.4 below three different wave fields are shown with their accompanying spectrum.

Obviously, an irregular wave field has more spread in wave frequencies, hence the spectrum will be quite broad. Moreover, harmonic waves all have the same frequency which means the spectrum can be visualised using one single arrow (referred to as delta-function). A combination between a full irregular wave field and purely harmonic waves can be thought of as a narrow spectrum. This means there is a modulated harmonic wave patters, covering multiple independent irregular waves. Hence wave groups can be identified.

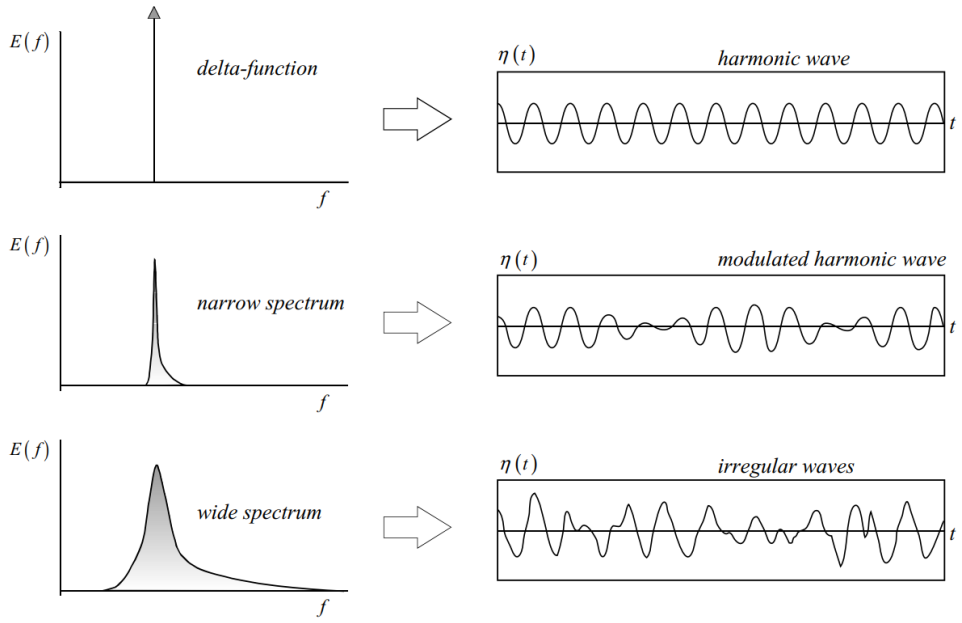

Figure 4.4: Regular and irregular wave fields and accompanying wave spectra [24]

4.1.5. Wave energy

Based on wave spectra, wave energy can be deduced rather straightforward as wave energy is expressed in terms of variance ($\overline{\eta^2}$) of the surface elevation [24]. Wave energy regarding harmonic waves is equal to $E_{\text{total}} = \rho_s g \overline{\eta^2}$. This means that the total energy easily follows by summing over all individual components, hence total wave energy equals the area of the wave spectrum as shown in Equation 4.7.

$$E_{energy}(f) = \rho g E_{variance}(f) \tag{4.7}$$

All components in Equation 4.7 above are briefly explained below.

- E_{energy} Represents the total wave energy [m^2/Hz]
- ρ_s Represents the density of sea water [kg/m^3], generally taken as $1,025 kg/m^3$
- g Represents the gravitational constant [m/s^2], generally taken as $9.81 m/s^2$
- $E_{variance}$ Represents variance density [m^2/Hz]

4.2. Motions

Offshore, environmental forces have major influences on vessel motions. These vessel motions, on their turn, have an an influence on cable motions at the chute (subsea power cable leaves the vessel at the chute). A vessel can be schematized as a 6DOF system [1, 40, 45]. At First, there are three motions sliding on the x-, y- and z-axis, named surge sway and heave respectively. Secondly, there are three additional motions which are rotations around the x-, y- and z-axis, named roll, pitch and yaw respectively.

Thus, overall there are three translations and three rotations. All motions are illustrated in Figure 4.5 below, and briefly explained in Table 4.1. Regarding all 6DOF, per DOF three more specific motions can be determined; the motion itself, motion velocity and motion acceleration [40]. Hence, overall 18 different motions can be distinguished.

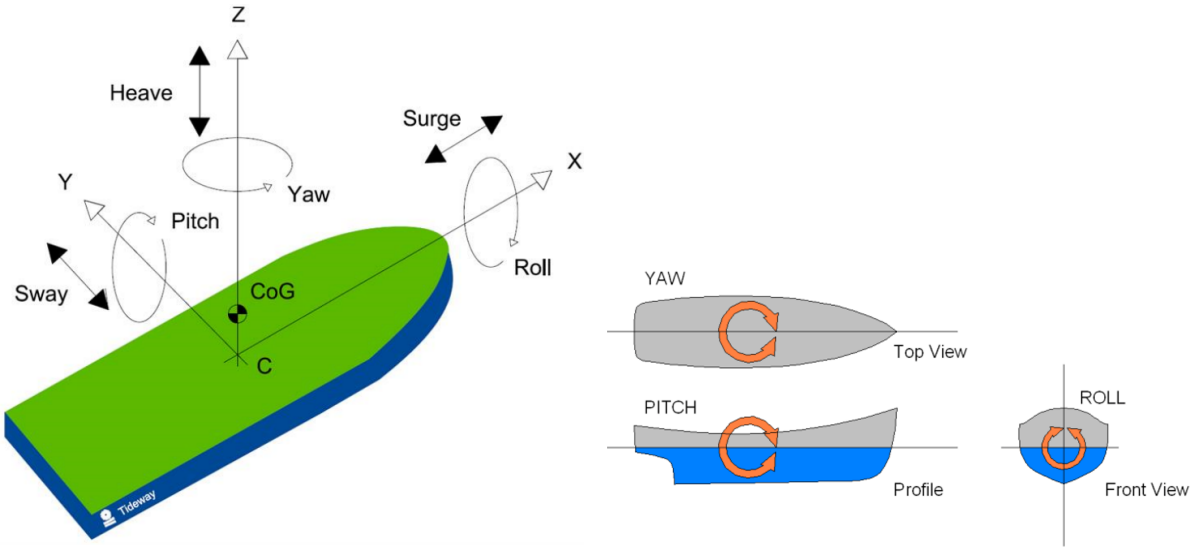

(a) 6 DOF vessel system

(b) Rotations

Figure 4.5: Vessel motions from COG [1, 49]

DOF	Name	Sign	DOF explanation	
DOF 1	Surge	ζ_1	Positive forward	Translation along x-axis
DOF 2	Sway	ζ_2	Positive to port	Translation along y-axis
DOF 3	Heave	ζ_3	Positive up	Translation along z-axis
DOF 4	Roll	ζ_4	Positive starboard down	Rotation around x-axis
DOF 5	Pitch	ζ_5	Positive bow down	Rotation around y-axis
DOF 6	Yaw	ζ_6	Positive bow to port	Rotation around z-axis

Table 4.1: 6 DOF right-handed vessel system [31]

An important note, however, is that all these 6DOF motions are calculated in the vessel's COG. This research, however, focuses on occurring motions at the chute. Therefore, a new convention for the chute motions is introduced to prevent confusion of terms. These local chute motions are further explained in the next section.

4.2.1. Local chute motions

As stated above, a new coordinate system and descriptions are required for chute motions to prevent confusion with the general 6DOF's. When considering the chute, however, only translations are interesting and rotations do not matter that much. This is because rotations in the COG, eventually result in translations of the chute. For example, if a vessel starts to pitch, this causes vertical motions at the chute. Moreover, rotations at the chute will actually not differ from rotations at the COG, since the entire vessel is rotated. For translations, there is a clear difference between translations at the COG and the chute.

Therefore, three main chute motions are indicated and named local chute x, local chute y and local chute z. For these three chute motions, it still holds that per motion the motion itself, motion velocity and motion acceleration are distinguished. The corresponding sign conventions are presented in Figure 4.6. In this figure, an OrcaFlex screenshot is shown and the chute motions are illustrated by means of an orange coordinate system.

There is one more motion to consider which is the motion in the direction of cable departure from the chute. This motion is visualized in Figure 4.7 below (within this thesis, these motions are referred to as chute cable motions). These chute cable motions can be constructed by combining chute x motions and chute z motions, by means of applying Pythagoras theorem and creating two right angled triangles (90^o). By means of these triangles, the contribution of both chute x motions and chute z motions can be rewritten towards the motion in cable departure direction. Obviously, chute cable motions are actually

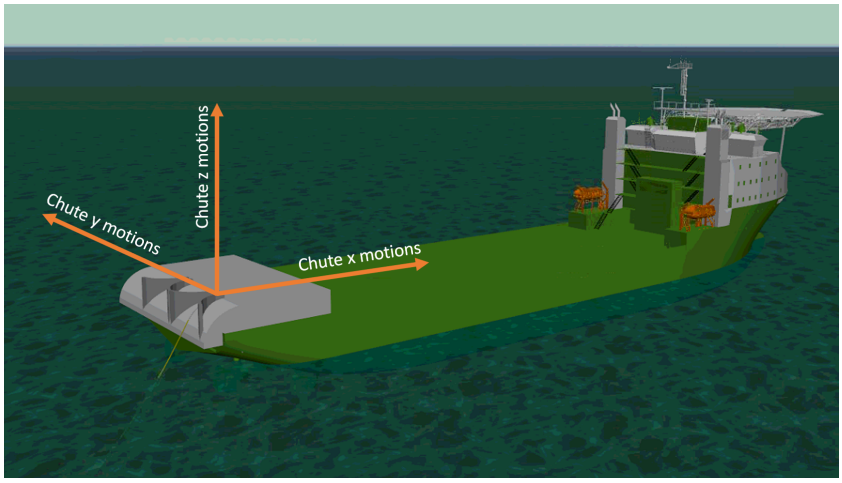

Figure 4.6: Local chute motions (adjusted screenshot taken from OrcaFlex)

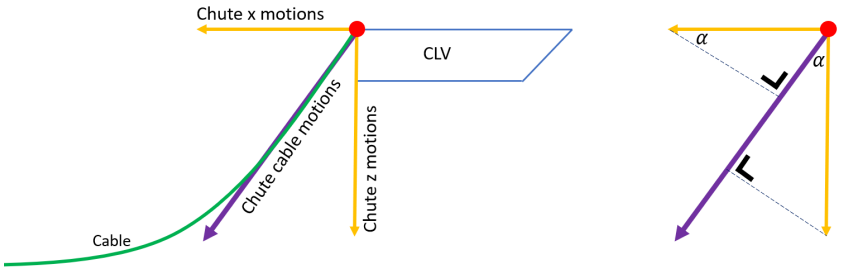

Figure 4.7: Illustration of motions in cable departure direction (CLV sideview)

a 3-dimensional appearance. However, during this thesis it was found that the contributions of chute y motions is so little that these are negligible.

Subsequently, in total 12 interesting motions at the chute have been defined, as presented in Table 4.2 below.

Motion	Motion explanation	
Motion 1	Chute x movement	m/m
Motion 2	Chute x velocity	m/s
Motion 3	Chute x acceleration	m/s^2
Motion 4	Chute y movement	m/m
Motion 5	Chute y velocity	m/s
Motion 6	Chute y acceleration	m/s^2
Motion 7	Chute z movement	m/m
Motion 8	Chute z velocity	m/s
Motion 9	Chute z acceleration	m/s^2
Motion 10	Chute cable movement	m/m
Motion 11	Chute cable velocity	m/s
Motion 12	Chute cable acceleration	m/s^2

Table 4.2: All local chute motions

4.2.2. Morison equation

To calculate hydrodynamic loading on structures, such as offshore platform legs and subsea power cables, the Morison equation is used. This equation originates from research performed in the 1950's. The original equation is presented below in Equation 4.8 [31, 48].

$$F = F_I + F_D = C_\mathrm{m} \Delta a_\mathrm{f} + \frac{1}{2} \rho C_\mathrm{d} A \left| v_\mathrm{f} \right| v_\mathrm{f} \tag{4.8}$$

The Morison equation is implemented within OrcaFlex. However, the original formula is slightly adjusted (as presented in Equation 4.9. The inertia term (F_I) is slightly reduced and regarding the drag component (F_D), the body-relative velocity is used instead of fluid velocity relative to the body. [31]

$$F = F_I + F_D = \underbrace{(C_{\mathrm{m}}\Delta a_{\mathrm{f}} - C_{\mathrm{a}}\Delta a_{\mathrm{b}})}_{\text{inertia}} + \underbrace{\frac{1}{2}\rho C_{\mathrm{d}} A\,|v_{\mathrm{r}}|\,v_{\mathrm{r}}}_{\text{drag}} \tag{4.9}$$

All components in Equation 4.8 and Equation 4.9 above are briefly explained below.

- F Represents the force applied on the structure per unit length (F_I=intertia component and F_D=drag component) [kN/m]
- C_m represents an inertial block coefficient [–]
- Δ Represents displaced fluid mass [kN]
- a_f Represents fluid acceleration relative to the earth [m/s^2]
- ρ Represents the density of the fluid (in this case sea water) [kg/m^3]
- C_d Represents a drag block coefficient [–]
- A Represents the area which endures drag [m^2]
- v_f Represents fluid velocity relative to the earth [m/s]
- C_a Represents an added mass coefficient regarding the body [–]
- a_b Represents the acceleration of the body relative to the earth [m/s^2]
- v_r Represents the fluid velocity relative to the body [m/s]

4.3. OrcaFlex software

Orcina OrcaFlex is software widely used for dynamic analyses of offshore marine systems. It is a leading software package developed especially developed for the offshore industry covering dynamic analysis of offshore marine systems such as cables, risers and anchor-systems.

In OrcaFlex simulations are performed based on so called simulation cases derived from a specific base case. The base case contains basic layout is, which consists of the vessel, specific subsea power cable and accompanying cable properties, water depth, and desired static bottom tension. Based on this base case model, simulation cases can be obtained. Each simulation case is derived from the base case, but to each individual simulation case a certain combination of H_s, T_p and α are assigned.

For this research, in the OrcaFlex base case model the subsea power cable was fixed to the chute. This represents reality as well, since onboard the CLV the cable is kept stationary due to the tensioner.

4.3.1. OrcaFlex sign conventions

The standard sign conventions implemented in OrcaFlex are illustrated below in Figure 4.8. Besides, in a 3D view, directions are defined by adding two angles; azimuth and declination.

- **Azimuth**
  Projection of x-axis on xy plane. Hence, the positive direction on the x-axis represents an azimuth of 0^o, and the positive direction on the y-axis represents an azimuth of 2700^o.
- **Declination**
  Declination represents the direction angle with the z-axis. Hence, in the positive direction on the z-axis the declination angle is 0^o, for any direction in the xy plane the declination angle is 90^o and in the negative direction on the z-axis the declination angle is 180^o.

Below, the azimuth projection is provided. In this figure a CLV is enclosed as well to give a clear overview. These conventions are the same for every analysis performed in OrcaFlex.

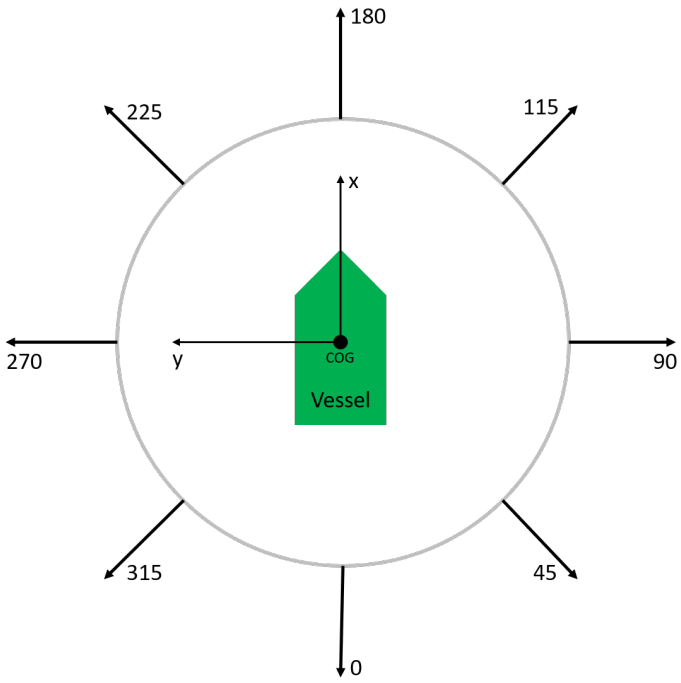

Figure 4.8: OrcaFlex directions and heading conventions, azimuth projection, all angles are in degrees [31] (adjusted)

As stated in the previous section, within this thesis not the COG is considered as coordinate system origin, but the chute location is as illustrated in Figure 4.6. The cable declination is also visualised in Figure 4.6.

How subsea power cable operations are precisely modelled in OrcaFlex is explained in the next few sections.

4.3.2. Wave trains

In order to model waves, so called 'wave trains' are set up. For each individual simulation case, based on the wave characteristic input parameters (H_s, T_p and $alpha$ combinations), the wave train is composed by combining regular wave components in order to create an irregular wave field to simulate a realistic offshore wave field environment.

In OrcaFlex, regular waves are specified in terms of wave height, wave period and incident wave direction relative to the vessel direction [31]. In order to create an irregular wave field, linear wave components are added on top of each other by means of linear superposition. Different phases for wave components can be obtained by changing the simulation origin time, wave origin time and specific seed number. All these components have different frequencies, which are generated by a frequency spectrum discretisation method. For this thesis, the equal energy method is applied, meaning certain wave components are chosen such that each component represents an equal amount of spectral energy (area under the spectrum).

Random wave trains are represented by a user-defined number of wave components, whose wave amplitudes and periods are selected by OrcaFlex itself. Below, in Figure 4.9 an example of a 1-directional (1D) JONSWAP spectrum is illustrated. This specific JONSWAP spectrum represents a 3-hour sea state based on a significant wave height of $4m$ and a wave peak period of $10s$. Besides, the modelled seed number is 12345 (OrcaFlex default). For each unique seed number, the resulting wave-train is always the same.

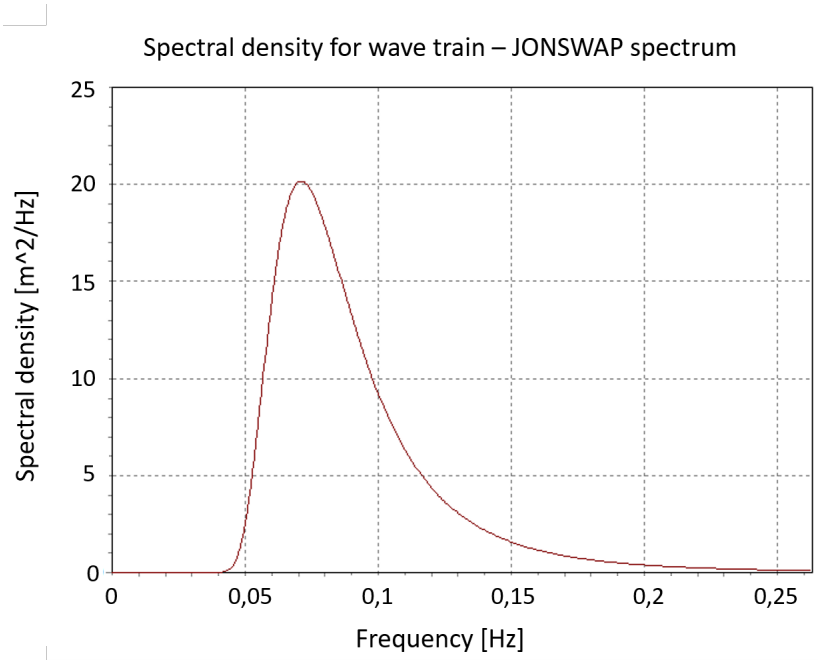

Figure 4.9: OrcaFlex JONSWAP example for seed number 12345 ($H_s = 4m$, $T_p = 10s$)

In order to verify whether OrcaFlex actually correctly generates an irregular wave field, there are two other interesting graphs to check; autocorrelation and overall sea elevation. These are presented in Figure 4.10a and Figure 4.10b respectively.

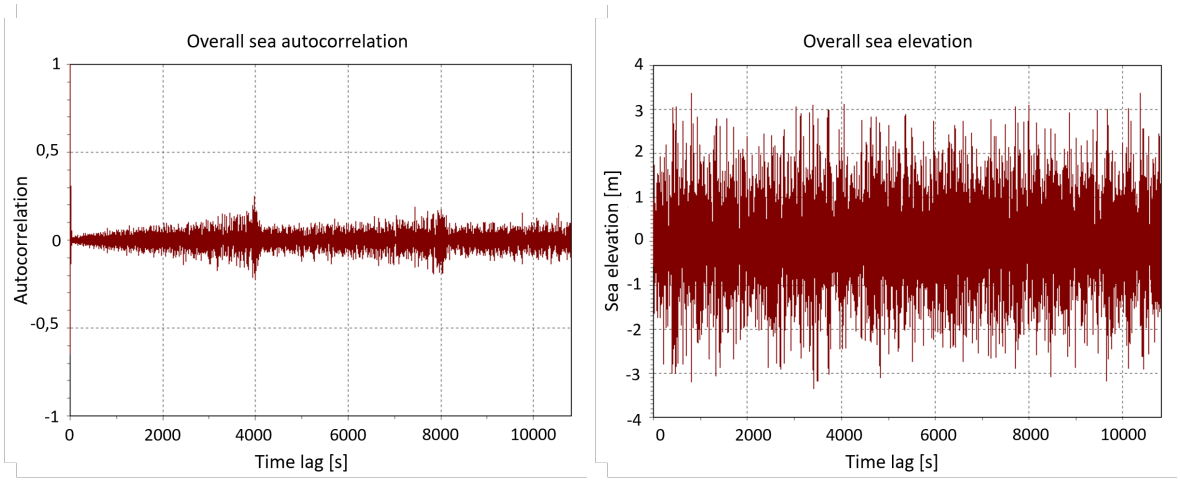

(a) Autocorrelation

(b) Overall sea elevation

Figure 4.10: Autocorrelation and overall sea elevation examples for seed number 12345 ($H_s = 4m$, $T_p = 10s$ & $\alpha = 180^o$)

The autocorrelation graphs is a manner to verify whether a certain discretisation represents reliable statistical modelling of a continuous spectrum process [31]. In the real world, this discretized continuous spectrum will decay to very small values after a short time. The decay is calculated using formula Equation 4.10 shown below.

$$\rho(\tau) = \frac{1}{\sigma^2}\mathrm{E}[\eta(t)\eta(t+\tau)] \tag{4.10}$$

All components in the equation above are briefly explained below.

- ρ Represents the autocorrelation factor [-]

- τ Represents a time lag [s]
- σ^2 Represents variance of sea surface elevation relative to still water level [m^2]
- E Represents an expectation operator [-]
- η Represents sea surface elevation [m]
- t Represents time [s]

For a single wave train, the calculation can be seen as an ergodic process (time averaged). This also holds when wave spreading is applied [31]. From Figure 4.10a it can be seen that indeed the autocorrelation factor decays to small numbers. This means that the generated wave field in OrcaFlex is indeed irregular and correct.

Another graph to verify whether the spectrum represents an irregular wave field, is the overall sea elevation graph. This graphs is presented in Figure 4.10b. It is clear that there is repetition of regular wave groups, hence the wave field is irregular.

When simulation other seed numbers in orcaFlex, it is always helpful to check the resulting JONSWAP, autocorrelation and sea elevation graphs to see whether the created wave field is indeed irregular and there are no visual peculiarities.

4.3.3. Simulation cases OrcaFlex model

A aforementioned, OrcaFlex cases are based upon one base case. In this base case, the normal lay configuration is modelled, hence the water depth is set at a certain value, and specific characteristics such as layback, static bottom tension etc. are implemented. Based on this base case model various wave loading possibilities are set-up, which are all possible H_s, T_p and α combinations (H_s and T_p possibilities are location specific, and $alpha$ is generally taken from 0^o to 330^o in steps of 30^o). By combining the base case with all wave loading scenarios, finally a lot of different simulation cases are set-up.

All these cases are modelled in the time-domain, which according to DNV-GL rules means in a period of 3-hours has to be modelled for each independent OrcaFlex simulation case. During this simulation, the vessel start to move due to the waves, hence the cable starts to move as well.as the cable is fixed to the chute of the vessel.

4.4. Subsea power cable modelling

As aforementioned, in water a subsea power cables can essentially be schematized as a catenary. However, in OrcaFlex cable modelling is somewhat more refined, and finite element modelling (FEM) is incorporated. Within FEM, the lumped mass model (LMM) is implemented as well.

4.4.1. FEM line model

In the end each type of line is a collection of properties such as bending stiffness, diameter and mass per unit length. Within OrcaFlex, subsea power cables are modelled as lines by a combination of the LMM and FEM. By applying LMM the entire line is split up in multiple segments and modelled as a series of lumps which are connected by springs. These springs are massless and represent a certain segment between two nodes. Each segment can have its own properties such as length, buoyancy, drag, mass etc. which have been lumped at the two ends of each segment at so called nodes. [31]

A typical line FEM model is presented in Figure 4.11a. There is a clear visual of the difference between the actual modelled pipe and the discretised OrcaFlex model. OrcaFlex software makes use FEM, and divides the line in a series of line segments. These segments are modelled using the lumped mass method as explained above. Essentially, each node is a straight rod representing both half-segments on both sides of the specific node. Of course, the two end nodes are somewhat different since these represent only one half-segment. The nodes are lumped, hence forces and moments are only applied at these points along the line model. Each segment of the model is a massless element and only axial and torsional properties are modelled. Bending properties are represented by the spring-damper on the ends of each segment, between the segment itself and the neighbouring node. This is presented in the structural model in Figure 4.11.

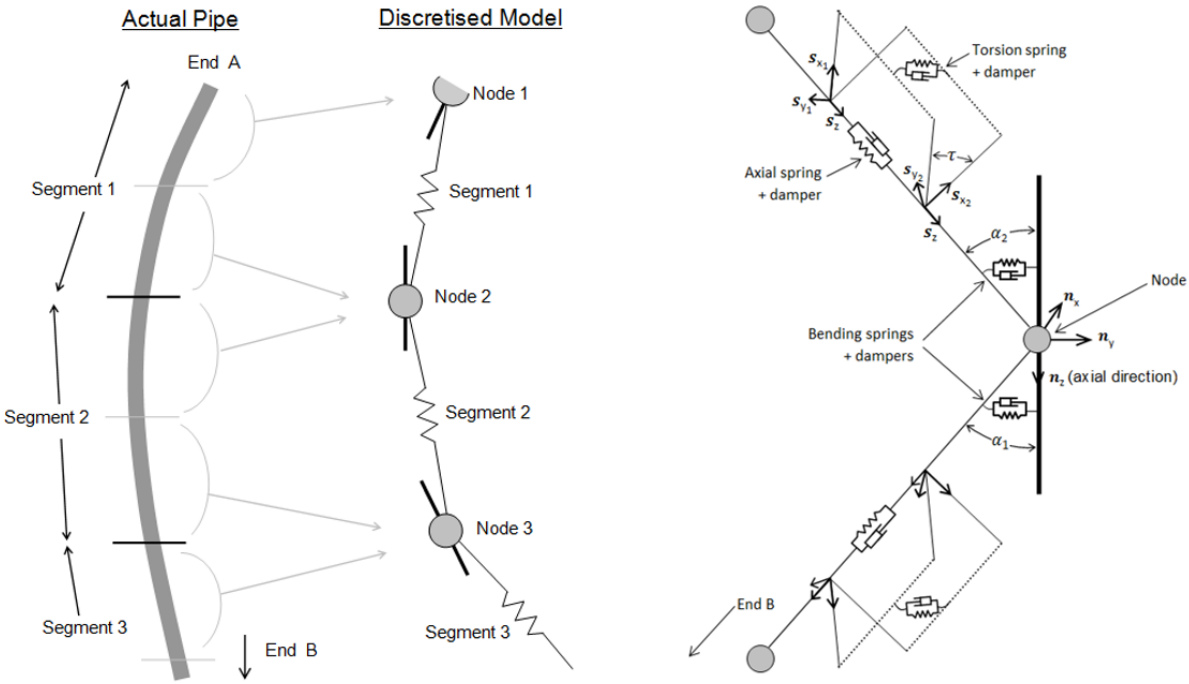

(a) OrcaFlex FEM line model

(b) Detailed OrcaFlex structural line model

Figure 4.11: Visualization OrcaFlex line models [31]

Taking a more detailed look at the structural model, as presented in Figure 4.11, it is clear that each individual segment is modelled as two rods connecting via three spring-damper systems; axial-, rotational- and torsional spring-damper systems. It is, however, possible to ignore torsion in the model. This means that both segment halves can twist freely and no line torsional properties accounted for.

The axial system is present in the middle of each segment. This system is used to translate axial stiffness and axial damping in the model of the specific line. This is done by applying equal (and opposite) forces on both segment end nodes.

The rotational system is present in the axial direction of a certain node (n_z) and the axial direction of a certain segment (s_z). This spring-damper system is used in order to model bending properties.

At last, the torsional system is present in the middle of each segment. This system is used to translate torsional properties in the model of the specific line. This is done by applying equal (and opposite) moments of torque on both segment end nodes.

4.4.2. LMM model

By applying FEM the line, in this case subsea power cable, is split into multiple segments and noded. This is were the LMM comes in. By applying the LMM, all forces are converted to these nodes. Starting with the equations of motions (EoM's), eventually the precise forces acting on each independent mode are determined. The precise LMM calculation is explained in more detail in Appendix B section B.4.

4.5. Multi system dynamics

Before subsea power cable operability calculations can start, the first step is to decide whether to work in a time- or frequency-domain, e.g. whether the EoM's will be solved by means of a spectrum or not [17, 24, 33]. Each manner has its own advantages and disadvantages, but the main difference that calculations based on a frequency-domain analysis are much faster [7].

4.5.1. Time-domain

As defined by DNV-GL [15], within time domain calculations, waves are characterised by a certain wave height and wave period. These somewhat deterministic waves are modelled using a specific constant time-step. For each specific time-step, and for each individual wave, the structural responses is analysed. Because each time-step is analysed separately, these type of calculations require a lot of computational power.

Since the EoM's are solved per time step, the time-domain method can be applied to every structural problem possible. Consequently, time-domain modelling is usually used to solve non-linear problems [17].

4.5.2. Frequency-domain

Within frequency-domain calculations on the other hand, waves are characterised by wave frequency [15]. The wave heights are not required, meaning that in the frequency-domain wave loads are complex and hence have both a real and an imaginary part. These real and imaginary parts combined express the precise load and a certain phase shift. This phase shift is with respect to the undisturbed incoming wave field. On the contrary to time-domain calculations, frequency-domain calculations do not demand much computational power, thus limited power resources will suffice or these calculations. Besides, calculations based on frequency domain are much faster as well and therefore frequency-domain is often preferred over time domain [7].

A disadvantage of frequency-domain calculations is that these are only applicable for linear problems (linear EoM's), hence not for nonlinear problems. Linear EoM's will lead to results that are easy to interpret. Moreover, multi-body problems are solved independently and the end results can easily be added in order to obtain final motion results. [17]

Before frequency-domain calculations can be performed, the data needs to be converted from the original format to the frequency domain [13, 33]. This is done by means of a transfer function [7, 13]. The Fourier transform is the most commonly applied and justified transfer function method to convert such data. Over the years, research has led to the Fast Fourier Transform (FFT), also known as the discrete Fourier Transform [44]. The FFT is further elucidated in Appendix B section B.5.

4.5.3. RAO's

The FFT is used throughout many different research fields [44]. However, regarding offshore engineering, and especially ship motions and waves, the implemented complex transfer function $H(\omega)$ is also referred to as an Response Amplitude Operator (RAO). [26, 40]

$$RAO(\omega) = \frac{\hat{F}(\omega)}{-\omega^2(m+a) + i\omega b + c} = \frac{\hat{z_a}}{\xi_a} \tag{4.11}$$

All components in the equation above are briefly explained below.

- $\hat{F}(\omega)$ Represents wave force [kN]
- ω Represents wave frequency [Hz]
- m Represents the mass matrix [kg]
- a Represents the added mass matrix [kg]
- b Represents the damping coefficient matrix [-]
- c Represents the restoring coefficients matrix [-]
- $\hat{z_a}$ Represents heave amplitude [m]
- ξ_a Represents the wave amplitude [m]

RAO's are commonly used in order to predict ship motions in different sea states. Therefore, also while performing operability calculations RAO's are essential as input information. Since RAO's are rather theoretic and complex formulas, in order to quantify the ROA's in-basin model tests are performed. Each company uses its own RAO's as these are vessel dependant, and they strive to model as close to reality as possible.

4.5.4. QTF's

Wave loads on a vessel can result from (and expressed in) first, second and even higher order terms. The first order, linear, terms usually have the highest contribution. However, second order terms can cause nonlinear effects that are smaller but can have significant contributions in specific cases.

In order to account for second order wave drift loads, quadratic transfer functions (QTF's) are required. Just like RAO's, QTF's are vessel dependant hence each company determines their own QTF's based on in house tests. More mathematical descriptions are enclosed in Appendix B section B.6.

4.5.5. Most probable maximum

In order to simulate a 'worst-case scenario', the highest possible occurring wave has to be composed. This particular wave is also known as the Most Probable Maximum (MPM), which is essentially the value of the maximum of a variable with the highest probability [13]. Since the method is based on probability studies a, both a time period and a probability-density function (PDF) are required. Typically, as stated by DNV-GL a 3-hour sea state is used which is Gaussian distributed [13]. Hence, the MPM is at the peak frequency of the PDF (generally this peak frequency coincides with the peak frequency of sea state).

As aforementioned, the MPM is based on a Gaussian PDF. Waves on the other hand are Rayleigh distributed [24, 26]. This means that for the Gaussian PDF a certain confidence interval (CI) is required, which highly influences the resulting MPM value. In the standard definition of the MPM a probability of exceedance of 63.2% is applied [13]. The formulas to calculate the MPM are presented below.

In Equation 4.12 the formula to determine the total MPM is presented. [13, 31, 58]

$$MPM = \mu + \sigma\sqrt{2\ln(n)} \tag{4.12}$$

The components in Equation 4.12 above are explained briefly below.

- μ Represents the mean wae height [m]
- σ Represents the wave height standard deviation [m]
- $\sqrt{2\ln(n)}$ Represents the MPM factor, in which n is the total number of events [#] (number of waves in the entire duration)

Within the total MPM calculation, a specific MPM factor can be distinguished ($\sqrt{2\ln(n)}$). Often, as a quick approximation, n is taken as 1000 events which results in a MPM factor of $\sqrt{2\ln(1000)} = 3.72$. However, there is also a more accurate formula to determine the MPM factor, which is provided in Equation 4.13.

$$MPM \quad factor = \sqrt{2\ln(n)} = \sqrt{2\ln\left(\frac{Duration}{T_z}\right)} \tag{4.13}$$

The components in Equation 4.13 above are explained briefly below.

- $Duration$ Represents the total duration in time [s], for 3-hours this is $10,800s$
- T_z Represents the zero crossing-up wave period [s] Appendix B section B.2

By applying Equation 4.13, the MPM factor is calculated by precisely determining the number of events in the total duration. As aforementioned, in this definition of the MPM a probability of exceedance (ϵ) of 63.2% is applied. This probability of exceedance, obviously, can be changed hence the MPM factor formula changes. This is illustrated by means of Equation 4.14.

$$MPM \quad factor = \sqrt{2\ln\frac{\left(\frac{Duration}{T_z}\right)}{\ln\frac{1}{1-\epsilon}}} \tag{4.14}$$

An important note is that the MPM factor represents the total sea elevation. Since it holds that wave height equals two times the wave amplitude ($H = 2 * a$)), it also holds that $3.72 = 2 * 1.86$. Hence, when applying the MPM factor for wave amplitudes, the MPM factor needs to be divided by two.

4.6. Final OrcaFlex model set up

Two base cases have been composed for this thesis, as presented in Figure 4.12. One base case is based on of a water depth of $30m$ (indicating shallow water) and one base of a water depth of $150m$ is created in order to investigate multiple cable catenary shapes. For both base cases, a static bottom tension of $5.00kN$ was persisted for continuity throughout catenary shapes.

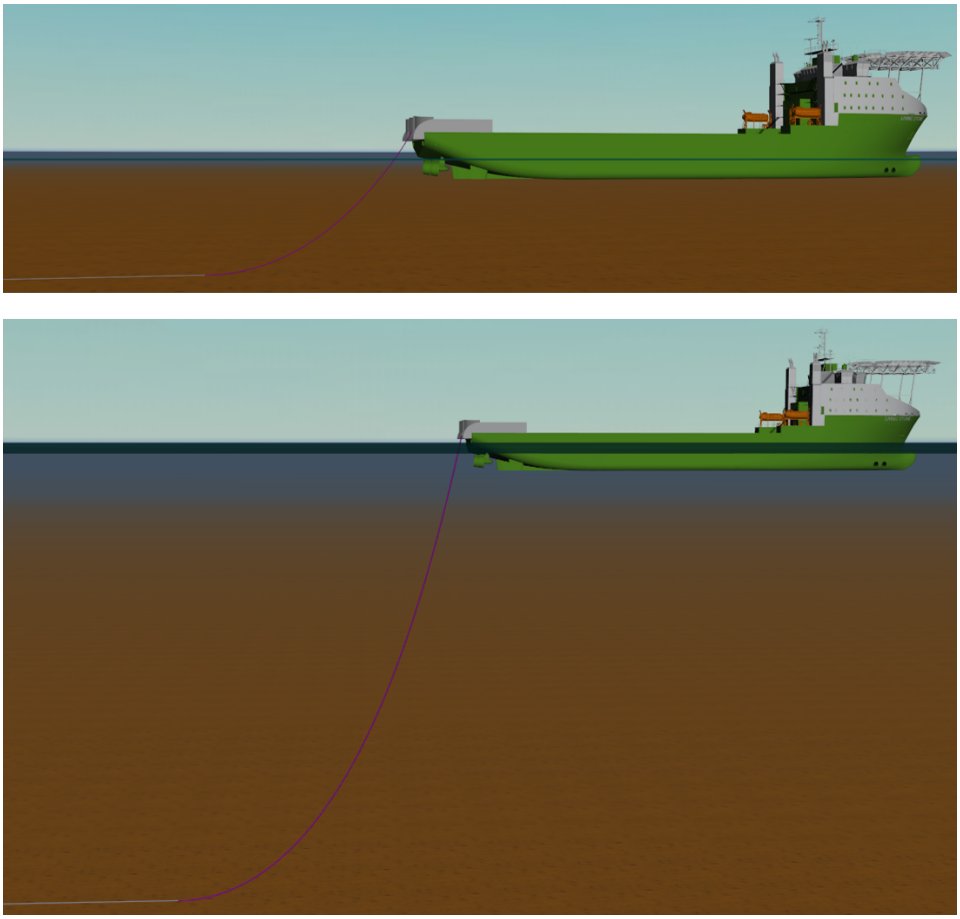

Figure 4.12: OrcaFlex base cases shallow (top) and deep water (bottom)

The simulated vessel is a CLV named the Living Stone, and its coorespinding RAO and QTF sets have been loaded into the model as well. By means of single $H_s - T_p$ combinations, a 1D JONSWAP is created hence the wave train was set up (based on default seed numer 12345 and equal energy discretisation). All environmental loading conditions are based on typical North Sea conditions, as further explained in section 5.4. Since the focus of the thesis is on extreme motions, the MPM factor is included as well. The MPM presented in Equation 4.13 is modelled, based on the total duration and zero crossing-up wave period.

For kinematics above water level, meaning predictions of both velocities and accelerations above the mean water level, a certain stretching needs to be applied. In this thesis, vertical stretching is applied by means of Equation 4.15.

$$E(z) = \frac{\cosh(k(d+z))}{\sinh(kd)} \qquad [31] \tag{4.15}$$

In case $z > 0$, $E(0)$ is applied, since otherwise the amplification would present unrealistic results. All components in Equation 4.15 above are briefly explained below.

- $E(z)$ Represents a certain scaling factor [-]
- k Represents wave number [rad/m]
- d Represents water depth [m]
- z Represents the height above mean sea level [m]

In the OrcaFlex model, the subsea power cable is fixed to the chute and the vessel is stationary, hence it is not sailing and the subsea power cable is not rolled-off from the storage turntable. To account for hydrodynamic loading, the Morison equation is implemented as well.

5

Limiting motion analysis

Up till now, in chapter 3 three main subsea power cable integrity limits have been established; minimum bending radius (MBR), minimum bottom tension (BT) and maximum top tension (TT). Besides, in chapter 4 OrcaFlex wave and cable modelling have been described.

This chapter covers the identification process of a limiting motion during normal cable lay operations, that can be appointed as a predictor. Therefore, the three determined cable integrity criteria are plotted against the 12 investigated chute motions, in order to find a link between cable integrity and chute motions. In total, four different subsea power cables are analysed. Typical inter-array cable 1 is assigned as a main experimental cable, whereas the remaining three cables are considered as control cables that are investigated for verification and validation aspects.

5.1. Subsea power cable data

As explained in chapter 3 no two subsea power cables are completely identical. There are, however, similarities in cable layer composition. Therefore, for this thesis four different types of subsea power cables are investigated to ensure verified and valid results.

To comply with confidentiality affairs, all analysed subsea power cables in this thesis are referred to as typical inter-array cables and typical export cables. Of both cable types, two cables are chosen based on differences in mechanical cable properties and different manufacturers. A few properties are summarized in Table 5.1 to illustrate the general differences. The entire cable specifics, including cross-sections, are enclosed in Appendix D Appendix C.

Cable characteristic	Typical inter-array cable 1 (main)	Typical inter-array cable 2	Typical export cable 1	Typical export cable 2
Manufacturer	A	B	B	C
HVAC or HVDC	HVAC	HVAC	HVAC	HVDC
Cores $[mm^2]$	3*300	3*300	3*1800	1*1300
Diameter $[mm]$	136	144	276	123
Mass in sea water $[kg/km]$	12,090	14,000	60,000	28,000

Table 5.1: Summary of modelled subsea power cable mechanical properties

Corresponding cable integrity limits a provided by the cable manufacturers is given in Table 5.2.

Cable integrity limit	Typical inter-array cable 1 (main)	Typical inter-array cable 2	Typical export cable 1	Typical export cable 2
MBR limit $[m]$	1.95	1.9	4.3	4.0
BT limit $[kN]$	-17	-12.5	-15	0
TT limit $[kN]$	170	85	300	149

Table 5.2: Summary of modelled subsea power cable integrity limits

From Table 5.1 and Table 5.2 it clear that there are quite some differences between the investigated subsea power cables, both regarding mechanical properties and and their integrity limits. Regarding these integrity limits, TT is an upper limit which may not be exceeded and both MBR and BT are lower limits .

For this chapter, typical inter-array cable 1 is assigned as main experimental cable and sensitivity assessments, whereas the remaining three cables are considered as as control cables that are investigated in verification and validation studies.

5.2. Initial local chute motion analysis

In order to investigate which motions show a proper relation w.r.t. the concluded cable integrity criteria, as a first step typical inter-array cable 1 is simulated in minor offshore conditions on a water depth of $50m$ with significant wave heights ranging from 1.5 to $4m$ in steps of $0.5m$ and wave peak periods of $7, 8$ and $9s$. The base case of this simulation is visualized in Figure 5.1, and the accompanying static report is provided in Table 5.3 (a static report comprises of six static parameters, hence without hydrodynamic loading).

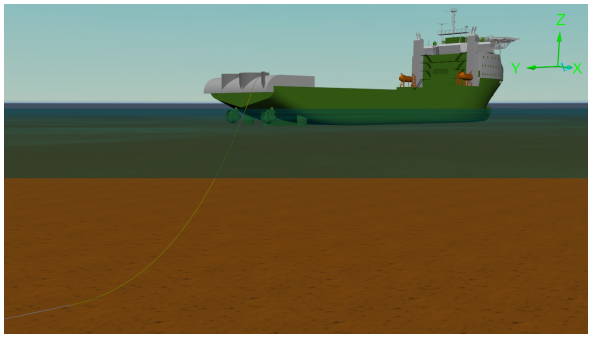

Figure 5.1: Initial chute motion analysis base case (OrcaFlex screenshot)

Parameter	Unit	Value
Water depth	m	50
Static layback	m	69.10
Static cable declination	deg	155.30
Static bending radius	m	42.50
Static top tension	kN	13.34
Static bottom tension	kN	5.00

Table 5.3: Static report - Initial 6 DOF motion analysis

In this step, the focus is on 9 chute x, chute y and chute z motions, hence chute cable motions are not taken into account within this step. The results of this initial analysis are presented by means of scatter graphs (all graphs are enclosed in Appendix D section D.1). Each independent motion is plotted against all three cable integrity criteria. In Figure 5.2, the results of all chute x, chute y and chute z motions are shown, plotted against the cables bending radius (BR). The dots represent all OrcaFlex cases, which are essentially all possible H_s, T_p and α combinations. Therefore, each individual plot in Figure 5.2 contains the same amount of data points.

For all OrcaFlex simulation cases, the maximum occurring motions are extracted. The focus is on the extreme occurring motions as the goal is to identify a limiting motion for cable lay operations. All other occurring motions in the time trace are not that much of interest, since the cable integrity limits are more likely to be breached in case of the most extreme occurring motions.

From Figure 5.2, it is clear that the relation between chute z motions and BR indicates to be the best. The graphs showing the chute x and chute y motions both contain more scatter. This observation also holds for the other two cable criteria, BT and TT (these results are enclosed in Appendix D section D.1).

Another remark is that the relation between BR and chute z motions seems to flatten out when moving towards higher motions, velocities and accelerations. This observation can be explained since at a certain point, it simply takes too much force to bend the cable even further. Besides, the bending stiffness shows nonlinear behaviour. This could also contribute to the asymptotic observation.

Based on the results of this initial analysis, several more advanced test cases are set up. However, first a proper method to compare the different motion relations with each other is required. This method is introduced in the next section.

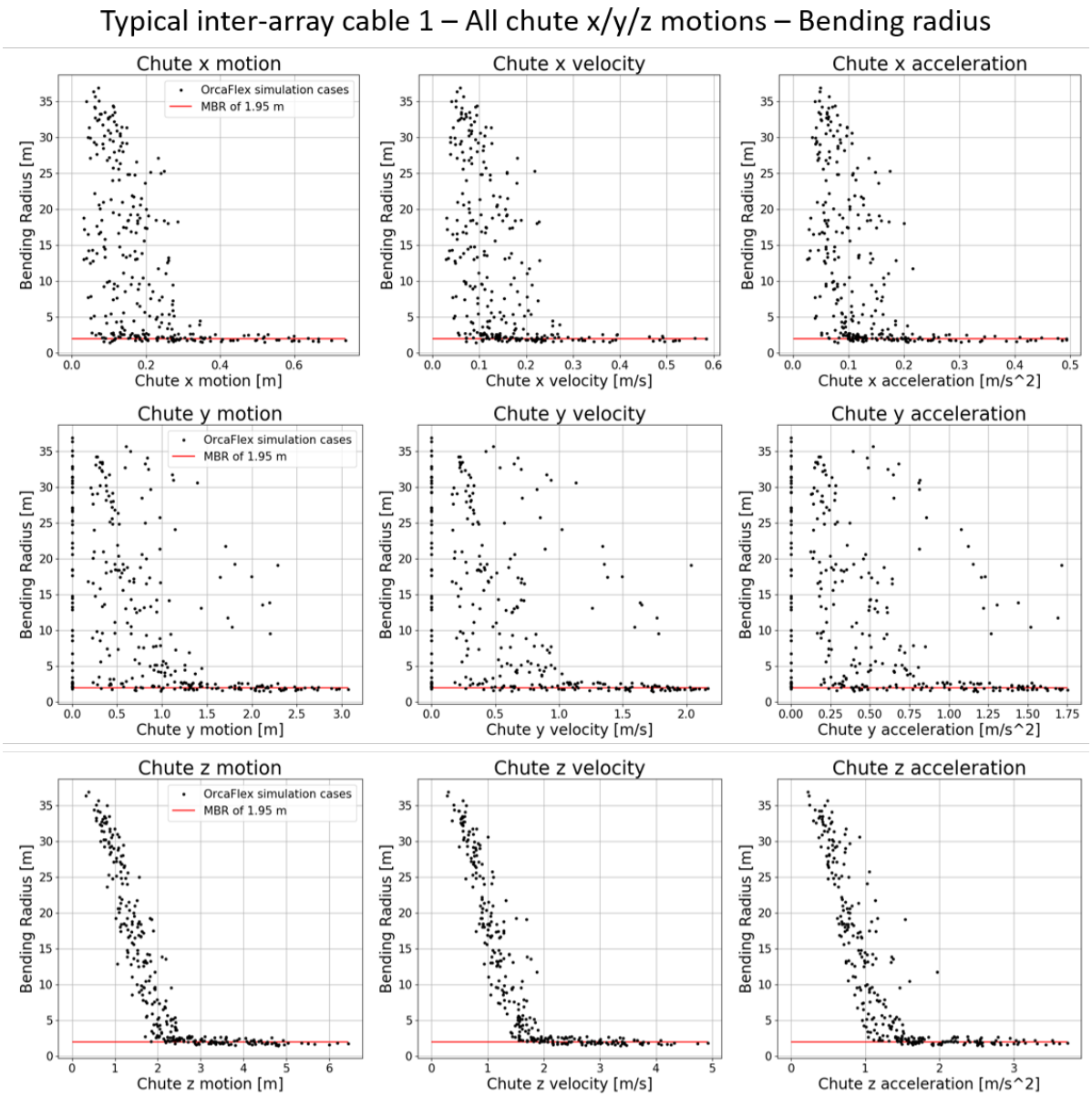

Figure 5.2: Initial motion analysis - All chute x/y/z motions w.r.t. - Bending radius

5.3. Line of best fit

To investigate which motion(s) has the best relation with respect to the cable integrity criteria a mathematical procedure is performed to find a 'best fit'. By means of least mean square (LMS) fitting method, a line of best fit is composed through a set of data points by minimizing the sum of squares of the existing vertical offsets (residuals) [56]. There are various type of LMS methods, both linear and nonlinear. Since subsea power cable operations are nonlinear, the applied LMS method must also be nonlinear. Types of nonlinear LMS analyses are exponential-, logarithmic-, polynomial- and power law fitting [56].

5.3.1. Underfit and overfit

Fitting distributions is tricky since data can be interpreted in various manners which can either be correct or false. A good illustration of this phenomenon is shown in Figure 5.3. In all three graphs the data points are exactly identical. However, the line of best fit is chosen differently for each graph, hence various LMS methods are applied. Which of all three LMS methods estimates the correct best fitted line trough all data points depends both on what needs to be investigated and how well fitted the data needs to be, since essentially all graphs can be used for different purposes.

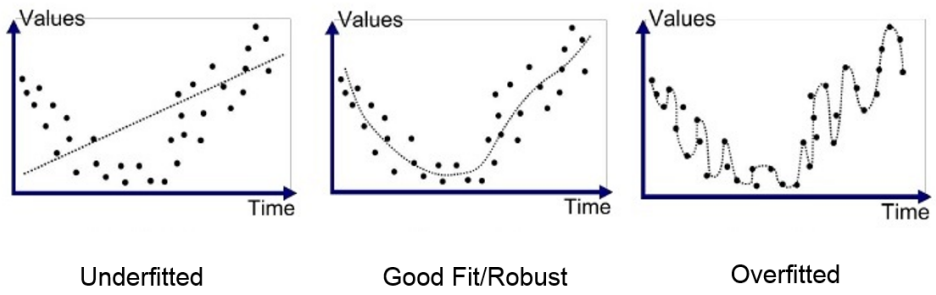

Figure 5.3: Overfitting, proper fitting and underfitting [5]

When a data set is underfitted, this means the underlying structure of the data set is not captured in the line of best fit due to a lack of missing features. Overfitting on the other hand, means that the model tries too hard to find a fit and too much features are used causing a complex fit in which every data point is connected. Overfitting is especially risky in the case of outliers in the data set, since these will have a lot of influence on the line of best fit. [5]

5.3.2. Exponential LMS fitting

Based on the resulting scatter graphs in Figure 5.2, exponential LMS fitting seems to give the best results out of the aforementioned nonlinear fitting methods. In this thesis, however, the exponential fitting base function is slightly modified in order to account for a line of best fit which does not start at the origin $(0, 0)$. Therefore, an additional parameter (C) is added as described below. In Equation 5.1, A, B and C are fitting parameters. [57]

More detailed information about exponential LMS fitting is enclosed in Appendix D section D.2.

$$y = A * e^{-B*x} + C \tag{5.1}$$

5.3.3. Regression

Based on the line of best fit a regression analysis can be performed. Regression is also known as goodness of fit. This goodness of fit is indicated by an R-squared (R^2) value, hence R^2 is a statistical measure of how close the original data points are w.r.t. the composed line of best fit. In literature, R-squared is also commonly referred to as regression coefficient and the coefficient of determination. The formula in order to determine the regression coefficients is given below in Equation 5.2. [16, 30, 56]

$$R^2 = \frac{Explained\ \ variance\ \ of\ \ the\ \ model}{Total\ \ variance\ \ of\ \ the\ \ model} = 1 - \frac{SS_{xy}^2}{SS_{xx} * SS_{yy}} \tag{5.2}$$

The components in Equation 5.2 above are explained briefly below.

- R^2 Represents the R-squared value, also known as regression coefficient
- SS_{xx} Represents sum of squares of the x variable
- SS_{yy} Represents sum of squares of the y variable
- SS_{xy}^2 Represents corrected sum of products x and y

The precise calculation of the variance terms (SS_{xy}^2, SS_{xx}^2 and SS_{yy}^2) is enclosed in Appendix D section D.2. The closer regression coefficient R^2 is to 1, the better the fit.

5.4. Test cases

In the section 5.2, based on an initial chute motion analysis, chute z motions indicate to provide proper relations against the cable integrity criteria. However, as mentioned in the introduction, there are also rumours in the Offshore industry that in fact the motions in the direction of cable departure are the limiting motions regarding normal cable operations [18]. Since those results are not completely open to the public, these motions are also taken into account in the following limiting motion identifying steps.

As aforementioned, typical inter-array cable one is chosen as the main experimental subsea power cable. Therefore this typical inter-array cable 1 is analysed in more detail, thus several test cases are set-up. These test cases are based on North Sea conditions. The simulated significant wave heights, wave peak periods and wave directions are listed below.

- **Significant wave height (H_s)**
  Range from $1.5m$ to $4m$ in steps of $0.5m$
- **Wave peak period (T_p)**
  Range from $7s$ to $15s$ in steps of $1s$
- **Wave direction (α)**
  Range from 0 to 330 degrees in steps of 30 degrees (0^o represents the same direction as 360^o)

Besides, two water depths are analysed. A water depth of $30m$ is chosen to simulate shallow water conditions and a water depth of $150m$ is chosen to simulate deep water, since these are common for normal cable lay operations in the North Sea. Further along this thesis a water depth of $30m$ is also referred to as shallow water, and a water depth of $150m$ is referred to as deep water. The main difference between both water depths, is that the cable catenary has a different shape, as in deep water the cable is leaving the chute almost vertically. This is illustrated in Figure 5.4. The top figure represents the OrcaFlex model in shallow water, and the bottom figure represents deep water.

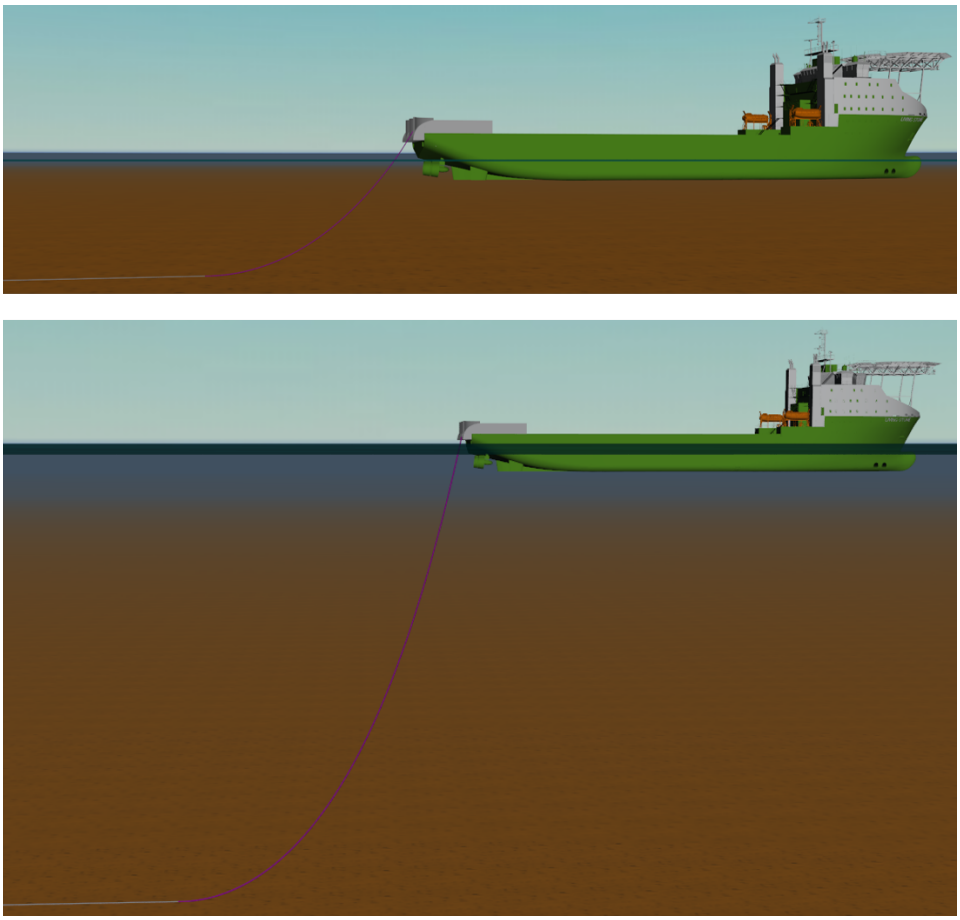

Figure 5.4: OrcaFlex typical inter-array cable 1 base cases for shallow water (top) and deep water (bottom)

5.4.1. Typical inter-array cable 1 test cases

Typical inter-array cable 1 is a 3*300mm^2 HVAC inter-array cable. An intersection and list of all specific cable properties is enclosed in Appendix C section C.1.

Static reports of the normal lay configurations (identical to the screenshots presented in Figure 5.4) for both shallow and deep water are provided below. From

Parameter	Unit	Value
Water depth	m	30
Static layback	m	58.93
Static cable declination	deg	149.03
Static bending radius	m	43.06
Static top tension	kN	11.05
Static bottom tension	kN	5.00

Table 5.4: Static report - Typical inter-array cable 1, shallow water $30m$

Parameter	Unit	Value
Water depth	m	150
Static layback	m	101.50
Static cable declination	deg	167.16
Static bending radius	m	43.32
Static top tension	kN	25.19
Static bottom tension	kN	5.00

Table 5.5: Static report - Typical inter-array cable 1, deep water $150m$

From Table 5.4 and Table 5.5, the differences between the normal cable lay configurations become quite clear. An important note is that both configurations are created such that the static bottom tension is $5.00kN$ for both cases. This is done to ensure continuity throughout the thesis, hence every cable simulation is performed with a static bottom tension of $5.00kN$. This parameter is therefore also part of the sensitivity study accompanying this chapter.

5.5. Results

The results of the typical inter-array cable 1 test cases, both for shallow and deep water are presented in Figure 5.5 and Figure 5.6 below. Note that these figures only contain BR results. Results for the other analysed cable integrity criteria, BT and TT, are enclosed in Appendix D section D.4.

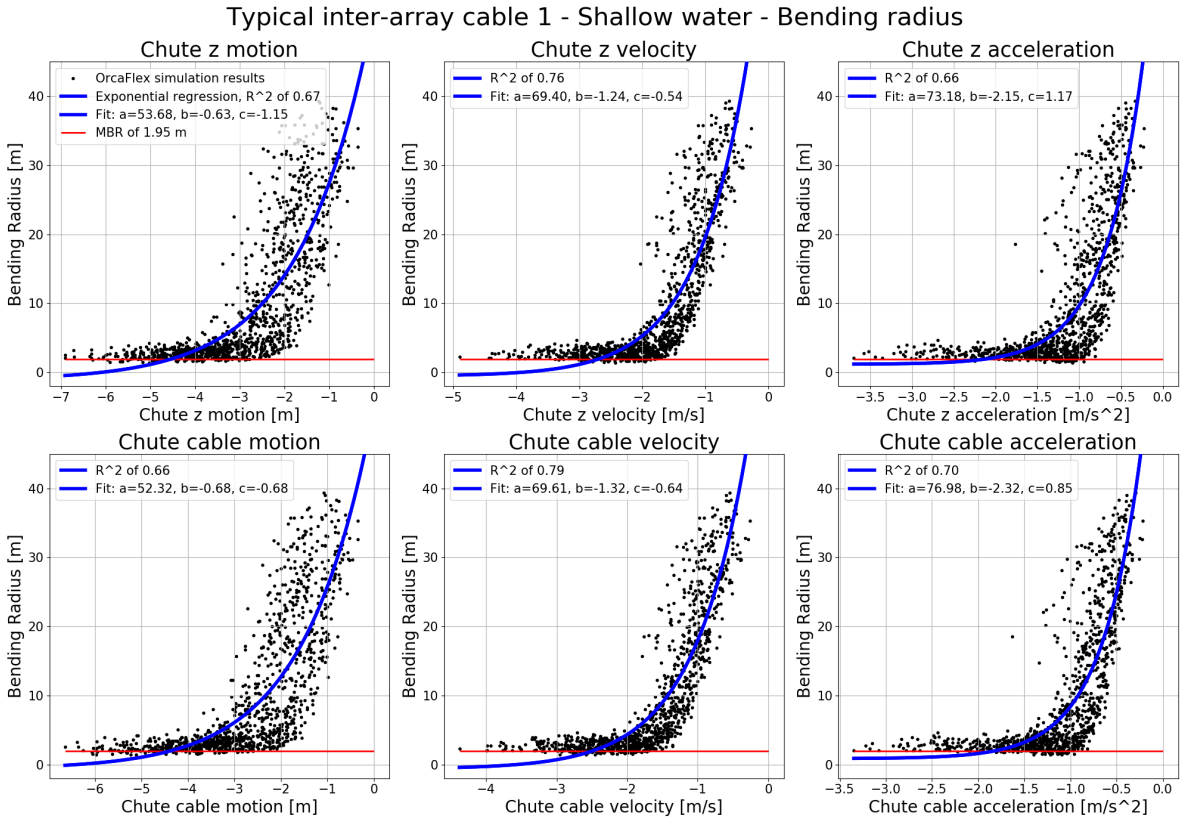

Figure 5.5: Regression coefficient results typical inter-array cable 1 w.r.t. MBR in shallow water ($30m$)

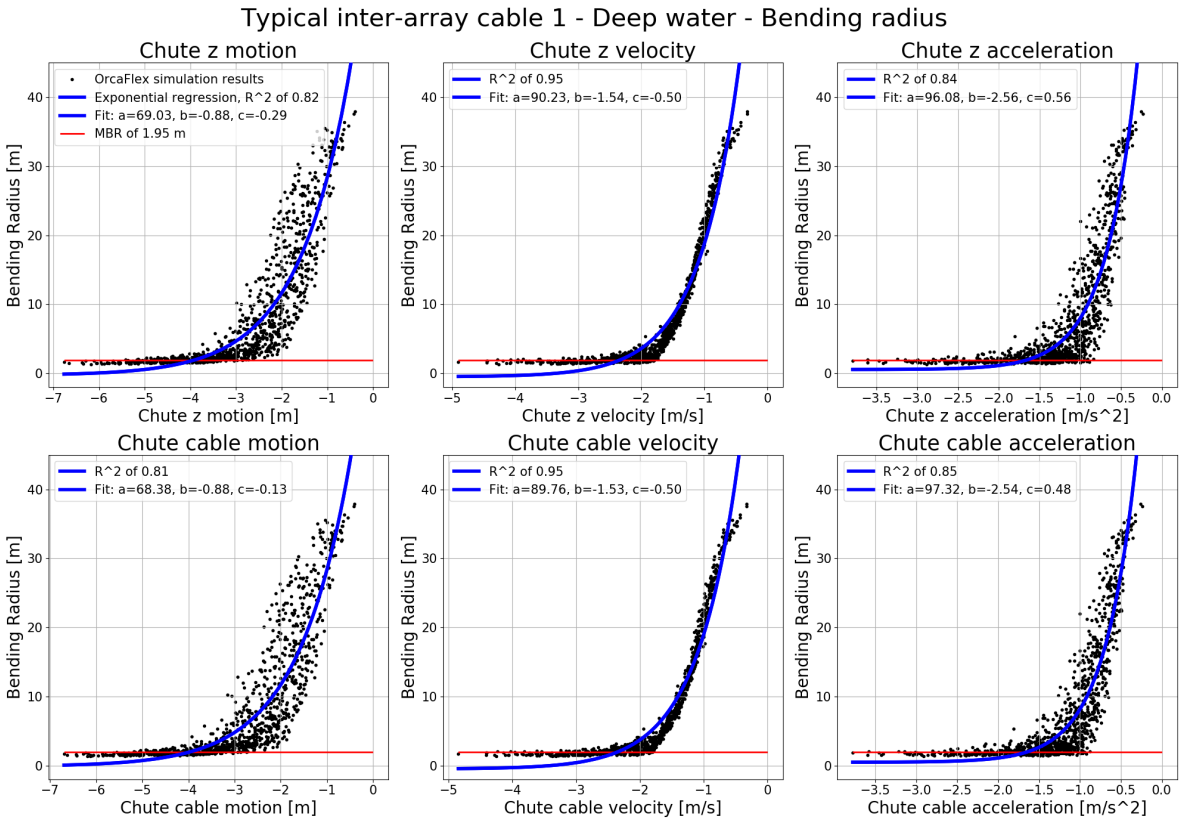

Figure 5.6: Regression coefficient results typical inter-array cable 1 w.r.t. MBR in deep water ($30m$)

In the figures above, the exponential line of best fit is drawn in bold blue and the accompanying regression coefficients and specific exponential fit parameters are presented in the legends as well. Again, the dots represent all OrcaFlex simulation cases (all possible H_s, T_p and α combinations), hence individual plot in contains the same amount of data points. This manner of presenting is persisted throughout the entire thesis.

The drawn line of best fit, however, does give a good indication of the entire relation, but especially in the flattening tail this exponential line of best fit does seem to be quite off.

From the shown graphs it can be concluded that for both shallow and deep water, both the chute z velocity and chute cable velocity seem to be proper limiting motion predictors. Especially in deep water the relation seems really good. The fact that the velocity relations in deep water indicate a better fit than the relations in shallow water can be clarified. When moving towards deeper water depths, the cable automatically leaves the chute in a more vertical position (as illustrated in Figure 5.4). Therefore, chute z motions become most the most important.

Regarding the other cable integrity criteria, BT and TT, all scatter graphs for the chute z motions and chute cable motions are enclosed in Appendix D section D.4. In general these results indicate the same limiting motion predictors; cable z velocity and cable chute velocity. All results for typical-inter array cable 1, both in shallow and deep water, are gathered in Table 5.6 and Table 5.7 respectively.

Motion	Typical inter-array cable 1		
	BR	BT	TT
Chute z motion	0.67	0.70	0.68
Chute z velocity	**0.76**	**0.81**	**0.88**
Chute z acceleration	0.66	0.72	0.77
Chute cable motion	0.66	0.68	0.58
Chute cable velocity	**0.79**	**0.82**	**0.88**
Chute cable acceleration	0.70	0.76	0.80

Table 5.6: Typical inter-array cable 1 - All regression coefficient (R^2) results - Shallow water ($30m$)

Motion	Typical inter-array cable 1		
	BR	BT	TT
Chute z motion	0.82	0.75	0.63
Chute z velocity	**0.95**	**0.82**	0.89
Chute z acceleration	0.84	0.69	**0.91**
Chute cable motion	0.81	0.74	0.58
Chute cable velocity	**0.95**	**0.83**	0.88
Chute cable acceleration	0.85	0.70	**0.91**

Table 5.7: Typical inter-array cable 1 - All regression coefficient (R^2) results - Deep water ($150m$)

In Table 5.6 and Table 5.7 all chute z motion and chute cable motion regression coefficient results are gathered. Overall, for both the velocities seem to indicate good predictors. Regarding top tension in deep water, however, chute z accelerations and chute cable accelerations seem to indicate even better fits than the corresponding velocities. The differences compared to the velocities are, however, minor.

5.6. Verification and validation

There are multiple aspects within this limiting motion identification process that need to be verified and validated. Regarding verification at first an other normal lay configuration is simulated, by changing the static bottom tension of the base case model. Besides, another CLV is modelled to verify whether the limiting motion results comply with each other.

To validate the obtained results, the remaining three subsea power cables are simulated to check whether the indicated limiting motions are identical for all cables.

5.6.1. Normal lay configuration

Subsea power cables modeling is a nonlinear process. Therefore, the configuration in which a subsea power cable is modelled can have much influence on the limiting motion identification process performed in this thesis. In order to verify the obtained limiting motions, a sensitivity analysis is performed on the normal lay configuration.

The normal lay configuration changes significantly due to three main factors; static bottom tension, water depth and type of subsea power cable (due to different cable properties). Differences in static departure angle, static layback length, static top tension and static bending radius result from adjusting the aforementioned factors. The effect of multiple water depths and different subsea power cables are already covered in other sections of this thesis, hence the static bottom tension as parameter remains.

So far, all calculations have been executed based on a static bottom tension of $5.0kN$. To model other normal lay configurations, typical inter-array cable 1 is modelled based on three additional static bottom tensions ($2kN$, $10kN$ and $20kN$) all in shallow water. Thus, in total data of three additional configurations is obtained. The effect of using other static bottom tensions is shown in the four tables below showing the static reports. The higher the static bottom tension is modelled, the longer the static layback, the higher the static BR, the and the lower the cable declination angle (more horizontal).

Parameter	Unit	Value
Water depth	m	30
Static layback	m	38.00
Static cable declination	deg	160.90
Static bending radius	m	18.38
Static top tension	kN	8.10
Static bottom tension	kN	2.00

Table 5.8: Static report - Typical inter-array cable 1, static bottom tension 2kN

Parameter	Unit	Value
Water depth	m	30
Static layback	m	58.93
Static cable declination	deg	149.03
Static bending radius	m	43.06
Static top tension	kN	11.05
Static bottom tension	kN	5.00

Table 5.9: Static report - Typical inter-array cable 1, static bottom tension 5kN

Parameter	Unit	Value
Water depth	m	30
Static layback	m	84.05
Static cable declination	deg	137.56
Static bending radius	m	88.76
Static top tension	kN	16.44
Static bottom tension	kN	10.00

Table 5.10: Static report - Typical inter-array cable 1, static bottom tension 10kN

Parameter	Unit	Value
Water depth	m	30
Static layback	m	116.69
Static cable declination	deg	127.23
Static bending radius	m	153.05
Static top tension	kN	26.27
Static bottom tension	kN	20.00

Table 5.11: Static report - Typical inter-array cable 1, static bottom tension 20kN

All resulting scatter graphs are presented in Appendix D section D.5. The regression coefficient results (R^2) for the additional normal lay configurations are gathered in Table 5.12 below.

Typical inter-array cable 1			
Motion	**Static bottom tension of** $2kN$		
	BR	BT	TT
Chute z motion	0.71	0.75	0.75
Chute z velocity	**0.78**	**0.86**	**0.85**
Chute z acceleration	0.63	0.74	0.69
Chute cable motion	0.71	0.74	0.70
Chute cable velocity	**0.80**	**0.86**	**0.87**
Chute cable acceleration	0.66	0.77	0.72
	Static bottom tension of $10kN$		
	BR	BT	TT
Chute z motion	0.64	0.66	0.63
Chute z velocity	**0.77**	**0.80**	**0.89**
Chute z acceleration	0.71	0.74	0.82
Chute cable motion	0.61	0.62	0.47
Chute cable velocity	**0.78**	**0.80**	**0.86**
Chute cable acceleration	0.76	0.79	**0.86**
	Static bottom tension of $20kN$		
	BR	BT	TT
Chute z motion	0.58	0.60	0.58
Chute z velocity	**0.74**	**0.77**	**0.89**
Chute z acceleration	**0.74**	**0.77**	0.86
Chute cable motion	0.53	0.53	0.38
Chute cable velocity	0.73	0.74	0.81
Chute cable acceleration	**0.79**	**0.82**	**0.89**

Table 5.12: Various static bottom tensions - Inter-array cable 1 regression coefficient results - Shallow water ($30m$)

From Table 5.12 it can be concluded that, again, both chute z velocity and chute cable velocity seem to be the best limiting motion predictors. In the $20kN$ static bottom tension case, however, accelerations indicate to have an even better fit. These differences between the velocities and accelerations are

however, again, very minor.

5.6.2. Simulate another vessel

So far, all OrcaFlex simulations have been performed based on the Living Stone CLV. Therefore, another CLV is modelled as well for exactly the same wave conditions. For confidentiality reasons, the exact name of the other CLV is not mentioned. This CLV is chosen such that the dimensions are completely different. Whereas the Living stone has a length of $161m$, the other CLV has a length of $88.2m$. And where the Living Stone has a breadth of $32.2m$, the other CLV has a breadth of $24m$. Most important is that this other CLV is chosen as a vessel much smaller compared to the Living Stone.

The resulting scatter graphs are enclosed in Appendix D section D.6. The regression coefficients are gathered in Table 5.13 below.

Motion	Typical inter-array cable 1		
	BR	BT	TT
Chute z motion	0.69	0.71	0.81
Chute z velocity	**0.86**	**0.84**	**0.91**
Chute z acceleration	0.63	0.68	0.83
Chute cable motion	0.70	0.68	0.79
Chute cable velocity	**0.86**	**0.84**	**0.91**
Chute cable acceleration	0.64	0.69	0.84

Table 5.13: Typical inter-array cable 1 - All regression coefficient (R^2) results - Shallow water ($30m$) - Other CLV

From Table 5.13, it is immediately clear that the regression coefficients both the chute z velocity and chute cable velocity indicate eminent results. Hence, when modelling another vessel this has no influence on the indicated best limiting motion predictor.

Taking a better look at the resulting scatter graphs, as enclosed in Appendix D section D.6, there is however a clear difference between the maximum occurring motions even though the same environmental conditions were implemented. For the Living Stone the maximum modelled chute z velocity was for example just under $-5m/s$, whereas the maximum modelled chute z velocity for the other vessel is just over $-10m/s$. This is clarified by the fact the the other vessel is simply much smaller than the Living Stone, and each vessel has its own RAO's and QTF's. Since the vessel is smaller, the vessel will simply move more in identical wave conditions. Consequently, by modelling the other CLV not only the MBR limit was breached (in case of the Living Stone), but since the motions are higher the cables top tension limit is breached as well.

Even though there is a clear difference between maximum occurring motions between the Living Stone and the other CLV, the MBR limit seems to be breached around the same chute z velocity, just under $-2m/s$.

This other CLV is currently not operational anymore, hence the precise RAO's and QTF's are hard to verify and validate. Therefore, this other CLV is not modelled in the quantification step in this research.

5.6.3. Multiple subsea power cable validation

So far, all experiments were performed by modelling typical-inter array cable 1. To ensure valid results, however, the remaining three control cables are modelled as well both in shallow and deep water conditions with a static bottom tension of $5kN$.

The static reports for each subsea power cable are enclosed in Appendix D section D.3, and all resulting scatter graphs are presented in Appendix D section D.4.

In Table 5.14 and Table 5.16 the final R^2 values of the regression analysis regarding the inter-array cables are presented, whereas in Table 5.15 and Table 5.17 the final R^2 values of the regression analysis regarding the export cables are presented.

Shallow water regression all 4 subsea power cables

Motion	Typical inter-array cable 1			Typical inter-array cable 2		
	BR	BT	TT	BR	BT	TT
Chute z motion	0.67	0.70	0.68	0.71	0.65	0.68
Chute z velocity	**0.76**	**0.81**	**0.88**	**0.81**	**0.76**	**0.89**
Chute z acceleration	0.66	0.72	0.77	0.69	0.67	0.80
Chute cable motion	0.66	0.68	0.58	0.70	0.62	0.58
Chute cable velocity	**0.79**	**0.82**	**0.88**	**0.83**	**0.76**	**0.89**
Chute cable acceleration	0.70	0.76	0.80	0.74	0.70	0.82

Table 5.14: Regression coefficient results - Typical inter-array cables 1 and 2 - Shallow water ($30m$)

Motion	Typical export cable 1			Typical export cable 2		
	BR	BT	TT	BR	BT	TT
Chute z motion	0.76	0.77	0.76	0.76	0.77	0.74
Chute z velocity	**0.83**	**0.90**	**0.85**	**0.84**	**0.90**	**0.88**
Chute z acceleration	0.69	0.75	0.70	0.72	0.77	0.75
Chute cable motion	0.75	0.74	0.72	0.75	0.74	0.68
Chute cable velocity	**0.85**	**0.91**	**0.87**	**0.86**	**0.91**	**0.89**
Chute cable acceleration	0.72	0.78	0.73	0.75	0.80	0.78

Table 5.15: Regression coefficient results - Typical export cables 1 and 2 - Shallow water ($30m$)

Deep water regression all 4 subsea power cables

Motion	Typical inter-array cable 1			Typical inter-array cable 2		
	BR	BT	TT	BR	BT	TT
Chute z motion	0.82	0.75	0.63	0.85	0.78	0.61
Chute z velocity	**0.95**	**0.82**	0.89	**0.97**	**0.83**	**0.88**
Chute z acceleration	0.84	0.69	**0.91**	0.85	0.71	0.87
Chute cable motion	0.81	0.74	0.58	0.84	0.76	0.56
Chute cable velocity	**0.95**	**0.83**	0.88	**0.97**	**0.83**	**0.88**
Chute cable acceleration	0.85	0.70	**0.91**	0.86	0.72	**0.88**

Table 5.16: Regression coefficient results - Typical inter-array cables 1 and 2 - Deep water ($150m$)

Motion	Typical export cable 1			Typical export cable 2		
	BR	BT	TT	BR	BT	TT
Chute z motion	0.87	0.75	0.55	0.85	0.79	0.60
Chute z velocity	**0.99**	**0.99**	0.90	**0.97**	**0.97**	**0.91**
Chute z acceleration	0.86	0.89	**0.95**	0.86	0.87	**0.91**
Chute cable motion	0.86	0.73	0.50	0.84	0.77	0.56
Chute cable velocity	**0.99**	**0.99**	0.88	**0.97**	**0.97**	0.90
Chute cable acceleration	0.87	0.90	**0.95**	0.87	0.88	**0.91**

Table 5.17: Regression coefficient results - Typical export cables 1 and 2 - Deep water ($150m$)

From Table 5.14 and Table 5.15 it is clear that in shallow water for both typical inter-array cables and both typical export cables, chute z velocity and chute cable velocity appear to be the motions with highest regression coefficients for all cable integrity criteria. Comparing chute z velocity against chute cable velocity indicates that the chute cable velocity has a slightly better regression coefficient or equal as chute z velocity.

Regarding deep water (Table 5.16 and Table 5.17), however, there seems to be a bit more spreading in which motion has the best. Again chute z velocity and chute cable velocity seem to show proper

relations, but regarding maximum top tension chute z acceleration and chute cable acceleration also indicate proper fits. Comparing chute z motions against the chute cable motions, all R^2 values are identical. This makes sense since moving from shallow towards deeper waters the chute z component will have the overhand w.r.t. chute x motions in contributing the motions in the chute cable motions as explained in subsection 4.2.1.

5.7. Conclusions

This section contains conclusions regarding the limiting motion identification process as followed in this thesis chapter.

Out of all 12 investigated chute motions, eventually two seem to indicate a proper overall relation as expressed in a regression coefficient. These two motions are chute z velocity and chute cable velocity, hence the vertical velocity at the chute and the velocity in the direction of cable departure. When moving to deeper water both motions show almost identical regression coefficients. Besides, in deep water the regression coefficients are even higher for both chute z velocity and chute cable velocity compared to shallow water. This makes sense since in deep water the subsea power cable leaves the CLV almost vertically, hence in the chute z direction.

Regarding top tensions in deeper water, however, chute z accelerations and chute cable accelerations indicate even better fits than the corresponding velocities. These gains in the acceleration regression coefficients are, however, minor.

The same results were obtained during verification and validation steps. When adjusting the normal lay configuration (by modelling several static bottom tensions), and modelling another vessel again chute z velocity and chute cable velocity indicate the highest regression coefficients. And again, in some cases the accompanying accelerations regression coefficient are just a little bit better. These observations also hold for the validation process, in which multiple subsea power cables were modelled with varying cable properties.

All together, both chute z velocities and chute cable velocities seem to be good limiting motion predictors. The velocities are preferred over the resulting accelerations, since the velocities always provide a good fit and the accelerations are negligible better in just a few cases. In reality it is, however, easier to monitor chute z motions then chute cable motions. This is because chute z motions can be easily determined by means of a frequency domain vessel motion analysis, and transferred from the COG to the chute. To obtain chute cable motions on the other hand requires implementation of a continuously varying declination angle, which comes with extra prediction and monitoring tasks. Therefore, based on the research performed within this thesis, chute z velocities are indicated as proper limiting motion predictors.

6

Motion quantification method

In chapter 5, eventually chute z velocity has been identified as the overall limiting motion for normal subsea power cable lay operations. In this chapter a quantification method is set-up in order to quantify these limiting chute z velocities.

Within this chapter, again, one subsea power cable is chosen as a main experimental cable whereas the remaining three cables are considered as control cables to ensure a valid results. In this chapter, however, typical export cable 1 is considered as the main experimental cable. Typical export cable 1 is preferred over typical inter-array cable 1 since for the latter cable, only the MBR criteria is breached.

In motion analyses, often a probability of exceedance is used to determine certain limits [26, 40]. However, specific RAO sets are implemented in these calculations. One of the main ideas behind this thesis is that eventually all cable integrity limits are converted into one limiting motion, independent of which vessel is used. Therefore, this probability of exceedance method is not desired anymore since RAO sets are vessel dependant. Therefore, a new method to quantify the limiting chute z velocity has to be set-up.

The exponential LMS fitting method applied in chapter 5 provided proper results regarding the overall relation and identification process of chute z velocity as limiting motion. But to make a proper quantification another method needs to be implemented since exponential LMS fitting is, especially in the lower and higher velocity tails, somewhat inaccurate. Especially, around higher (negative) velocities are interest for this quantification step, since this is the area where eventually cable integrity limits (MBR, BT and TT) will breach.

6.1. Percentile method

The quantification approach applied in this thesis in based on percentiles. By splitting the scatter graphs into multiple (vertical) bins, per bin a certain percentile can be calculated. By composing a line between all these percentiles eventually an intersection between the chute z velocity and subsea power cable integrity criteria is obtained if the particular cable integrity limit is breached. This means that in the end for each subsea power cable three quantifications will be made, for each cable integrity criterion one. These three quantifications among each other will most likely give different results, of which only one can be limiting during cable laying operations in practice. This is the lowest value as this is associated with the first integrity criteria that will be breached.

Calculating percentiles is based on the index of a certain array. All modelled cable integrity limits (as modelled in OrcaFlex) are combined into an array of in total N indices, ascending from the lowest value (index$= 1$) to the highest value (highest possible index out of data points). Based on this ascending array, the $q^{th}_{percentile}$ index is determined by applying Equation 6.1 [37]. Note that in the formula $N-1$ is applied. This is since the difference (distance) between the first and last element has to be investigated whilst setting up a percentile line, and not the total amount of data points.

$$Index = (N-1) * \frac{q^{th}_{percentile}}{100} \tag{6.1}$$

All components in Equation 6.1 are briefly explained below.

- $Index$ Represents the $q^{th}_{percentile}$ index of the total array [#]
- N Represents the total amount of data points [#]
- $q^{th}_{percentile}$ Represents the to be investigated percentile [%]

The resulting $q^{th}_{percentile}$ index from Equation 6.1 will most likely not be an integer. Therefore, an interpolation method is required. There are multiple kind of interpolation methods that are frequently used within percentile calculations, such as linear, lower, higher, midpoint and nearest neighbour. In this research, linear interpolation is applied because the distribution is fairly smooth. This linear interpolation method is based on Equation 6.2. [37]

$$Percentile_{value} = Index_{low} + (Index_{high} - Index_{low}) * Frac \tag{6.2}$$

All components in Equation 6.1 are briefly explained below.

- $Percentile_{value}$ Represents the final percentile value [-]
- $Index_{low}$ Represents the value in the composed array on the determined percentile index in Equation 6.1 rounded off to the lowest possible integer [#]
- $Index_{high}$ Represents the value on the determined percentile index rounded off to the highest possible integer [#]
- $Frac$ Represents the corresponding fractional part [-]

An example to illustrate the percentile method and implemented linear interpolation procedure is presented in the box below.

Example 90^{th} ***percentile:***

Array = $[3, 8, 6, 9, 4, 2, 4, 5, 3, 6]$ (composed using a random number generator)
Listed array = $[2, 3, 3, 4, 4, 5, 6, 6, 8, 9]$
Index array = $[1, 2, 3, 4, 5, 6, 7, 8, 9, 10]$

Based on the listed array, from small to high, Equation 6.1 can be applied.

$$Index = (10 - 1) * \frac{90}{100} = 8.1$$

Thus the values belonging to indices 8 and 9 of the listed array need to be linearly interpolated, and the fractional part is 0.1.
Following the resulting listed and index arrays, index 8 has a value of 6 and index 9 holds a value of 8. Now, Equation 6.2 can be applied.

$$Percentile_{value} = 6 + (8 - 6) * 0.1 = 6.2$$

Consequently, the 90^{th} percentile of the randomly generated array is 6.2.

In the DNV-GL code, it is stated that the probability of exceeding the calculated extreme hydrodynamic loading the operation period shall not exceed 10% [13]. Hence, offshore operations need to be determined based on 90% certainty. Moreover the DNV-GL code contains specific information regarding percentiles. There is no specific prescribed percentile, but there is a recommendation of choosing a qth-percentile between $90\% - 95\%$. [13]

Therefore, the qth-percentile applied within this thesis is 90%. This means, that in 90% of all the simulation cases the limit needs to be preserved, and in the remaining 10% of the cases cable integrity limits may be breached. Since this percentile is applied per bin, this 90% certainty does no necessarily hold for all simulation cases together.

6.1.1. Percentile line

Based on the scatter graphs created in chapter 5, and applying the percentile function explained above, a percentile line can be composed through all percentiles. This is done by dividing the x-axis (representing chute z velocity) in multiple bins. Per bin the percentile can be calculated, thus for each bin the resulting percentile is determined. Through these midpoints of the percentiles per bin, a linear line is plotted which indicates the percentile line. Of course this line is highly dependent on the amount of data points per bin, amount of bins, and 90^{th}-percentile applied in the percentile function. [42, 43]

Based on this composed 90^{th}-percentile line, the chute z velocities can be quantified at the intersection point between the percentile line and horizontal line representing a cable limit. It is not necessarily the case that all three cable integrity are breached. However, in case one or more limits are breached, the lowest quantified chute z velocity is taken as guiding limiting motion.

To compose this percentile line, especially around the higher (negative) chute z velocities more data is required in order to apply proper percentile statistics. Therefore, based on the resulting scatter graphs from chapter 5 certain interesting chute z velocity ranges are distinguished. These ranges are specified close around the cable integrity limits, since this is the area to focus on since in these regions the chute z velocities likely to breach cable integrity limits. How these cases are precisely obtained is elucidated in the next section.

6.1.2. Define extra cases

As aforementioned, the area around the intersection point between motion and cable integrity criteria is of high interest during the quantification. In order to ensure robust and accurate results more data needs to be generated in these specific areas. In OrcaFlex this can be done by simulating the exact same OrcaFlex cases, but for multiple seed numbers.

Changing the seed number, essentially comes down to changing the wave train phase. OrcaFlex is based on random wave trains, which are defined by a user-defined number of wave components. In order to assign a phase to these wave components, OrcaFlex makes use of a random number generator in combination with a user-defined seed to assign phases. This particular sequence is a repeatable process, hence the same seed (in same conditions) will always be assigned to the same phases, consequently leading the exact same wave train. [31]

To obtain more data points required for percentile statistics at higher chute z velocities, all OrcaFlex cases within the interesting range are simulated for five different seed numbers. These ranges are clarified in Appendix E section E.1. These ranges are chosen closely around cable integrity limits in order to generate more data in those regions. Hence, the scatter clouds around the limits will be enlarged.

To conclude which OrcaFlex cases are interesting for a specific seed number, all possible North Sea environmental cases (see section 5.4) are simulated for each extra seed number. This is done by means of a vessel motion analysis in the frequency-domain, hence no subsea power cable is incorporated. If the the chute z velocity of a certain OrcaFlex case falls within the predefined range, this case is modelled again in the time-domain with the attached subsea power cable.

Thus, by modelling multiple seed numbers, extra data can be generated. The outcomes will be similar to the original seed number (default OrcaFlex seed number is 12345), but there will be some variations in the precise chute z velocities and accompanying, BR's, BT's and TT's. When changing the seed number, it is useful to always check the resulting JONSWAP, autocorrelation graph and total sea elevation graphs to verify whether the created wave field is indeed irregular and there are no visible peculiarities.

6.2. Results

As aforementioned, the percentile line is constructed by splitting the x-axis (chute z velocity) in bins. For this analysis, three different binwidths ($1m/s$, $0,5m/s$ and $0,25m/s$) are investigated to obtain verified results.

In Figure 6.1 and Figure 6.2 three graphs with different binwidths for typical export cable 1 with respect to MBR and BT respectively in shallow water conditions are presented. The differences in binwidths is clearly indicated by means of the vertical blue dotted lines. The quantified chute z velocities are indicated with a yellow star, and the precise value is also listed in the legends. Since the TT limit is not breached for this specific cable configuration, these graphs are not shown. The graphs presented below contain all data points for 5 seed numbers. All other graphs, for different amounts of seed

numbers, are gathered in Appendix E Appendix E.

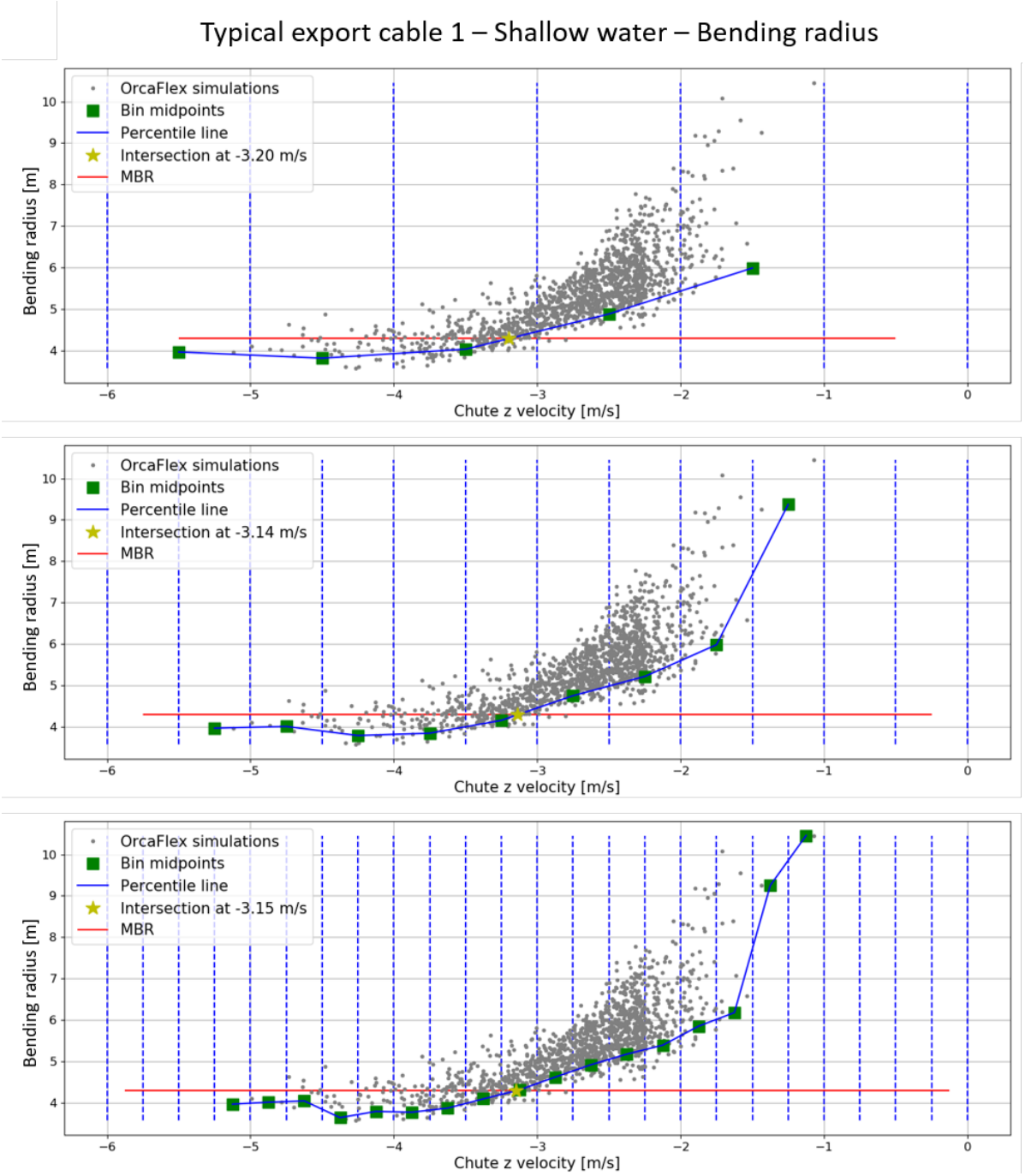

Figure 6.1: Quantification graphs w.r.t. MBR limit - Typical export cable 1 - Shallow water ($30m$) - All binwidths for 5 seeds data

From Figure 6.1 it is clear that the limiting chute z velocity, for the MBR cable integrity criteria, is somewhere between $-3.14s$ and $-3.20/s$, depending on the chosen binwidth. These results indicate that the binwidth, in this case, does not have much influence on the final quantified chute z velocity.

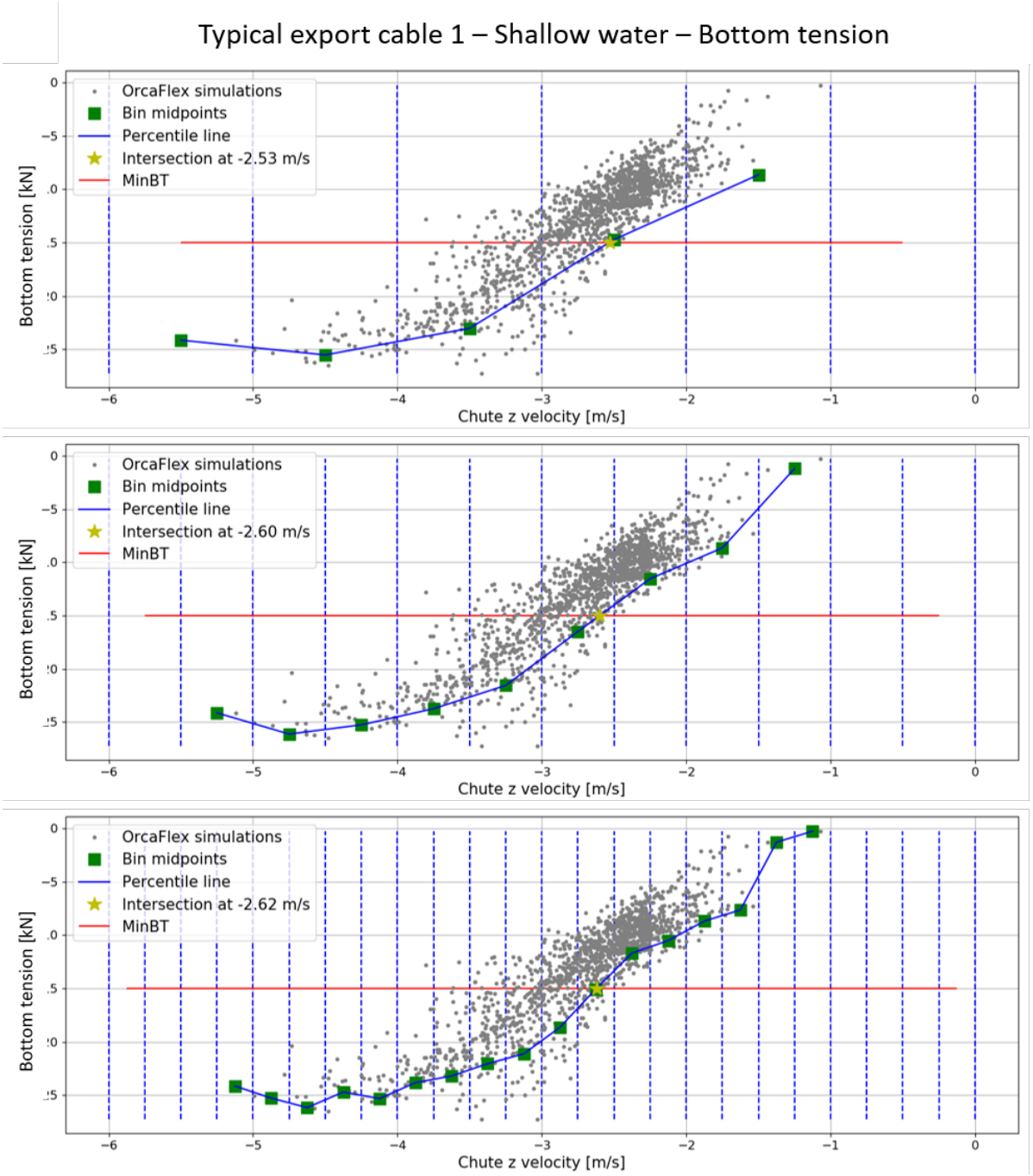

Figure 6.2: Quantification graphs w.r.t. BT limit - Typical export cable 1 - Shallow water ($30m$) - All binwidths for 5 seeds data

From Figure 6.2 it is clear that the limiting chute z velocity, for the BT cable integrity criteria, is somewhere between $-2.53m/s$ and $-2.62m/s$, depending on the chose binwidth. These results indicate that the binwidth, in this case, does not have much influence on the final quantified chute z velocity.

Comparing the quantified chute z velocities for cable limits MBR and BT, for this specific cable configuration BT is more critical than BR since the BT limit is breached earlier. Therefore, the limiting chute z velocity is, in this case, associated with BT.

The presented percentile lines in Figure 6.1 and Figure 6.2 all show the same overall behaviour, a downward trend from the top right to the bottom left. This is logical since at more extreme chute z velocities, the cable is compressed to the TDP with a higher force, hence the BR decreases and BT increases. However, the fact that the percentile line is going up again between chute z velocities of $-4m/s$ and $-5m/s$ is simply incorrect. The reason for this is that there are too little data points in this

area to apply proper percentile statistics.

To get a better overview of the chute z velocity results from the percentile line method, all quantified chute velocities for export cable 1 in both shallow and deep water are gathered in Table 6.1. If a certain cell contains an x, this means there is no intersection between the chute z velocity and cable integrity criterion. Besides, if a cell is empty this means there are no intersections available to determine an average.

Typical export cable 1 - Shallow water					Typical export cable 1 - Deep water			
Bin width	**1 m/s**	**0.5 m/s**	**0.25 m/s**		**1 m/s**	**0.5 m/s**	**0.25 m/s**	
	5 Seed numbers			**Average**	**5 Seed numbers**			**Average**
BR	-3.20	-3.14	-3.15	-3.16	-2.65	-2.80	-2.86	-2.77
BT	-2.53	-2.60	-2.62	-2.58	-2.30	-2.51	-2.59	-2.47
TT	x	x	x		x	x	x	
	4 Seed numbers			**Average**	**4 Seed numbers**			**Average**
BR	-3.21	-3.14	-3.15	-3.17	-2.65	-2.81	-2.87	-2.78
BT	-2.54	-2.60	-2.63	-2.59	-2.29	-2.51	-2.59	-2.46
TT	x	x	x		x	x	x	x
	3 Seed numbers			**Average**	**3 Seed numbers**			**Average**
BR	-3.23	-3.19	-3.16	-3.19	-2.65	-2.80	-2.86	-2.77
BT	-2.55	-2.63	-2.64	-2.61	-2.31	-2.52	-2.60	-2.48
TT	x	x	x		x	x	x	
	2 Seed numbers			**Average**	**2 Seed numbers**			**Average**
BR	-3.19	-3.17	-3.16	-3.17	-2.61	-2.80	-2.86	-2.76
BT	-2.52	-2.63	-2.62	-2.59	-2.30	-2.51	-2.60	-2.47
TT	x	x	x		x	x	x	
	1 Seed numbers			**Average**	**1 Seed numbers**			**Average**
BR	-3.23	-3.19	-3.23	-3.22	-2.64	-2.79	-2.86	-2.76
BT	-2.53	-2.65	-2.65	-2.61	-2.31	-2.51	-2.60	-2.47
TT	x	x	x		x	x	x	
Average (BR)	-3.21	-3.17	-3.17		-2.64	-2.80	-2.86	
Average (BT)	-2.53	-2.62	-2.63		-2.30	-2.51	-2.60	
Average (TT)								

Table 6.1: Chute z velocities [m/s] for typical export cable 1 in shallow water ($30m$) and deep water ($150m$)

Table 6.1 gives a clear insight in the limiting chute z velocities for typical export cable 1, since the table essentially contains a summary of all graphs enclosed in Appendix E Appendix E.

From these results, several observations stand out. A first observation is that the TT limit is never breached. Whether a certain cable limit is breached is, of course, dependant on the static cable configuration and environmental loads (North Sea conditions) applied on the vessel.

A second observation is that between BR and BT the limiting failure criterion is BT (as BT is breached before BR is breached w.r.t. chute z velocities). This also all depends on the base case cable configuration that was modelled in combination with the applied hydrodynamic loading.

A third observation is that regarding the average over the amount of data points, indicated by the amount of seed numbers, seems to be consistent. This observation holds for both water depths, and for both BR and BT. Regarding binwidths, there is however some more variance within the quantified chute z velocities. In general differences between binwidths of $1m/s$ and $0.5m/s$ are bigger than the differences between binwidths of $0.5m/s$ and $0.25m/s$. This indicates that binwidth of $1m/s$ is too large. This phenomenon is also clearly observed in the presented percentile line graphs as shown in Figure 6.1 and Figure 6.2. Neighbouring bins are important for the percentile line to adapt a certain shape, and for binwidths of $1m/s$ the step is simply too inaccurate.

All together, the results of export cable 1 indicate the proposed method provides sufficient results when implementing a bin size of no less than $0.5m/s$. Besides, the number of modelled seed numbers does not seem to effect the quantified chute z velocities that much. In the end, the purpose of this chapter was to set up a proper method to quantify the limiting chute z velocities. Therefore, the

percentile line method is further investigated during verification and validation steps in the next section.

6.3. Verification and validation

There are several aspects within the proposed chute z velocity quantification that need to be verified and validated. Regarding verification, first the number of data points is investigated by means of a sensitivity study. Besides, the binwidths are studies in more detail as well. To validate, the percentile line method is performed for the three remaining subsea power cables as well to check whether the method provides proper and stable results.

6.3.1. Multiple subsea power cable validation

As already touched upon in the previous section, the quantified chute z velocities over the multiple amount of seed numbers actually does not differ that much. On the other hand, binwidth does have a significant impact on the determined chute z velocities. hence, a more detailed sensitivity study has been conducted. In Appendix E section E.3 the results of this analysis for all modelled subsea power cables are enclosed, both for shallow and deep water conditions.

This sensitivity analysis is based on the combination of the absolute error (between specific quantified chute velocity and chute z velocity average) and confidence intervals (CI's). The underlying formula is presented in Equation 6.3.

$$\text{CI} = 100 - \frac{ABS(\text{Chute z velocity} - \text{Averaged chute z velocity})}{\text{Averaged chute z velocity}} * 100\% \tag{6.3}$$

To determine these CI's, firstly the percentile line method needs to be executed on all subsea power cables, both in shallow and deep water. These results are presented in Table 6.2, Table 6.3, Table 6.4 and Table 6.5.

Quantified chute z velocity motions in [m/s] for inter-array cables in shallow water

Typical inter-array cable 1					Typical inter-array cable 2			
Bin width	**1 m/s**	**0.5 m/s**	**0.25 m/s**		**1 m/s**	**0.5 m/s**	**0.25 m/s**	
	5 Seed numbers			**Average**	**5 Seed numbers**			**Average**
BR	-2.30	-2.1	-1.99	-2.13	x	x	x	
BT	x	x	x		-2.27	-2.27	-2.28	-2.27
TT	x	x	x		5.01	4.94	4.79	4.91
	4 Seed numbers			**Average**	**4 Seed numbers**			**Average**
BR	-2.29	-2.09	-1.97	-2.12	x	x	x	
BT	x	x	x		-2.27	-2.23	-2.27	-2.26
TT	x	x	x		5.04	4.96	x	5.00
	3 Seed numbers			**Average**	**3 Seed numbers**			**Average**
BR	-2.28	-2.08	-1.96	-2.11	x	x	x	
BT	x	x	x		-2.29	-2.27	-2.28	-2.28
TT	x	x	x		5.04	4.96	x	5.00
	2 Seed numbers			**Average**	**2 Seed numbers**			**Average**
BR	-2.25	-2.07	-1.97	-2.10	x	x	x	
BT	x	x	x		-2.23	-2.22	-2.28	-2.24
TT	x	x	x		x	x	x	
	1 Seed numbers			**Average**	**1 Seed numbers**			**Average**
BR	-2.34	-2.05	-1.95	-2.11	x	x	x	
BT	x	x	x		-2.37	-2.27	-2.38	-2.34
TT	x	x	x		x	x	x	
Average (BR)	-2.29	-2.08	-1.97					
Average (BT)					-2.29	-2.25	-2.30	
Average (TT)					5.03	4.95	4.79	

Table 6.2: Results quantification method limiting chute z velocity [m/s] typical inter-array cables in shallow water

From Table 6.2 it stands out regarding typical inter-array 1 only the BR limit is breached, whilst regarding typical inter-array cable 2 BR is the only limit that is not breached. An explanation for this observation can be traced back to the differences in cable properties. For typical inter-array cable 2 the bending stiffness is higher than the bending stiffness of typical inter-array cable 1. This means that typical inter-array cable 1 is more flexible, hence will bend earlier. Moreover, whether certain cable integrity limits are breached all depends on the normal lay cable configuration and the specific cable properties.

There seems to be less variance in the averages over the columns (amount of seed numbers accounted for), than in the averages over the rows (binwidth). This indicates that the choice of binwidth has a larger effect on the quantified chute z velocities than the amount of simulated seed numbers.

Quantified chute z velocity motions in [m/s] for export cables in shallow water

Typical export cable 1					Typical export cable 2			
Bin width	**1 m/s**	**0.5 m/s**	**0.25 m/s**		**1 m/s**	**0.5 m/s**	**0.25 m/s**	
	5 Seed numbers			**Average**	**5 Seed numbers**			**Average**
BR	-3.20	-3.14	-3.15	-3.16	-1.44	-1.60	-1.65	-1.56
BT	-2.53	-2.60	-2.62	-2.58	-1.26	-1.40	-1.50	-1.39
TT	x	x	x		x	x	x	
	4 Seed numbers			**Average**	**4 Seed numbers**			**Average**
BR	-3.21	-3.14	-3.15	-3.17	-1.44	-1.60	-1.65	-1.56
BT	-2.54	-2.60	-2.63	-2.59	-1.25	-1.40	-1.50	-1.38
TT	x	x	x		x	x	x	x
	3 Seed numbers			**Average**	**3 Seed numbers**			**Average**
BR	-3.23	-3.19	-3.16	-3.19	-0.92	-1.59	-1.65	-1.39
BT	-2.55	-2.63	-2.64	-2.61	-0.80	-1.38	-1.49	-1.22
TT	x	x	x		x	x	x	
	2 Seed numbers			**Average**	**2 Seed numbers**			**Average**
BR	-3.19	-3.17	-3.16	-3.17	-1.03	-1.59	-1.66	-1.43
BT	-2.52	-2.63	-2.62	-2.59	-0.85	-1.38	-1.49	-1.24
TT	x	x	x		x	x	x	
	1 Seed numbers			**Average**	**1 Seed numbers**			**Average**
BR	-3.23	-3.19	-3.23	-3.22	-1.14	-1.61	-1.66	-1.47
BT	-2.53	-2.65	-2.65	-2.61	-0.92	-1.41	-1.50	-1.28
TT	x	x	x		x	x	x	
Average (BR)	-3.21	-3.17	-3.17		-1.19	-1.60	-1.65	
Average (BT)	-2.53	-2.62	-2.63		-1.02	-1.39	-1.50	
Average (TT)								

Table 6.3: Results quantification method limiting chute z velocity [m/s] typical export cables in shallow water

From Table 6.3 it is clear that for both typical export cables both BR and BT limits are breached. However, comparing the resulting chute z velocities of both cables there are major differences, almost a factor 2. This difference can also be traced back to the specific cable properties. Typical export cable 1 consists of three large cores whilst typical export cable 2 only has one single smaller core. Hence properties such as bending stiffness, weight in air and diameter are completely different.

Another observation is that the spread regarding the averages of typical export cable 1 is less than the spread regarding the averages of typical export cable 2, both w.r.t. column averages and row averages for binwidths of $1m/s$. This implies that this binwidth is simply to large to apply proper statistics.

Quantified chute z velocity motions in [m/s] for inter-array cables in deep water

Typical inter-array cable 1					Typical inter-array cable 2			
Bin width	**1 m/s**	**0.5 m/s**	**0.25 m/s**		**1 m/s**	**0.5 m/s**	**0.25 m/s**	
	5 Seed numbers			**Average**	**5 Seed numbers**			**Average**
BR	-1.69	-1.89	-1.85	-1.81	-2.48	-2.31	-2.24	-2.34
BT	-1.58	-1.79	-1.86	-1.74	-1.55	-1.78	-1.86	-1.73
TT	x	x	x		4.13	3.90	3.73	3.92
	4 Seed numbers			**Average**	**4 Seed numbers**			**Average**
BR	-1.76	-1.96	-1.85	-1.86	-2.48	-2.39	-2.27	-2.38
BT	-1.58	-1.79	-1.86	-1.74	-1.56	-1.78	-1.86	-1.73
TT	x	x	x		3.97	3.81	3.83	3.87
	3 Seed numbers			**Average**	**3 Seed numbers**			**Average**
BR	-1.77	-1.97	-1.85	-1.86	-2.48	-2.28	-2.22	-2.33
BT	-1.58	-1.79	-1.86	-1.74	-1.55	-1.78	-1.85	-1.73
TT	x	x	x		3.96	3.80	3.90	3.89
	2 Seed numbers			**Average**	**2 Seed numbers**			**Average**
BR	-1.77	-2.03	-1.86	-1.89	-2.48	-2.39	-2.24	-2.37
BT	-1.63	-1.82	-1.87	-1.77	-1.57	-1.79	-1.87	-1.74
TT	x	x	x		3.97	3.71	3.58	3.75
	1 Seed numbers			**Average**	**1 Seed numbers**			**Average**
BR	-1.80	-2.15	-1.86	-1.94	-2.51	-2.55	-2.29	-2.45
BT	-1.64	-1.83	-1.88	-1.78	-1.57	-1.79	-1.87	-1.74
TT	x	x	x		3.94	3.69	x3.60	3.74
Average (BR)	-1.76	-2.00	-1.85		-2.49	-2.38	-2.25	
Average (BT)	-1.60	-1.80	-1.87		-1.56	-1.78	-1.86	
Average (TT)					3.99	3.78	3.73	

Table 6.4: Results quantification method limiting chute z velocity [m/s] typical inter-array cables in deep water

From Table 6.4 it is clear that in deep water for typical inter-array cable 2 all cable integrity limits get breached, and for typical inter-array cable 1 TT is the only cable integrity limits that does not get breached.

An other observation is that regarding both inter-array cables, there seems to be less variance in the averages over the columns (amount of seed numbers accounted for), than in the averages over the rows (binwidth). This indicates that the choice of binwidth has a larger effect on the quantified chute z velocities than the amount of simulated seed numbers.

Quantified chute z velocity motions in [m/s] for export cables in deep water

Typical export cable 1					Typical export cable 2			
Bin width	**1 m/s**	**0.5 m/s**	**0.25 m/s**		**1 m/s**	**0.5 m/s**	**0.25 m/s**	
	5 Seed numbers			**Average**	**5 Seed numbers**			**Average**
BR	-2.65	-2.80	-2.86	-2.77	-1.21	-1.67	-1.75	-1.54
BT	-2.30	-2.51	-2.59	-2.47	-1.08	-1.49	-1.62	-1.40
TT	x	x	x		x	x	x	
	4 Seed numbers			**Average**	**4 Seed numbers**			**Average**
BR	-2.65	-2.81	-2.87	-2.78	-1.21	-1.67	-1.75	-1.54
BT	-2.29	-2.51	-2.59	-2.46	-1.09	-1.49	-1.62	-1.40
TT	x	x	x		x	x	x	
	3 Seed numbers			**Average**	**3 Seed numbers**			**Average**
BR	-2.65	-2.80	-2.86	-2.77	-1.19	-1.67	-1.75	-1.54
BT	-2.31	-2.52	-2.60	-2.48	-1.07	-1.50	-1.62	-1.40
TT	x	x	x		x	x	x	x
	2 Seed numbers			**Average**	**2 Seed numbers**			**Average**
BR	-2.61	-2.80	-2.86	-2.76	-1.25	-1.68	-1.76	-1.56
BT	-2.30	-2.51	-2.60	-2.47	-1.10	-1.51	-1.62	-1.41
TT	x	x	x		x	x	x	x
	1 Seed numbers			**Average**	**1 Seed numbers**			**Average**
BR	-2.64	-2.79	-2.86	-2.76	-1.29	-1.68	-1.76	-1.58
BT	-2.31	-2.51	-2.60	-2.47	-1.11	-1.52	-1.62	-1.42
TT	x	x	x		x	x	x	
Average (BR)	-2.64	-2.80	-2.86		-1.23	-1.67	-1.75	
Average (BT)	-2.30	-2.51	-2.60		-1.09	-1.50	-1.62	
Average (TT)								

Table 6.5: Results quantification method limiting chute z velocity [m/s] typical export cables in deep water

From Table 6.5 it follows that in no cases the subsea power cable's top tension is breached. In both cases only BR and minimum BT are breached, and in both cases BT is the limiting criterion since those chute z velocities are smaller than the limiting motions accompanying BR.

An other observation is that regarding both export cables, there seems to be less variance in the averages over the columns (amount of seed numbers accounted for), than in the averages over the rows (binwidth). This indicates that the choice of binwidth has a larger effect on the quantified chute z velocities than the amount of simulated seed numbers.

6.3.2. Data points and binwidth

Based on the chute z velocities as quantified for all four subsea power cables in the previous section, it seems that the chosen binwidth has more influence on the limiting chute z velocity than the amount of data points (indicated by modelled number of seeds). The sensitivity results regarding the CI's is enclosed in Appendix E section E.3.

The performed sensitivity analysis indicates that out of the conducted research most confidence intervals with respect to binwidth are high in the 90% range. However, for typical export cable 2 in shallow water, there are also some CI's as low as 65%. This means that for typical export cable 2 there were not enough data points to obtain robust results and there is quite some spread in the quantified chute z velocities.

Regarding the amount of modelled seed numbers, the performed sensitivity analysis indicates that out of the conducted research most confidence intervals with respect to amount of seeds are over 99%. An interesting observation is that for typical export cable 2 in shallow water (which also showed large spread regarding binwidth), the sensitivity analysis based on the amount of simulated seed numbers indicated good CI's.

Hence, these observations are in line with the previously determined results. The amount of modelled seeds has less influence on the quantification method than the chosen binwidth.

6.4. Conclusions

The goal of this chapter was to set up a robust chute z velocity quantification method, in which all cable integrity properties are converted into one chute z velocity limit. A probability of exceedance method to determine limits required specific vessel dependant RAO sets. Therefore, a percentile line is introduced. To compose this percentile line all extreme chute z velocities, obtained from OrcaFlex simulations, are split into multiple bins. Per bin, a certain $90^{th}_{percentile}$ is calculated, which represents a value for which 90% are above this value and the remaining 10% of the cases is under this value. By composing a linear line through all these percentiles per bin, eventually a percentile line is obtained. Subsequently, there are two parameters that are important regarding the introduced percentile line; binwidth and amount of data points. Based on the conducted research, the chosen binwidth has more influence on the precise chute z velocity quantification than the amount of data points.

With respect to the quantification method itself, the binwidth has a clear influence on the constructed percentile lines. Between binwidths of $1m/s$ and $0.5m/s$ the difference in chute z velocities is however larger than the difference between binwidths of $0.5m/s$ and $0.25m/s$. Hence, the quantified limiting motion seems to divert to a certain value. Therefore, binwidths must not be chosen larger than $0.5m/s$ for this method to provide robust results. Regarding the amount of data points per bin (indicated by the number of modelled seeds), there seem to be less differences in quantified chute z velocities. However, no minimum amount of data points could be indicated since this differs per modelled subsea power cable.

Therefore, to conclude this chapter, the introduced percentile line is indeed a method to obtain a better idea of the chute z velocities at which the cable integrity criteria (MBR, BT and TT limits) get breached. Besides, the method can also be used to quantify these limiting chute z velocities. Out of the three investigated binwidths, it follows that the method provides robust results based on binwidths no larger than $0.5m/s$. Regarding the minimum number of data points per bin, however, no precise amount of data points could be extracted since this is quite different for all the researched subsea power cables within this thesis. Moreover, the latter of course also depends on how accurate the final quantifications need to be.

7

Motion-based forecasting

In the previous chapter, a method was set up to quantify the occurring limiting motions during normal cable lay operations. This chapter covers a preliminary study to investigate the gain of implementing a motion-based forecasting approach within cable operation workability studies.

Instead of modelling entire 2D forecast spectra, a superimposed JONSWAP is created by means of wind waves and swell contributions. In the motion forecast model, this superimposed JONSWAP is compared against the original 1D JONSWAP. In total a period of 8 days is analysed, in which various wave conditions occur.

7.1. Wave spreading

In the current OrcaFlex simulations directional spreading is not accounted for as these simulations are based on a 1D JONSWAP spectrum, which are composed by one total sea state consisting of one H_s-T_p combination. However, this is just a simplification of the entire wave field, as a wave spectrum in reality is always 2D as there is always some case of directional wave spreading.

In order to obtain a 2D spectrum, a directional component needs to be accounted for. The general expression for a 2D wave spectrum is given below in Equation 7.1. [12, 13, 24, 47]

$$S(\omega, \theta) = S(\omega) * D(\theta) \tag{7.1}$$

All components in Equation 7.1 are briefly explained below.

- $S(\omega, \theta)$ Represents a function for the entire directional wave spectrum [m^{2}s]
- $S(\omega)$ Represents a wave spectrum [m^{2}s/rad]
- $D(\theta)$ Represents a directional spreading function [rad]

There is no exact formulation for spreading function $D(\theta)$. Research has proven that the maximum of this particular distribution is in the same direction as incoming wind, as usually wind induced waves travel in the wind direction, hence wave energy travels downstream. The most common applied spreading function is based on a $\cos$-squared component. The general expression is presented below in Equation 7.2. In some references, the same function is also referred to as $D(\theta) = \cos^{2s}\theta$. [12, 32, 60]

$$D(\theta) = \cos^{n}\theta \tag{7.2}$$

The components in Equation 7.2 above are explained briefly below.

- n Represents a certain spreading parameter [-]
- θ Represents the wave direction from the weather forecast [rad]

The effect of applying the directional spreading function is illustrated in Figure 7.1.

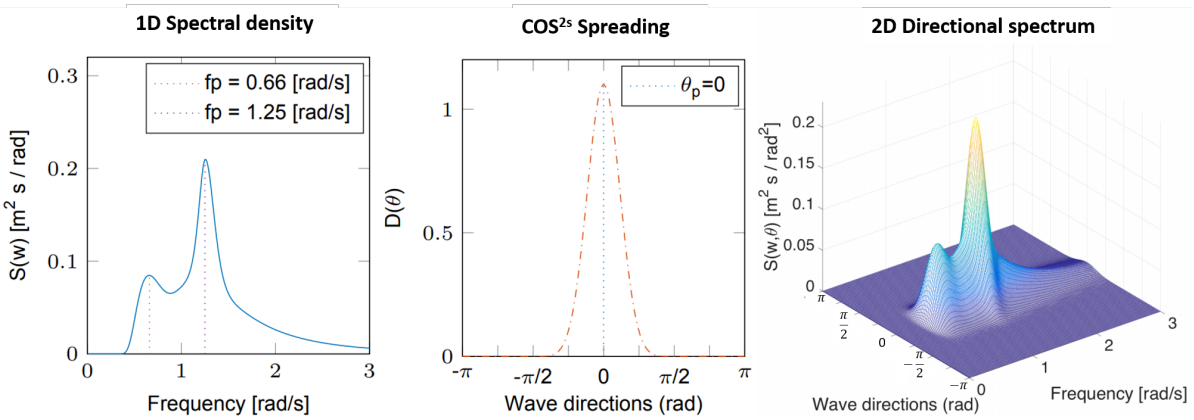

Figure 7.1: Combine 1D wave spectrum with directional wave spreading (cosine approximation) to obtain a 2D wave spectrum [24, 31, 33]

In the first graph (left) an example of a 1D spectral density of some wave field is shown. The effect of spreading function $\cos(\theta)$ is illustrated in the middle graph. The larger spreading parameter n is taken, the less directional spreading is applied. By combining the first two graphs, in the end the 2D spectrum is obtained.

The chosen value for spreading parameter n is of paramount importance since this factor has a large influence of the amount of applied directional spreading. For swell, usually a spreading parameter of $n = 10$ is used, and for wind waves a spreading parameter of $n = 4$ is applied. These factors are clarified by the fact that swell originate from a further location, hence are more developed waves. Therefore there is less wave spreading, hence a larger spreading factor is implemented. Wind waves, however, are less developed and so there is more spreading in these waves. [12]

7.2. Weather forecasts

Weather information is bought via specialized weather forecasting companies. These companies can provide location specific weather forecasts. In the current workability assessment, all calculations are performed based on the total sea states as defined by single $H_s - T_p$ combination to create a 1D JONSWAP spectrum. This 1D spectrum is modelled in OrcaFlex for various vessel headings (incident wave angles α). These $H_s - T_p$ combinations are provided for certain specific time periods of for example $\frac{1}{2}$ or 1 hour. Within this 1D JONSWAP, wave spreading is not accounted for.

Weather forecasters, however, can provide more detailed data including directional information and even entire 2D forecasts as well. Besides, more specific $H_s - T_p$ and θ combinations for wind waves and swell contributions can be provided. Differences between these wave types are clearly illustrated in Figure 4.1. Wind waves are rather young wind-induced waves, hence the wave periods are also rather short and there is a lot of directional spreading in these waves. Swell, however, originates from further locations so these waves are more developed leading to higher wave periods compared to wind waves. Besides, since swell originates from a storm somewhere far away there is less directional spreading. Moreover, the directions of wind waves and swell are not necessarily equal.

The combination of both wind waves and swell contributions therefore represented by a $H_s - T_p$ and θ combination for wind waves and a $H_s - T_p$ and θ combination for swell (for a specific time period). By incorporating the directional distributions of wind sea waves and swell, eventually a superimposed JONSWAP can be composed as stated in the DNV-GL codes (see Figure 7.3). [12]

7.2.1. Dataset

For this thesis, no entire 2D spectra have been used since there was no sufficient data available. Since this is merely a preliminary study to indicate the effects of implementing an entire motion-based forecasting method, a superimposed JONSWAP is created based on both wind waves and swell contributions.

In total 8 days of real forecasted data has been used (equal to 192 hours). This data contains total

sea state information listed per hour (one $H_s - T_p$ and θ combination). Besides, for each hour the wind and swell sea states are provided as well. All data is presented in Figure 7.2, containing four graphs each showing the total sea waves, wind waves and swell.

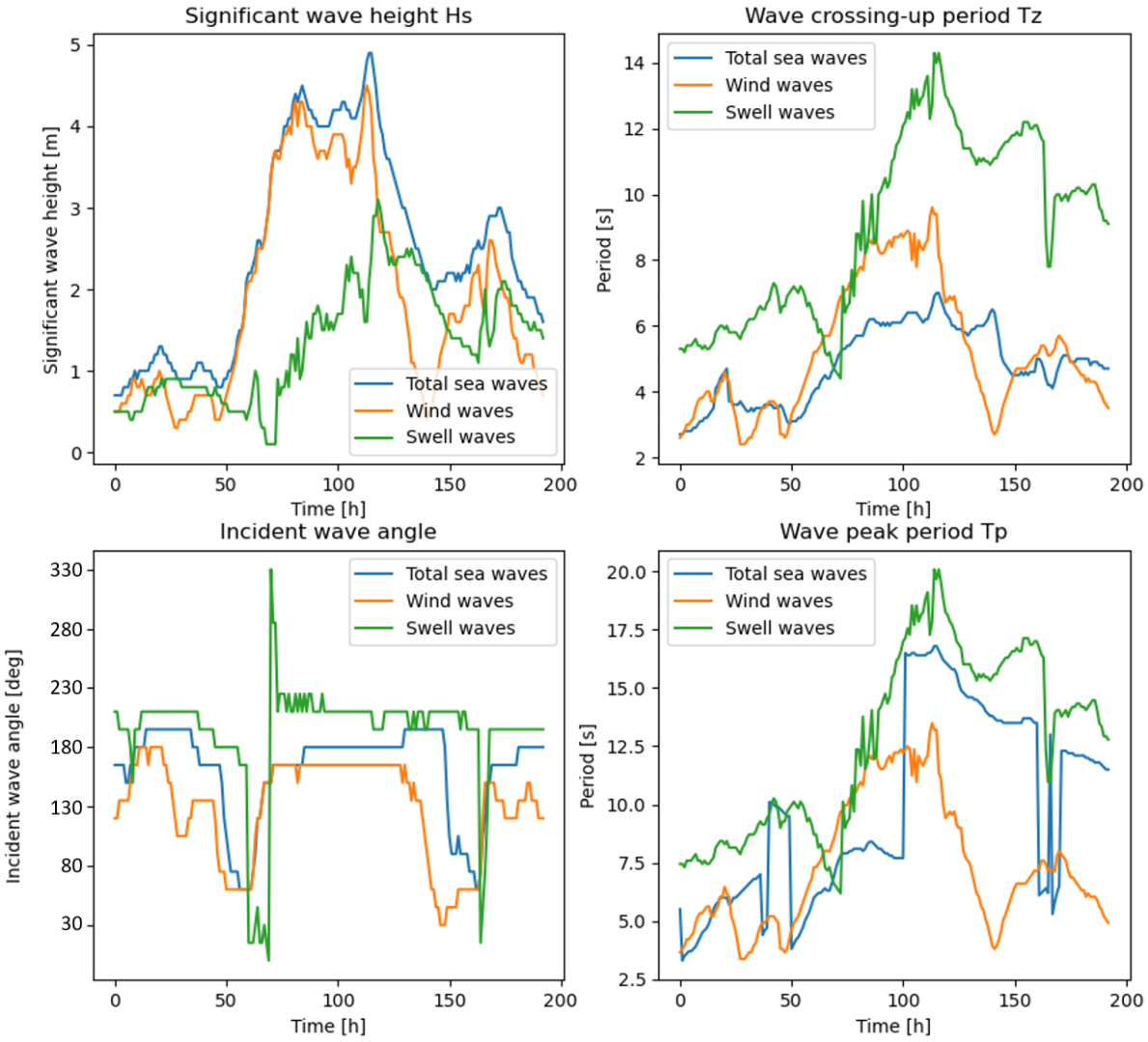

Figure 7.2: Real weather forecast information April 2^{nd} to April 8^{th}

From Figure 7.2 the precise differences between the total sea waves, wind waves and swell waves are illustrated. This dataset was chosen such that a significant wave height varying between $1m$ and $4m$ was covered, meaning there are obvious differences in environmental loading conditions.

From Figure 7.2, several observations stand out. Firstly, taking a look at the significant wave heights and wave periods (both T_p and T_z), it doesn't necessarily need to be the case that wind and swell wave data can simply be added or subtracted. These two contributions can either strengthen or weaken each other, which means that the total sea state does not always reveal to be the highest wave height (sometimes the total sea wave height coincides with wind sea wave height) or longest wave period.

Another remark is that wave directions, indicated as incident wave angle, indeed changes continuously over the total time of 192 hours. These directional differences are visualized in the next section.

The $T_p's$ for swell and wind waves were not part of the dataset, but the accompanying $T_z's$ is. The wave peak periods of swell and wind waves is calculated as if these were not part of the original dataset. These $T_p's$,for swell and wind waves, have been calculated by means of Equation 7.3. An iteration was carried out on the peak enhancement factor since γ depends on T_p.

$$\frac{T_z}{T_p} = 0.6673 + 0.05037\gamma - 0.006230\gamma^2 + 0.0003341\gamma^3 \qquad [12,\ 13]. \tag{7.3}$$

The components in Equation 7.3 above are explained briefly below.

- T_z Represents zero up-crossing wave period [s]
- T_p Represents wave peak period [s]
- γ Represents peak enhancement factor [-] (see Equation 4.4)

7.2.2. Differences total sea waves and superimposed wind + swell sea waves

From the dataset, observation hour 150 specifically, the 2D wave spectra for both total sea waves (Figure 7.3a) and the combination of wind waves and swell (Figure 7.3b) are illustrated below.

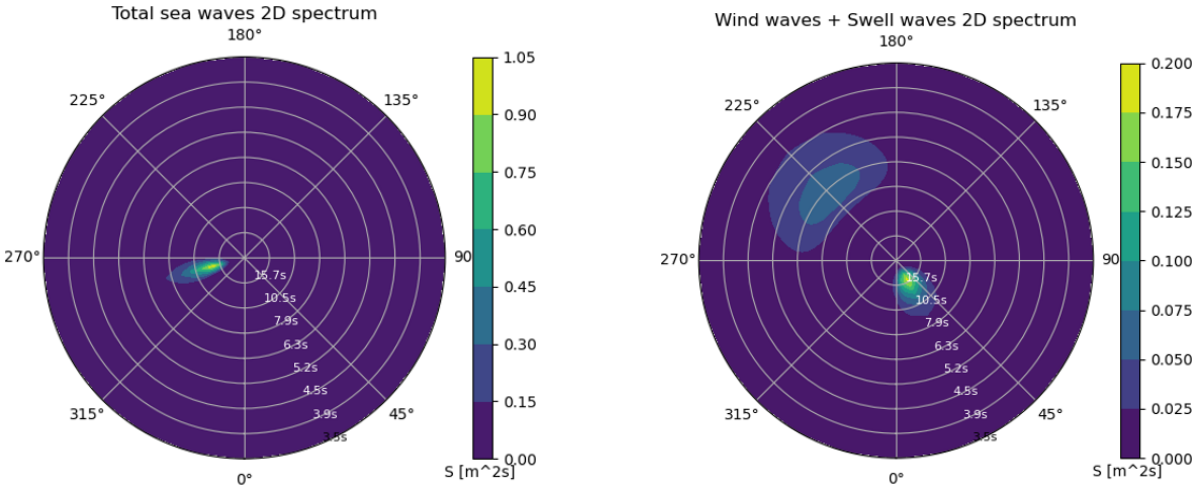

(a) 1D JONSWAP spectrum, total sea waves

(b) 2D superimposed JONSWAP spectrum, wind waves + swell

Figure 7.3: Differences 1D JONSWAP and superimposed 2D JONSWAP

In this figure, the same sign conventions as presented in subsection 4.3.1 are applied. Besides, the wave energy is visualised by means of the colorbar, and the radial axis contains the wave period.

Based on Figure 7.3, there is a big difference regarding both wave directions and wave energy in the spectra. In Figure 7.3b the upper more spread wave field represents wind waves, and the more dense wave field represents swell (please note that the wave period increases inwards the radial axis).

7.3. Motion forecast model

Based on the 1D JONSWAP's and 2D superimposed JONSWAP's, all $192 hours$ of data are modelled in a frequency-domain vessel motion analysis. This is done by means of Python, in which the Living Stone and corresponding RAO sets were implemented. There is no need for a FFT since the JONSWAP spectrum is a representation of the sea state in the frequency-domain.

In order to simulate the maximum occurring chute z velocities, MPM factors are included as well. The DNV-GL prescribed 3-hour MPM is accounted for, based on the calculated T_z. This means, that for every hour, the 3-hour MPM factor slightly changes.

In the end, the resulting chute z velocities need to be compared to some determined chute z velocity limit. For this study, based on the results of the studied quantification method, a limiting chute z velocity of $2m/s$ is chosen. The results of chapter 6 indicated some higher and lower values, hence $2m/s$ seems like a proper starting point for this specific model.

If this $2m/s$ chute z velocity limit is exceeded, operations cannot take place, and if the limit is not exceeded operations can take place.

7.4. Results

This section contains the chute z velocity forecast results. All these results are presented by means of four individual graphs. In the first two graphs, the chute z velocity is plotted for five different vessel headings for both the total sea state and the swell + wind sea state. This is done to get an idea of how the chute z velocity changes over time for multiple vessel headings.

The last two graphs contain the entire motion forecast for every possible vessel heading (also for both the total sea state and the swell + wind sea state). The colors are based on the chute z velocity. As explained in the model set up, when the chute z velocity exceeds $2m/s$, the model regards this vessel heading as not workable. These motion forecasts contain every possible vessel heading, from 0 to 360 degrees. Obviously, the determined chute z velocity criterion of $2m/s$ will be crossed in some occasions. However, as this criterion represents a hard limit, the colorbar does not provide information above chute z velocities over $2m/s$.

7.4.1. 3-hour MPM motion forecast

The results of the 3-hour chute z velocity forecasts are presented in Figure 7.4.

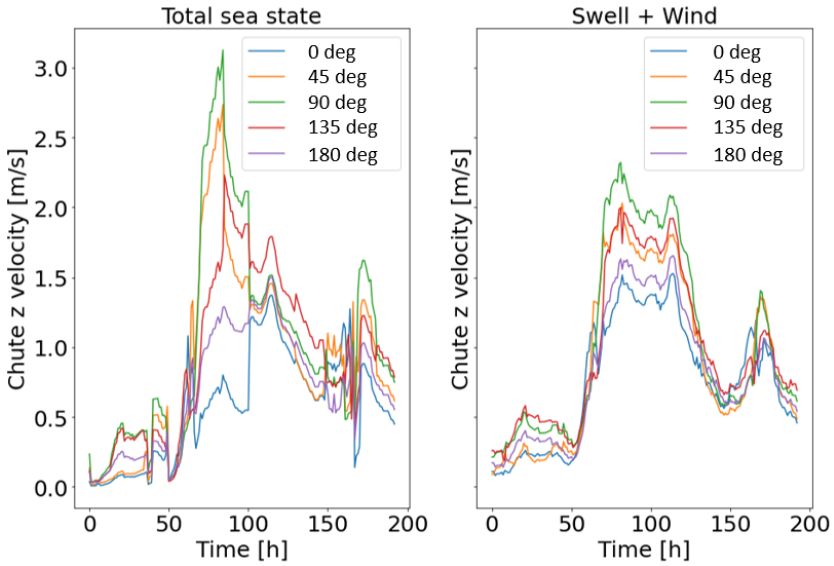

(a) Chute z velocities for 5 different vessel headings

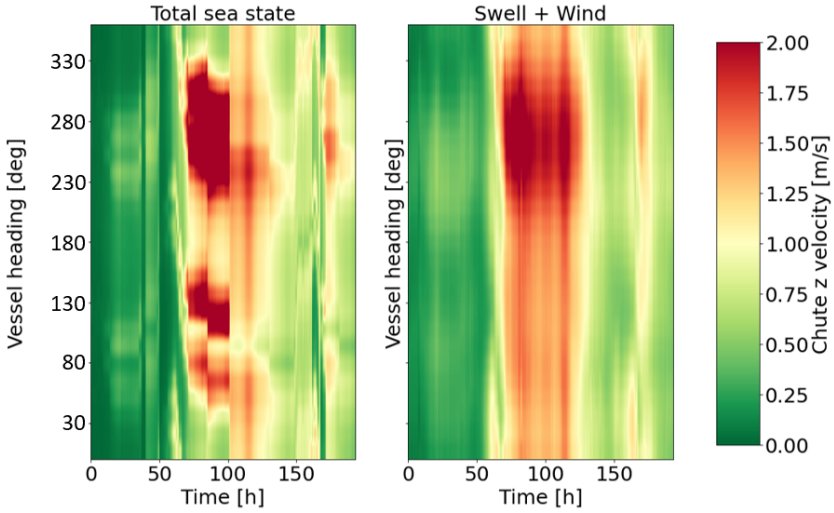

(b) Total chute z velocity forecasts

Figure 7.4: 3-hour MPM chute z velocity response forecast

7.5. Conclusions

Comparing the total sea states (left figures) with the swell + wind (right figures), there are some noticeable observations. The motions forecast based on the superimposed swell + wind sea JONSWAP's looks more smoothed than the forecast representing total sea states. Figure 7.4a clearly indicates that the higher peaks from the total sea state chute z velocity forecast are somewhat downscaled in the swell + wind sea states. Also, the lower peaks from the total sea state forecast seem a bit upscaled in the swell + wind sea state.

This smoothing occurrence is also clearly visible in Figure 7.4b. What this smoothing occurrence essentially comes down to is that when changing the vessel heading direction based on the swell + wind sea state, the effect on the chute z velocity is less compared to changing vessel heading based on the total sea state.

Another observation is that for both methods in general the sea state forecasts actually do not differ that much from each other. Therefore, the current total sea state method does provide proper outcomes. The obtained results, however, indicate that optimization is possible by splitting the total sea states into both swell and sea waves contributions and accounting for wave spreading. For example, taking a look around modelled hour 75 in Figure 7.4, an operation with heading restriction at $135deg$ could not be performed when workability is based on the total sea states, but in case workability would be based on swell + wind waves sea states the operation would be possible.

8

Discussion

This chapter contains a discussion of the conducted theoretical aspects, data collection, modelling choices, results and interpretation covered in this thesis. The sections are structured in line with the thesis reading guide (which is at its turn based upon the composed research questions presented in section 2.3).

8.1. Subsea power cables and cable integrity

No two power cables are completely identical due to differences in project requirements, specifications, manufacturers and materials. Within this research, four typical power cables are investigated (two inter-array cables and two export cables). Cable manufacturers, however, also keep innovating themselves hence the modelled cables within this thesis remain just a few out of many possible subsea power cables types. Consequently, one main experimental subsea power cable was chosen and the remaining three have been used for verification and validation purposes.

Eventually, for normal cable lay operations all mechanical processes and cable limits are covered by three main cable integrity criteria (MBR, BT and TT limits). These three limits are also the three main integrity limits implemented in the current workability assessment. By implementing motion-based forecasting (MBF), however, these cable integrity limits are eventually converted into one limiting chute z velocity which needs to be monitored.

8.2. OrcaFlex modelling

Obviously, it is rather difficult to completely mimic nonlinear offshore operations. Within this thesis a lot of OrcaFlex simulations have been conducted. OrcaFlex is a widely applied software package developed especially for the offshore industry covering dynamic analysis of offshore marine systems such as cables, risers and anchor-systems. Hence, this software itself is verified and validated against other software packages and real-time data for various operations. Although OrcaFlex is widely used in the offshore industry, there are also some limitations which must be mentioned.

The first, and arguably most important limitation, is that there is always some kind of randomness involved regarding wave train set up. This makes it hard to compare OrcaFlex results with other tools. However, since this thesis was entirely conducted using OrcaFlex and for quantification of limiting chute z velocities percentile statistics have been incorporated as well, the comparisons remain viable.

A second limitation is that numerical errors can occur by running too large time steps in time-domain simulations. OrcaFlex cable modelling is performed in the time-domain, and the software is created in such a manner that calculations can be solved as much as possible. However, in some cases the modelled time step does provide outcomes, but these results are not viable since there is an underlying numerical error. Therefore, the time histories of the simulated OrcaFlex files are thoroughly checked for the 'worst' incident wave angles, 60, 120, 210 and $270deg$. If a certain $H_s - T_p$ combination shows a numerical error (a large inexplicable peak in e.g. top tension), all other larger wave heights and periods will most likely contain a numerical error as well. These specific cases need to be re-simulated with a smaller time step and then checked again for numerical errors. Throughout this thesis the most common cases that generate numerical errors have been checked, but it can not be guaranteed that

no numerical errors still exist somewhere. Consequently, not every OrcaFlex simulation was executed based on the same time step.

One of the goals within this thesis was to gain insight in a relation between cable integrity and maximum vessel motions. Therefore, a lot of OrcaFlex simulations have been performed and only the extreme occurring motions per different OrcaFlex case have been gathered. Another manner to gain insight in a relation between cable integrity and vessel motions, is to gather much more data out of the executed 3-hour sea state OrcaFlex simulations. This way the focus is more on entire relations and less on extreme motions.

8.3. Identification analysis

To identify a certain motion as a predictor to implement into MBF, 12 different chute motions have been studied. Three of these are related to motions in cable departure directions (chute cable motions). To calculate these chute cable motions, the departure angle is required. For this thesis, this departure angle was chosen as the static departure angle resulting from the static cable configuration layout. In reality this angle is obviously not static at all, but changing continuously due to both vessel and cable movements. This means that the cable departure angle is in fact not a static angle, hence the static angle applied in this research is an approximation for simplicity reasons. Therefore, the resulting motions in cable departure direction provide merely a prediction. Moreover, it would be difficult to implement motions in the direction of cable departure in MBF. Predicting and converting vessel motions from the COG to chute motions at the chute is merely a translation of the vessel motions which can simply be implemented into a MBF method. Predicting the cables departure angle based on weather forecasts, however, is a totally different process as both the vessel and the cable will move due to environmental wave loading. The vessel motions can be predicted, but the cable motions are not that straightforward to forecast.

Another aspect to highlight is the applied line of best fit. Based on some quick tests, exponential LMS fitting indicated to be the best LMS method to incorporate into this thesis. This LMS method does result in a rather good line, but taking a better look at the scatter graphs indicates that the function does not hold that well for every case. Regarding MBR, the tail in higher chute z velocities is not always represented that well, and the same holds for the other tail in the lower chute z velocities. For bottom tension, especially regarding the inter-array cables, again the tail in the higher chute z velocity region is not represented that well.

In the conducted research, chute z velocity was eventually chosen as a proper limiting motion predictor. Therefore, in the following steps only the chute z velocity motion has been investigated.

8.4. Quantification method

In order to quantify the investigated limiting motion, multiple seed numbers have been simulated in OrcaFlex to obtain more data around the limit. As aforementioned, however, there are more options to obtain more data points by not focusing on the extremes per 3-hour simulation but extracting more data points from this 3-hour analysis as explained in section 8.2.

To finally draw a certain percentile line, a certain percentile needs to be chosen. Within this thesis the 90^{th} percentile has been chosen since this in line with DNV-GL standards. However, this is merely a guideline than a rule. Therefore, implementing e.g. a 80^{th} percentile line, workability would increase but the amount of failing cases would be higher as well. Hence, the higher this percentile is chosen, less failing cases will be allowed. Consequently, the lower the this $q^{th}_{\lfloor percentile}$ is chosen the higher the eventual workability will be.

Besides, when setting up this percentile line some type of interpolation needs to be implemented between the two cornering data points. Linear interpolation has been applied in this research since the cornering data points are relatively close to each other. There are, however, more interpolation methods such as lower, higher, midpoint and nearest neighbour interpolation methods.

As addressed in the thesis, the influence of outliers needs to be accounted for as well. Regarding the proposed method, outliers do not have much influence as long as they are not part of the used 90^{th} percentile indices. If an outlier would be part of the interpolation, this would result in inaccurate chute z velocities.

Three different binwidths have been investigated; a binwidth of $1m/s$, a binwidth of $0.5m/s$ and at last a binwidth 0f $0.25m/s$. Obviously, there are much more variations possible. However, these bin-

widths were chosen as they each represent a factor divided by 2. Choosing binwidth is dependant on how accurate the final quantified chute z velocity needs to be. To quantify based on smaller binwidths, however, in general more data points are required. As the quantified chute z velocity results showed sufficient results for these binwidths, no further binwidths have been analysed.

The conducted quantification method is only based on one vessel since only verified and total information of one CLV was available. For the identification step another vessel has been modelled to verify the identified limiting motion. This other CLV, however, is not operational at the moment and the accompanying RAO's and QTF's are therefore not completely verified and validated. Hence, this other vessel was not incorporated in the quantification step of this thesis.
Whether MBR, minimum allowable BT or maximum allowable TT is limiting depends on cable properties and offshore operation type. In this research, top tension was never assigned as the governing criterion, but this does not necessarily mean it never is. For example, in very harsh conditions (a storm) and when the CLV has to go into survival mode, top tension does get very important. The fact that within all investigated cable cases TT is never limiting is hence merely a coincidence, as this depends on subsea power cable properties and offshore circumstances.

8.5. Motion-based forecasting

Unfortunately no entire 2D wave spectra data were available to investigate during this research, hence the conducted research is merely an exploratory step. The current 1D JONSWAP workability study is compared to a superimposed JONSWAP in which both swell and wind sea waves are combined. Moreover, by means of applying standard directional spreading parameters on this superimposed JONSWAP a 2D wave spectrum was mimicked. Subsequently, this mimicked 2D spectrum is still based on a standard JONSWAP spectrum, hence still an simplification/indication of the real 2D wave spectrum.

Moreover, the investigated data set to compose these 1D and 2D spectra consisted of a total period of $8days$ (with a time step of $1hour$). Thus in total $192hours$ of workability studies based on a 1D JONSWAP and a 2d superimposed JONSWAP have been compared. Although the results indicated a clear difference, the total time period of $8days$ remains rather short.

Once again, it must be noted that the implemented MBF method provides merely preliminary results as the superimposed 2D spectrum is still based on standard JONSWAP shapes.

9

Conclusions and recommendations

The growing demand for subsea power cables triggers both offshore contractors and subsea power cable manufacturers to keep developing themselves. Since this thesis was conducted at an offshore contractor, the focus of this thesis was on workability studies. The current 1D JONSWAP approach does provide proper outcomes, but there are always manners to optimize the margins. Within this thesis, a MBF method is implemented in workability studies in order to investigate whether this could optimize subsea power cable installation operations.

This chapter covers both the final conclusions of the conducted research and recommendations for further research. Before presenting the final conclusions and recommendations, the main research question as defined in section 2.3 is repeated and additionally the sub-questions are repeated as well. The main research question is:

How is workability of offshore cable installation improved by shifting workability towards local limiting motions at the chute instead of the conventional workability method?

Pursued by the following sub-questions:

1. Which mechanical properties and processes determine subsea power cable integrity during offshore cable installation?
2. Which occurring motions at chute level are limiting per cable failure mechanism during the normal cable laying procedure?
3. How can the values of these limiting vessel motions at chute level be quantified?
4. How can the offshore installation workability in practice be improved by implementing motion-based forecasting combined with limiting motions compared to the conventional workability analyses?

9.1. Conclusions

The conclusions are presented per sub-question in the next four sections.

9.1.1. Cable integrity limits

Based on a literature study and inhouse knowledge, in the end three main cable integrity criteria for normal cable lay operations have been identified. Together, these three cover all mechanical processes and cable properties within normal lay operations.

- Minimum bending radius $[m]$ occurring over entire cable length from chute to TDP
- Minimum bottom tension $[kN]$ at TDP
- Maximum top tension $[kN]$ at the chute

These cable integrity limits are independent of each other, meaning they do not strengthen or weaken each other.

Regarding MBR, BT and TT, both extreme maximum and extreme minimum motions need to be investigated since not all maximum positive and maximum negative motions within one wave are precisely opposite to each other. Since both MBR and BT become most critical during downward chute motions, these motions are investigated looking into negative maximum motions. However, top tension becomes critical when the CLV's chute is moving upwards, hence positive motions need to be investigated.

9.1.2. Limiting motion during normal cable laying operations

For this research, the chute motions have been investigated to obtain an overall limiting chute motion, covering both BR, BT and TT limits. Out of all 12 distinguished chute motions eventually chute z velocity (vertical velocity [m/s] at the chute) is indicated as the limiting motion during normal cable lay operations.

The results of the limiting motion identification analysis indicate that both chute z velocity and chute cable velocity (in the direction of cable departure) indicate very good relations to all three cable integrity limits. These two motions are highly correlated since chute z velocity has a major contribution in constructing the chute cable velocity. Moving towards deeper water, this correlation gets higher and higher since chute x velocity is overruled by chute z velocity contribution as the cable is leaving the chute more vertically. Since offshore chute z motions are much more easy to measure and interpret than chute cable motions, the chute z velocity was indicated as the best predicting limiting motion. Besides, the constructed chute cable motions are merely estimations since these have been calculated based on a static cable departure angle. In reality, however, this angle will never be static but continuously change due to the CLV's motion responses.

9.1.3. Motion quantification method

Within this thesis a percentile line method is introduced in order to quantify the limiting chute z velocities. To compose this percentile line, all extreme chute z velocities obtained from OrcaFlex simulations are split into multiple bins. Per bin, a certain $90^{th}_{percentile}$ is calculated, which represents a value for which 90% are above this value and the remaining 10% of the cases is under this value. By composing a linear line through all these percentiles per bin, eventually a percentile line is obtained.

Based on the conducted research, it shows that the chosen binwidth has more influence on the precise chute z velocity quantification than the amount of data points. With respect to the quantification method itself, the binwidth has a clear influence on the constructed percentile lines. Between binwidths of $1m/s$ and $0.5m/s$ the difference in chute z velocities is however much larger than the difference between binwidths of $0.5m/s$ and $0.25m/s$. Hence, the quantified limiting motion seems to divert to a certain value. Therefore, binwidths must not be chosen larger than 0.5m/s for this method to provide robust results.

Regarding the amount of data points per bin, there seem to be less differences in quantified chute z velocities. However, no minimum amount of data points could be indicated since this differs per modelled subsea power cable.

The introduced percentile line is indeed a method to obtain a better idea of at which chute z velocities cable integrity criteria get breached. Besides, the method can also be used to quantify these limiting chute z velocities. To obtain precise guidelines that can be followed, however, more research is required.

9.1.4. Implementation of motion-based forecasting

Based on the chute z velocity forecasting model, it can be concluded that accounting for wave spreading and splitting the total sea states into swell and wind wave contributions, has a smoothing effect on workability studies. This means that when changing the vessel heading direction based on a superimposed 2D swell + wind sea state, the effect on the chute z velocity is less compared to changing vessel heading based on the 1D total sea state. Essentially, the higher chute z velocity peaks from the 1D total sea state are downscaled when accounting for wave spreading, whereas the the lower chute z velocity peaks from the 1D total sea state are upscaled when accounting for wave spreading. Based on this research, it can be concluded that for both methods the sea state forecasts actually do not differ that much from each other. Therefore, the current total sea state method does provide proper outcomes.

The obtained results, however, indicate that optimization is possible by splitting the total sea states into both swell and sea waves contributions and accounting for wave spreading.

9.2. Recommendations

The main idea behind the research described in this thesis was to investigate the possibility of implementing MBF in subsea power cable operations, and subsequently explore what the effect on workability will be when implementing a MBF approach. During this thesis several aspects for future research came forward.

9.2.1. Verification and validation

At first, five general recommendations are presented which are all focused on more verification and validation.

To start, more subsea power cables need to be assessed. In this research four typical cables, two inter-array and two export, have been assessed but each cable shows different behaviour as no two cables are completely identical.

Another recommendation is to simulate more divergent cable lay configurations. Based on the results of this thesis, the maximum top tension is never the limiting failure criteria. This does not necessarily imply that top tension is never the limiting factor. Therefore, by investigating more diverse cable lay configurations (essentially more cable catenary shapes) a more overall picture can be obtained.

Moreover, this thesis only focuses on normal cable laying operations. It would be interesting to investigate whether chute z velocity is also a good limiting motion predictor during a 1^{st} and 2^{nd} end pull in and other more specialized cable operations.

Another aspect is that the entire research is conducted by modelling the same CLV for all cases. Therefore, it is recommended to also repeat the identification and quantification steps taken in this thesis for a completely different CLV to check how these results relate to one another.

At last, the MBF introduced in this thesis is merely a preliminary study. To investigate the effect of implementing a MBF method better, total 2D wave spectra data is required which is not based on standard JONSWAP spectrum assumptions.

9.2.2. Cable integrity limits

Subsea power cable manufacturers are somewhat secretive regarding precise cable limit calculations and applied safety factors. For their workability studies, offshore contractors depend completely on the cable data provided by the cable manufacturers. Therefore, it is recommended to either work more closely with the cable manufacturers or start inhouse tests to verify these cable limits. Gaining more knowledge of where such cable limits originate from could provide new insights which can be further developed into workability studies. Actively contributing in JIP's also provides new industry insights and could lead to new collaborations.

9.2.3. Limiting motion identification

Within this research, the identification of which chute motion shows the best correlation with the cable integrity criteria is merely based on an LMS method combined with a regression analysis. Out of all OrcaFlex simulations, only the extreme occurring chute x, chute y and chute z motions have been gathered. The overall link between cable integrity and vessel motions can therefore be further expanded, by not only investigating the maximum occurring motions but the overall relations between cable integrity and vessel motions. Moreover, in the presented scatter graphs multiple data points, representing various motions, are extracted from the same Orcaflex cases. Hence another opportunity for future work is to check how these different motions can be combined to better understand cable behaviour. To clarify, in this analysis, vertical motions have been split into three chute z motions (motion itself, motion velocity and motion acceleration). However, these three might correlate with each other and sa deeper 3D matrix analysis might provide more insights regarding the limiting motion.

Another point for future work is related to the MBR cable integrity limit. In the presented scatter graphs, for higher motions the BR indicates asymptotic behaviour towards the MBR limit. This can be clarified by the fact that at a certain point the cable just cannot bend further. However, due to these asymptotes, the precise cable behaviour is hard to observe. Future work can be performed by diving more into this asymptotic behaviour in order to explain this phenomenon better.

9.2.4. Limiting motion quantification

Within this thesis, the introduced percentile method has been used to determine the final limiting chute z velocities. There are, however, multiple variables to compose this percentile line depending on chosen $q^{th}_{percentile}$, binwidth and amount of data points per bin. Within this research, only $90^{th}_{percentile}$ have been investigated. Future work could investigate the sensitivity of this percentile. Besides, no precise minimum amount of data points per bin could be determined to produce robust results. This is also an aspect that could be further investigated.

Besides, future work could be focused on an other method for quantification of the limiting motions. As aforementioned, there is a frequently applied method based on the probability of exceedance of certain motions. This method was not applied in this thesis because vessel dependant RAO sets are incorporated in the calculation. It would, however, still be interesting to also quantify the limiting chute z velocity based on a max probability of exceedance of 10% and comparing these to obtained limiting motions resulting from the introduced percentile line method.

9.2.5. Motion-based forecasting implementation

Based on the conducted research, the most important recommendation is to implement entire 2D wave spectra forecasts (and not superimposed JONSWAP's combined with a wave spreading factor). By eliminating the basic JONSWAP spectral shape from the forecast and implementing entire 2D spectra, the workability assessment is modelled closer to real sea states.

Bibliography

[1] World Maritime Affairs. Ship motion: 6 degrees of freedom (dof), 2019. URL https://www.worldmaritimeaffairs.com/ship-motion-6-degrees-of-freedom-dof/.

[2] International Energy Agency. World energy outlook 2019, 2019. URL https://www.iea.org/reports/world-energy-outlook-2019.

[3] A.W. Lewis; R.N. Allos. *JONSWAP's parameters: sorting out the inconsistencies*. Ocean Engineering, 1990.

[4] Q. Bai; Y. Bai. *Subsea Pipeline Design, Analysis, and Installation*. Elsevier, 2014.

[5] A. Bhande. *What is underfitting and overfitting in machine learning and how to deal with it*. Medium Greyatom, 2018.

[6] Offshore Wind Programme Board. *Overview of the offshore transmission cable installation process in the UK*. Offshore wind Programme Board, 2015.

[7] A. Pegalajar-Jurado; M. Borg; H. Bredmose. *An efficient frequency-domain model for quick load analysis of floating offshore wind turbines*. European Academy Of Wind Energy, 2018.

[8] I. Komusanac; D. Fraile; G. Brindley. *Wind energy in Europe in 2018; trends and statistics*. Wind Europe, 2019.

[9] United Nations Climate Change. What is the paris agreement?, 2015. URL https://unfccc.int/process-and-meetings/the-paris-agreement/what-is-the-paris-agreement.

[10] Cigre. *Recommendations for mechanical testing of submarine cables*. Technical report, Working group B.1.43, 2015.

[11] F. Diepenmaat. *MSc. Thesis Literature Study - Optimizing Offshore Cable Operations - A study Identifying, Quantifying and Implementing Limiting Motions within Conventional Cable Laying*. TU Delft, DEME Offshore, 2020.

[12] DNV-GL. *Recommended practice DNV-RP-C205 - Environmental conditions and environmental loads*. DNV-GL, 2010.

[13] DNV-GL. *DNVGL-ST-N001 Marine operations and marine warranty (Edition: 2016-06)*. DNV-GL, 2016.

[14] DNV-GL. *Energy Transition Outlook 2019 Executive Summary - A global and regional forecast to 2050*. DNV-GL, 2019.

[15] DNV-GL. What is the difference between a frequency domain and a time domain mooring analysis?, 2020. URL https://www.dnvgl.com/software/FAQ/What-is-the-difference-between-a-frequency-domain-and-a-time-domain.mooring-analysis.html.

[16] Minitab Blog Editor. Regression analysis: How do i interpret r-squared and assess the goodness-of-fit?, 2013. URL https://blog.minitab.com/en/adventures-in-statistics-2/regression-analysis-how-do-i-interpret-r-squared-and-assess-the-goodness-of-fit.

[17] K. Eigenraam. *Partly submerged crane suspended jacket*. Delft University of Technology & Heerema Marine Contractors, 2020.

[18] MO4 Next Level Forecasting. *MO4 Business Case Offshore Wind Part 1: Cable Lay*. MO4 Next Level Forecasting, 2018.

[19] L. Renforth; M. Seltzer-Grant; M. Foxall. *Experiences in the Condition Monitoring and Testing of Subsea High Voltage Cables in the UK Offshore Industries*. HVPD Ltd Manchester, UK, 2019.

[20] DEME Group. About deme group - activities, 2013. URL https://www.deme-group.com/#paragraph-112.

[21] DEME Group. Living stone - dp3 cable installation & multipurpose vessel - technology specifications facts, 2021. URL https://www.deme-group.com/technologies/living-stone.

[22] Westwood Global Energy Group. Offshore wind propels subsea cable demand, 2018. URL https://www.westwoodenergy.com/reports/subsea-cable-tracker-2018-2022.

[23] J. Herdiyanti. *Comparisons Study of S-Lay and J-Lay Methods for Pipeline Installation in Ultra Deep Water*. Universititet i Stavanger, Facultie of Science and Technology, 2013.

[24] L.H. Holthuijsen. *Waves In Oceanic And Coastal Waters*. Cambridge University Press, 2007. ISBN 978-0-521-86028-4.

[25] P. Homewood. Hornsea offshore wind farm opens–at huge cost to energy customers, 2019. URL https://notalotofpeopleknowthat.wordpress.com/2019/06/06/hornsea-offshore-wind-farm-opens-at-huge-cost-to-energy-customers/.

[26] J.M.J. Journee; W.W. Massie; R.H.M. Huijsmans. *OFFSHORE HYDROMECHANICS Third Edition*. Delft University of Technology, 2015.

[27] International Renewable Energy Agency (IRENA). *Perspectives For The Energy Transition - Investment Needs for a Low-Carbon Energy System*. International Energy Agency (IEA) and International Renewable Energy Agency (IRENA), 2017.

[28] W.J. Pierson; G. Neumann; R.W. James. *Practical Methods for Observing and Forecasting Ocean Waves by Means of Wave Spectra and Statistics*. Washington, US, 1955.

[29] I. Jonoski. *Fatigue analysis for offshore power cable installation*. Delft University of Technology & DEME Offshore NL, 2020.

[30] J. Kenney; E. Keeping. *Mathematics of Statistics. Volume 1*. D. Van Nostrand Company, Princeton, 1962.

[31] Orcina Ltd. United Kingdom. Orcaflex help manual 10.3e, 2020. URL https://www.orcina.com/webhelp/OrcaFlex/Default.htm.

[32] M.S. Longuet-Higgins. *Observations of the Directional Spectrum of Sea Waves Using the Motions of a Floating Buoy*. Ocean Wave Spectra, Prentice-Hall Inc., Englewood Cliffs, 1963.

[33] A. Lotgering. *Can motion measurements during an offshore heavy lift operation on-line help to make a more accurate prediction of the vessel response and decision making operation*. Mocean & Delft University of Technology, 2017.

[34] McKinsey. *Global Energy Perspective 2019: Reference Case*. Energy Insights by McKinsey, 2019.

[35] H. Mitsuyasu. *On the growth of spectrum of wind-generated waves (I)*. Kyushu University, Reports of Research Institute for Applied Mechanics, 1968.

[36] H. Mitsuyasu. *On the growth of spectrum of wind-generated waves (II)*. Kyushu University, Reports of Research Institute for Applied Mechanics, 1969.

[37] Python NumPy Module. *Statistics - NumPy API reference - numpy.percentile*. Python NumPy Module, 2021.

[38] W.J. Pierson; L. Moskovitz. *A proposed spectral form for fully developed wind seas based on the similarity theory of S. A. Kitaigorodskii*. J. Geophys. Res., 1964.

[39] W.H. Munk. *Origin and generation of waves*. Proc. 1st Conference Coastal Engineering (Long Beach), New York, ASCE, 1950.

[40] P. Naaijen. *Course Notes; Motions and Loading of Structures in Waves, Part I MT44020 2019-2020*. Delft University of Technology, 2019.

[41] T. Nakajima. *On the Dynamic Analysis of Multi-Component Mooring Lines*. University of Tokyo, 1982.

[42] R. Newson. *Robust confidence intervals for median and other percentile differences between groups*. State Technical Bulletin, 2000.

[43] R. Newson. *Confidence intervals for rank statistics: Percentile slopes, differences, and ratios*. The Stata Journal, 2006.

[44] U. Oberst. *The Fast Fourier Transform*. Society for Industrial and Applied Mathematics, 2007.

[45] D. Prasanna. The ships motions at sea, 2014. URL `https://hubpages.com/travel/theshipsmotionsatsea`.

[46] C. Rice. Wire rope discard standards, 2017. URL `https://www.drillsafe.co.za/drillsafe-articles/wire-rope-discard-standards`.

[47] T. Duarte; S. Gueydon; J. Jonkman; A. Sarmento. *Computation of Wave Loads under Multidirectional Sea States for Floating Offshore Wind Turbines*. National Renewable Energy Laboratory, 2014.

[48] J.R. Morison; M.D. O'Brien; J.W. Johnson; S.A. Schaaf. *The force exerted by surface waves on piles*. Petrol Trans AIME, 1950.

[49] Tideway Offshore Solutions. *Guideline Cable Lay Operations*. Tideway, 2016.

[50] Tideway Offshore Solutions. *Living Stone - DP3 CABLE INSTALLATION & MULTIPURPOSE VESSEL*. Tideway Offshore Solutions, 2016.

[51] D. Sotiriadis. *Motion based cable integrity limits for quadrant assisted pull-in operations on submarine inter-array cables*. Delft University of Technology & Boskalis, 2020.

[52] C. Strang-Moran. *Subsea cable management: Failure trending for offshore wind*. Offshore Renewable Energy Catapult, 2020.

[53] V.A. Mamatsopoulos; C. Michailides; E.E. Theotokoglou. *An Analysis Tool for the Installation of Submarine Cables in an S-Lay Configuration Including "In and Out of Water" Cable Segments*. Journal of Marine Science and Engineering, 2020.

[54] F. van Dorst. *Subsea Cable Installation; Beatrice Offshore wind Farm*. Seaway Heavy Lifting, 2019.

[55] J.H. Vugts. *Handbook of bottom founded offshore structures Part 1; General features of offshore structures and theoretical background*. Eburon, 2013. ISBN 978-9-059-72796-0.

[56] E. Weisstein. Least squares fitting, 2021. URL `https://mathworld.wolfram.com/LeastSquaresFitting.html`.

[57] E. Weisstein. Least squares fitting - exponential, 2021. URL `https://mathworld.wolfram.com/LeastSquaresFittingExponential.html`.

[58] P. Wellens. *Course Notes; Motions and Loading of Structures in Waves, Part II MT44020 2019-2020*. Delft University of Technology, 2019.

[59] D.J. Wilkens. The bathtub curve and product failure behavior part one - the bathtub curve, infant mortality and burn-in, 2002. URL https://www.weibull.com/hotwire/issue21/hottopics21.htm.

[60] W.J. Pierson; J.J. Tuttle; J.A. Wooley. *The theory of the refraction of a short-crested Gaussian sea surface with application to the northern New Jersey coast*. ASCE Cambridge, 1952.

[61] T. Worzyk. *Submarine power cables; Design, installation, repair, environmental aspects*. Springer, 2009.

A

Appendix - Problem statement

This appendix contains additional background information regarding chapter 1 (introduction) and chapter 2 (problem statement).

A.1. Offshore software packages

Regarding the offshore industry there are several software packages that are frequently used. The most common software packages are listed below.

- **Ansys Aqwa**
  Finite Element Analysis (FEA) software for structural engineering
- **Flexcom**
  Versatile software package specially designed for marine and offshore engineering
- **Orcina OrcaFlex**
  Dynamic analysis of offshore marine systems
- **Principia**
  FEA software for offshore wind turbines

At DEME Offshore NL, OrcaFlex is used for subsea power cable workability assessments. OrcaFlex is rather user-friendly and easy to interpret. Currently, in order to perform operability calculations, several additional software packages used as well. These are Excel and Python.

Orcina OrcaFlex is a leading software package developed especially for the offshore industry covering dynamic analysis of offshore marine systems such as cables, risers and anchor-systems.

Between OrcaFlex and Excel, a smart plug-in is available and OrcaFlex even provides their own Excel processing sheet. Around this plug-in, a processor has been built in order to set up all cases with Excel, automatically execute these in OrcaFlex and extract the required data back to excel. Hence, Excel is used as a pre- and post-processor, which required only one OrcaFlex base case. Various environmental loading conditions are combined with this base case to create all kind of different OrcaFlex cases (all derived from the base case)

Furthermore, the foundation of OrcaFlex is based on Python code which means it is possible to extend or adjust an analysis by means of writing a Python Script using an OrcaFlex plug-in. This could useful when computing compute more inconvenient calculations for pre-processing or post-processing of OrcaFlex data.

A.2. Methodology overview

The research methodology persisted within the thesis is clearly illustrated in Figure A.1. Starting at the top with '*Define problem statement*' and ending with '*Conclusions and recommendations*'. In between, all steps are explained and two feedback loops are present as well to improve the quality of the simulation process.

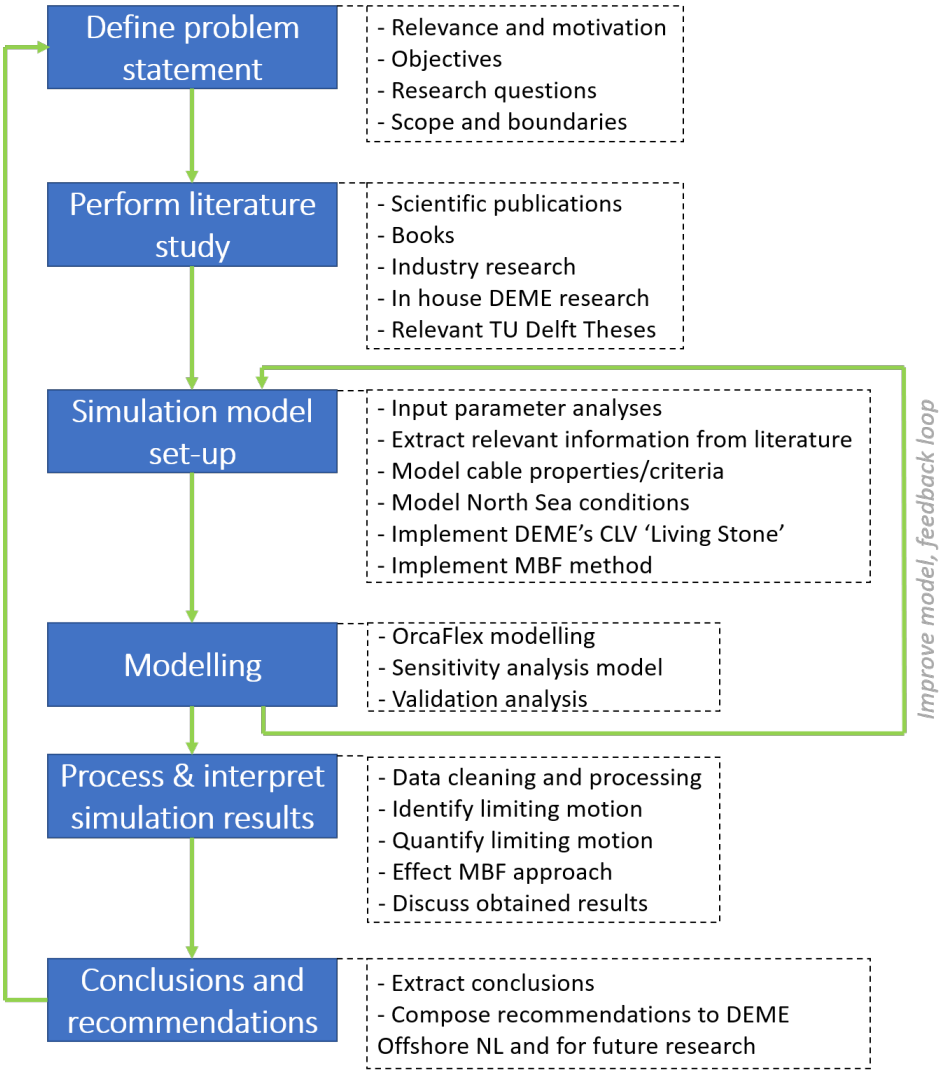

Figure A.1: Research methodology overview

B

Appendix - OrcaFlex modelling

This appendix contains more detailed information with respect to chapter 4, hence both the offshore environment and OrcaFlex modelling software.

B.1. DEME's Living Stone CLV

In this section an overview of the most important 'Living Stone' characteristics are provided. The Living Stone is DEMEs most recent DP3 installation & multipurpose operation vessel. The Living Stone is plays an active part in DEMEs fleet, and is widely used regarding cable operations in Europe. The vessel was constructed in 2016, and had its first trip on september 18^{th} 2016. Onboard there is, amongst other equipment, a helicopter deck, an active heave compensated crane, two cable spools,a fall pipe and a chute.

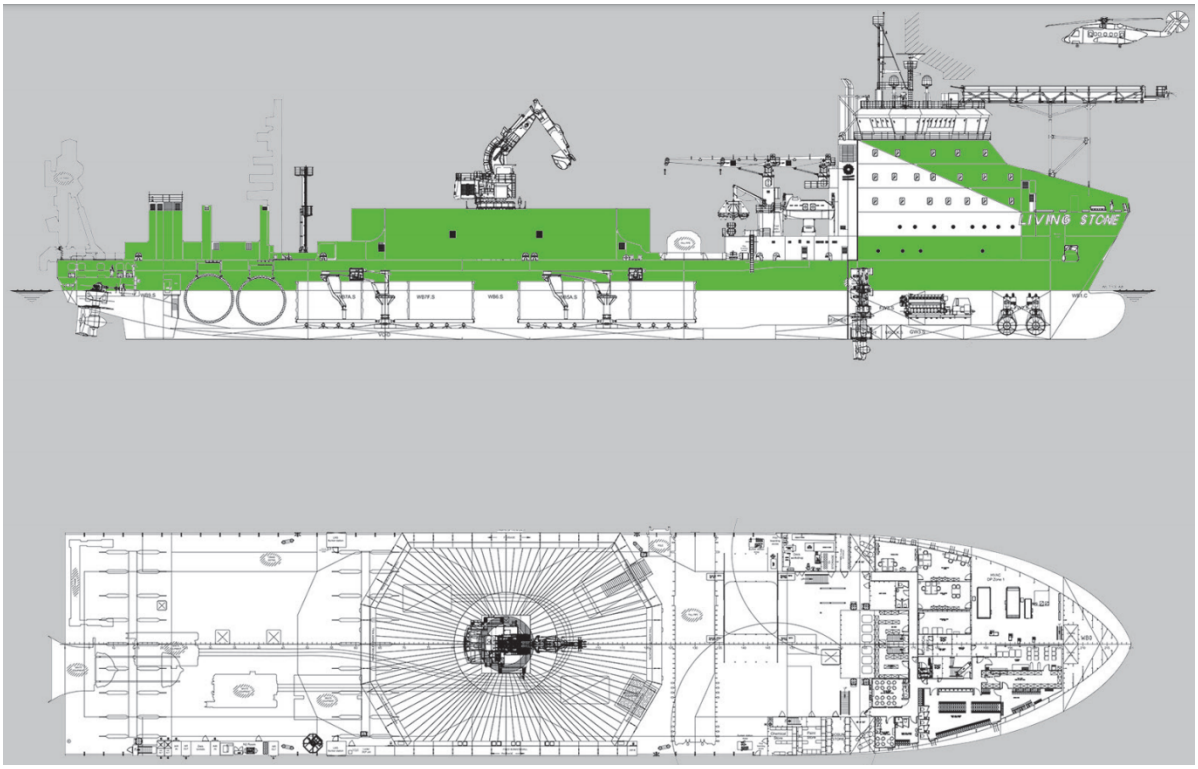

Figure B.1: Technical drawing DP3 cable installation & multipurpose vessel 'Living Stone' [50]

Most important Living Stone characteristics

Parameter	Additional information	Unit	Value
Dimensions	length o.a.	[redacted]	m
	Breath o.a.	[redacted]	m
Power	Total installed	[redacted]	kW
Capacity Tanks	Maximum rock loading capacity	[redacted]	m^3
Rock Placement Storage	Maximum loading capacity	[redacted]	tonnes
Fall Pipe Diameter		[redacted]	mm
	Moulded depth	[redacted]	m
Crane Capacity	Active heave compensated	[redacted]	tonnes
Production Capacity	Maximum cable hold capacity	[redacted]	tonnes
Maximum Speed Loader		[redacted]	knots

Table B.1: Most important Living Stone characteristics [21]

B.2. Wave theory

As aforementioned, sea waves are irregular since they are a superposition of lots of single regular harmonic waves. Assuming $H = 2 \cdot a$ (wave height is equal two times the wave amplitude), the formula for a harmonic propagating wave in positive x-direction is Equation B.1.

$$\eta(x,t) = a\sin(\omega t - kx) \tag{B.1}$$

The components are briefly explained below.

- η Represents crest elevation [m]
- a Represents wave amplitude [m]
- ω Represents wave frequency [Hz], which is calculated as $\omega = \frac{2\pi}{T}$ in which T is the wave period [s]
- k Represents the wave number [$radm^{-1}$] , which is calculated as $k = \frac{2\pi}{L}$ in which L is the wave length [m]

This harmonic propagating wave has a velocity potential as given in Equation B.2.

$$\Phi = \hat{\Phi}(z)\cos(\omega t - kx) = \frac{\omega a}{k}\frac{\cosh(k(d+z))}{\sinh(kd)}\cos(\omega t - kx) \tag{B.2}$$

All components which haven't been explained before, are briefly explained below.

- Φ Represents the potential [m]
- d Represents the water depth [m]
- z Represents a certain depth coordinate [m], see Figure B.2 as an illustration

When differentiating the velocity potential to x and z, the orbital velocities in these directions can be determined. These formulas are given in Equation B.3 and Equation B.4.

$$u_x = \hat{u}_x(z)\sin(\omega t - kx) = \frac{d\Phi}{dx} = \omega a\frac{\cosh(k(d+z))}{\sinh(kd)}\sin(\omega t - kx) \quad (90^o \text{ out of phase with } \Phi) \tag{B.3}$$

$$u_z = \hat{u}_z(z)\cos(\omega t - kx) = \frac{d\Phi}{dz} = \omega a\frac{\sinh(k(d+z))}{\sinh(kd)}\cos(\omega t - kx) \quad (\text{in phase with } \Phi) \tag{B.4}$$

In deep and shallow water, these orbital velocities can be simplified since the hyperbolic functions in $\hat{u}_x$ and $\hat{u}_z$ can be simplified. This can also be illustrated by means of a particle velocity schematization in deep, intermediate and shallow water. This illustration is shown in Figure B.2.

As stated by Holthuijsen and DNV-GL in [13, 24], an ocean is regarded as deep water when individual water particles are not influenced by the seabed, meaning the orbital velocity can be seen as a perfect circular motion. This only holds when the d/L ratio is larger than 3. The ocean is regarded as intermediate water when the d/L ratio is between 0.05 and 0.5, and when the d/L ratio is lower than 0.05 the ocean is regarded as shallow water.

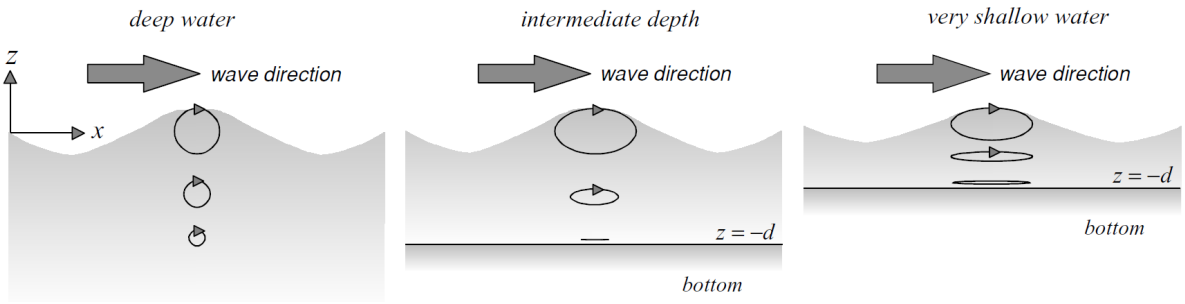

Figure B.2: Orbital particle velocity profiles in deep, intermediate and shallow water [24]

For ***deep water***, the orbital velocities in x and z direction respectively, are given in Equation B.5 and Equation B.6. Since the orbital velocity formulas are equal in x and z direction, the water particles are indeed not influenced by the seabed.

$$\hat{u}_x(z) = \omega a \frac{\cosh(k(d+z))}{\sinh(kd)} = \omega a e^{kz} \tag{B.5}$$

$$\hat{u}_z(z) = \omega a \frac{\sinh(k(d+z))}{\sinh(kd)} = \omega a e^{kz} \tag{B.6}$$

For ***shallow water***, the orbital velocities in x and z direction respectively, are given in Equation B.7 and Equation B.8. These orbital velocity formulas are not equal, thus the water particles are influenced by the seabed.

$$\hat{u}_x(z) = \omega a \frac{\cosh(k(d+z))}{\sinh(kd)} = \frac{ca}{d} \tag{B.7}$$

$$\hat{u}_z(z) = \omega a \frac{\sinh(k(d+z))}{\sinh(kd)} = \omega a \left(1 + \frac{z}{d}\right) \tag{B.8}$$

The dispersion relation is often applied is wave calculations as it directly relates wave length (or wave number) to wave frequency, hence not much calculations are required. The formula is presented in Equation B.9.

$$\omega^2 = gk\tanh(kd) \quad \text{or rewritten as} \quad L = \frac{gT^2}{2\pi}\tanh\left(\frac{2\pi d}{L}\right) \tag{B.9}$$

Additional wave statistics

Spectral moments, n-order spectral moment:

$$m_{n,a} = \int_0^\infty \omega^n \cdot S_a(\omega) \cdot d\omega \tag{B.10}$$

Root mean square:

$$H_{RMS} = \sqrt{m_0} \tag{B.11}$$

Significant wave height:

$$H_s = 4\sqrt{m_0} \tag{B.12}$$

Zero crossing-up wave period:

$$T_{02} = \sqrt{\frac{m2}{m0}} \tag{B.13}$$

B.3. Compose motions in direction of cable departure direction

In this section, the derivation of the chute motion in the direction of cable departure (referred to as chute cable motions) is explained in more detail. These chute cable motions can be constructed by combining chute x motions and chute z motions, by means of applying Pythagoras theorem and creating two right angled triangles (90^o). By means of these triangles, the contribution of both chute x motions and chute z motions can be rewritten towards the motion in cable departure direction. These procedures are illustrated in Figure B.3

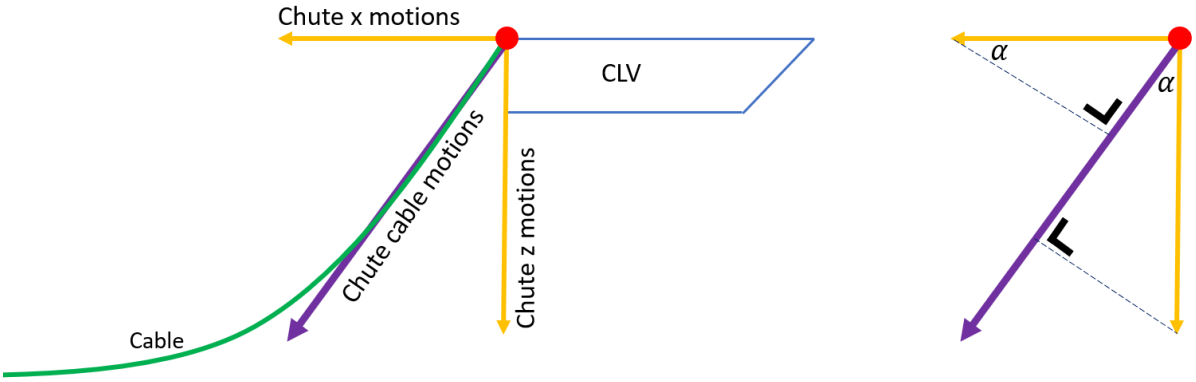

Figure B.3: Illustration of motions in cable departure direction (CLV sideview)

By means of these composed triangles, the contribution of both chute x motions and chute z motions can be rewritten towards the motion in cable departure direction. The required formulas to rewrite these contributions are given below in Equation B.14 and Equation B.15 respectively. To finally obtain the motion in cable departure direction, the rewritten x and z contributions can easily be added to each other as prescribed in Equation B.16. All these formulas hold for the motion itself, motion velocities and motion accelerations.

$$x_{contribution\ cable} = Chute\ x\ motions\ *\ \sin(\alpha) \tag{B.14}$$

$$z_{contribution\ cable} = Chute\ z\ motions\ *\ \cos(\alpha) \tag{B.15}$$

$$Chute\ cable\ motions = x_{contribution\ \ cable}\ +\ z_{contribution\ cable} \tag{B.16}$$

To verify whether Pythagoras is correctly applied to obtain the chute cable motions, a extreme deep water case is checked (static results of this case are enclosed in Table B.2.

When installing cables in extremely deep water the cable leaves the chute almost vertically, hence contributions in x-direction are negligible and only contributions in z-direction motions remain important. This means that the chute z motions and cable motions are expected to be the same.

These graphs clearly indicate that indeed the chute cable motions and chute z motions are the identical in deep water, hence contribution from chute x motions is negligible. This means that Pythagoras is incorporated correctly, and the equations presented above are indeed correct.

Examples of the composed scatter graphs are presented below in Figure B.4.

Parameter	Unit	Value
Water depth	m	1145
Static layback	m	80.50
Static cable declination	deg	172.14
Static MBR	m	16.70
Static top tension	kN	404.59
Static bottom tension	kN	5.00

Table B.2: Static report - Extreme deep water case to verify chute cable motion composition (1000m)

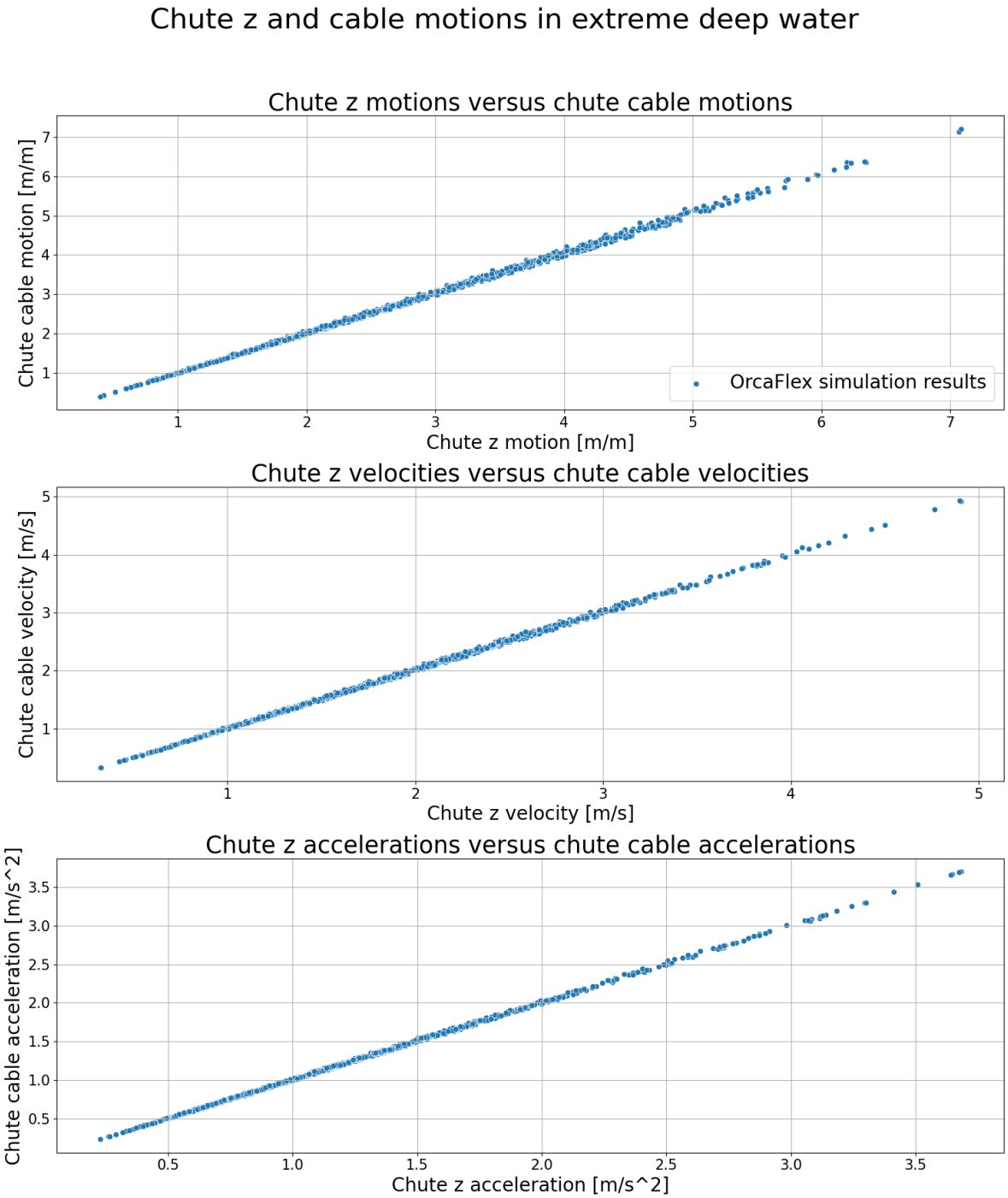

Figure B.4: Chute z motions versus chute cable motions in extreme deep water (1000m)

B.4. Lumped mass method

In order to analyse an entire catenary system it is useful to discretize the problem. By discretizing the catenary, the line is split into segments and each segment can be analysed separately. This method is also known as the lumpd mass method (LMM) and originates from 1959 (Walton & Polachtek). Since then, a lot of research has been done on the LMM, and it was Nakajima (1982) who composed the equations of motion that are still used today.

For horizontal and vertical directions, the following equations of motion (EoMs) hold. [41]

$$\left[M_j + A_{nj}\sin^2\theta_j + A_{tj}\cos^2\theta_j\right] * \ddot{x}_j + \left[A_{tj} - A_{nj}\right] * \ddot{z}_j \sin\theta_j \cos\theta_j = F_{xj} \tag{B.17}$$

$$\left[M_j + A_{nj}\cos^2\theta_j + A_{tj}\sin^2\theta_j\right] * \ddot{z}_j + \left[A_{tj} - A_{nj}\right] * \ddot{x}_j \sin\theta_j \cos\theta_j = F_{zj} \tag{B.18}$$

The components in the equations above are explained briefly below.

- M_j Represents masses of the jth lump [kg]
- A_{nj} Represents added masses of the jth lump in normal direction [kg]
- A_{tj} Represents added masses of the jth lump in tangential direction [kg]
- $\ddot{x}$ Represents accelerations of the jth lump in x-direction [m/s^2]
- $\ddot{z}$ Represents accelerations of the jth lump in z-direction [m/s^2]
- $\bar{\theta}_j$ Represents the angle and can be determined as $\bar{\theta}_j = \frac{1}{2}\left(\theta_{j-1} + \theta_j\right)$

These equations of motions can be simplified and written in matrix form by composing an added mass matrix $[m_a(t)]_j$.

$$\left(\begin{bmatrix} M & 0 \\ 0 & M \end{bmatrix}_j + [m_a(t)]_j\right)\begin{bmatrix} \ddot{x}(t) \\ \ddot{z}(t) \end{bmatrix}_j = \begin{bmatrix} F_x(t) \\ F_z(t) \end{bmatrix}_j \tag{B.19}$$

In which equations for the nodal components of the external forces (F_{xj} and F_{zj}) from Equation B.17, Equation B.18 and Equation B.19 are given below.

$$F_{xj} = T_j \cos\theta_j - T_{j-1}\cos\theta_{j-1} - f_{dxj} \tag{B.20}$$

$$F_{zj} = T_j \sin\theta_j - T_{j-1}\sin\theta_{j-1} - f_{dzj} - \delta_j \tag{B.21}$$

The components in the equations above are explained briefly below.

- F_{xj} Represents the external force in x-direction [kN]
- F_{zj} Represents the external force in z-direction [kN]
- T_j Represents tension in segment between jth and j+1th lumped masses [kN]
- δ_j Represents the weight in water of the lumped mass [kg]
- f_{dxj} Represents drag forces on the catenary in x-direction [kN]
- f_{dzj} Represents drag forces on the catenary in z-direction [kN]

These drag forces are proportional to the square of fluid velocity relative to the catenary line, and can be calculated by means of the following two equations.

$$f_{dxj} = -\frac{1}{2}\rho D_c \bar{l}\left[C_{dn}\sin\bar{\theta}_j|u_{nj}|u_{nj} - C_{dt}\cos\bar{\theta}_j|u_{tj}|u_{tj}\right] + \frac{1}{2}\rho A_{rx}C_{dx}|\dot{x}_j - c_j|(\dot{x}_j - c_j) \tag{B.22}$$

$$f_{dzj} = \frac{1}{2}\rho D_c \bar{l}\left[C_{dn}\cos\bar{\theta}_j|u_{nj}|u_{nj} + C_{dt}\sin\bar{\theta}_j|u_{tj}|u_{tj}\right] + \frac{1}{2}\rho A_{rz}C_{dz}|\dot{z}_j|\dot{z}_j \tag{B.23}$$

The components in the equations above are explained briefly below.

- f_{dxj} Represents drag forces on the catenary in x-direction [kN]
- f_{dzj} Represents drag forces on the catenary in z-direction [kN]
- ρ Represents density of sea water [kg/m^3], generally taken as 1,025kg/m^3
- D_c represents the equivalent diameter of mooring line [m]
- $\bar{l}$ Represents the original length of the line segment [m]
- C_{dn} Represents a drag coefficient normal to the mooring line [-]
- C_{dt} Represents a drag coefficient tangential to the mooring line [-]
- C_{dx} Represents coefficients of additional substances in x-direction [-]
- C_{dz} Represents coefficients of additional substances in z-direction [-]
- A_{rx} Represents projected areas in x-direction [m^2]
- A_{rz} Represents projected areas in z-direction [m^2]
- u_{nj} Represents velocity component normal to the mooring line [m/s]
- u_{tj} Represents velocity component tangential to the mooring line [m/s]

The velocity components u_{nj} and u_{tj} normal and tangential to the mooring line are given by

$$u_{nj} = -\left(\dot{x}_j - c_j\right)\sin\theta_j + \dot{z}_j\cos\theta_j \tag{B.24}$$

$$u_{tj} = \left(\dot{x}_j - c_j\right)\cos\theta_j + \dot{z}_j\sin\theta_j \tag{B.25}$$

The components in the equations above are explained briefly below.

- u_{nj} Represents velocity component normal to the mooring line [m/s]
- u_{tj} Represents velocity component tangential to the mooring line [m/s]
- c_j Represents the current velocity in horizontal direction at the jth lumped mass [m/s]

An additional constraint is required in order to solve all equations presented above from the LMM. This constraint is presented below.

$$(x_j - x_{j-1})^2 + (z_j - z_{j-1})^2 = \bar{l}^2\left(1 + \frac{T_{j-1}}{A * E}\right)^2 \tag{B.26}$$

The components in the equations above are explained briefly below.

- A Represents the cross-sectional area of the catenary line [m^2]
- E Represents Young's Modulus of elasticity

B.5. Fourier transform

To illustrate the Fourier transform the general EoM of a 1-DOF mass-spring-damper system is considered following an example by Pegalajar [7], see Equation B.27.

$$(m+a)\ddot{\xi}(t) + b\dot{\xi}(t) + c\xi(t) = F(t) \tag{B.27}$$

The components in Equation B.27 above are explained briefly below.

- m Represents mass matrix [kg]
- a Represents added mass matrix [kg]
- b Represents damping coefficients matrix
- c Represents restoring coefficients matrix
- $\xi(t)$ Represents the displacement from equilibrium position [m]
- $F(t)$ Represents an harmonic excitation force [kN]

The general 1-DOF equation can be converted into its complex format by introducing Fourier Transform $\hat{F}(t)$, and expressing the original excitation force $F(t)$ in terms of ω instead of time (t). The corresponding formula is given in Equation B.28. Furthermore, in the following formulas $\Re$ indicates the real part of the equations and i indicates the imaginary part of the equations.

$$F(t) = \Re\left\{\hat{F}(\omega)e^{i\omega t}\right\} \tag{B.28}$$

In the same manner as the excitation force $(F(t))$, the displacement can be converted into a real and imaginary part as well. This only holds when the transient part of the response is neglected. The formula for this steady-state system response is shown in Equation B.29.

$$\xi(t) = \Re\left\{\hat{\xi}(\omega)e^{i\omega t}\right\} \tag{B.29}$$

Finally, using Equation B.28 and Equation B.29 the general EoM from Equation B.27 can be rewritten as shown in Equation B.30.

$$\left[-\omega^2(m+a) + i\omega b + c\right]\hat{\xi}(\omega) = \hat{F}(\omega) \quad \rightarrow \quad \hat{\xi}(\omega) = \frac{\hat{F}(\omega)}{-\omega^2(m+a)+i\omega b+c} \equiv H(\omega)\hat{F}(\omega) \tag{B.30}$$

In which complex transfer function $H(\omega)$ is defined as $H(\omega) = \frac{1}{-\omega^2(m+a)+i\omega b+c}$

From Equation B.30, it can be derived that in the end only the Fourier Transform $\hat{F}(\omega)$ multiplied by complex transfer function $H(\omega)$ remains.

B.6. QTF's

Regarding DEME's Living Stone, QTF'a are predefined and can easily be loaded into OrcaFlex. All equations below are taken from the OrcaFlex manual. [31]

Wave drift load

$$\sum_{i=1}^{n}\sum_{j=1}^{n}\mathrm{Re}\left\{Q_{\mathrm{d}}\left(\beta_i,\beta_j,\tau_i,\tau_j\right)a_i a_j\exp\left[\mathrm{i}\left(\omega_i-\omega_j\right)t-\left(\phi_i-\phi_j\right)\right]\right\} \tag{B.31}$$

Sum frequency load

$$\sum_{i=1}^{n}\sum_{j=1}^{n}\mathrm{Re}\left\{Q_{\mathrm{s}}\left(\beta_i,\beta_j,\tau_i,\tau_j\right)a_i a_j\exp\left[\mathrm{i}\left(\omega_i+\omega_j\right)t-\left(\phi_i+\phi_j\right)\right]\right\} \tag{B.32}$$

In which $Q_{\mathrm{d}}\left(\beta_i,\beta_j,\tau_i,\tau_j\right)$ and $Q_{\mathrm{s}}\left(\beta_i,\beta_j,\tau_i,\tau_j\right)$ represent wave drift and frequency QTF's between interactions i and j.

Wave drift QTF, in complex-valued form:

$$Q_{\mathrm{d}}\left(\beta_1,\beta_2,\tau_1,\tau_2\right)=a_{\mathrm{d}}\left(\beta_1,\beta_2,\tau_1,\tau_2\right)\exp\left[-\mathrm{i}\phi_{\mathrm{d}}\left(\beta_1,\beta_2,\tau_1,\tau_2\right)\right] \tag{B.33}$$

Wave drift QTF, in complex-valued form

$$Q_{\mathrm{s}}\left(\beta_1,\beta_2,\tau_1,\tau_2\right)=a_{\mathrm{s}}\left(\beta_1,\beta_2,\tau_1,\tau_2\right)\exp\left[-\mathrm{i}\phi_{\mathrm{s}}\left(\beta_1,\beta_2,\tau_1,\tau_2\right)\right] \tag{B.34}$$

$a_{\mathrm{d}}\left(\beta_1,\beta_2,\tau_1,\tau_2\right)=$ wave drift amplitude, as specified in the data
$\phi_{\mathrm{d}}\left(\beta_1,\beta_2,\tau_1,\tau_2\right)=$ wave drift phase lag, in radians, relative to the difference frequency crest
$a_{\mathrm{s}}\left(\beta_1,\beta_2,\tau_1,\tau_2\right)=$ sum frequency amplitude, as specified in the data
$\phi_{\mathrm{s}}\left(\beta_1,\beta_2,\tau_1,\tau_2\right)=$ sum frequency phase lag, in radians, relative to the sum frequency crest.

C

Appendix - Investigated subsea power cable properties

In this Appendix an overview of four investigated subsea power cables and their properties is provided. References are not mentioned since these are confidential.

C.1. Typical 3*300mm2 HVAC inter-array cable 1

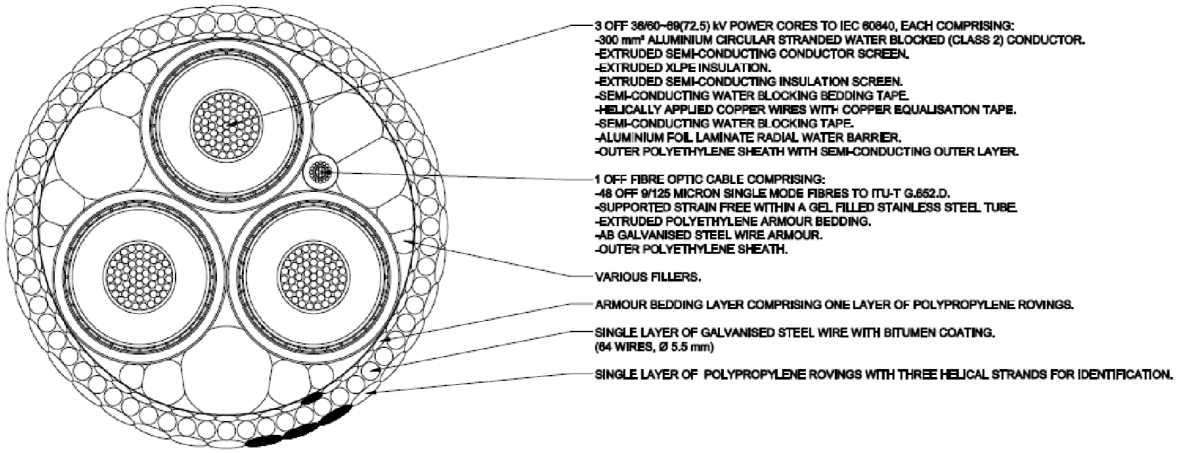

Figure C.1: Typical inter-array cable 1 cross section and listed components [-]

Cable limit	Unit	Value
Minimum bending radius (MBR)	m	1.95
Maximum top tension	kN	170
Minimum bottom tension	kN	-17

Table C.1: Cable limits typical inter-array cable 1 [-]

Parameter	Unit	Value
Cable diameter	mm	136
Unit mass in air	kg/km	25,800
Unit mass in seawater	kg/km	12,090
Specific gravity in seawater	m/s^2	1.81
Minimum breaking strength	kN	855
Maximum working load	kN	170
Maximum Torsion at working load	Nm	2,740
Axial stiffness	MN	304
Torsional stiffness (clockwise)	kNm^2/deg	1.86
Torsional stiffness (counter clockwise)	kNm^2/deg	0.621
Maximum permissible impact energy	KJ/m	15
Maximum sidewall pressure	kN/m	50
Maximum permissible crush load between two flat plates	kN/m	73
Minimum coling diameter	mm	10,000
Recommended minimum drop height	mm	10,000

Table C.2: Mechanical performance parameters typical inter-array cable 1 [-]

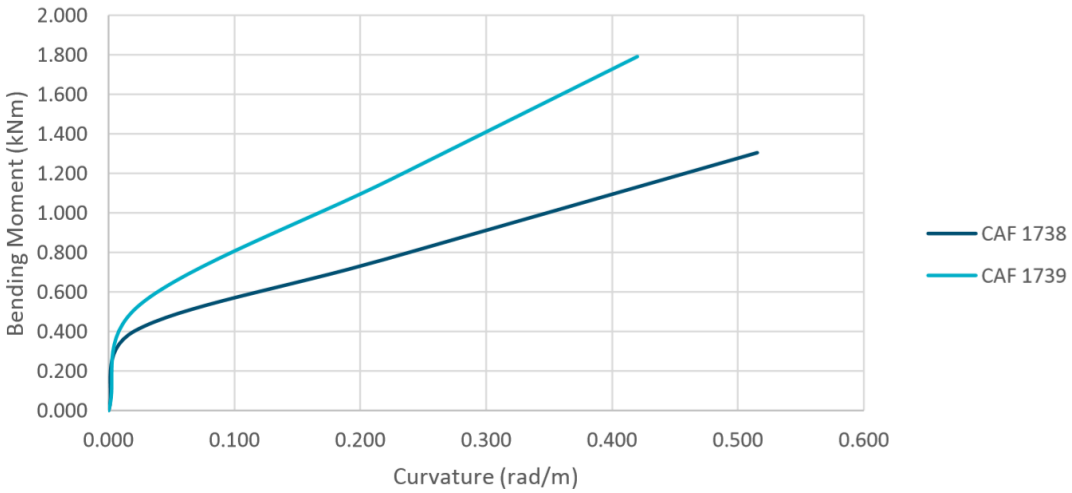

Figure C.2: Non-linear bending stiffness typical inter-array cable 1 [-]

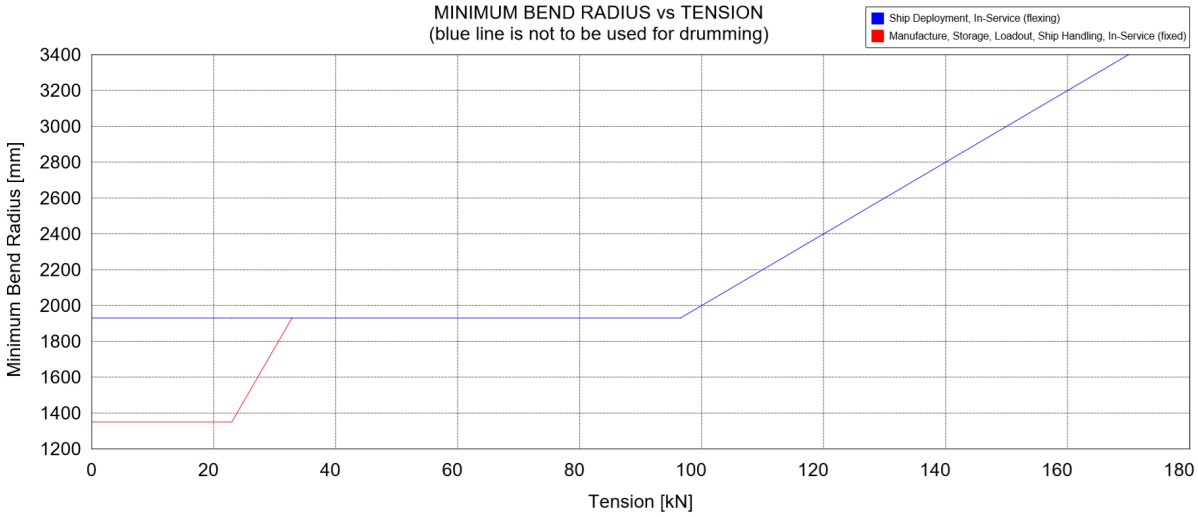

Figure C.3: Minimum bending radius versus working load typical inter-array cable 1 [-]

C.2. Typical 3*300mm2 HVAC inter-array cable 2

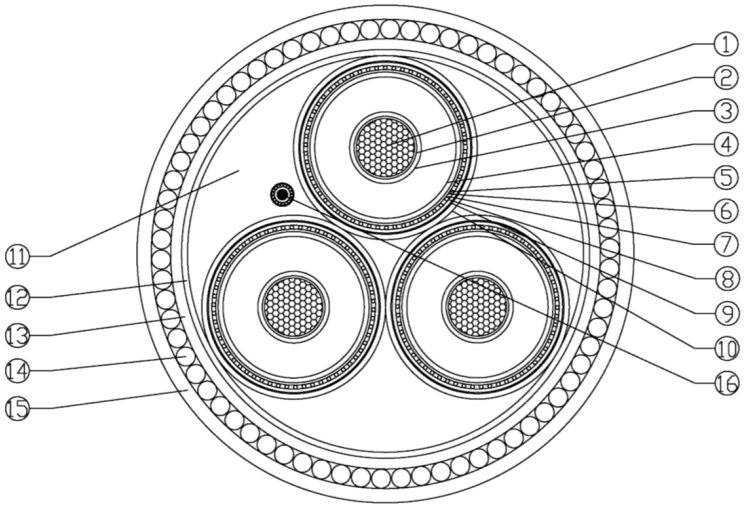

Figure C.4: Typical inter-array cable 2 cross section [-]

1	Water seal
2	Semiconducting tape
3	Conductor screen
4	XLPE Insulation
5	Non-metallic screen
6	Semiconducting tape(s)
7	Metallic screen
8	Semiconducting tape
9	Radial water-tightness
10	Sheath
11	Fillers
12	Binding tape
13	Polypropylene yarns
14	Armour
15	Polypropylene yarns
16	Armour

Table C.3: Typical inter-array cable 2 cable components [-]

Component	Unit	Value
Conductor diameter	mm	20.6
Inner semiconducting layer thickness	mm	1
XLPE insulation thickness	mm	9.4
Outer semiconducting layer thickness	mm	1
Radial water tightness barrier, thickness	mm	0.2
PE sheath thickness	mm	2.5
Core diameter	mm	57
Lay length of cores	m	2
Lay direction of cores	-	Left (s)
Armour wire diameter	mm	5.5
Lay length of armour wires	mm	2.1
Lay direction of armour wires	-	Left (s)
Cable diameter	mm	144

Table C.4: Typical inter-array cable 2 dimensional characteristics [-]

Cable limit	Unit	Value
Minimum bending radius (MBR)	m	1.9
Maximum top tension	kN	85
Minimum bottom tension	kN	-12.5

Table C.5: Typical inter-array cable 2 limits [-]

Parameter	Unit	Value
Cable diameter	mm	144
Unit mass in air	kg/km	30,000
Unit mass in seawater	kg/km	14,000
Specific gravity in seawater	m/s^2	1.82
Minimum bending radius (MBR)	m	1.9
Maximum working load	kN	85
Axial stiffness	MN	367.1
Bending stiffness	kNm^2	3.9
Torsional stiffness	kNm^2/rad	7.8
Maximum permissible impact energy	J	245
Maximum sidewall pressure	kN/m	33
Maximum allowable compression	kN	12.5
Crush load at tensioner	kN/m	55

Table C.6: Typical inter-array cable 2 mechanical performance parameters [-]

C.3. Typical 3*1800 mm2 HVAC export cable 1

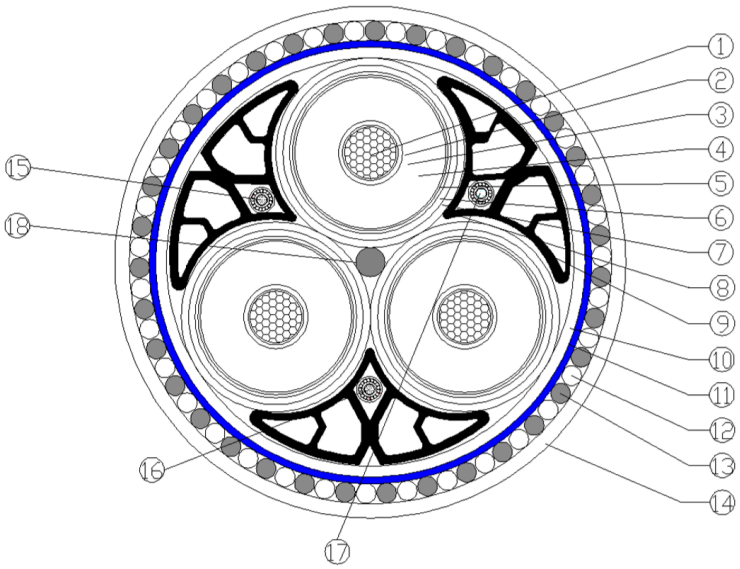

Figure C.5: Typical export cable 1 [-]

1	Water seal
2	Semiconducting tape(s)
3	Conductor screen
4	XLPE Insulation
5	Non-metallic screen
6	Semiconducting tape(s)
7	Metallic sheath
8	Semiconducting PE sheath
9	PE profile fillers
10	Semi-conducting tape(s)
11	Polypropylene yarns
12	Armour
13	Armour
14	Polypropylene yarns
15	Armour
16	Armour
17	Armour
18	Polypropylene filler

Table C.7: Typical export cable 1 cable components [-]

Cable limit	Unit	Value
Minimum bending radius (MBR)	m	4.3
Maximum top tension	kN	300
Minimum bottom tension	kN	-15

Table C.8: Typical export cable 1 limits [-]

Parameter	Unit	Value
Cable diameter	mm	276
Unit mass in air	kg/km	109,500
Unit mass in seawater	kg/km	60,000
Maximum working load	kN	300
Axial stiffness	MN	698
Bending stiffness	kNm^2	153
Torsional stiffness	kNm^2/rad	388
Maximum sidewall pressure	kN/m	70
Maximum allowable axial compression	kN	15

Table C.9: Typical export cable 1 mechanical performance parameters [-]

C.4. Typical 1*1300 mm2 HVDC export cable 2

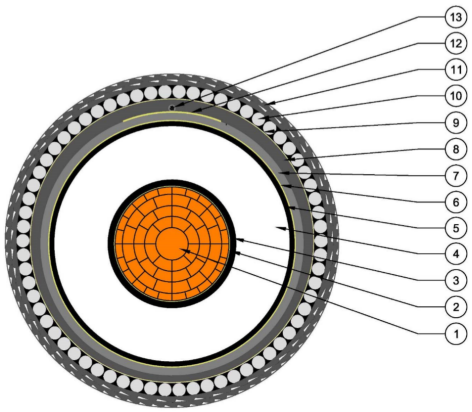

Figure C.6: typical export cable 2 cross section [-]

1	Conductor
2	Swellable tape
3	Conductor screen
4	Insulation
5	Insulation screen
6	Longitudinal water-block
7	Lead sheath
8	PE sheath
9	Bedding
10	Armour
11	Outer serving
12	Bedding tape
13	Fiber optic element

Table C.10: Typical export cable 2 components [-]

Cable limit	Unit	Value
Minimum bending radius (MBR)	m	4
Maximum top tension	kN	149
Minimum bottom tension	kN	0

Table C.11: Typical export cable 2 limits [-]

Parameter	Unit	Value
Cable diameter	mm	123
Unit mass in air	kg/km	38,000
Unit mass in seawater	kg/km	27,000
Maximum working load	kN	149

Table C.12: Typical export cable 2 mechanical performance parameters [-]

D

Appendix - Limiting motion identification

This appendix contains ... chapter 5.

D.1. Initial analysis results

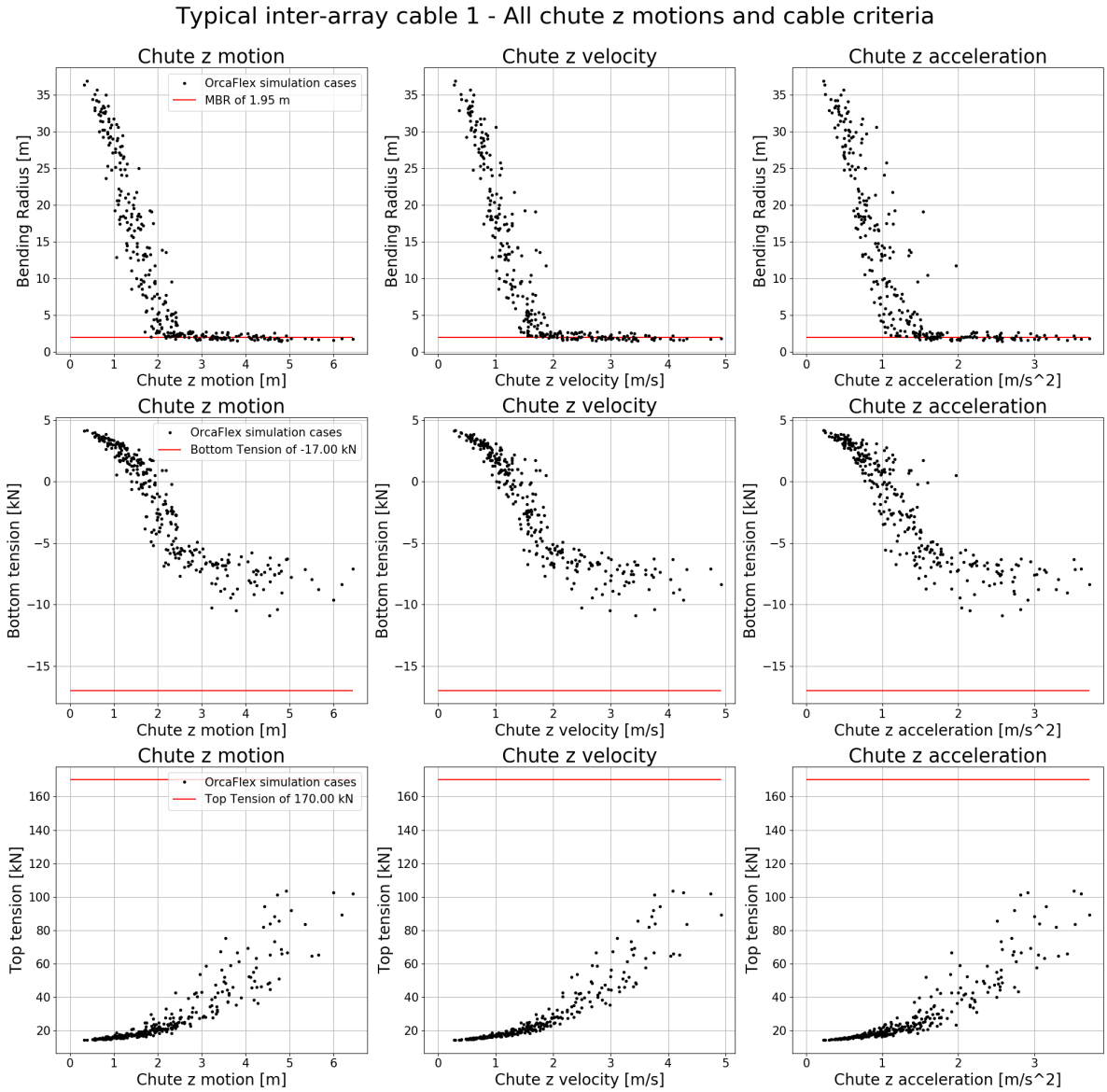

Figure D.1: Initial motion analysis, all chute z motions w.r.t. cable integrity criteria

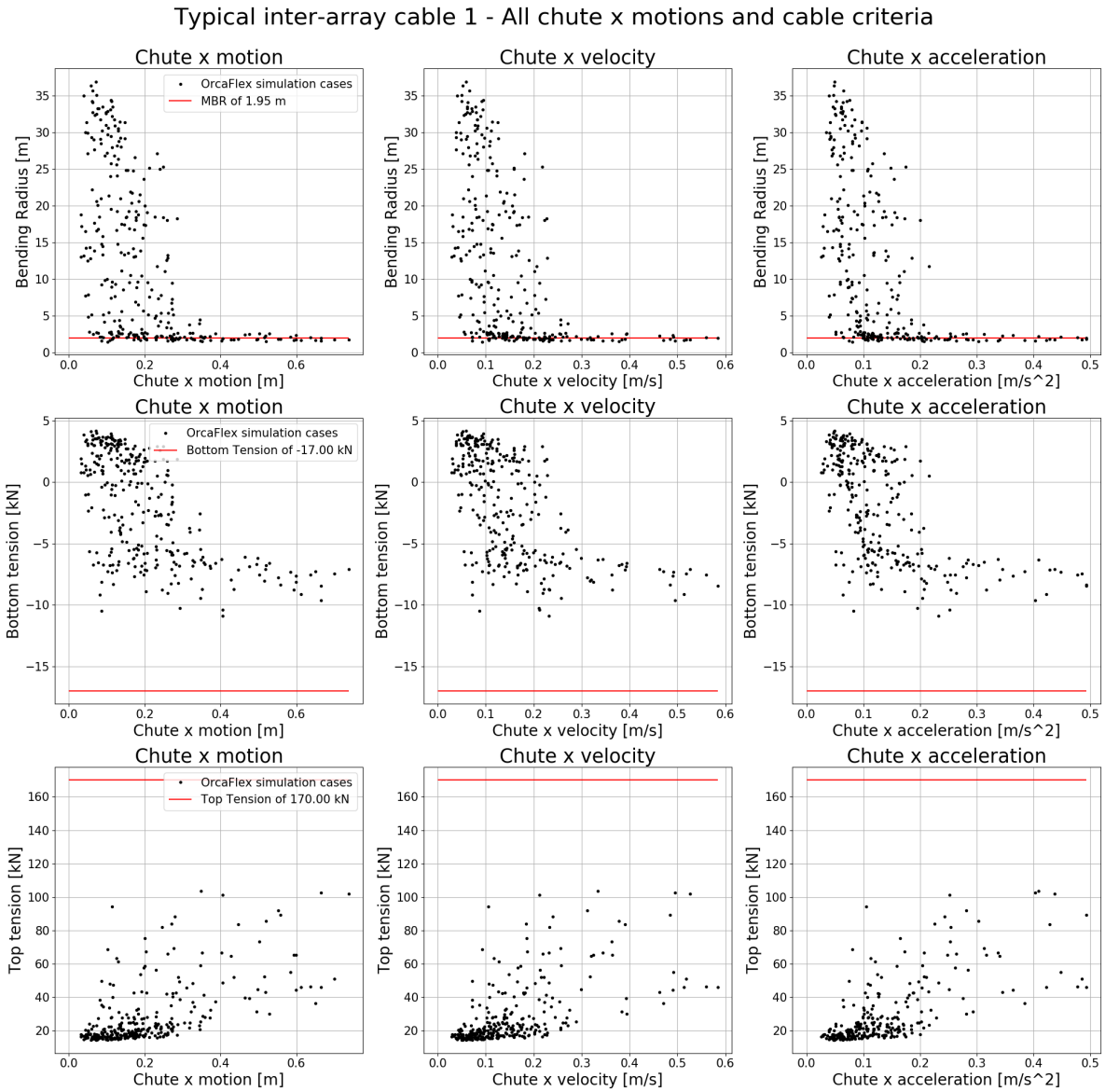

Figure D.2: Initial motion analysis, all chute x motions w.r.t. cable integrity criteria

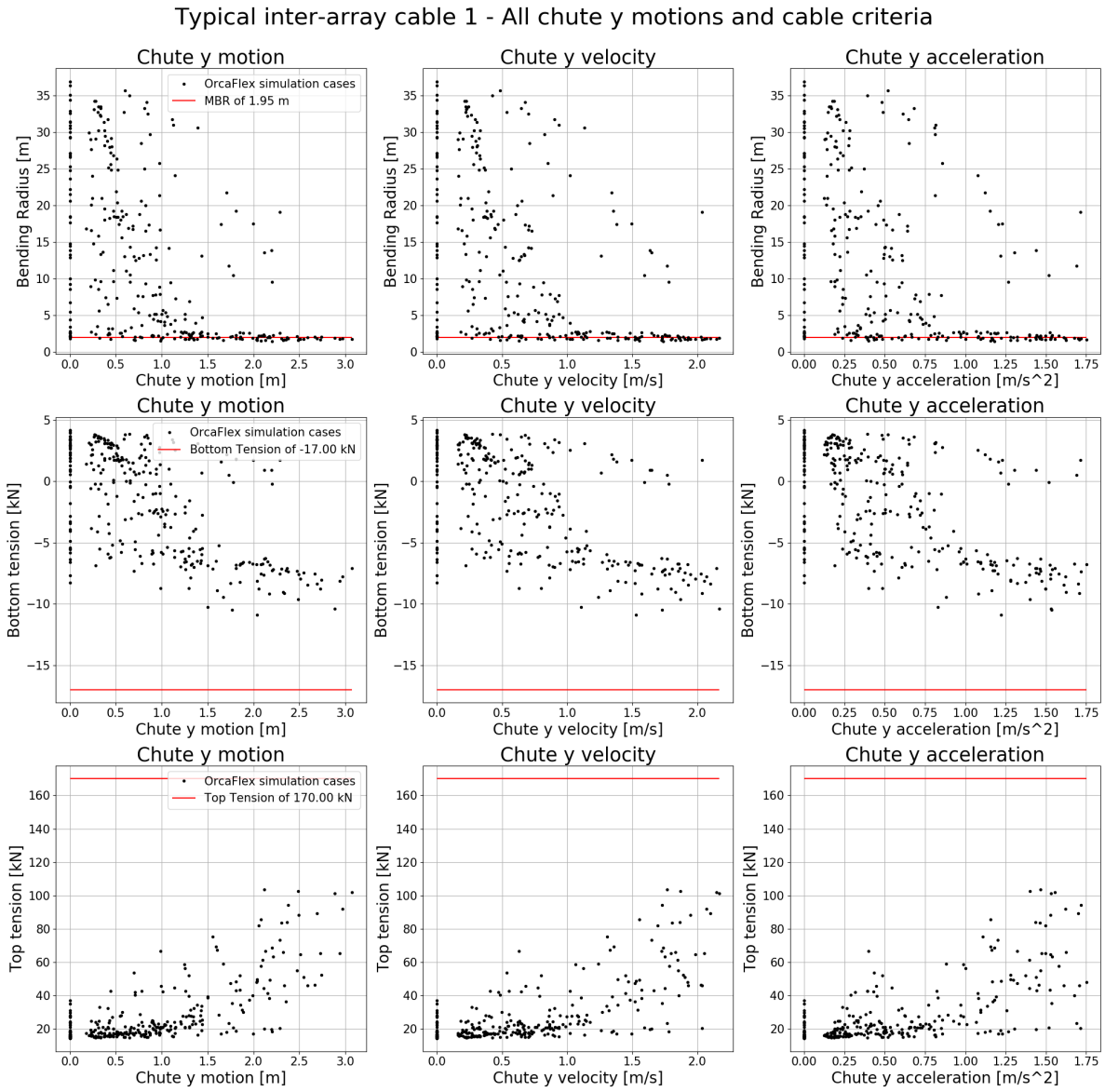

Figure D.3: Initial motion analysis, all chute y motions w.r.t. cable integrity criteria

D.2. Least Mean Square methods

Exponential LMS fitting

Based on the resulting scatter graphs in Figure 5.2, exponential LMS fitting seems to give the best results out of the aforementioned nonlinear fitting methods. The base function used for exponential LMS fitting is presented below in Equation D.1. When taking the logarithm of both sides, Equation D.2 arises. [57]

$$y = A * e^{-B*x} \tag{D.1}$$

$$\ln y = \ln A + Bx \tag{D.2}$$

Based on the equations listed above, the best-fit values can be determined by solving the following equations, in which $B = b$, $A = \exp a$ and n is the number of considered data points.

$$a\sum_{i=1}^{n} y_i + b\sum_{i=1}^{n} x_i y_i = \sum_{i=1}^{n} y_i \ln y_i \tag{D.3}$$

$$a\sum_{i=1}^{n} x_i y_i + b\sum_{i=1}^{n} x_i^2 y_i = \sum_{i=1}^{n} x_i y_i \ln y_i \tag{D.4}$$

$$\begin{bmatrix} \sum_{i=1}^{n} y_i & \sum_{i=1}^{n} x_i y_i \\ \sum_{i=1}^{n} x_i y_i & \sum_{i=1}^{n} x_i^2 y_i \end{bmatrix} \begin{bmatrix} a \\ b \end{bmatrix} = \begin{bmatrix} \sum_{i=1}^{n} y_i \ln y_i \\ \sum_{i=1}^{n} x_i y_i \ln y_i \end{bmatrix} \tag{D.5}$$

$$a = \frac{\sum_{i=1}^{n} \left(x_i^2 y_i\right) \sum_{i=1}^{n} \left(y_i \ln y_i\right) - \sum_{i=1}^{n} \left(x_i y_i\right) \sum_{i=1}^{n} \left(x_i y_i \ln y_i\right)}{\sum_{i=1}^{n} y_i \sum_{i=1}^{n} \left(x_i^2 y_i\right) - \left(\sum_{i=1}^{n} x_i y_i\right)^2} \tag{D.6}$$

$$b = \frac{\sum_{i=1}^{n} y_i \sum_{i=1}^{n} \left(x_i y_i \ln y_i\right) - \sum_{i=1}^{n} \left(x_i y_i\right) \sum_{i=1}^{n} \left(y_i \ln y_i\right)}{\sum_{i=1}^{n} y_i \sum_{i=1}^{n} \left(x_i^2 y_i\right) - \left(\sum_{i=1}^{n} x_i y_i\right)^2} \tag{D.7}$$

In this thesis, the exponential fitting base function is slightly modified in order to account for a line of best fit which does not start at the origin (0,0). Therefore, an additional parameter (c) is added as described below.

$$y = A * e^{-B*x} + c \tag{D.8}$$

Regression

To investigate which motion(s) has the best relation w.r.t. the cable integrity criteria, based on the line of best fit a regression analysis can be performed. Regression is also known ad goodness of fit. This is indicated by an R-squared (R^2) value, hence R^2 is a statistical measure of how close the original data points are w.r.t. the composed line of best fit, a s explained in the section above. In literature, R-squared is also commonly referred to as regression coefficient and the coefficient of determination. The formula in order to determine the regression coefficients is given below in Equation D.9. [16, 30, 56]

$$R^2 = \frac{Explained\ \ variance\ \ of\ \ the\ \ model}{Total\ \ variance\ \ of\ \ the\ \ model} = 1 - \frac{SS_{xy}^2}{SS_{xx} * SS_{yy}} \tag{D.9}$$

In which the variance terms are obtained by the following formulas. In Equation D.10 to Equation D.12, $\bar{x}$ and $\bar{y}$ both represent averages off all considered x_i and y_i respectively.

$$\mathrm{ss}_{xy} = \sum_{i=1}^{n} \left(x_i - \bar{x}\right)\left(y_i - \bar{y}\right) = \left(\sum_{i=1}^{n} x_i y_i\right) - n\bar{x}\bar{y} \tag{D.10}$$

$$\mathrm{ss}_{xx} = \sum_{i=1}^{n} \left(x_i - \bar{x}\right)^2 = \left(\sum_{j=1}^{n} x_i^2\right) - n\bar{x}^2 \tag{D.11}$$

$$\mathrm{ss}_{yy} = \sum_{i=1}^{n} (y_i - \bar{y})^2 = \left(\sum_{j=1}^{n} y_i^2 \right) - n\bar{y}^2 \tag{D.12}$$

D.3. Test cases control cables

D.3.1. Typical interarray cable 2

The second examined subsea power cable is also a typical 3*300mm^2 HVAC inter-array cable. An intersection and list of all specific cable properties is enclosed in section C.2. Regarding cable integrity criteria, the cable limits are listed below.

- MBR → $1.9m$
- Minimum bottom tension → $-12.5kN$
- Maximum top tension → $85kN$

Static reports of the normal lay configuration for both shallow and deep water are provided below.

Parameter	Unit	Value
Water depth	m	30
Static layback	m	58.10
Static cable declination	deg	152.35
Static MBR	m	40.03
Static top tension	kN	12.95
Static bottom tension	kN	5.00

Table D.1: Static report - Typical inter-array cable 2, water depth of $30m$

Parameter	Unit	Value
Water depth	m	150
Static layback	m	93.50
Static cable declination	deg	167.68
Static MBR	m	39.58
Static top tension	kN	28.65
Static bottom tension	kN	5.00

Table D.2: Static report - Typical inter-array cable 2, water depth of $150m$

D.3.2. Typical export cable 1

The third examined subsea power cable is a typical 3*1800mm^2 HVDC export cable. An intersection and list of all specific cable properties is enclosed in section C.3. Regarding cable integrity criteria, the cable limits are listed below.

- MBR → $4.3m$
- Minimum bottom tension → $-15kN$
- Maximum top tension → $300kN$

Static reports of the normal lay configuration for both shallow and deep water are provided below.

Parameter	Unit	Value
Water depth	m	30
Static layback	m	30.17
Static cable declination	deg	160.35
Static MBR	m	15.18
Static top tension	kN	35.35
Static bottom tension	kN	5.00

Table D.3: Static report - Typical export cable 1, water depth of $30m$

Parameter	Unit	Value
Water depth	m	150
Static layback	m	41.66
Static cable declination	deg	168.90
Static MBR	m	15.18
Static top tension	kN	105.51
Static bottom tension	kN	5.00

Table D.4: Static report - Typical export cable 1, water depth of $150m$

D.3.3. Typical export cable 2

The fourth, and last, examined subsea power cable is a typical 1*1300mm^2 HVDC export cable. An intersection and list of all specific cable properties is enclosed in section C.4. Regarding cable integrity criteria, the cable limits are listed below.

- MBR → $4m$
- Minimum bottom tension → $0kN$
- Maximum top tension → $149kN$

Static reports of the normal lay configuration for shallow and deep water are provided below.

Parameter	Unit	Value
Water depth	m	30
Static layback	m	38.60
Static cable declination	deg	159.98
Static MBR	m	20.11
Static top tension	kN	16.53
Static bottom tension	kN	5.00

Table D.5: Static report - Typical export cable 2, water depth of $30m$

Parameter	Unit	Value
Water depth	m	150
Static layback	m	61.42
Static cable declination	deg	171.16
Static MBR	m	20.25
Static top tension	kN	48.04
Static bottom tension	kN	5.00

Table D.6: Static report - Typical export cable 2, water depth of $150m$

D.4. Results all cables, BR, BT and TT

D.4.1. Typical inter-array cable 1 at 30m water depth

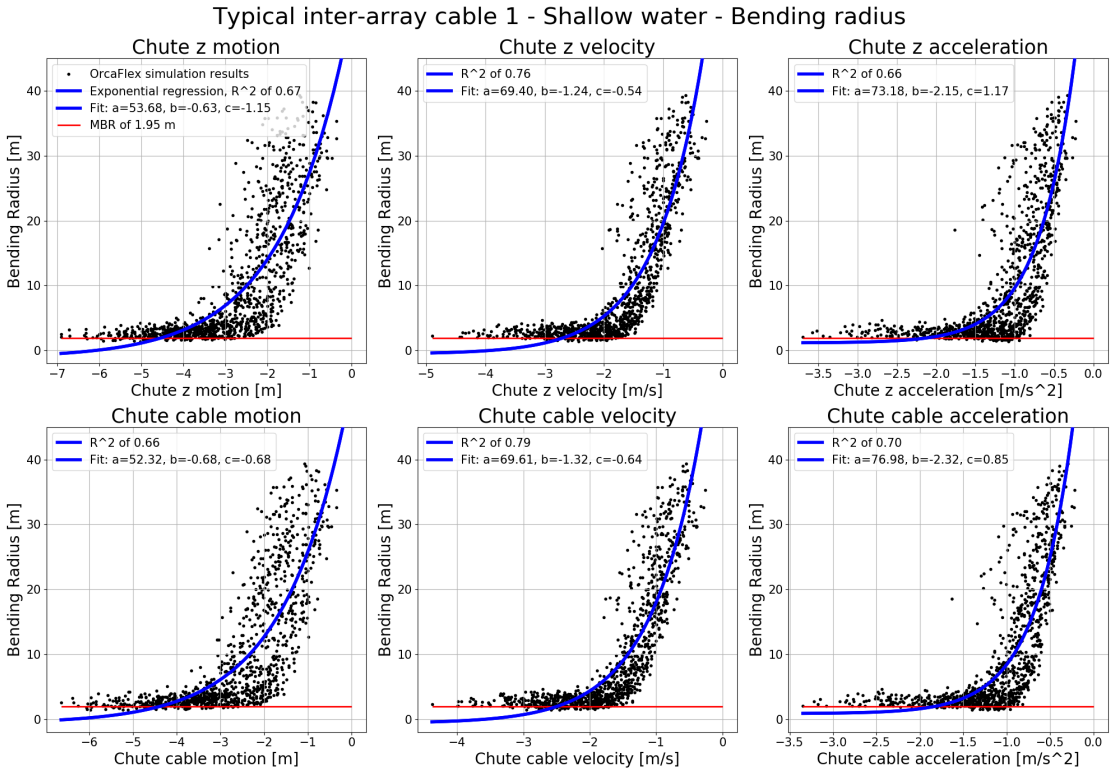

Figure D.4: Typical inter-array cable 1 at 30m water depth, MBR regression analysis

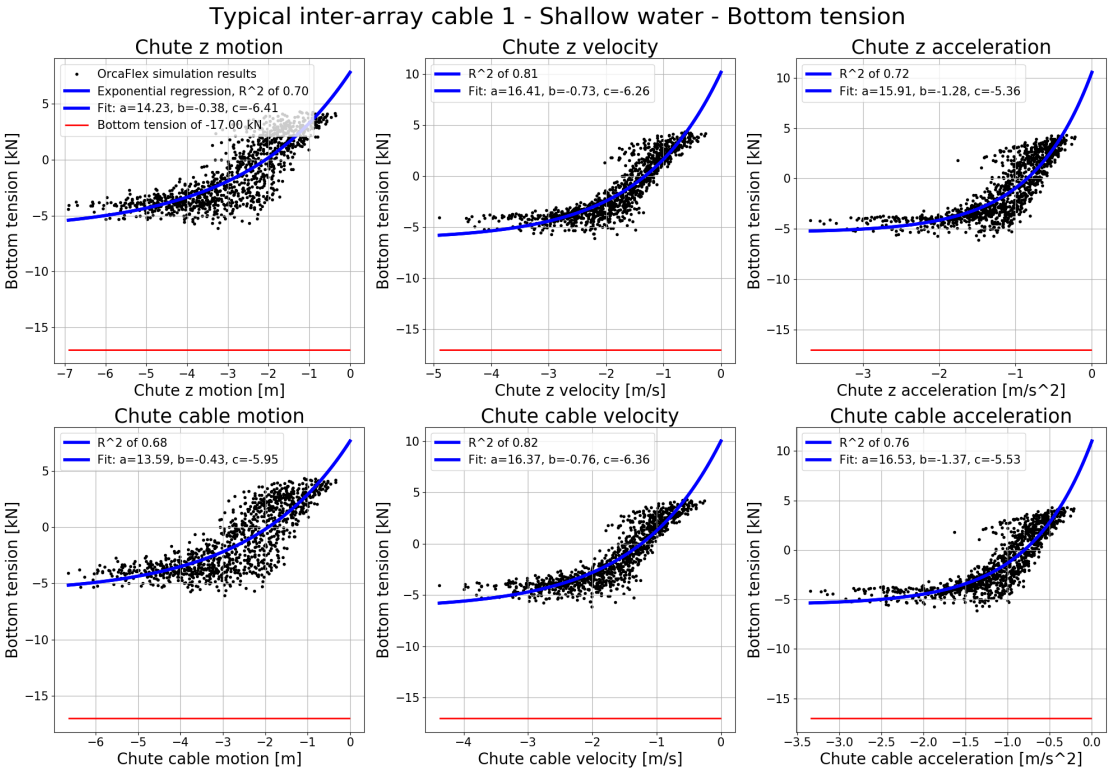

Figure D.5: Typical inter-array cable 1 at 30m water depth, BT regression analysis

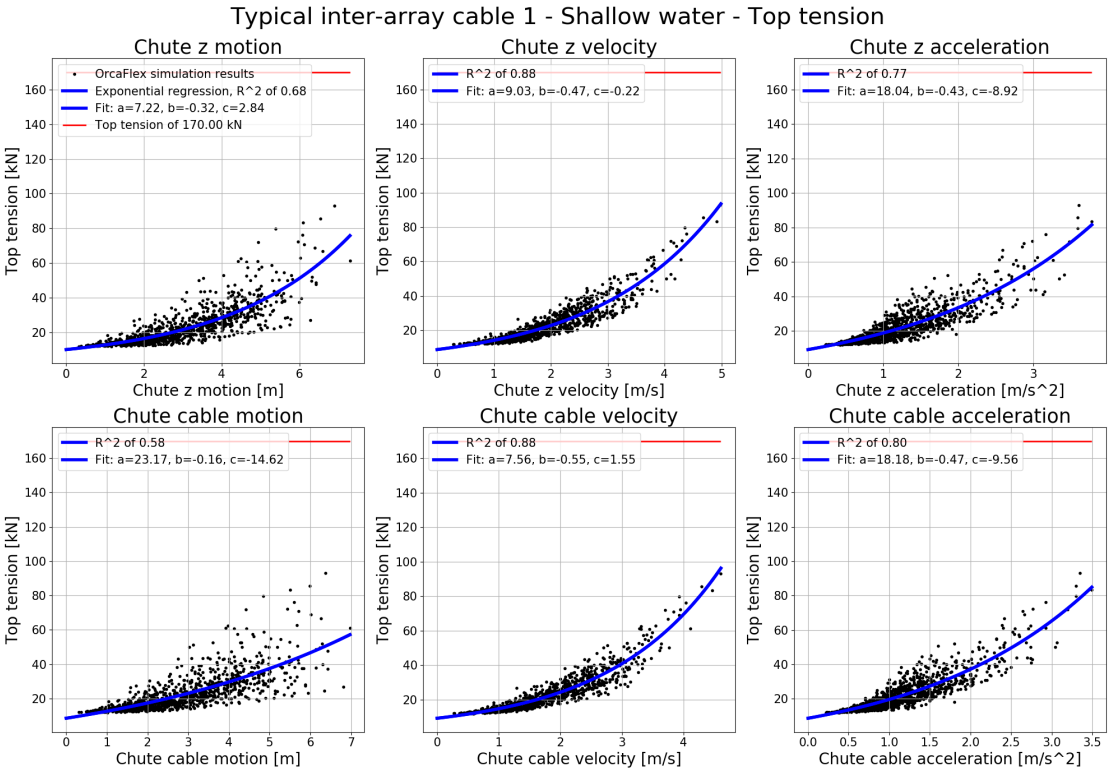

Figure D.6: Typical inter-array cable 1 at 30m water depth, TT regression analysis

D.4.2. Typical inter-array cable 2 at 30m water depth

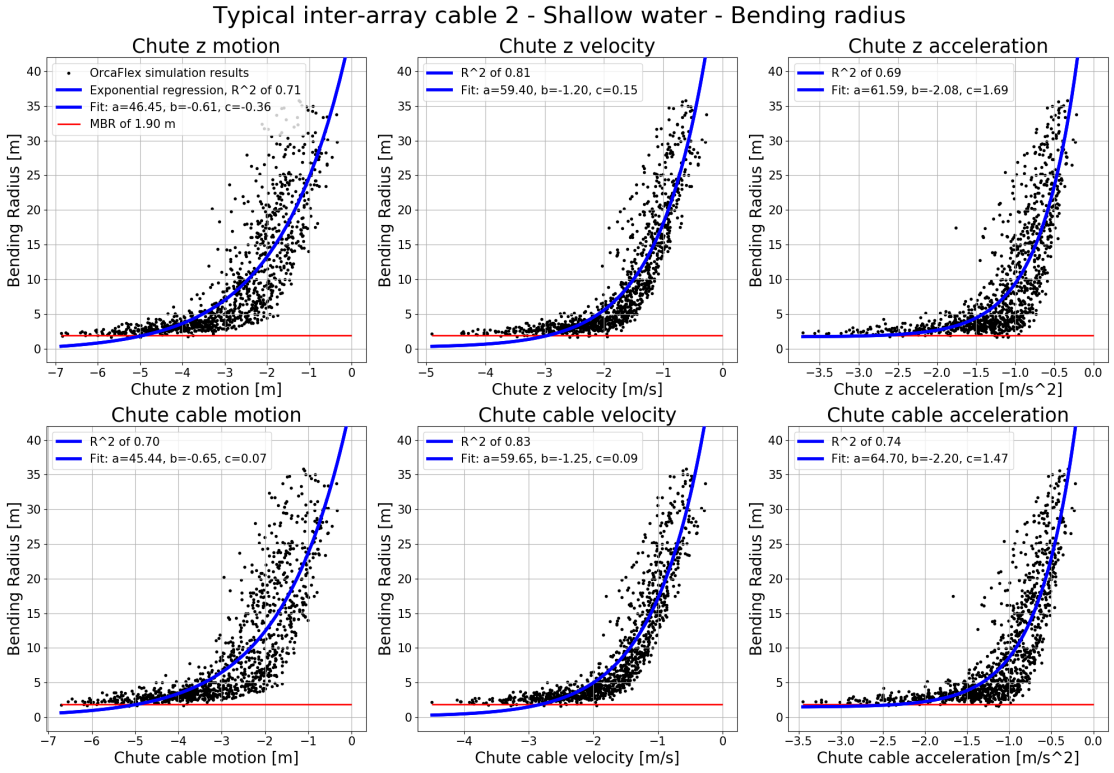

Figure D.7: Typical inter-array cable 2 at 30m water depth, MBR regression analysis

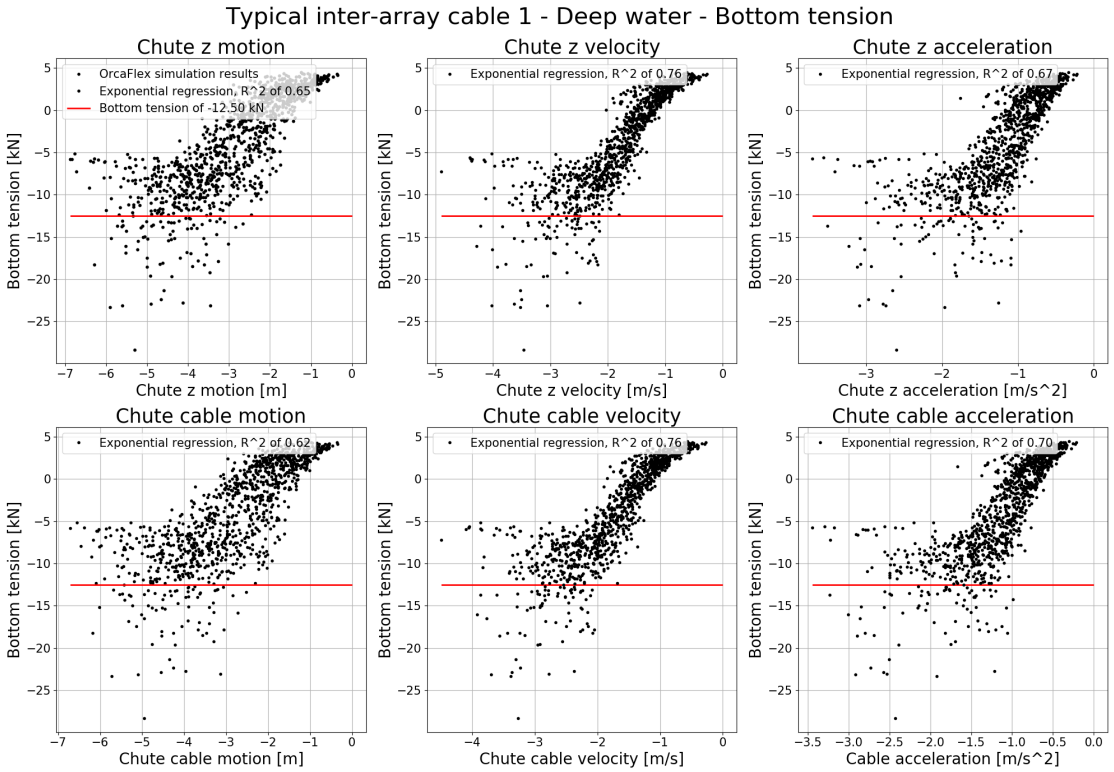

Figure D.8: Typical inter-array cable 2 at 30m water depth, BT regression analysis

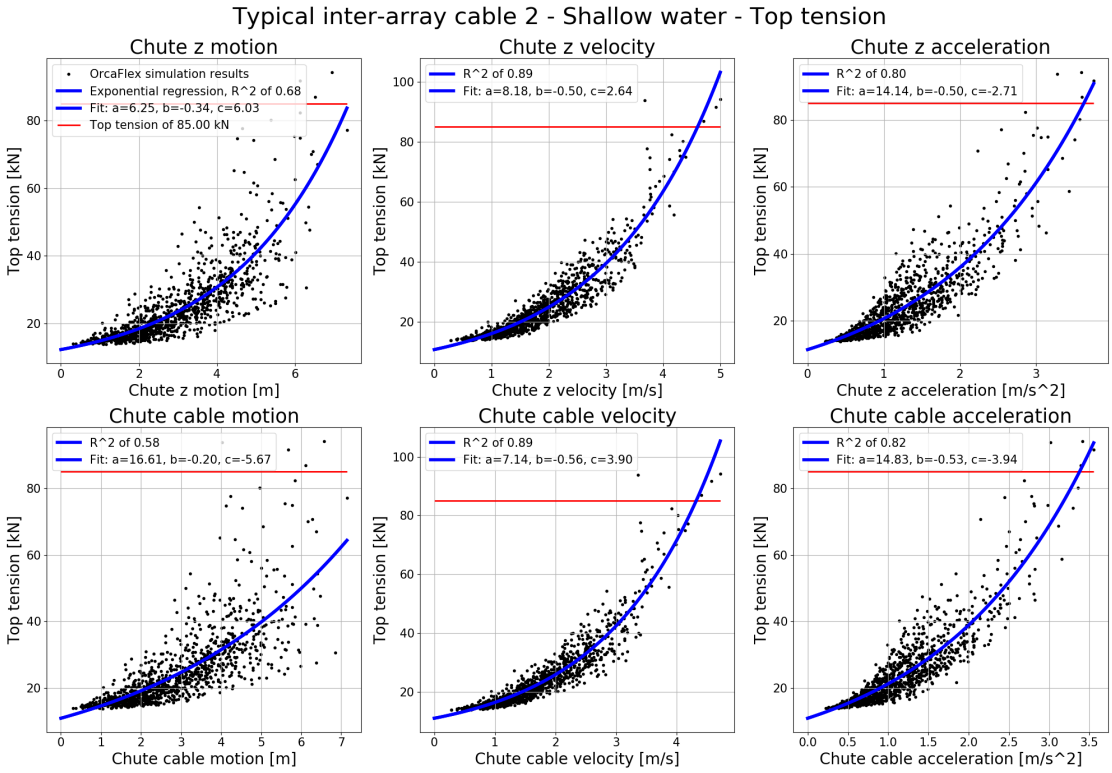

Figure D.9: Typical inter-array cable 2 at 30m water depth, TT regression analysis

D.4.3. Typical export cable 1 at 30m water depth

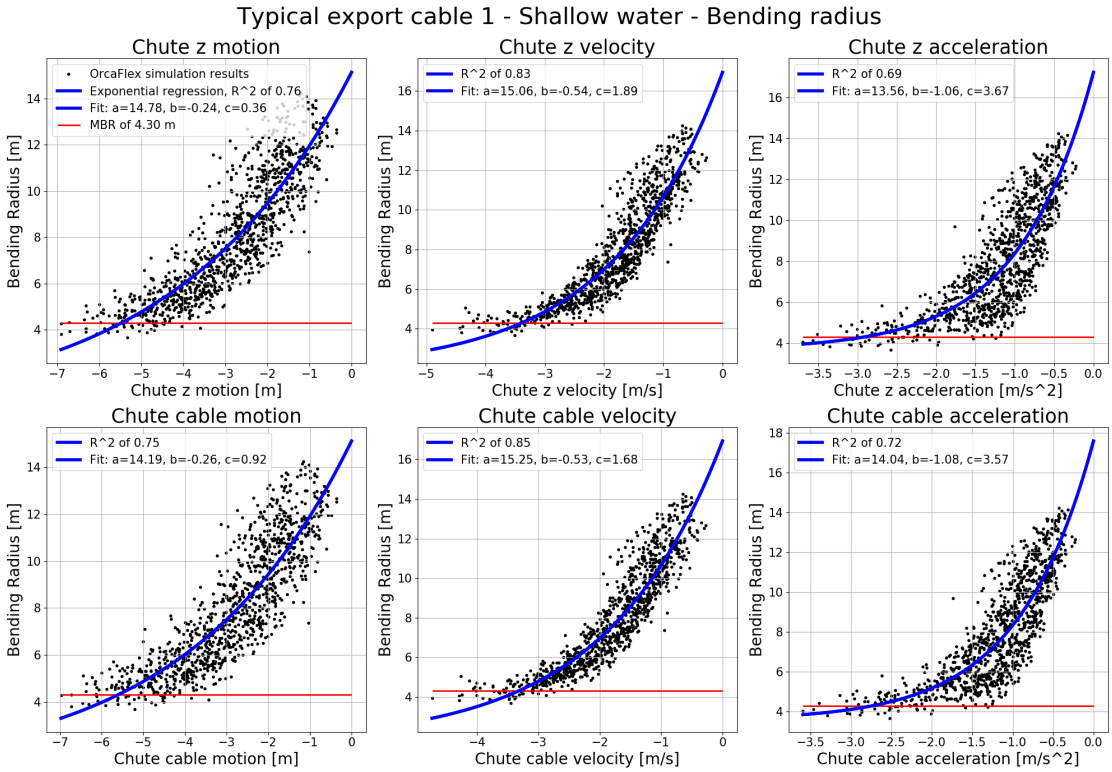

Figure D.10: Typical export cable 1 at 30m water depth, MBR regression analysis

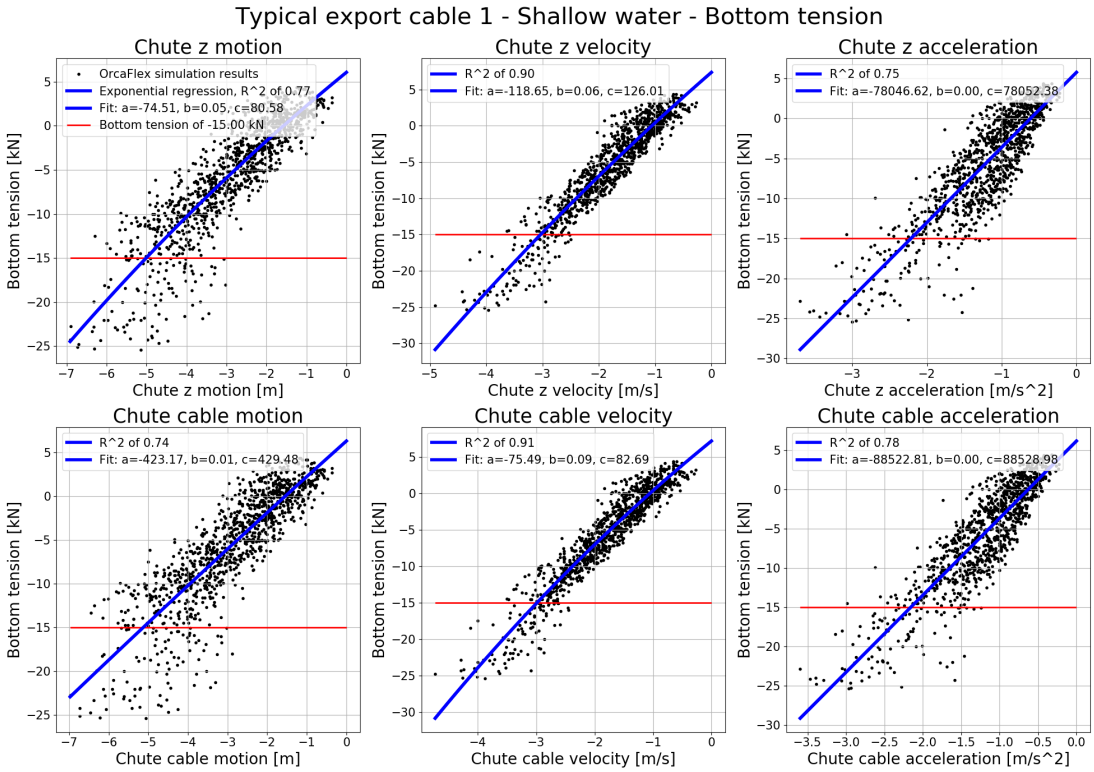

Figure D.11: Typical export cable 1 at 30m water depth, BT regression analysis

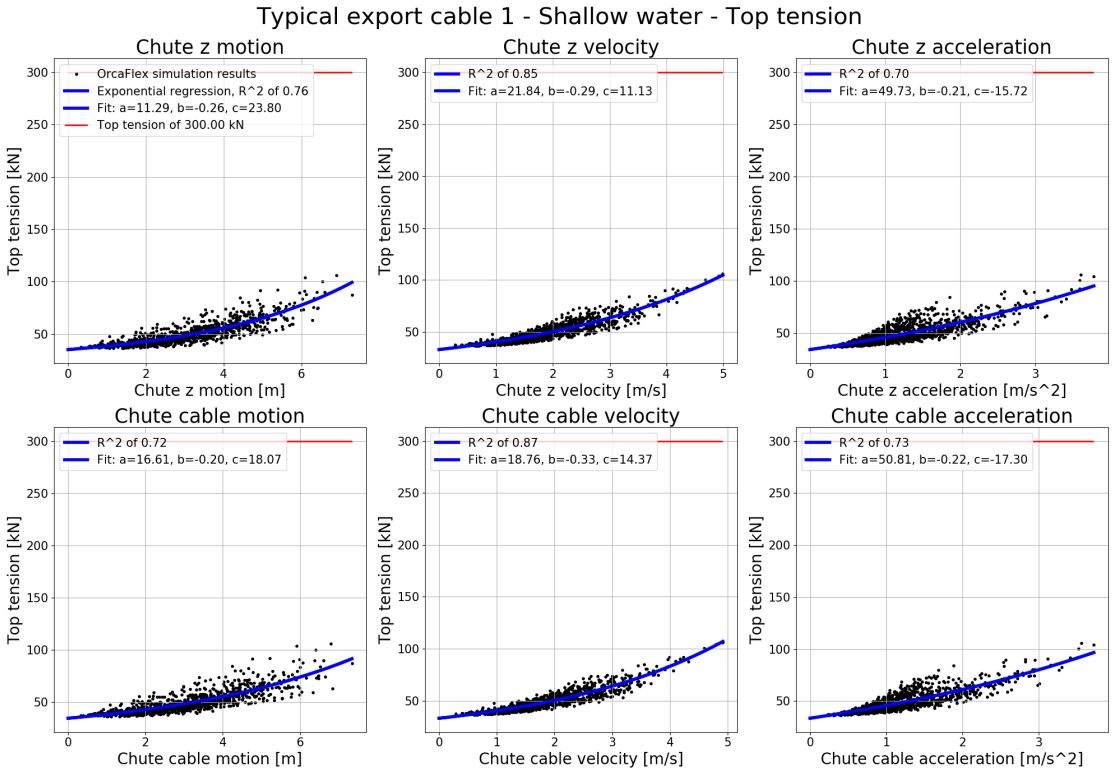

Figure D.12: Typical export cable 1 at 30m water depth, TT regression analysis

D.4.4. Typical export cable 2 at 30m water depth

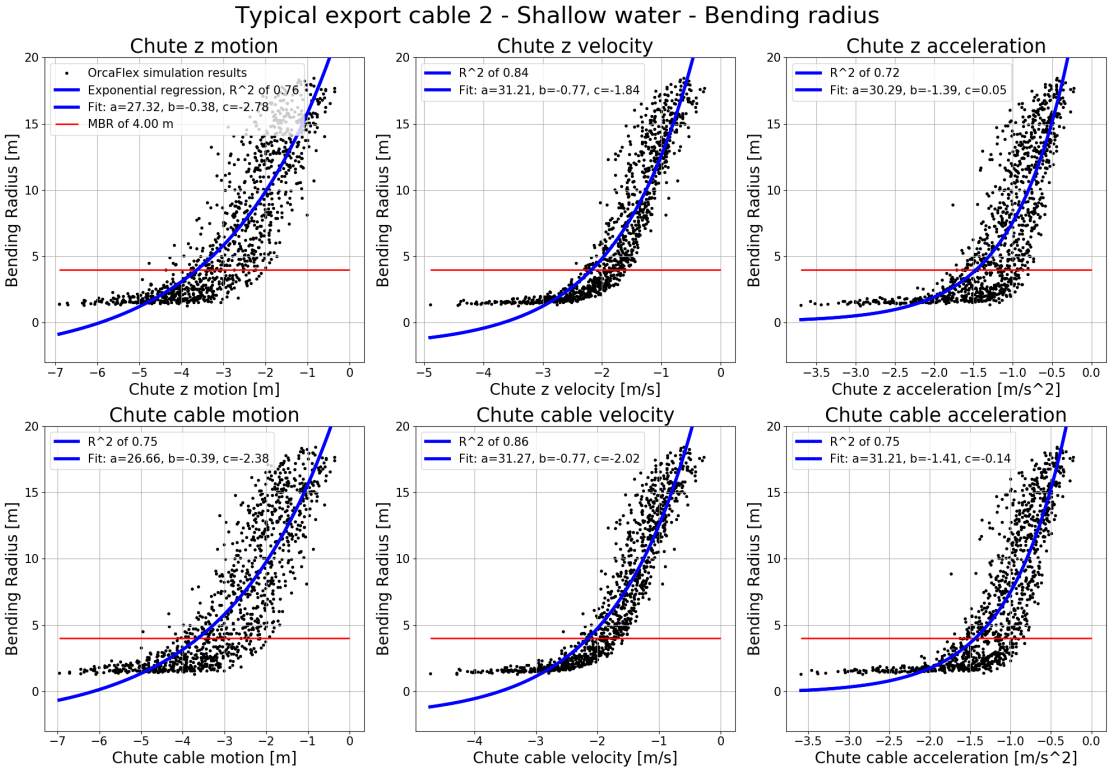

Figure D.13: Typical export cable 2 at 30m water depth, MBR regression analysis

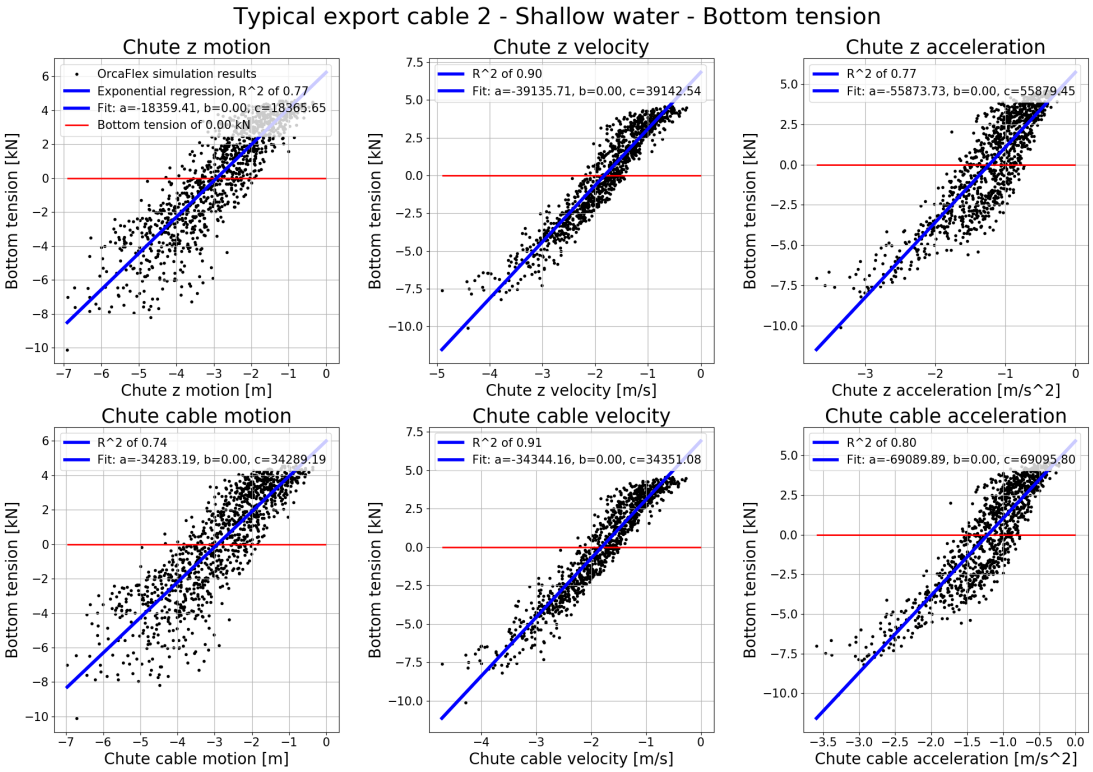

Figure D.14: Typical export cable 2 at 30m water depth, BT regression analysis

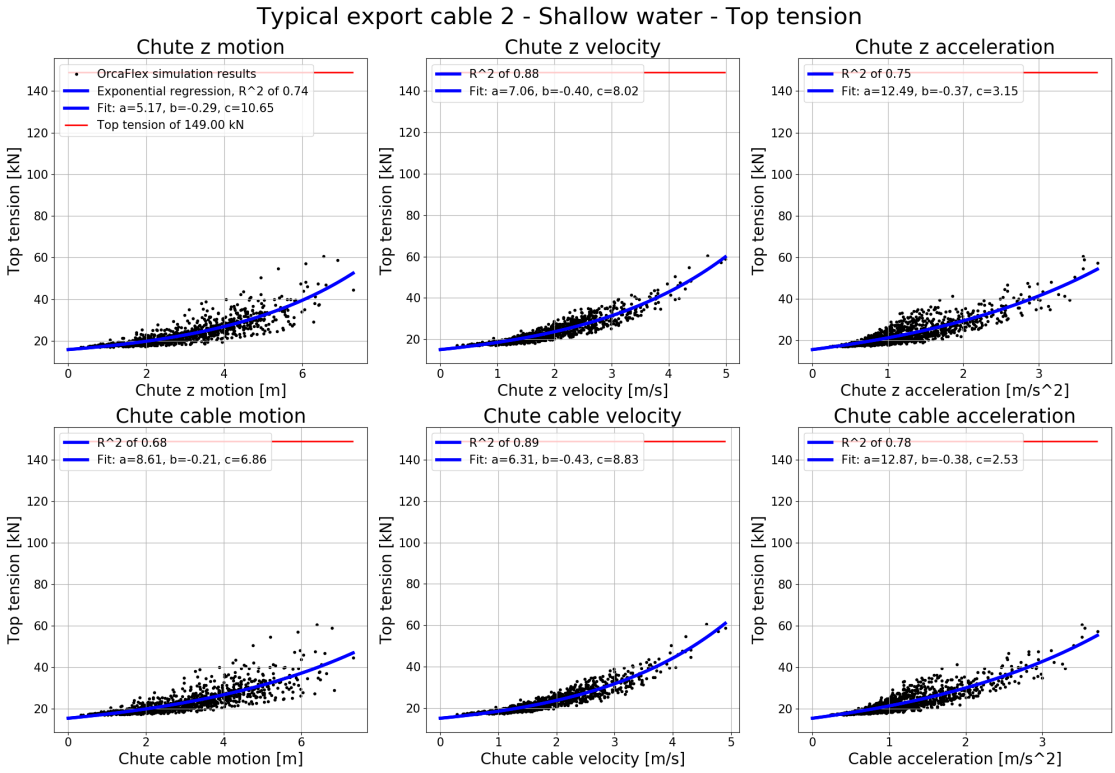

Figure D.15: Typical export cable 2 at 30m water depth, TT regression analysis

D.4.5. Typical inter-array cable 1 at 150m water depth

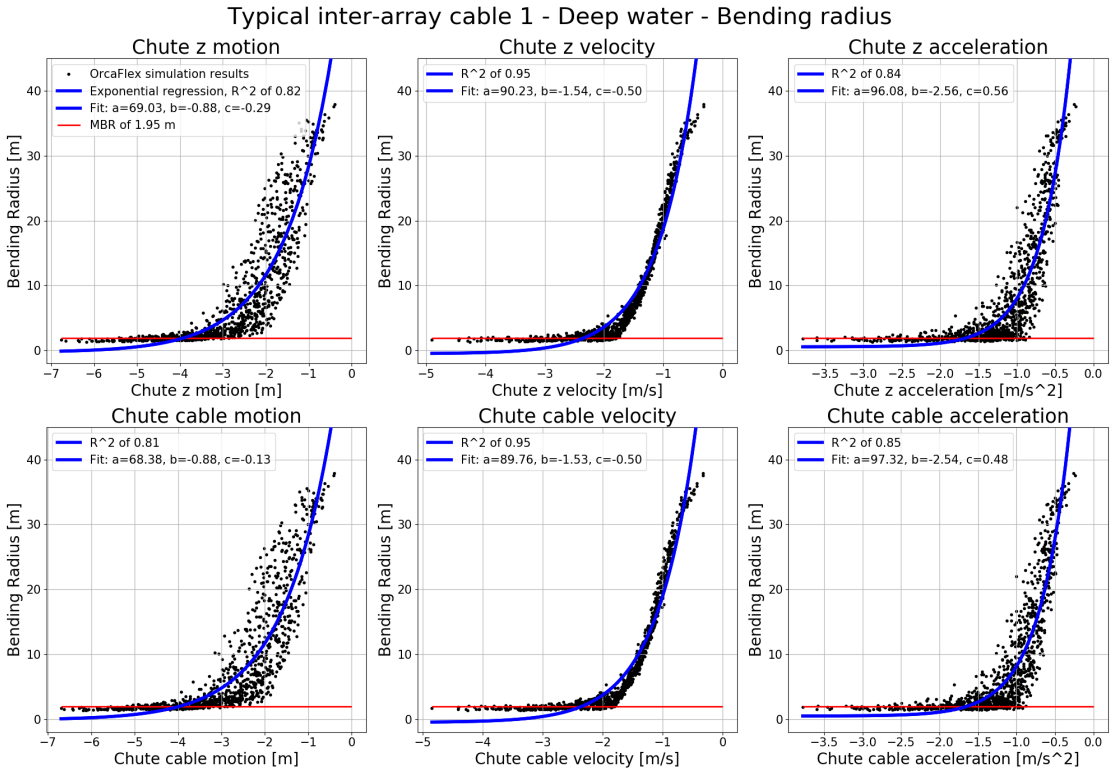

Figure D.16: Typical inter-array cable 1 at 150m water depth, MBR regression analysis

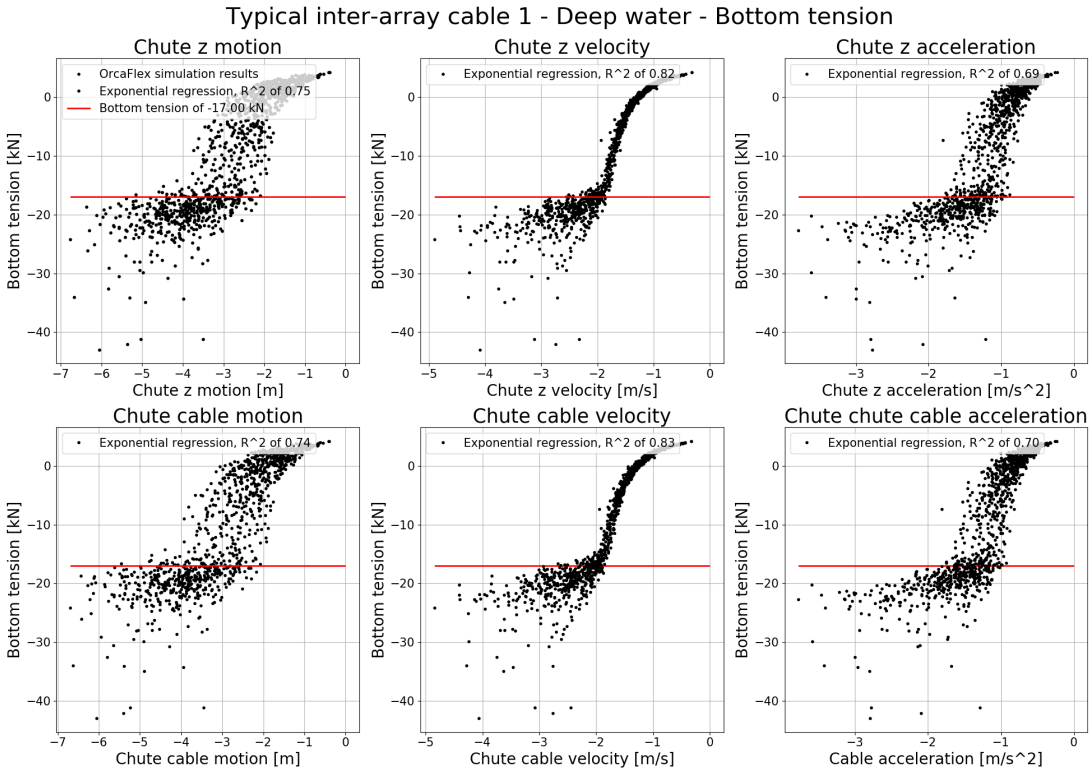

Figure D.17: Typical inter-array cable 1 at 150m water depth, BT regression analysis

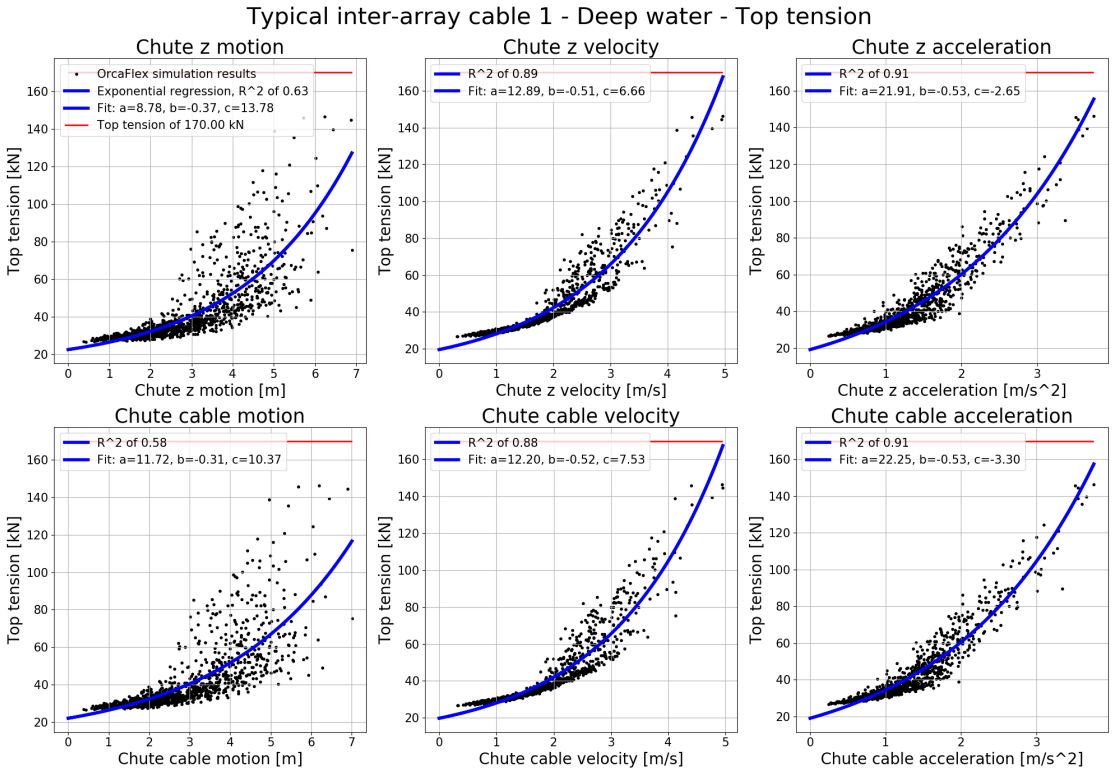

Figure D.18: Typical inter-array cable 1 at 150m water depth, TT regression analysis

D.4.6. Typical inter-array cable 2 at 150m water depth

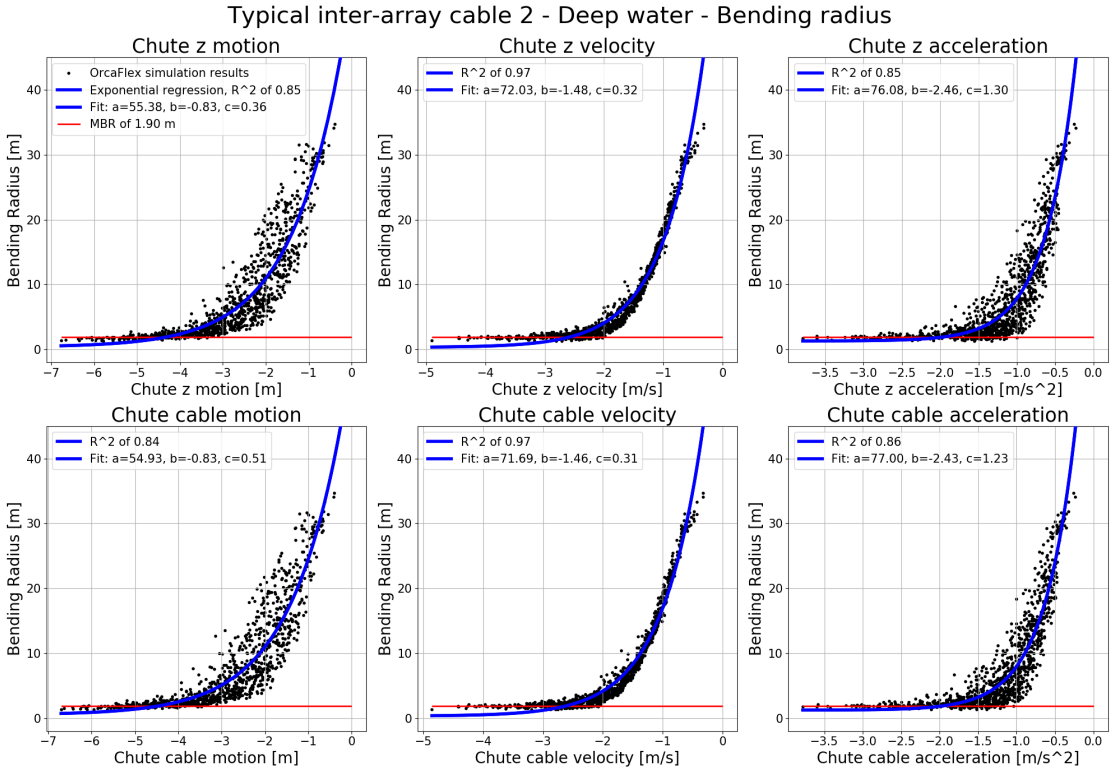

Figure D.19: Typical inter-array cable 2 at 150m water depth, MBR regression analysis

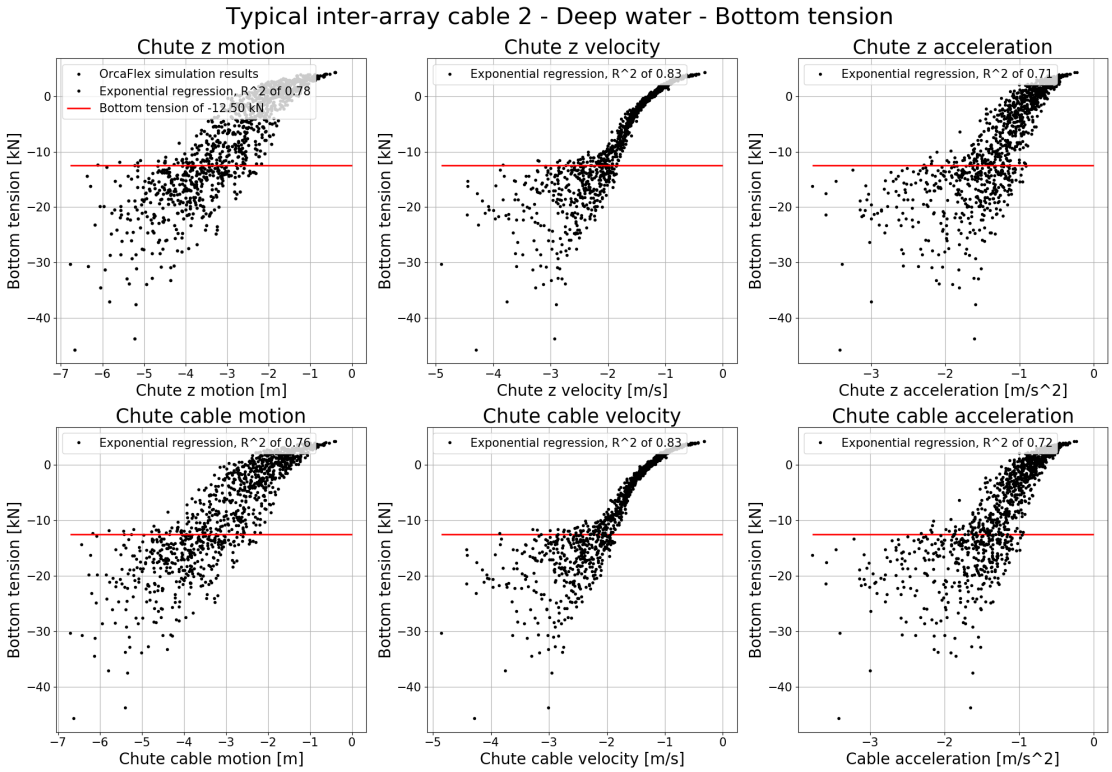

Figure D.20: Typical inter-array cable 2 at 150m water depth, BT regression analysis

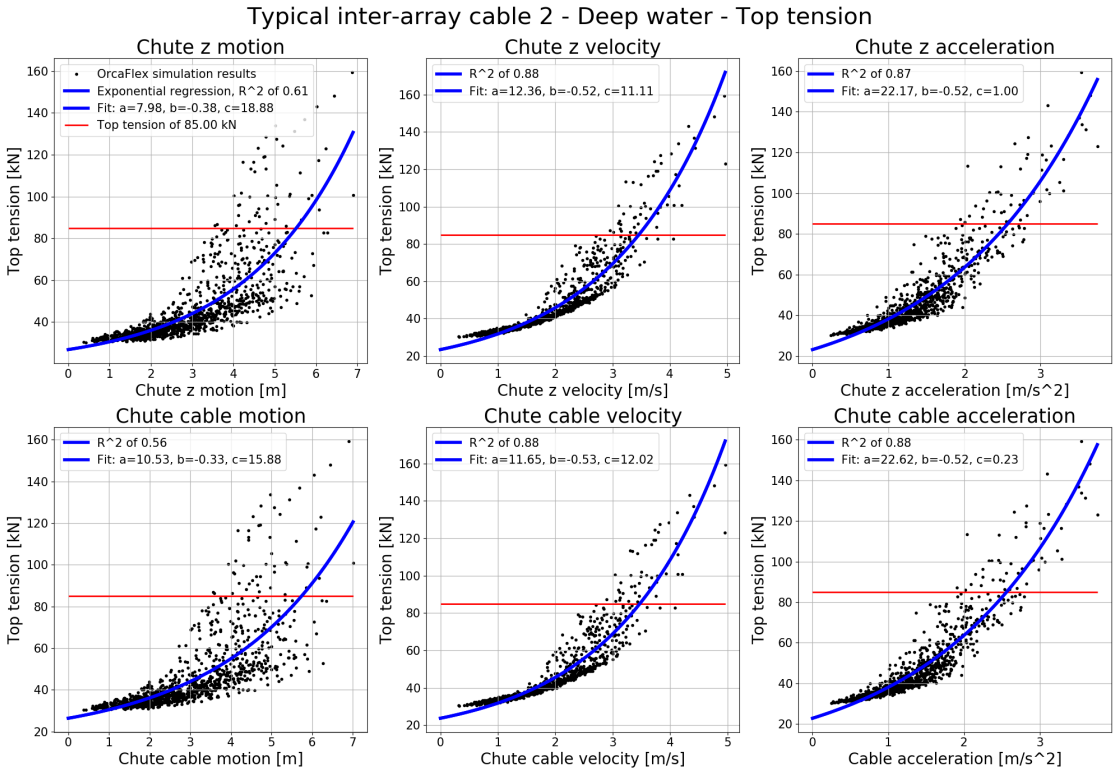

Figure D.21: Typical inter-array cable 2 at 150m water depth, TT regression analysis

D.4.7. Typical export cable 1 at 150 m water depth

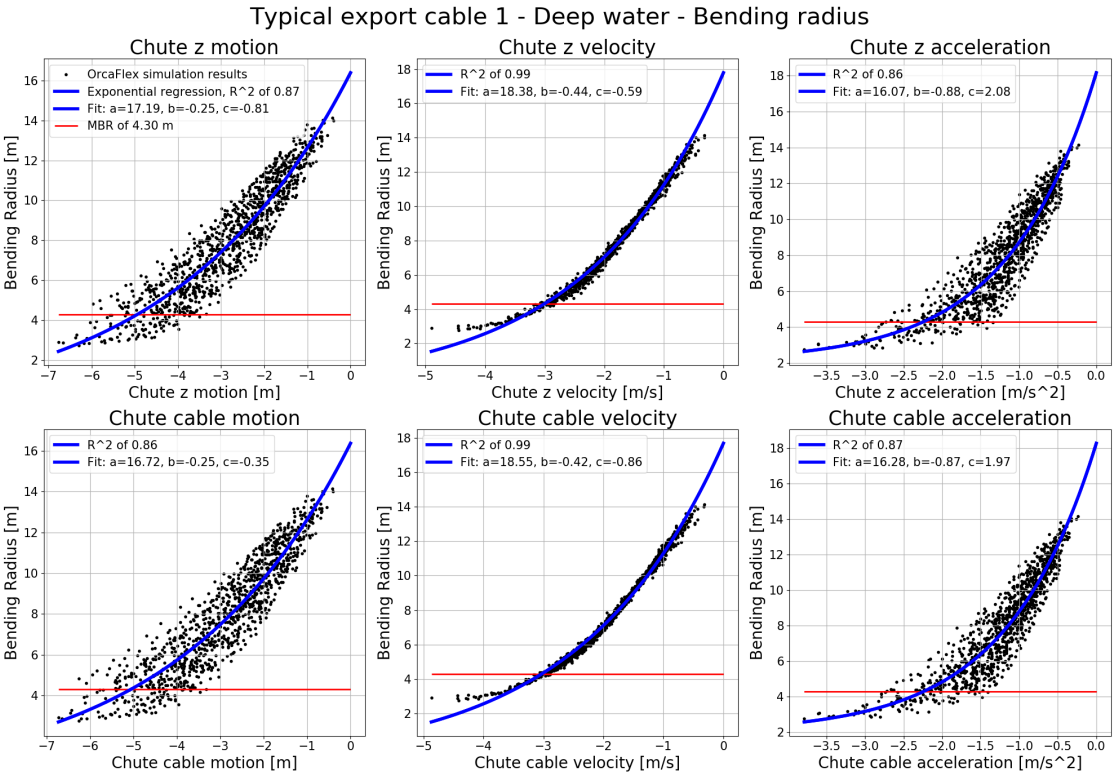

Figure D.22: Typical export cable 1 at 150m water depth, MBR regression analysis

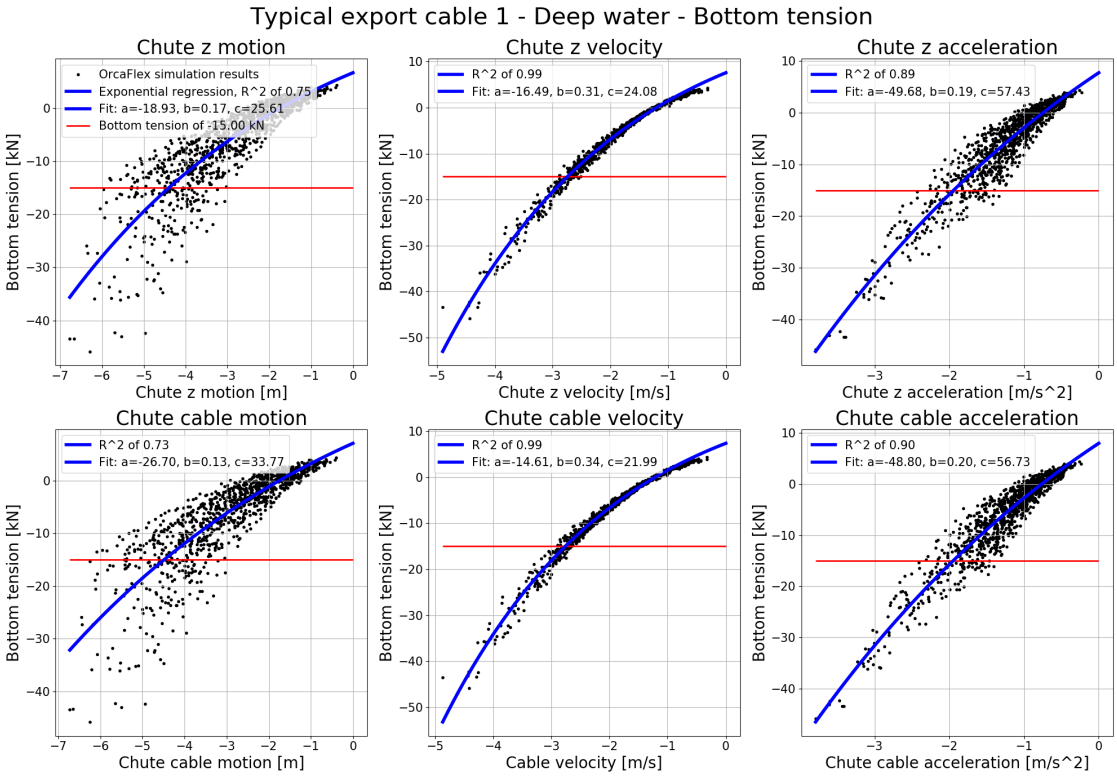

Figure D.23: Typical export cable 1 at 150m water depth, BT regression analysis

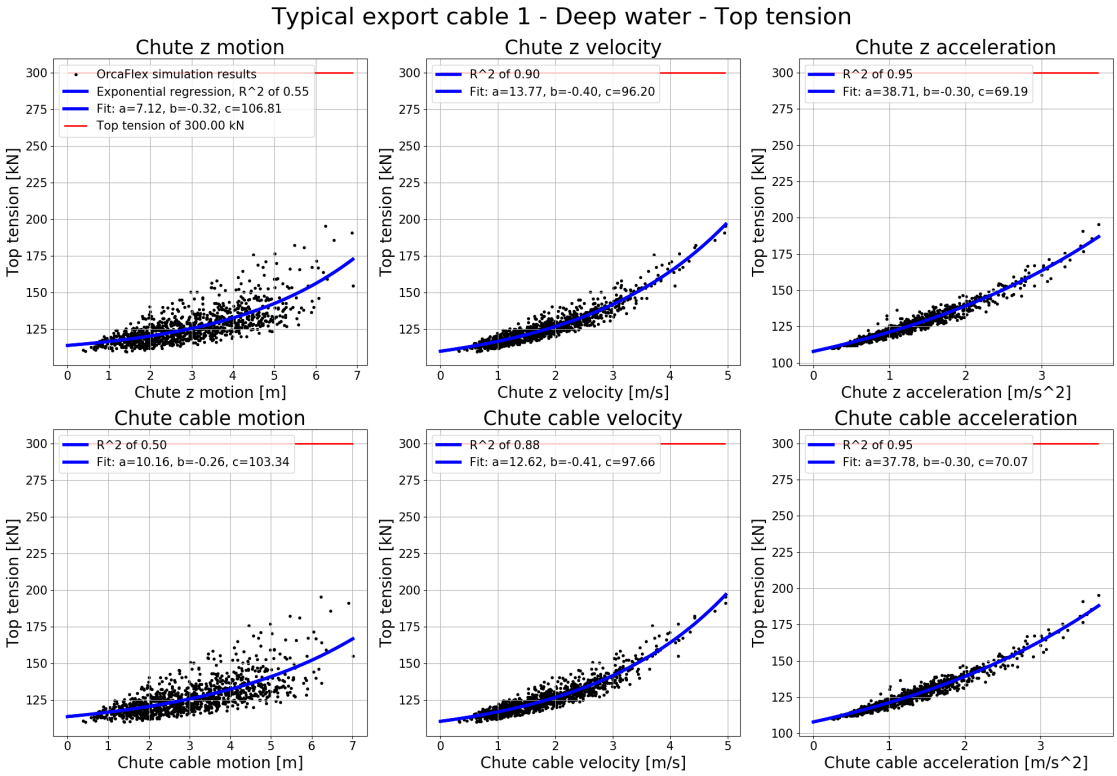

Figure D.24: Typical export cable 1 at 150m water depth, TT regression analysis

D.4.8. Typical export cable 2 at 150m water depth

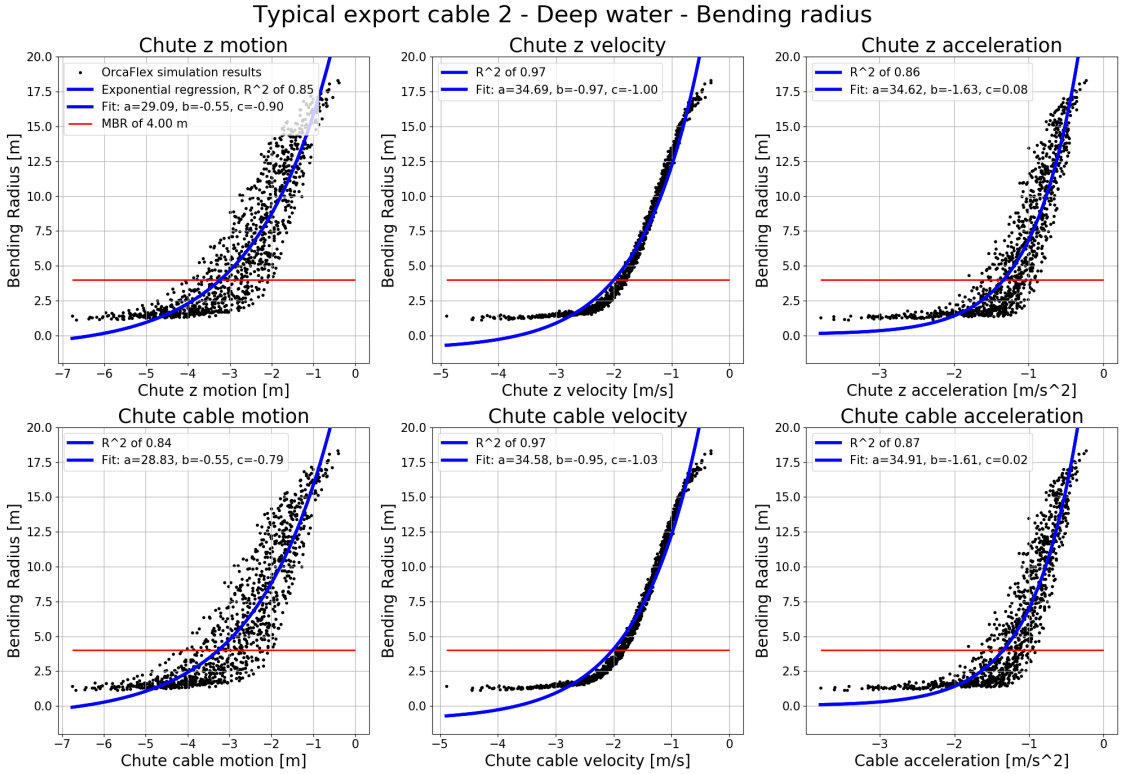

Figure D.25: Typical export cable 2 at 150m water depth, MBR regression analysis

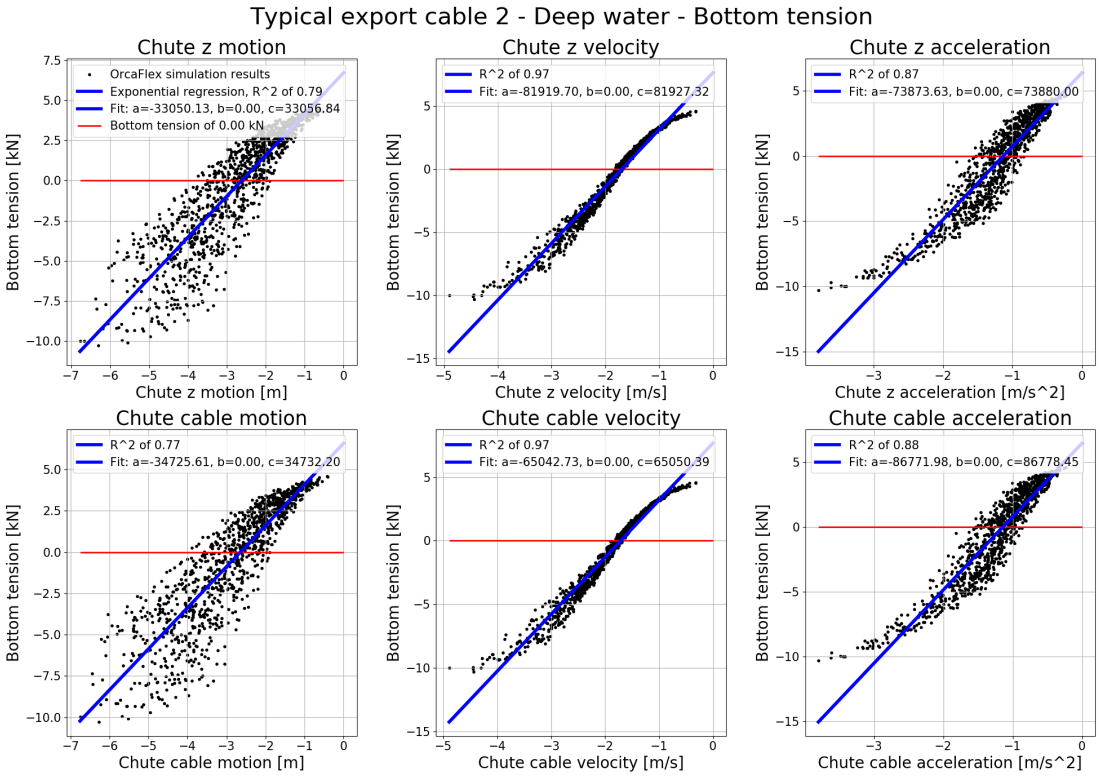

Figure D.26: Typical export cable 2 at 150m water depth, BT regression analysis

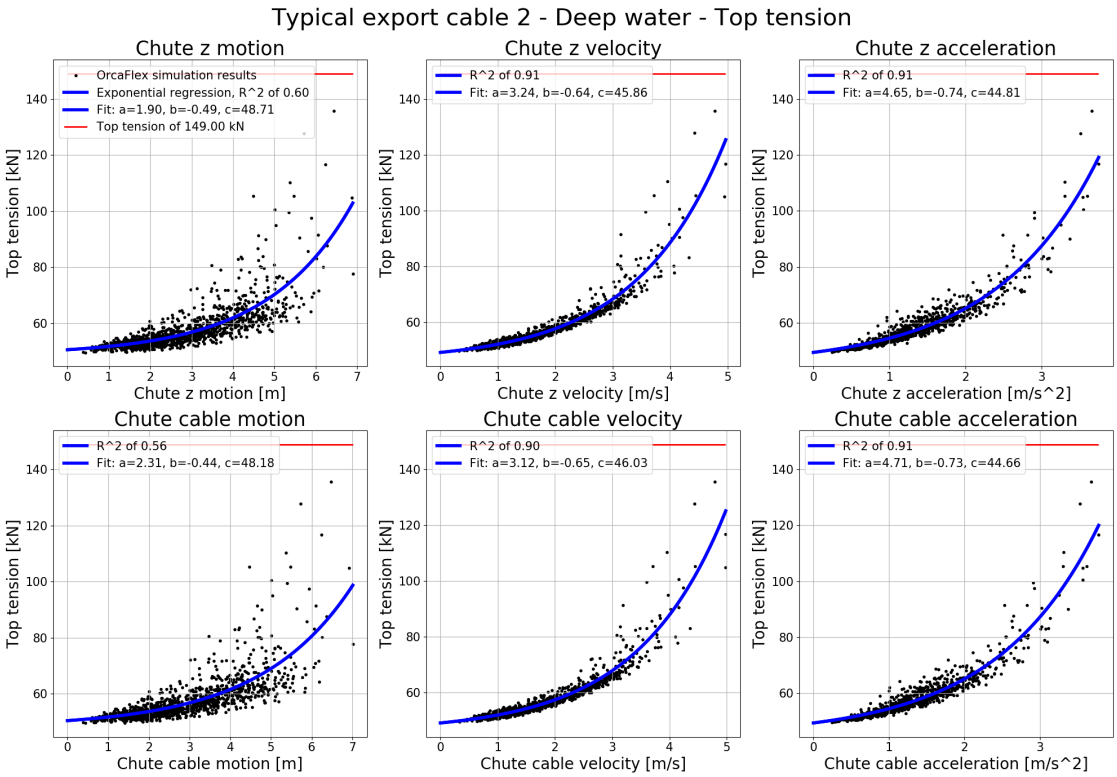

Figure D.27: Typical export cable 2 at 150m water depth, TT regression analysis

D.5. Normal lay configuration verification results

D.5.1. Typical inter-array cable 1, multiple static bottom tensions (2, 10 & 20 kN)

Minimum bending radius

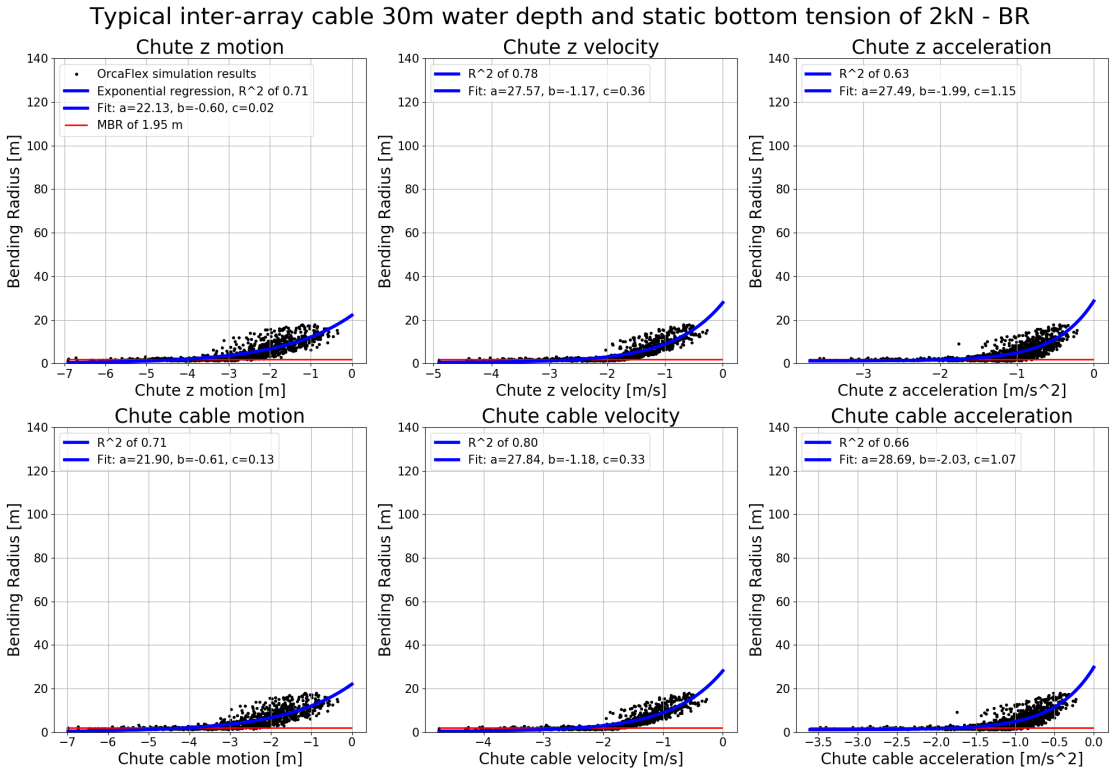

Figure D.28: Typical inter-array cable 1 at 30m water depth with a static bottom tension of 2kN, MBR regression analysis

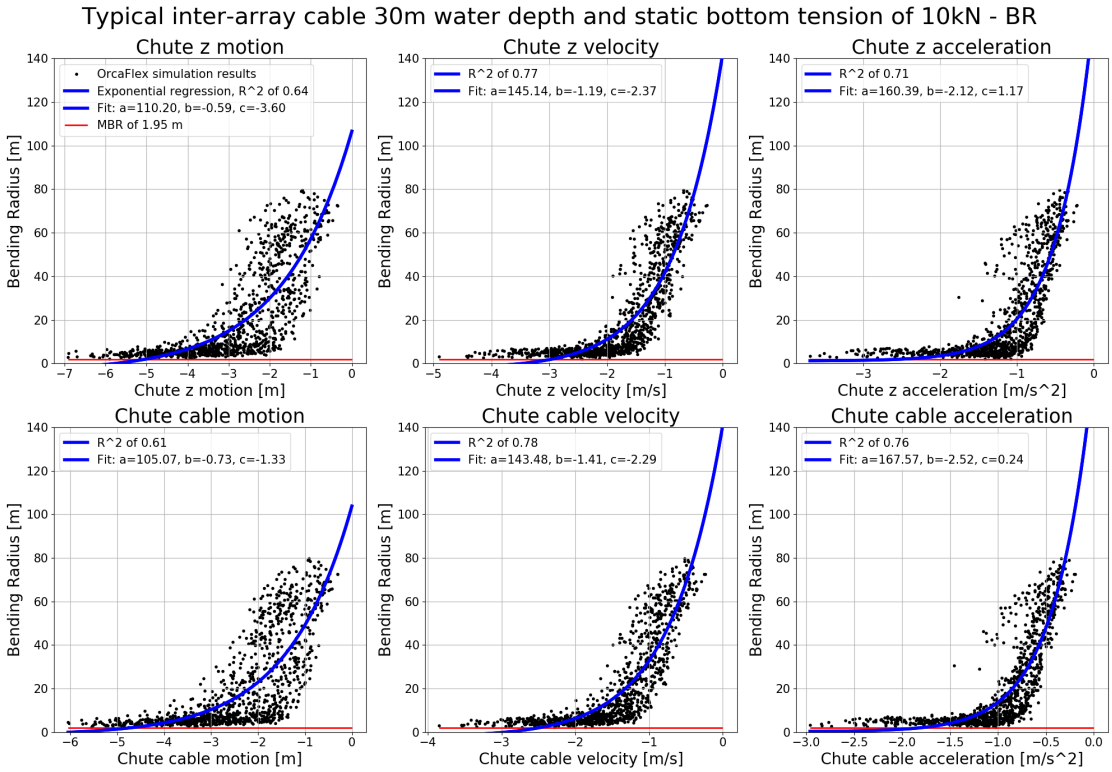

Figure D.29: Typical inter-array cable 1 at 30m water depth with a static bottom tension of 10kN, MBR regression analysis

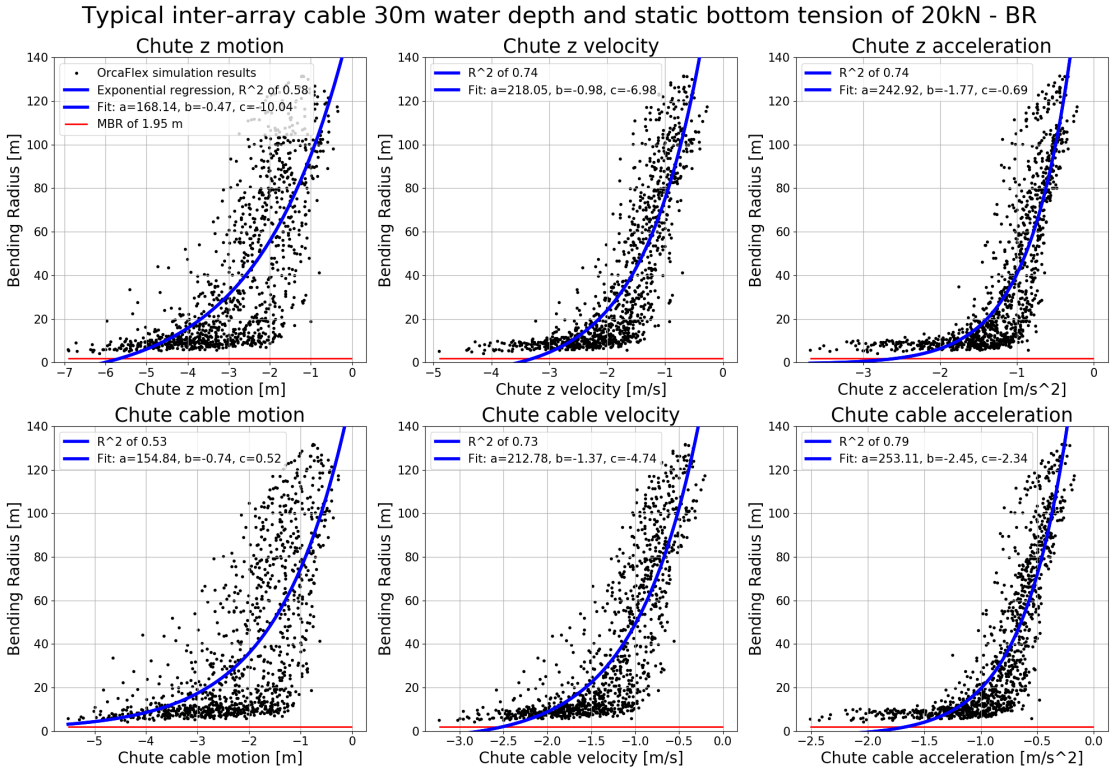

Figure D.30: Typical inter-array cable 1 at 30m water depth with a static bottom tension of 20kN, MBR regression analysis

Minimum bottom tension

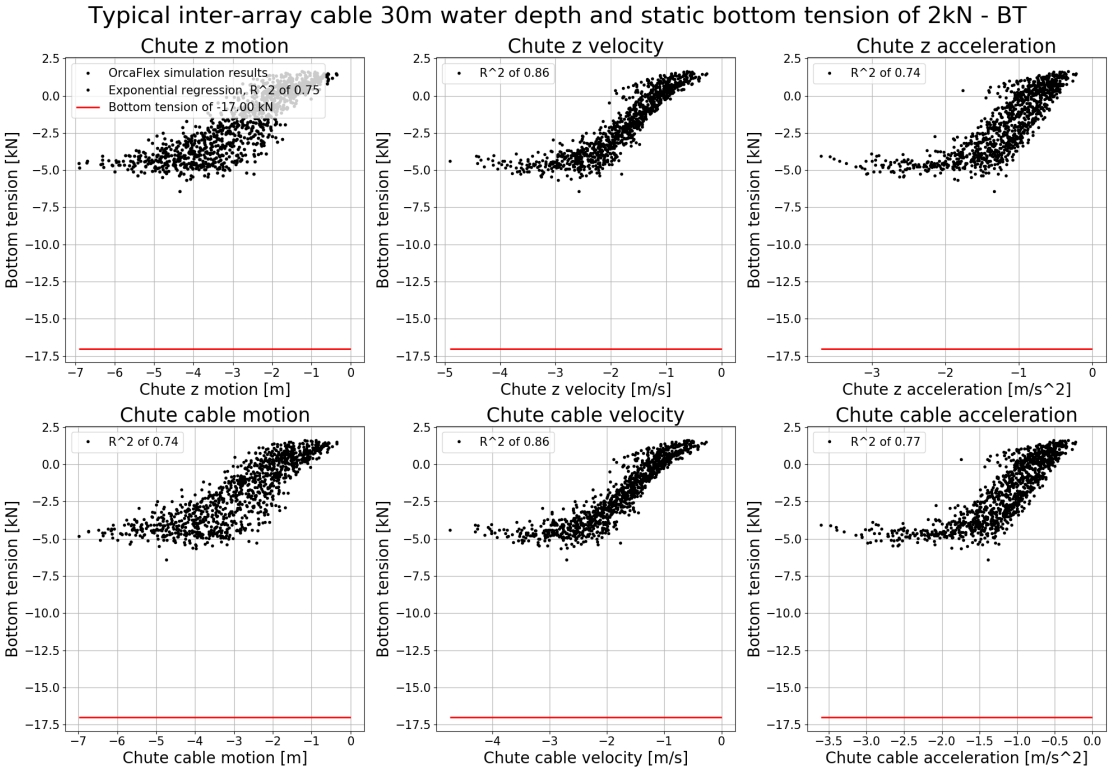

Figure D.31: Typical inter-array cable 1 at 30m water depth with a static bottom tension of 2kN, BT regression analysis

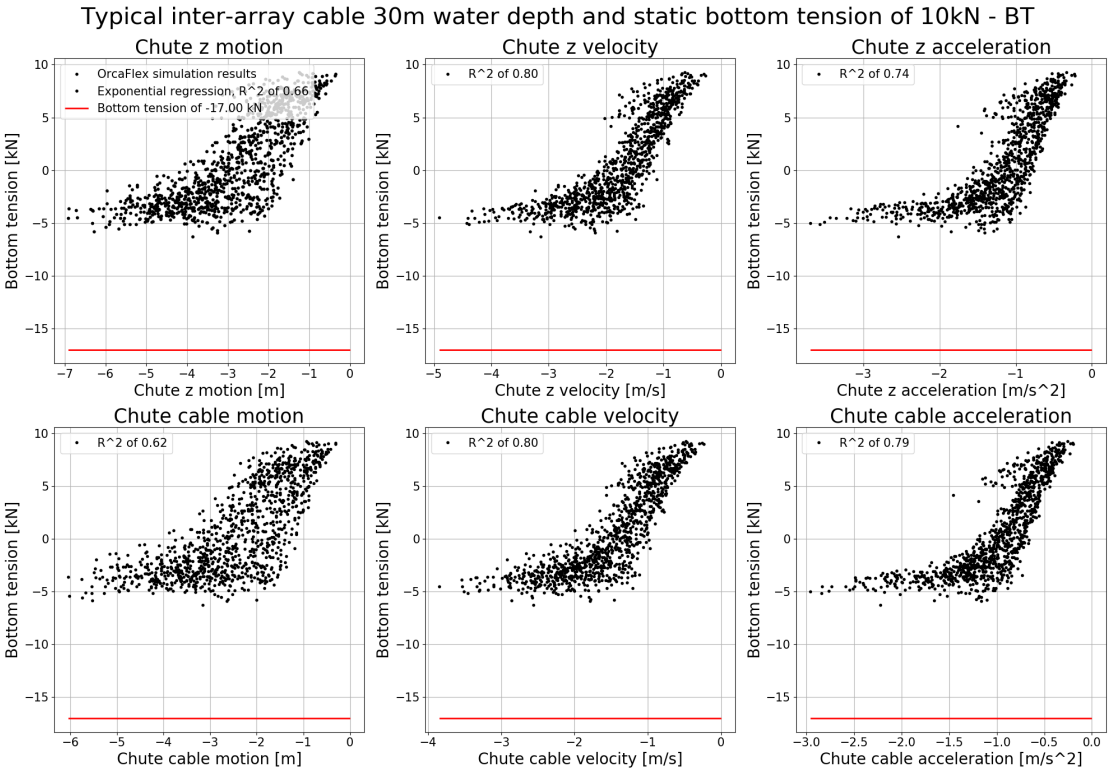

Figure D.32: Typical inter-array cable 1 at 30m water depth with a static bottom tension of 10kN, BT regression analysis

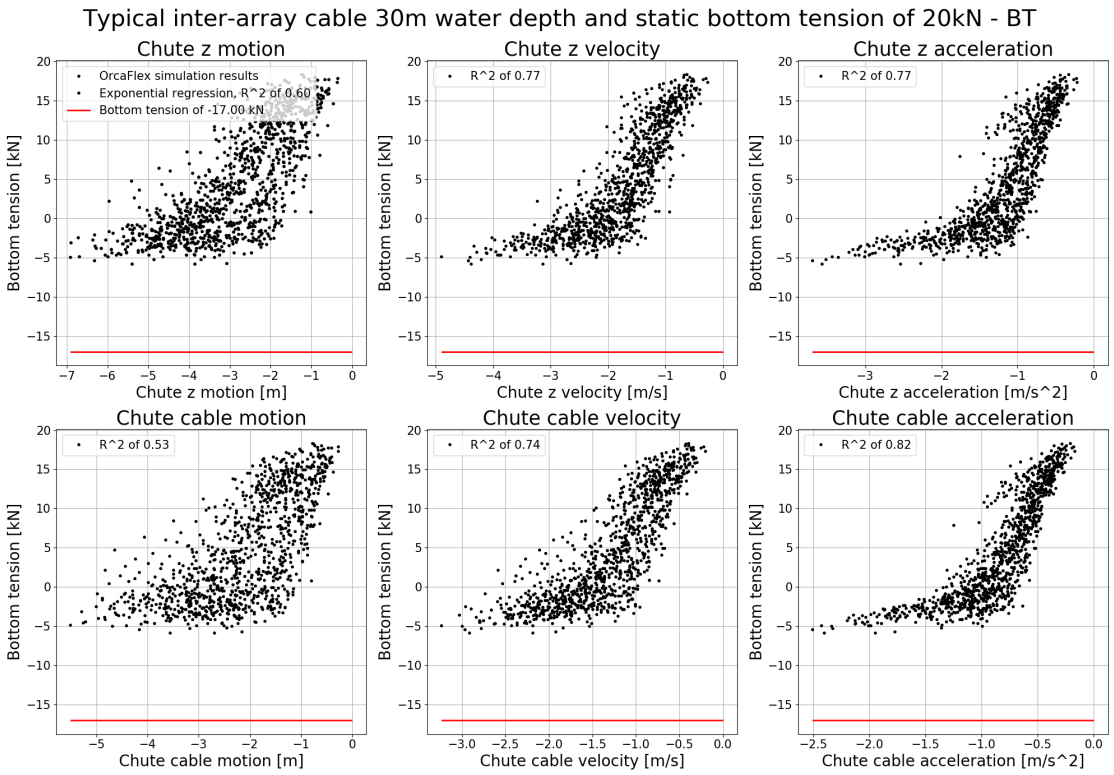

Figure D.33: Typical inter-array cable 1 at 30m water depth with a static bottom tension of 20kN, BT regression analysis

Maximum top tension

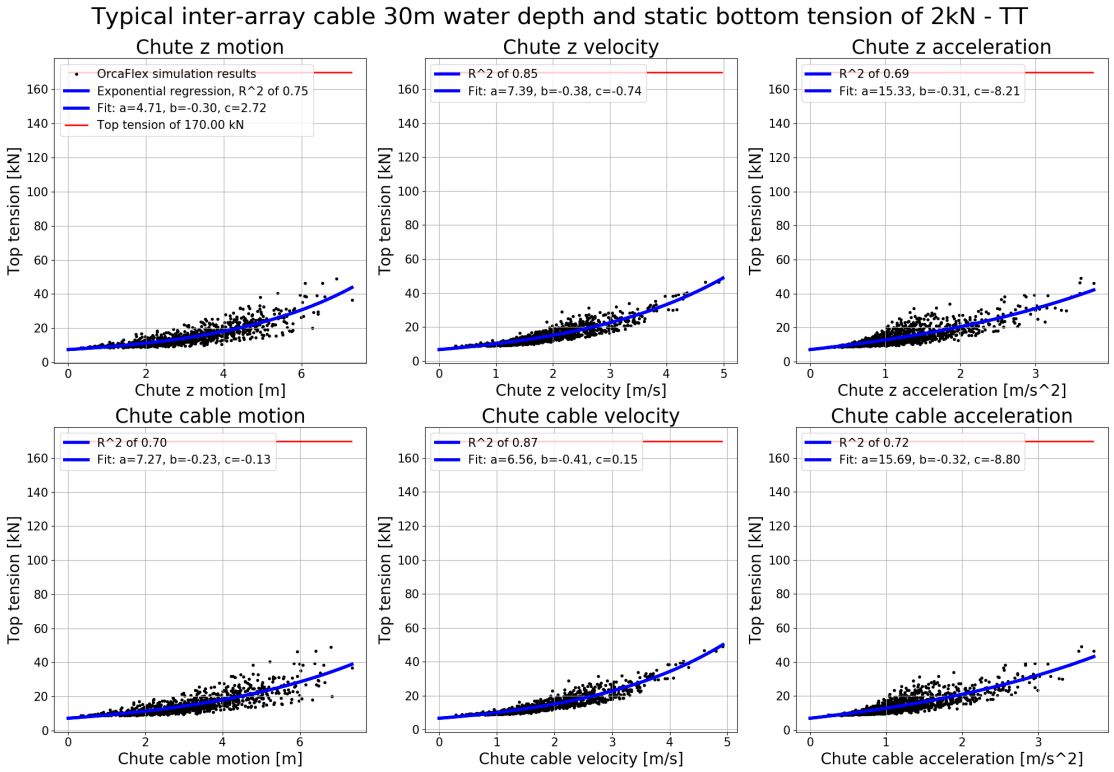

Figure D.34: Typical inter-array cable 1 at 30m water depth with a static bottom tension of 2kN, TT regression analysis

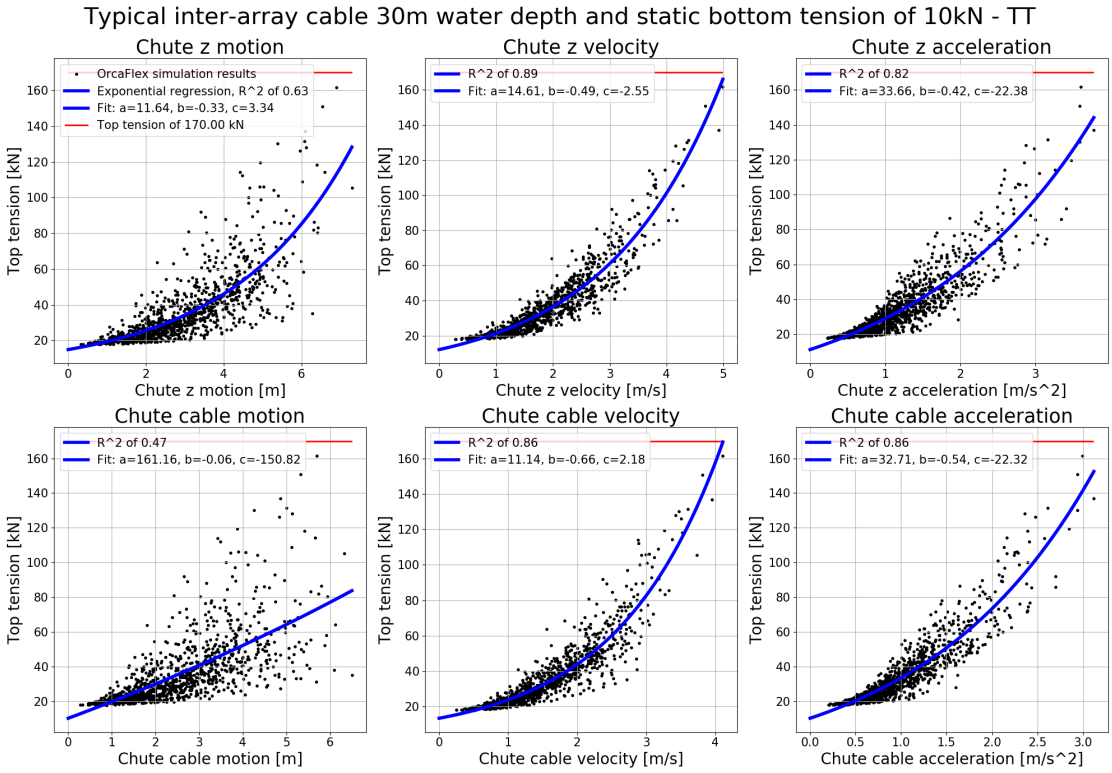

Figure D.35: Typical inter-array cable 1 at 30m water depth with a static bottom tension of 10kN, TT regression analysis

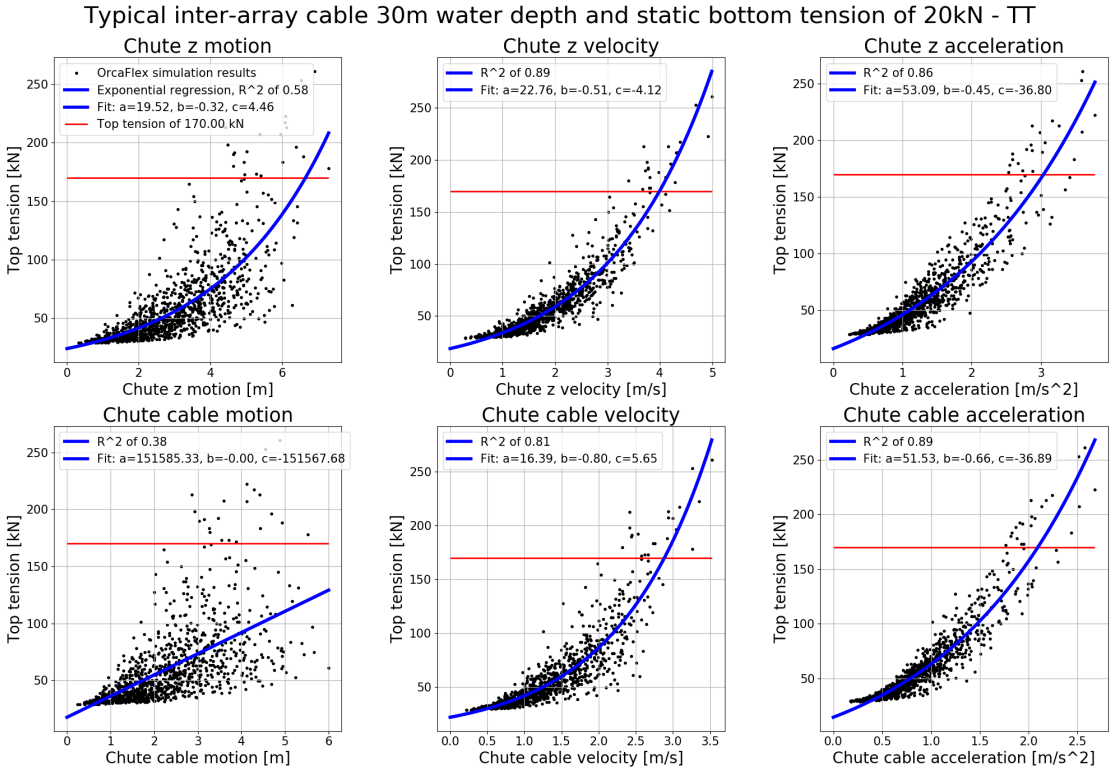

Figure D.36: Typical inter-array cable 1 at 30m water depth with a static bottom tension of 20kN, TT regression analysis

D.6. Another vessel verification results

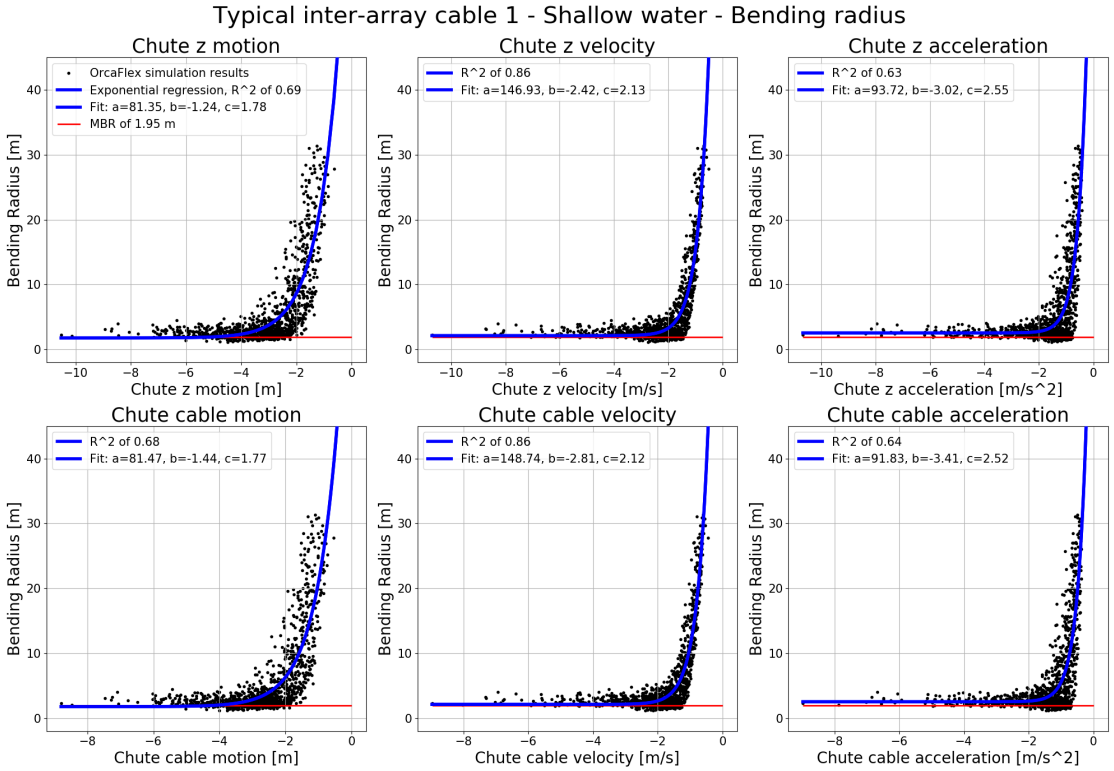

Figure D.37: Typical inter-array cable 1 at 30m water depth with a static bottom tension of 5kN, BR regression analysis, another vessel

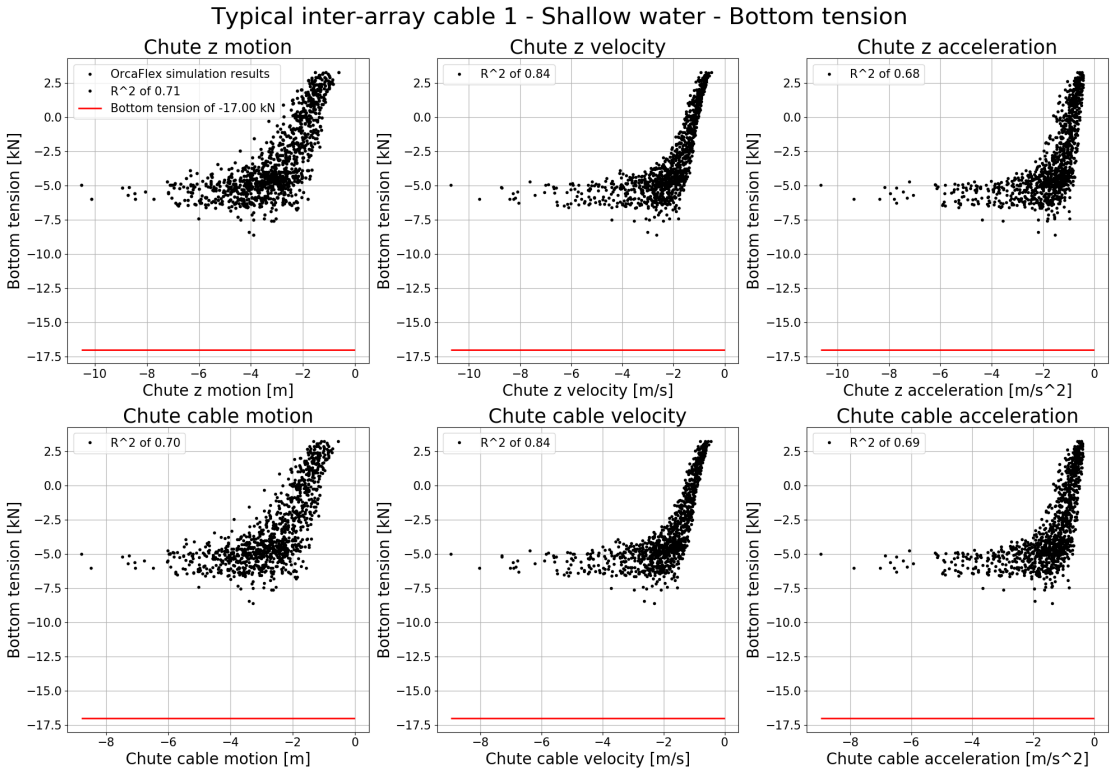

Figure D.38: Typical inter-array cable 1 at 30m water depth with a static bottom tension of 5kN, BT regression analysis, another vessel

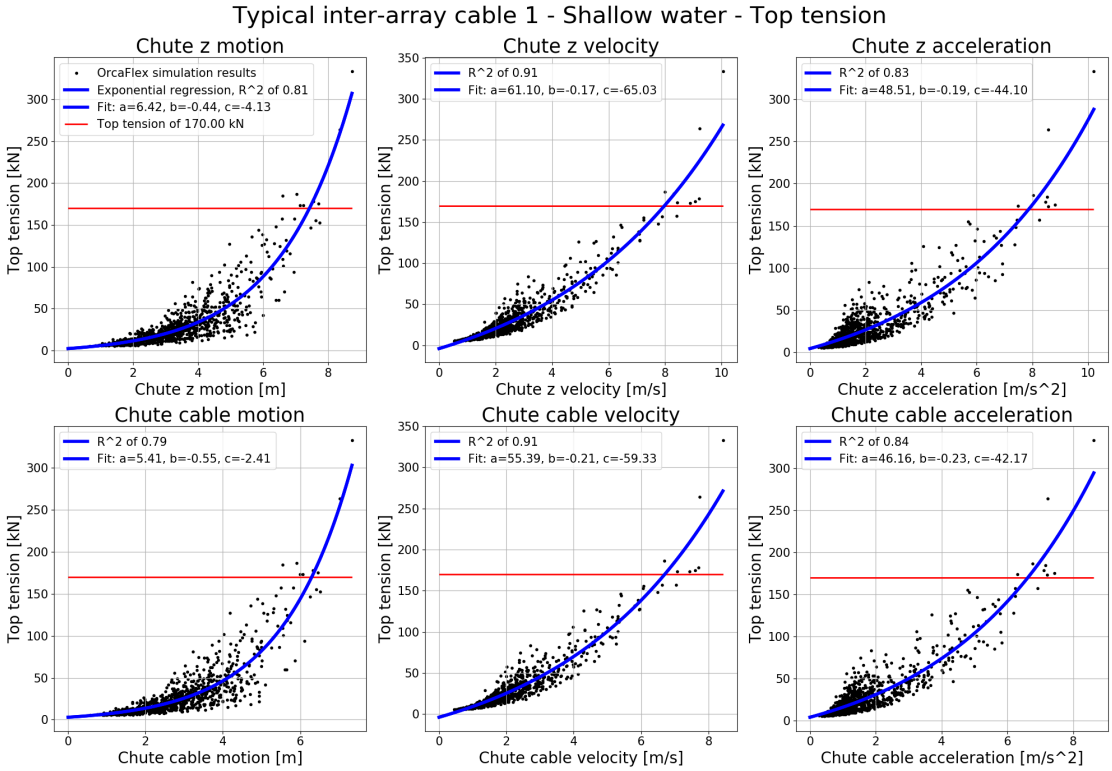

Figure D.39: Typical inter-array cable 1 at 30m water depth with a static bottom tension of 5kN, TT regression analysis, another vessel

D.7. Examine extreme minimum or extreme maximum motions

In the cable laying process, two extreme values occur; extreme minimum and maximum motions (also referred to as maximum positive and negative motions). To check which extreme needs to be assessed, scatter graphs are created in which on the x-axis the extreme maxima are plotted and on the y-axis the extreme minima are plotted. This is done for typical inter-array cable 1 and for typical export cable 1, on $30m$ water depth and $150m$ water depth.

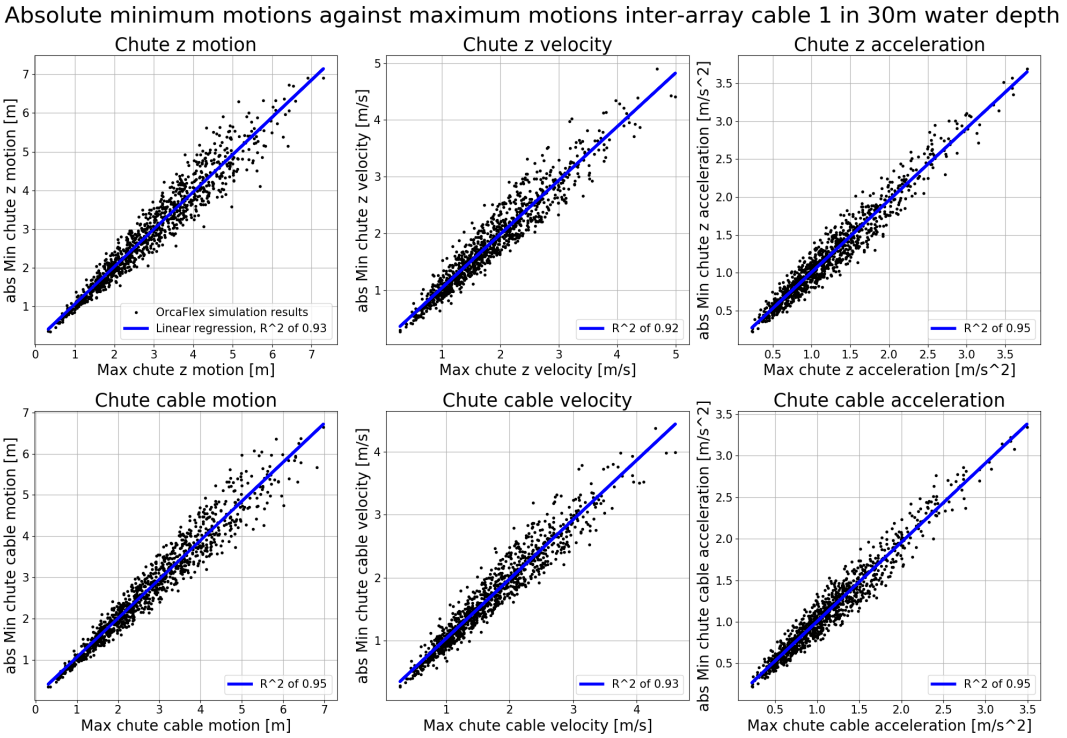

Figure D.40: Absolute minimum motions against maximum motions inter array cable 1 in 30m water depth

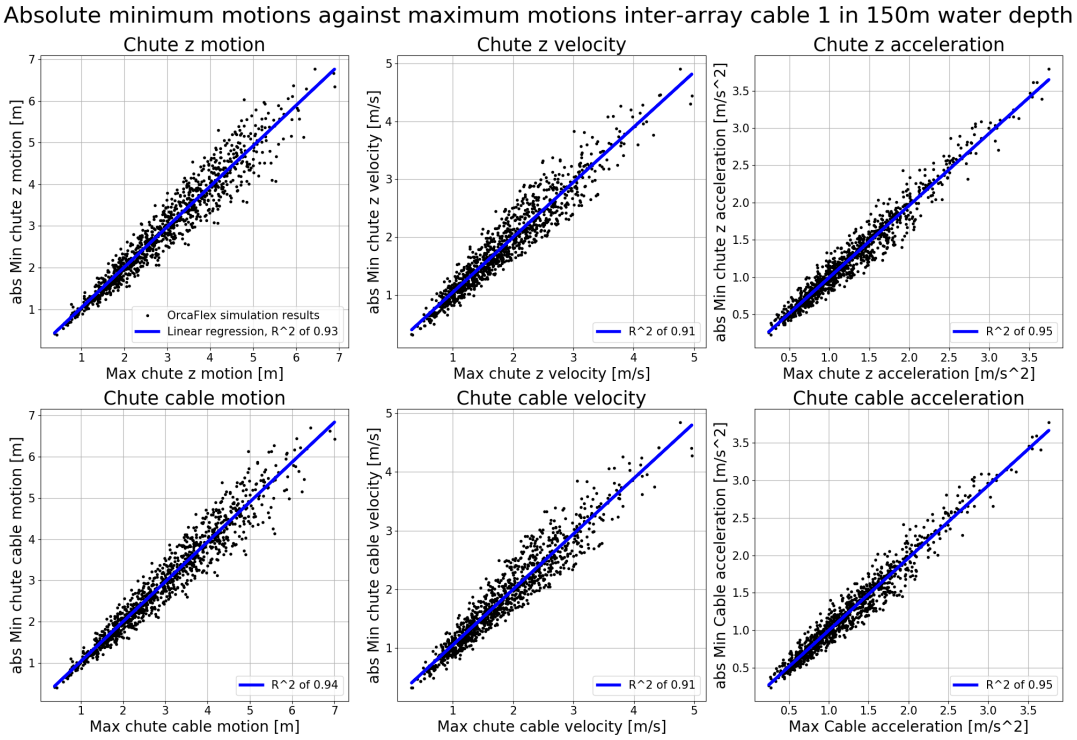

Figure D.41: Absolute minimum motions against maximum motions inter array cable 1 in 150m water depth

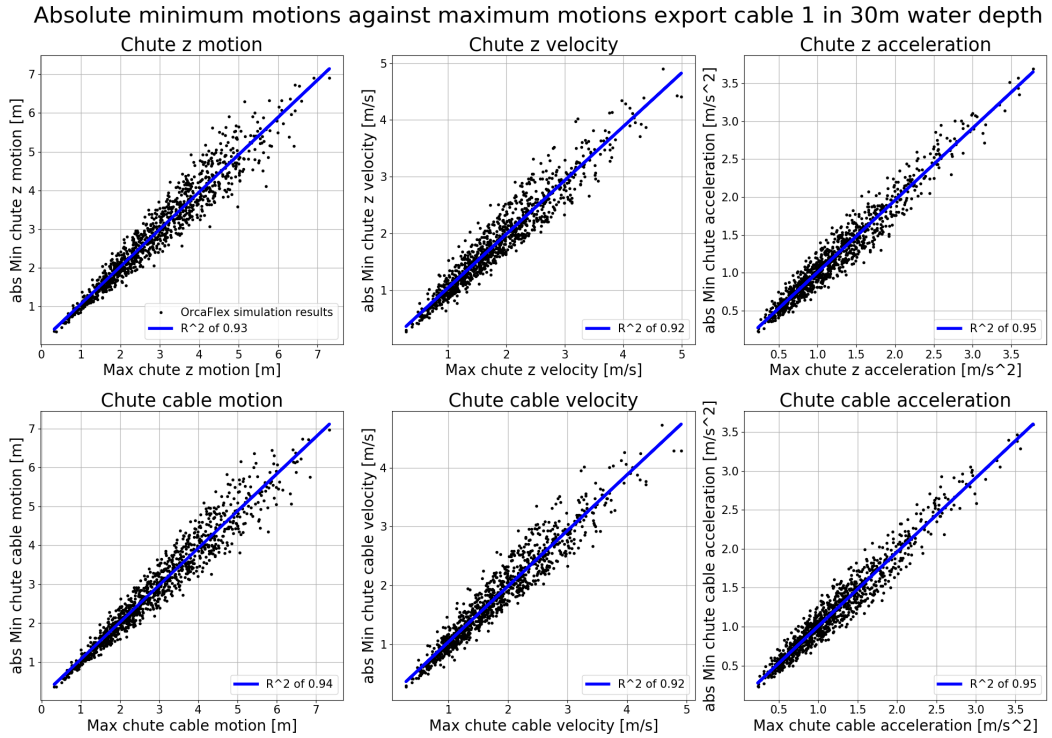

Figure D.42: Absolute minimum motions against maximum motions export cable 1 in 30m water depth

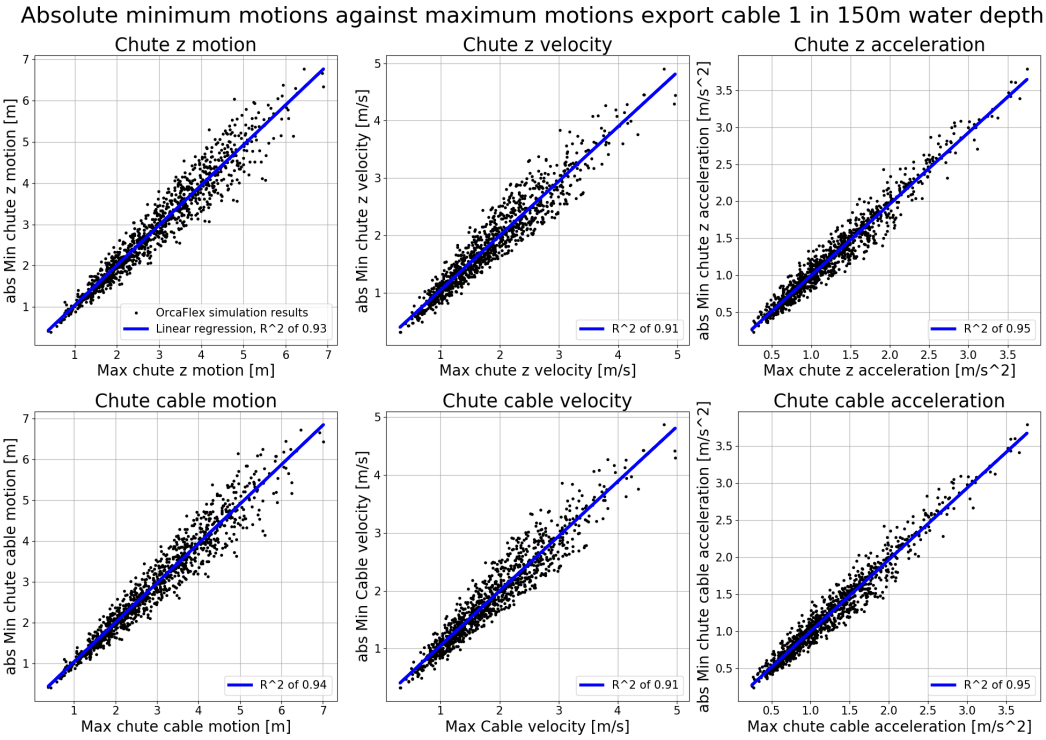

Figure D.43: Absolute minimum motions against maximum motions export cable 1 in 150m water depth

The composed graphs clearly visualize that the there is quiet a lot of scatter, which grows when moving towards higher motion values. The degree of scatter is described by a linear regression line in the form of $y = x$ in combination with a regression coefficient (further explained in subsection 5.3.3.

These graphs clearly indicate that extreme minima and extreme maxima are not opposite equal to each other. Hence both extremes need to be accounted for when identifying the limiting motions. Whether the extreme maxima or minima need to be accounted for is cable failure criteria dependant. Both MBR and minimum bottom-tension give the worst scenarios when the chute is moving downwards in the sea, thus extreme minima need to be assessed. Regarding the maximum top tension, however, the extreme occurs when the chute is moving upwards, hence extreme maxima need to be assessed.

E

Appendix - Limiting motion quantification

E.1. Interesting ranges

Shallow water chute z velocity ranges (water depth of $30m$)

- Typical inter-array cable 1 → chute z velocity from -1.5 to -5.0 [m/s]
- Typical inter-array cable 2 → chute z velocity from -1.8 to -5.0 [m/s]
- Typical export cable 1 → chute z velocity from -2.25 to -5.0 [m/s]
- Typical export cable 2 → chute z velocity from -1.5 to -2.5 [m/s]

Deep water chute z velocity ranges (water depth of $150m$)

- Typical inter-array cable 1 → chute z velocity from -1.6 to -5.0 [m/s]
- Typical inter-array cable 2 → chute z velocity from -1.7 to -5.0 [m/s]
- Typical export cable 1 → chute z velocity from -2.5 to -3.5 [m/s]
- Typical export cable 2 → chute z velocity from -1.5 to -2.5 [m/s]

E.2. Quantification graphs typical export cable 1

E.2.1. Quantification graphs typical export cable 1 in shallow water

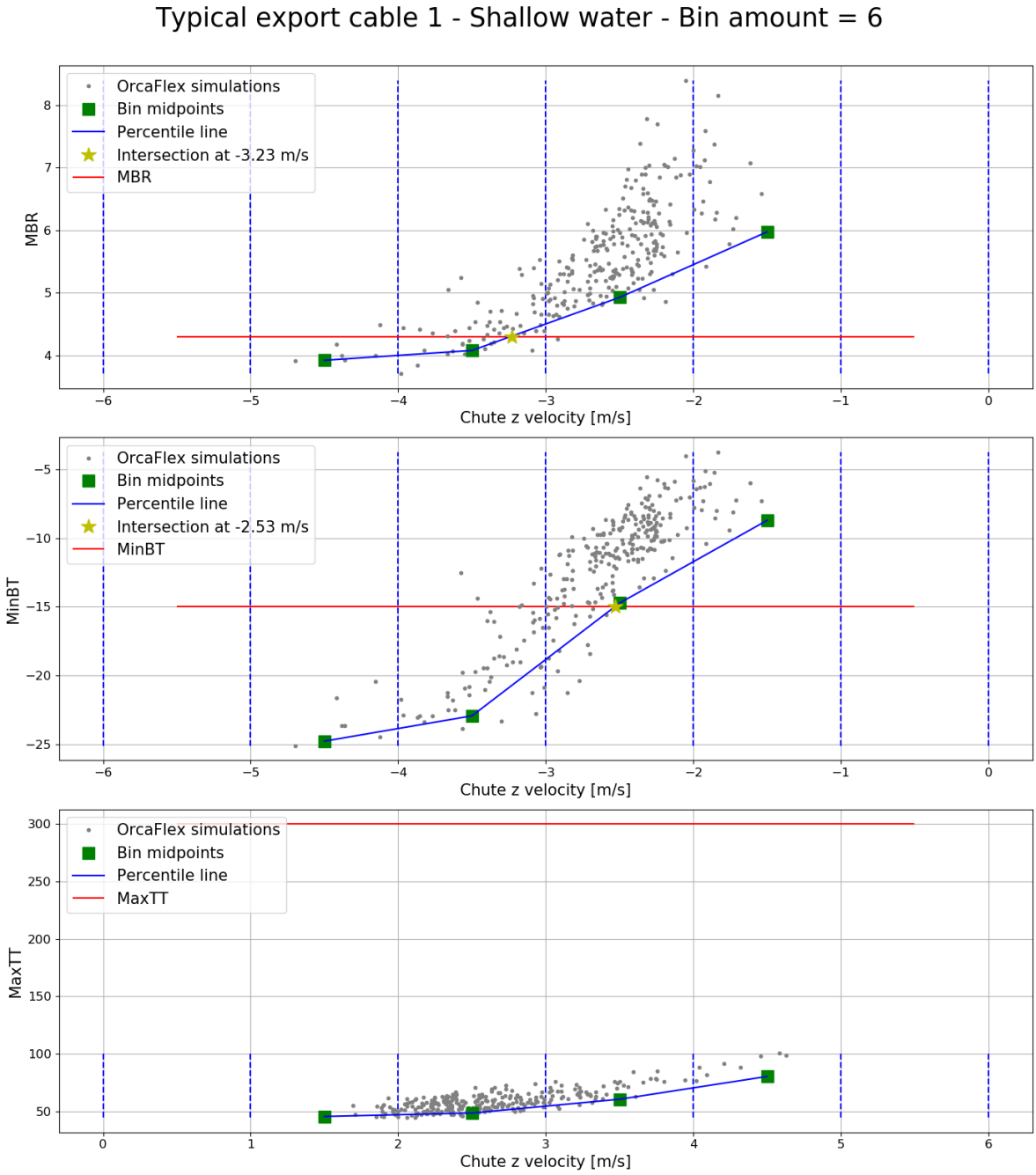

Figure E.1: Quantification graphs typical export cable 1 in shallow water ($30m$), 1 seed number, binwidth of $1m/s$

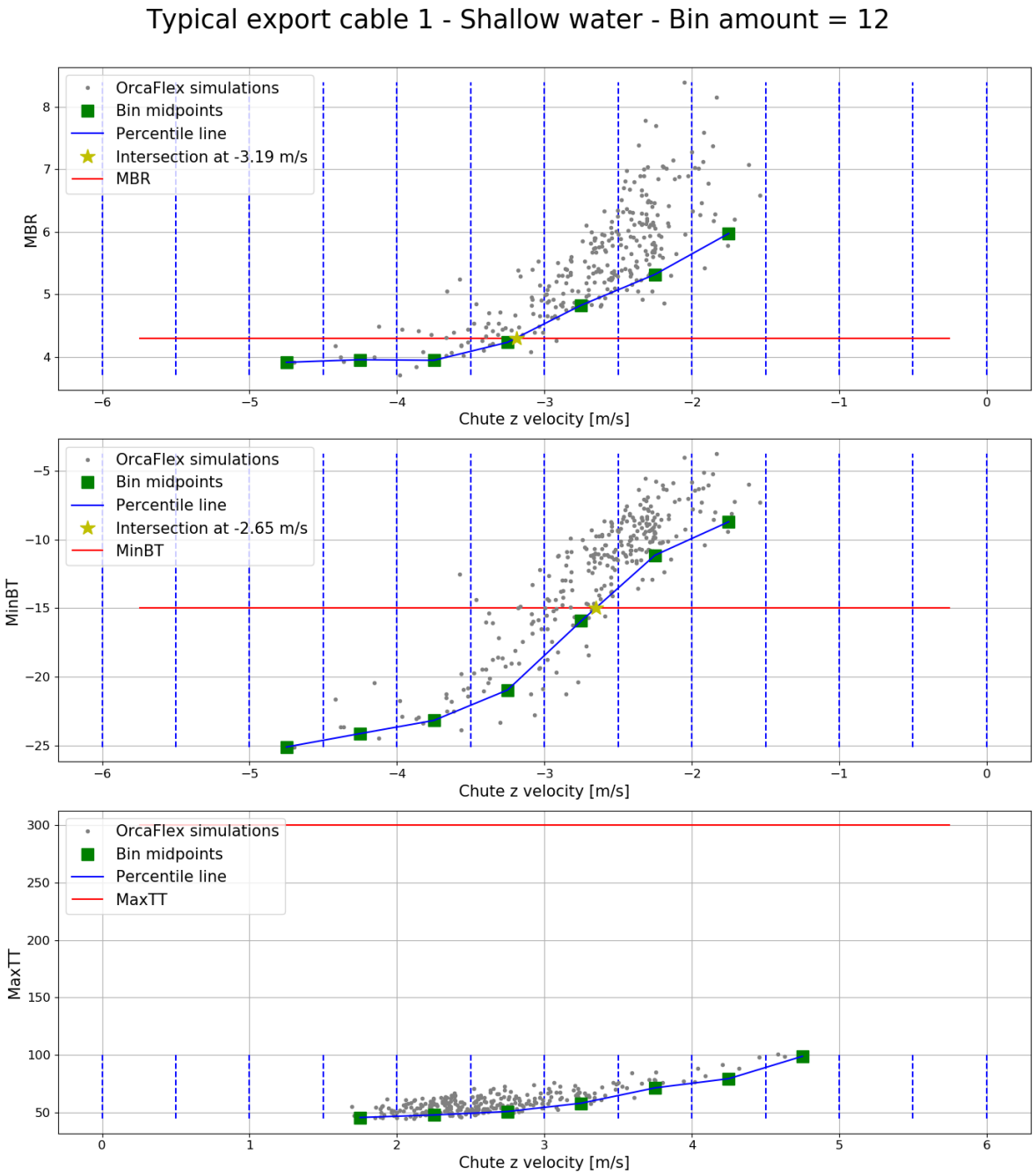

Figure E.2: Quantification graphs typical export cable 1 in shallow water ($30m$), 1 seed number, binwidth of $0.5m/s$

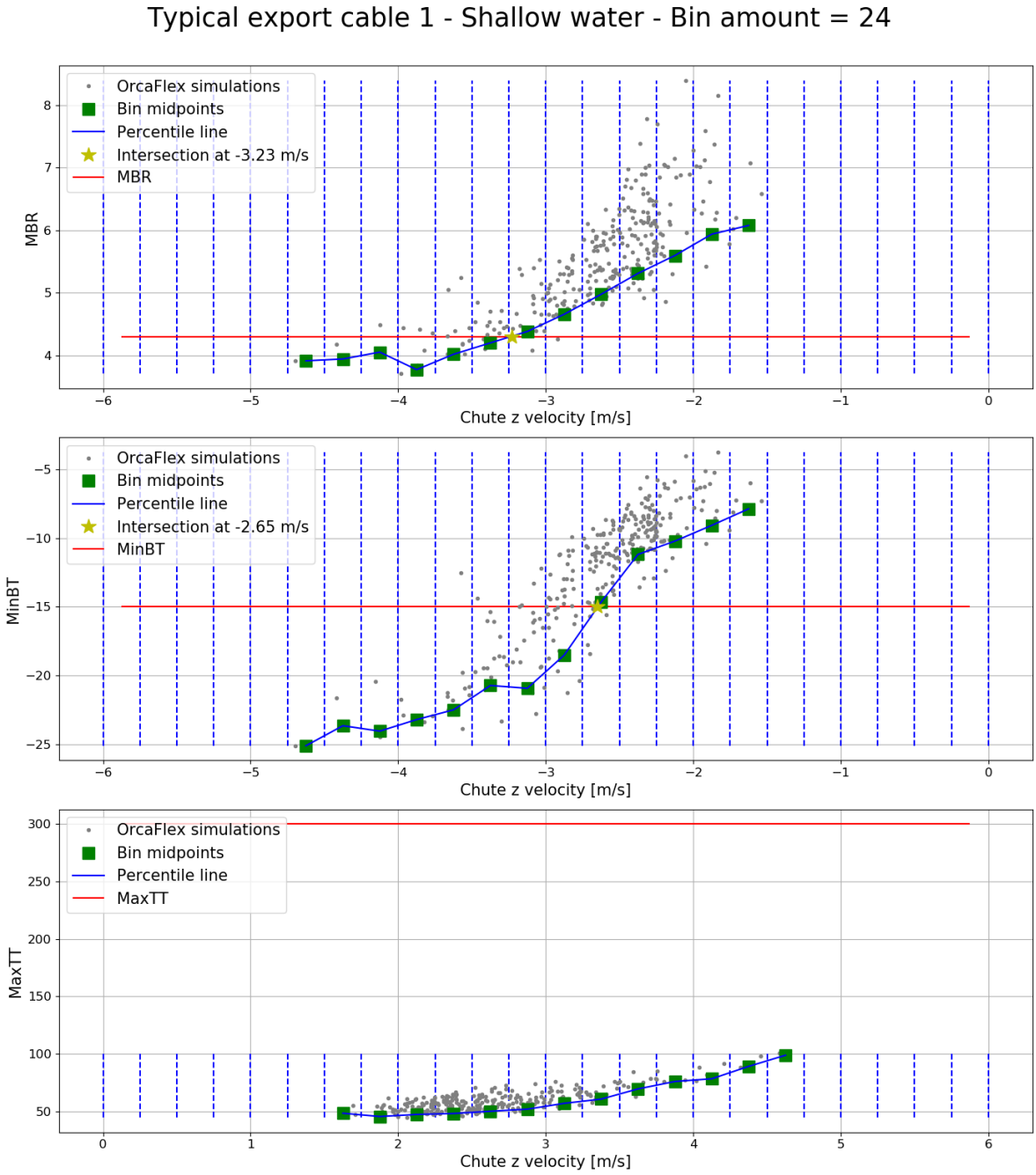

Figure E.3: Quantification graphs typical export cable 1 in shallow water ($30m$), 1 seed number, binwidth of $0.25m/s$

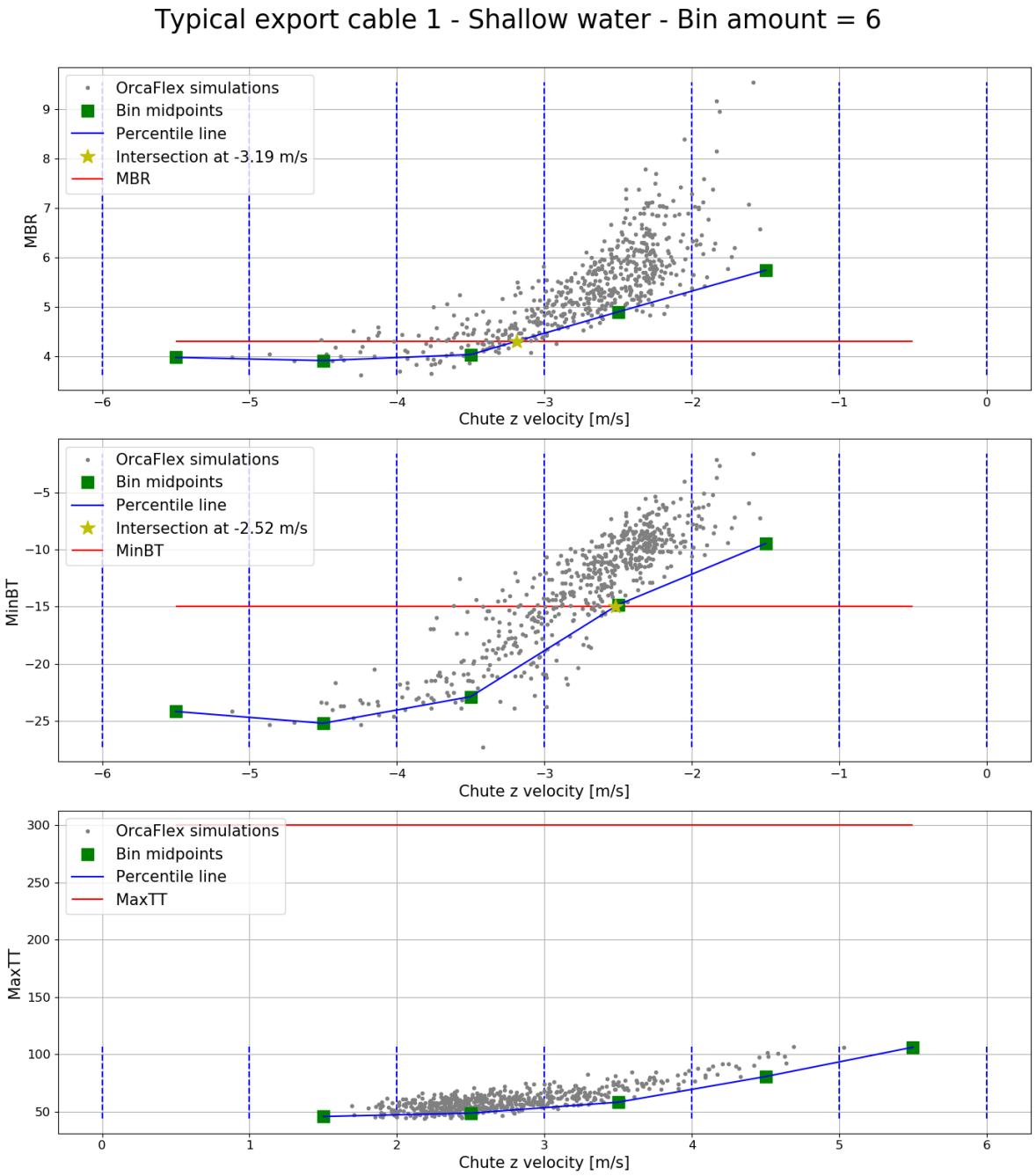

Figure E.4: Quantification graphs typical export cable 1 in shallow water ($30m$), 2 seed numbers, binwidth of $1m/s$

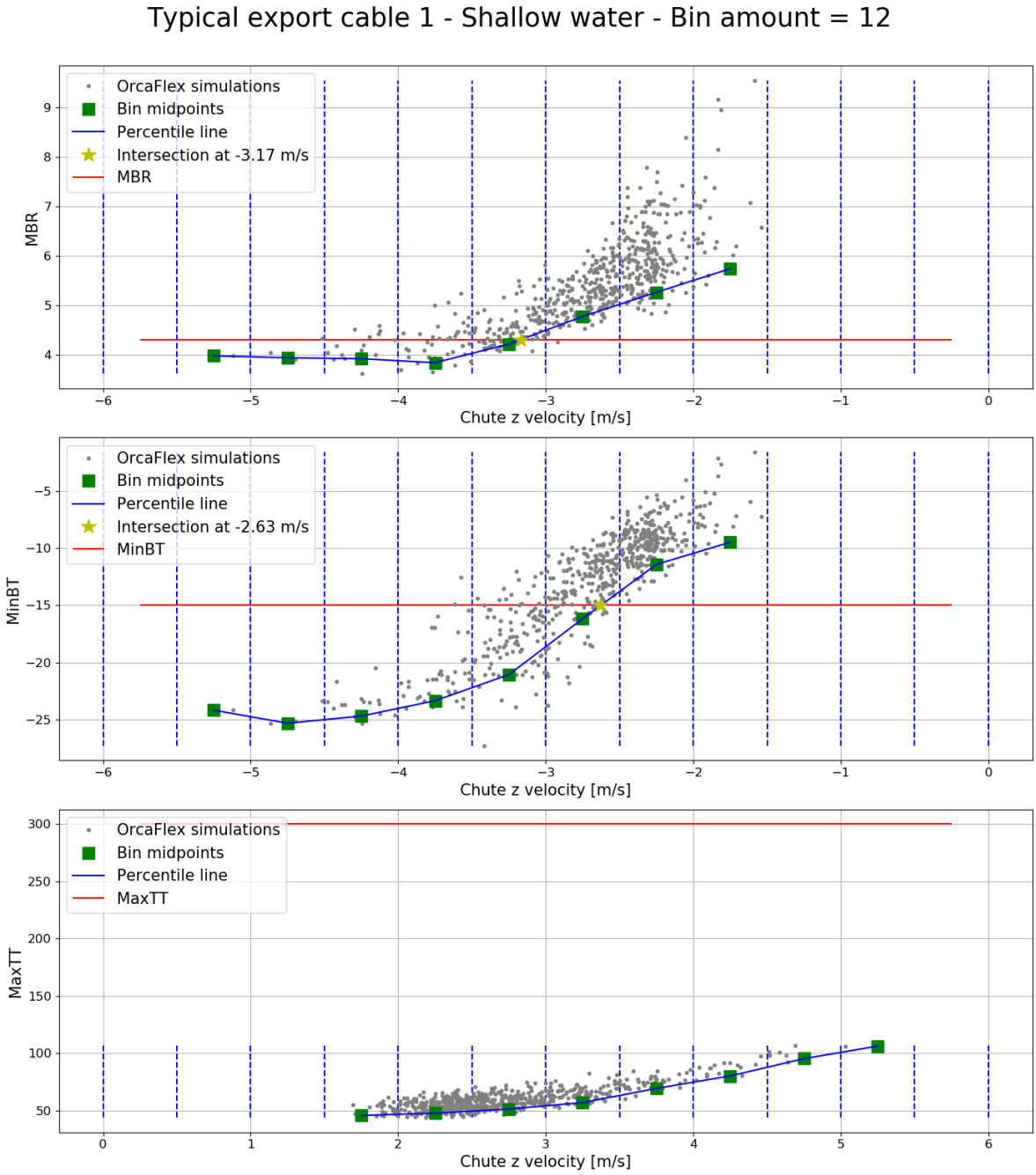

Figure E.5: Quantification graphs typical export cable 1 in shallow water ($30m$), 2 seed numbers, binwidth of $0.5m/s$

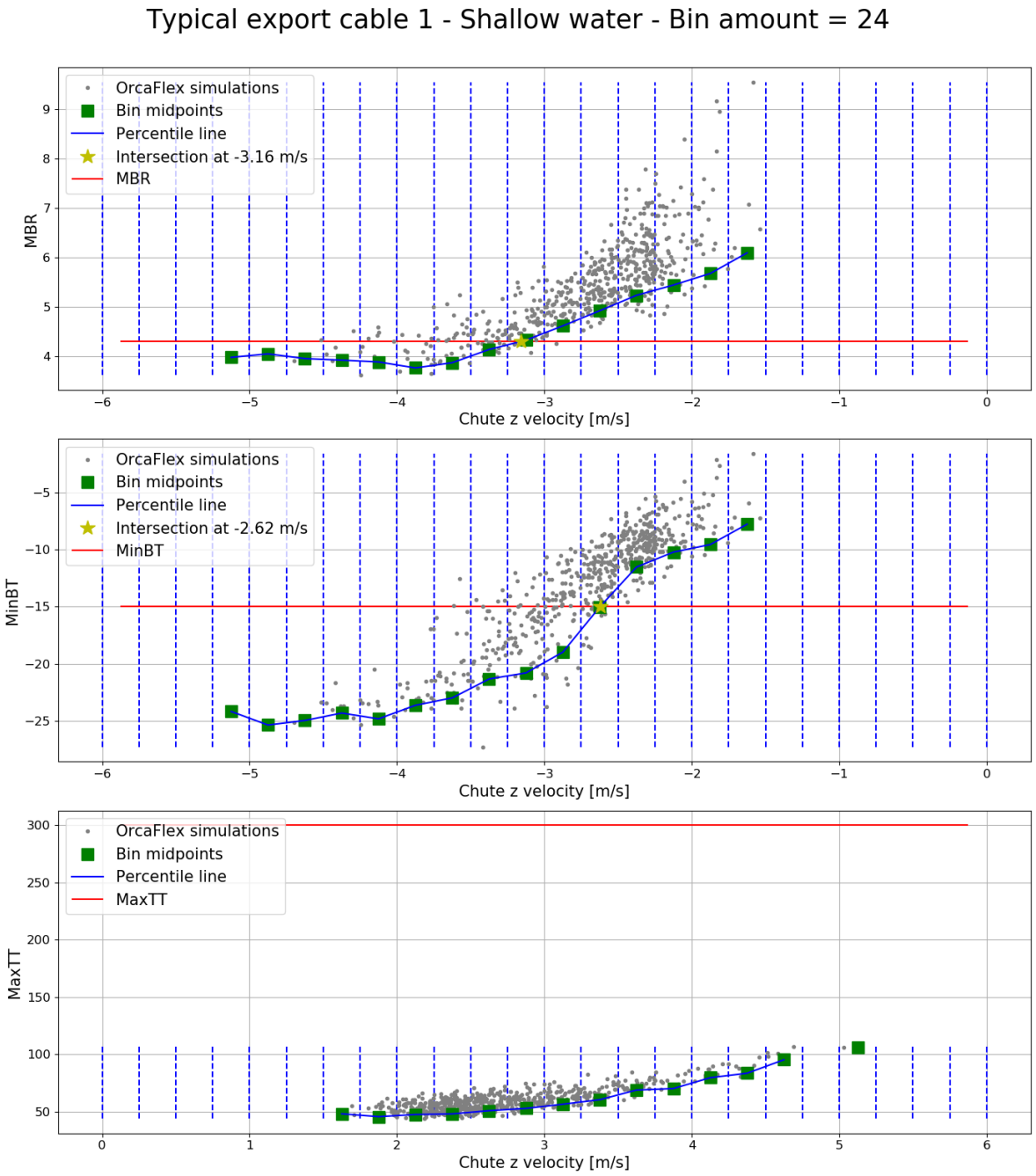

Figure E.6: Quantification graphs typical export cable 1 in shallow water ($30m$), 2 seed numbers, binwidth of $0.25m/s$

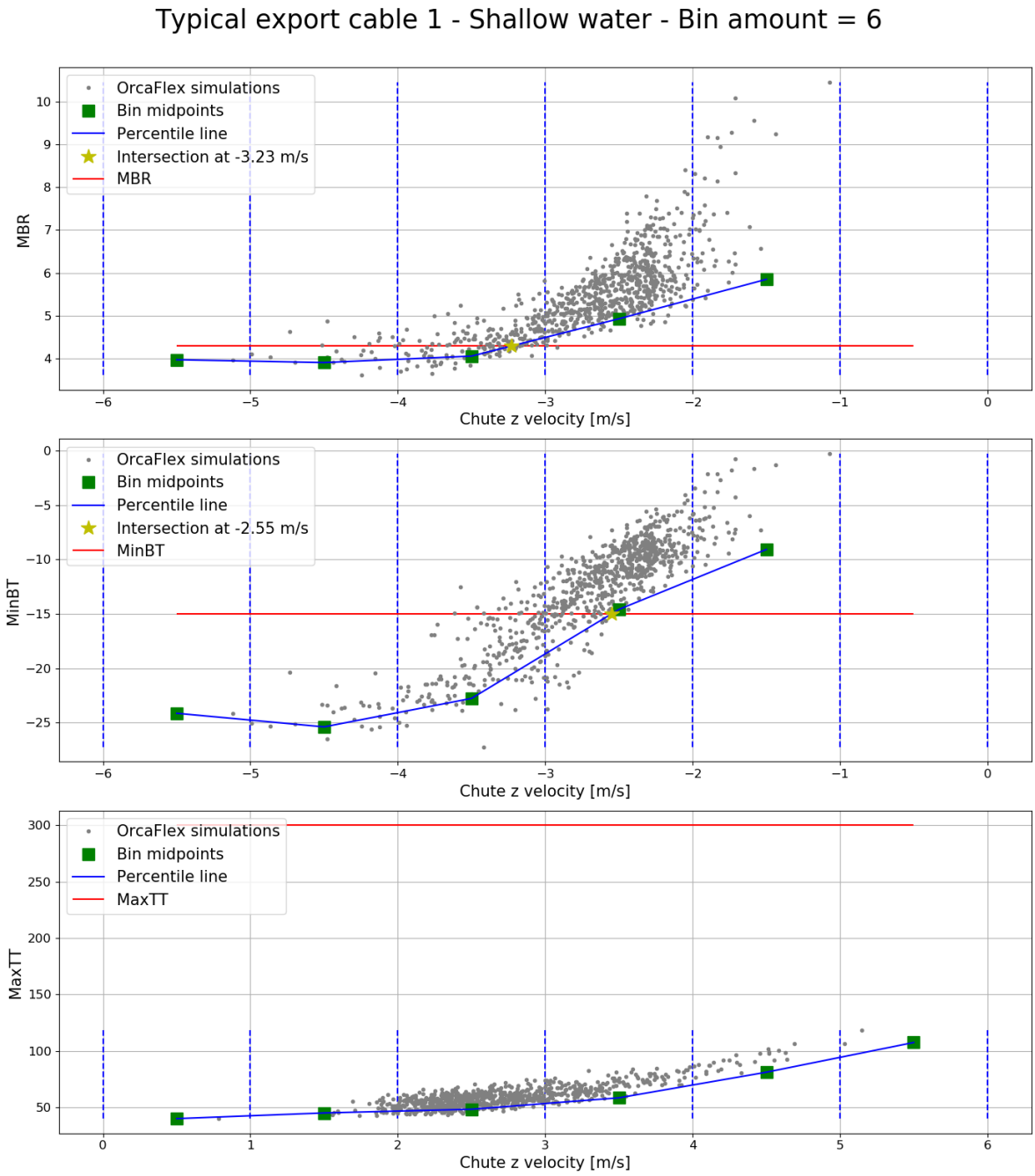

Figure E.7: Quantification graphs typical export cable 1 in shallow water ($30m$), 3 seed numbers, binwidth of $1m/s$

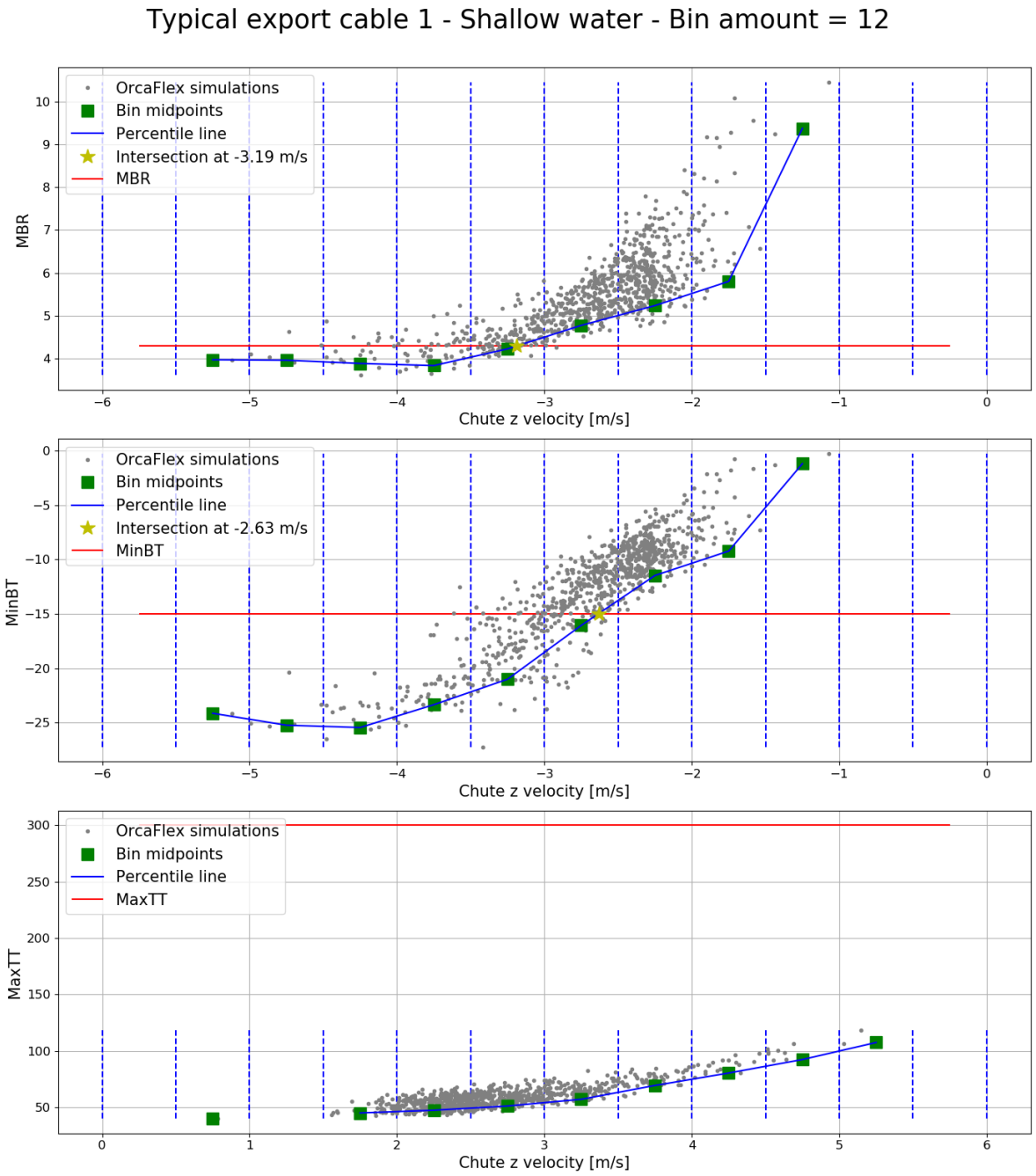

Figure E.8: Quantification graphs typical export cable 1 in shallow water ($30m$), 3 seed numbers, binwidth of $0.5m/s$

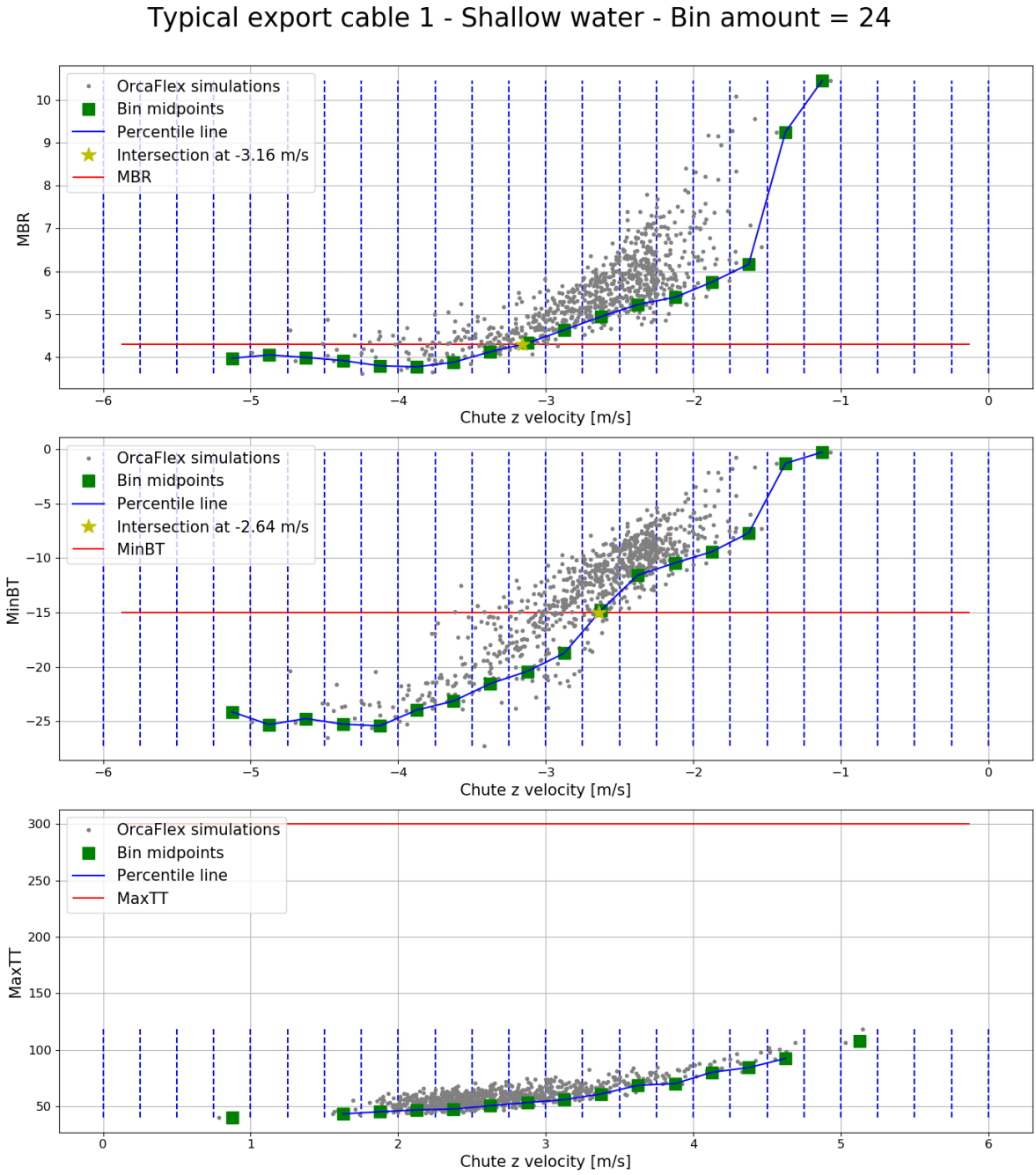

Figure E.9: Quantification graphs typical export cable 1 in shallow water ($30m$), 3 seed numbers, binwidth of $0.25m/s$

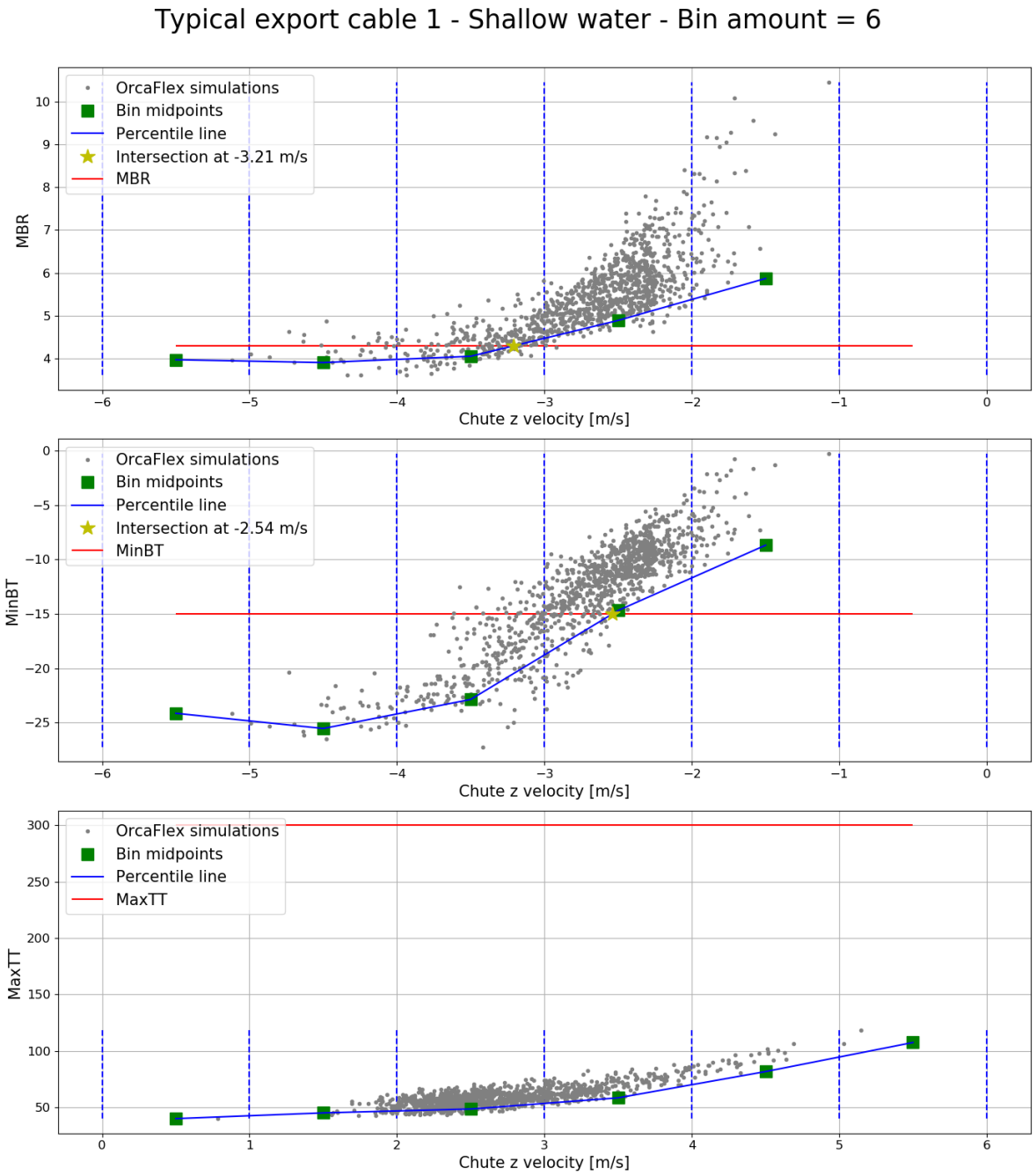

Figure E.10: Quantification graphs typical export cable 1 in shallow water ($30m$), 4 seed numbers, binwidth of $1m/s$

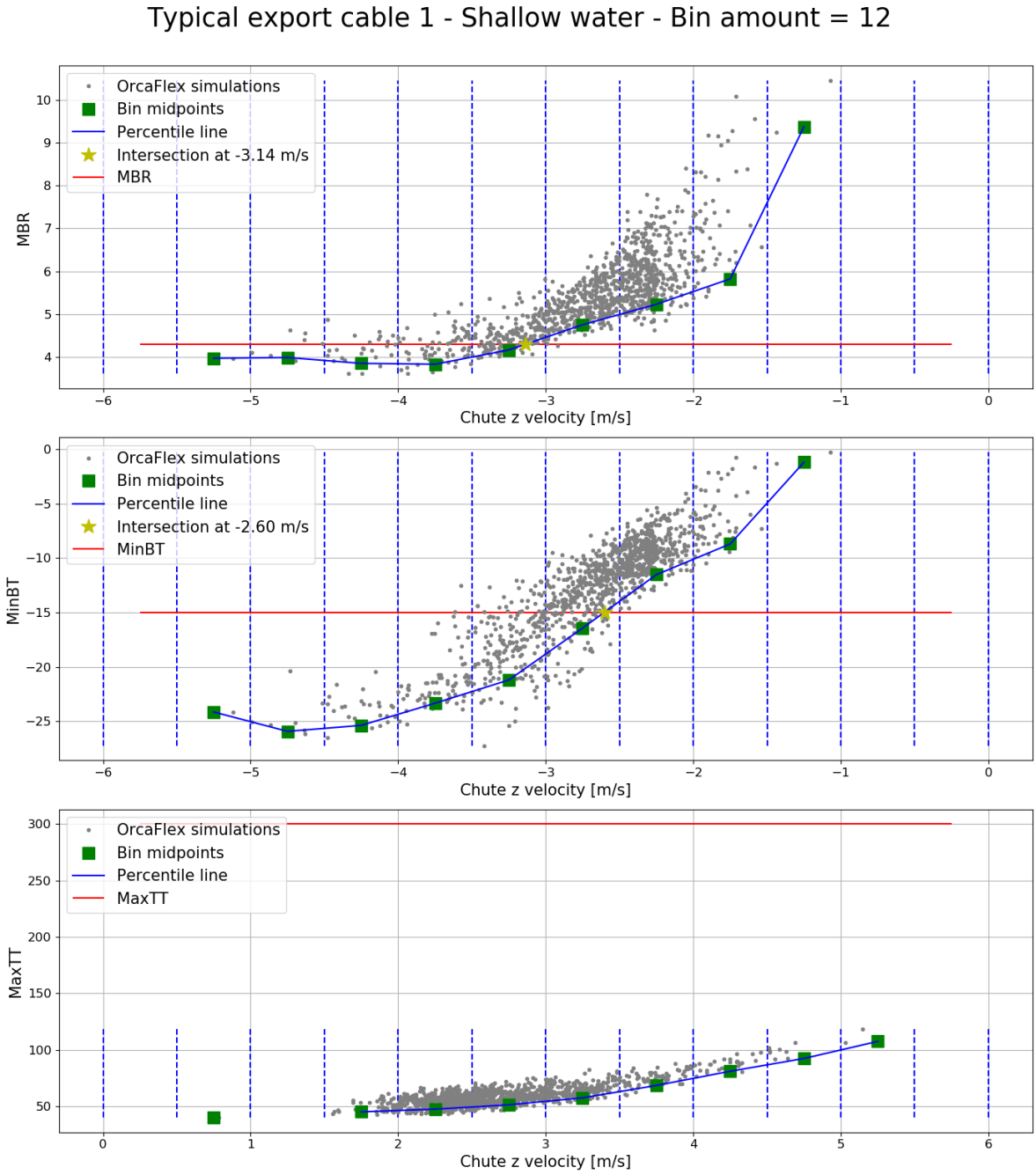

Figure E.11: Quantification graphs typical export cable 1 in shallow water ($30m$), 4 seed numbers, binwidth of $0.5m/s$

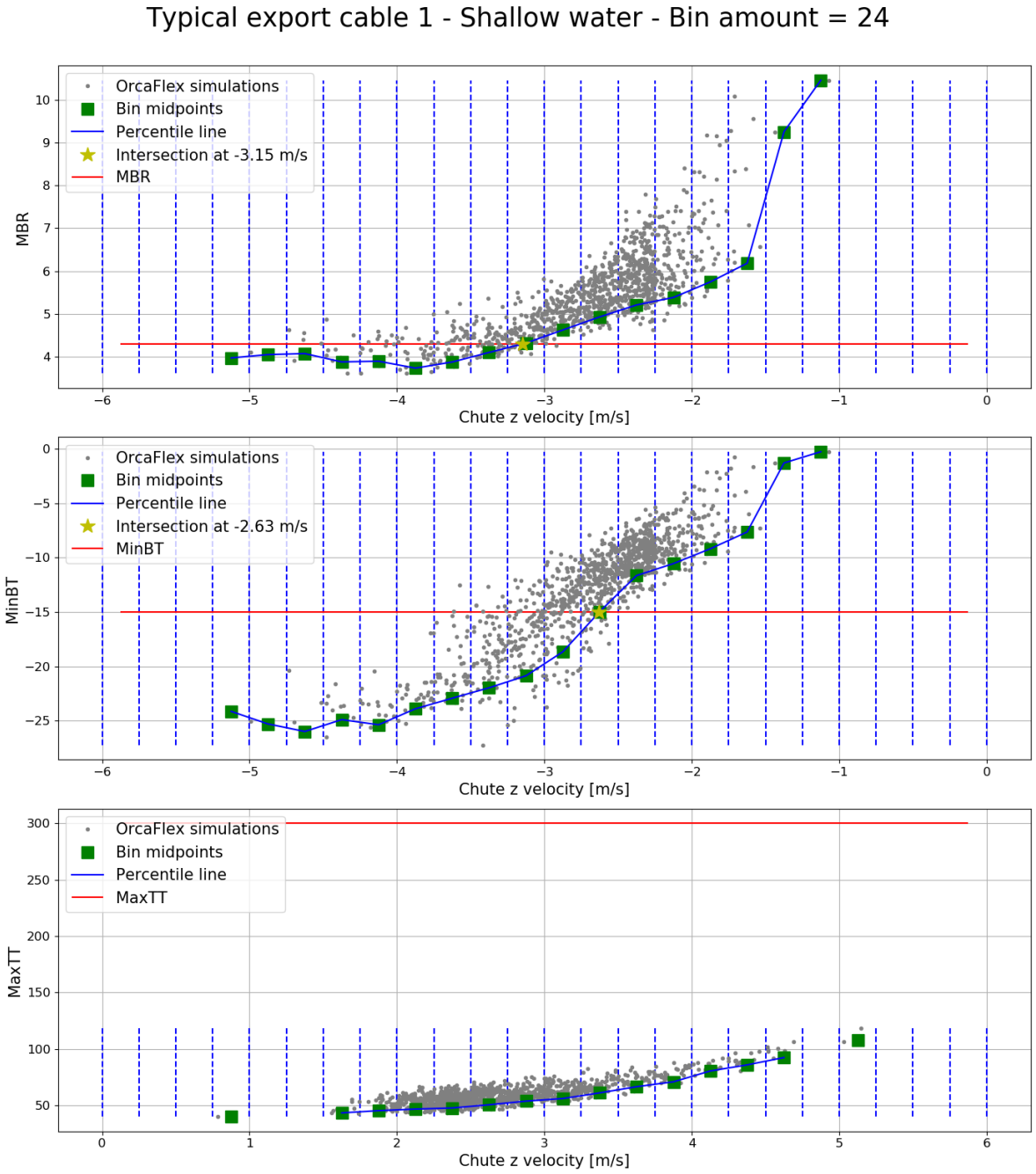

Figure E.12: Quantification graphs typical export cable 1 in shallow water ($30m$), 4 seed numbers, binwidth of $0.25m/s$

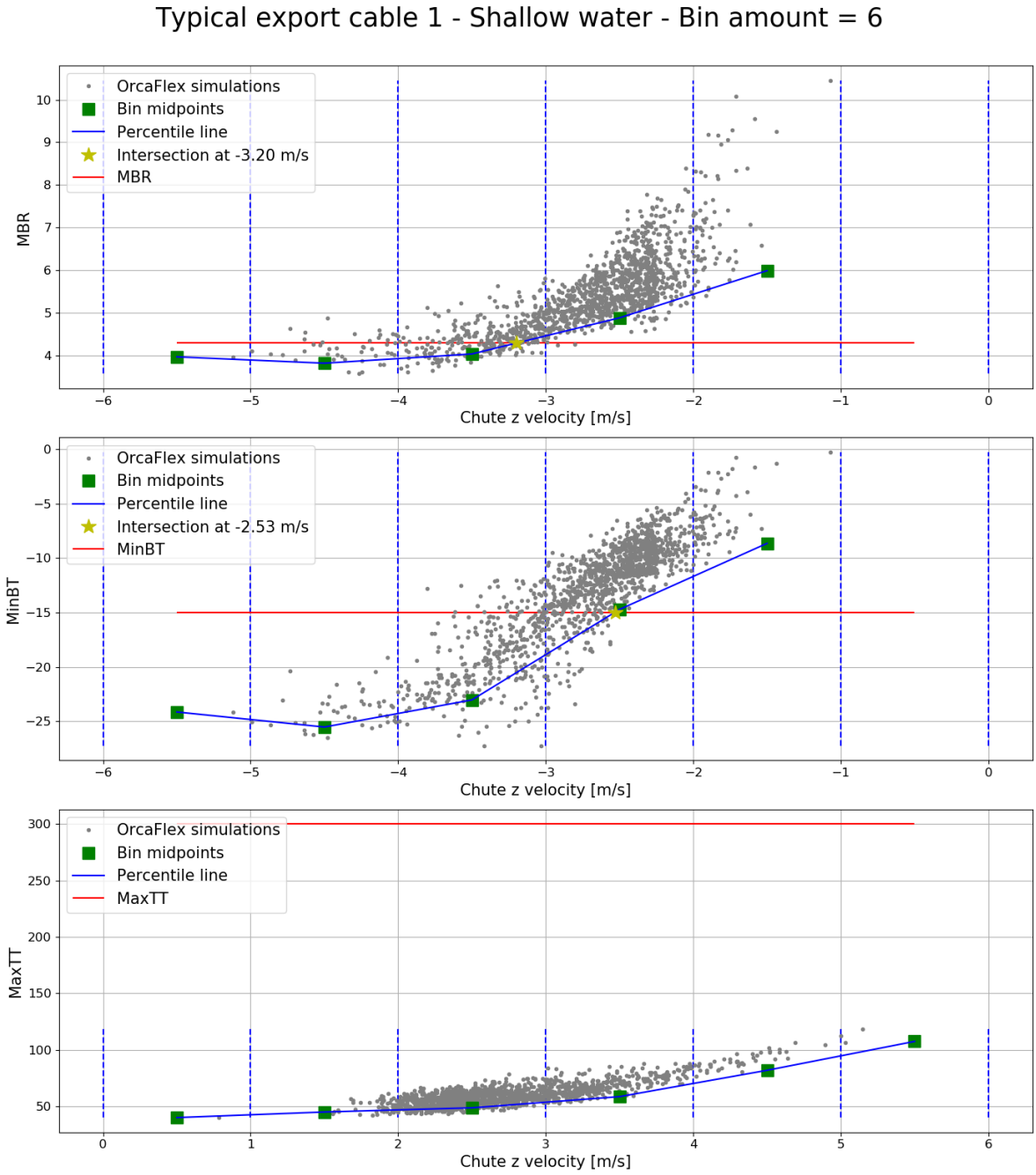

Figure E.13: Quantification graphs typical export cable 1 in shallow water ($30m$), 5 seed numbers, binwidth of $1m/s$

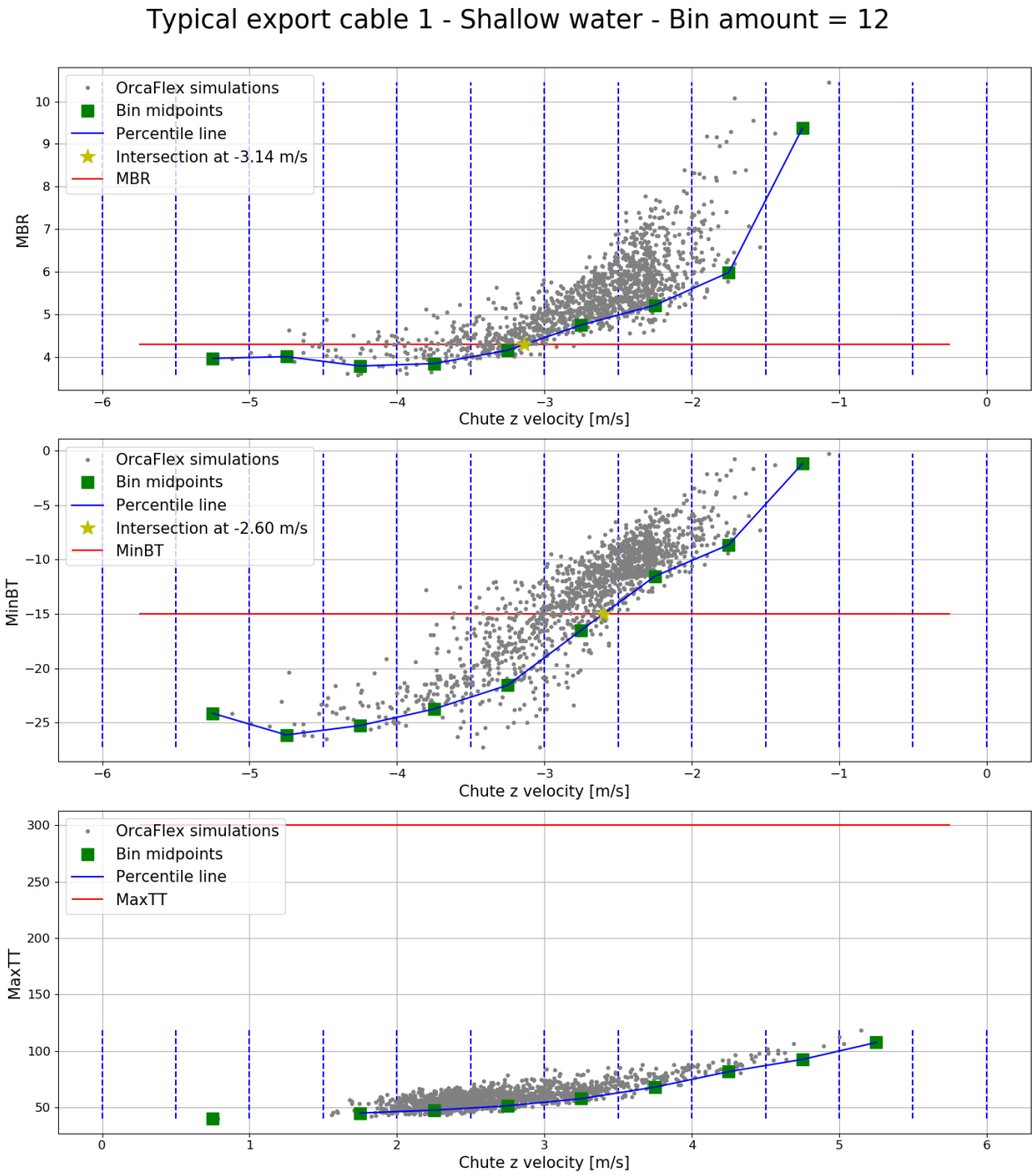

Figure E.14: Quantification graphs typical export cable 1 in shallow water ($30m$), 5 seed numbers, binwidth of $0.5m/s$

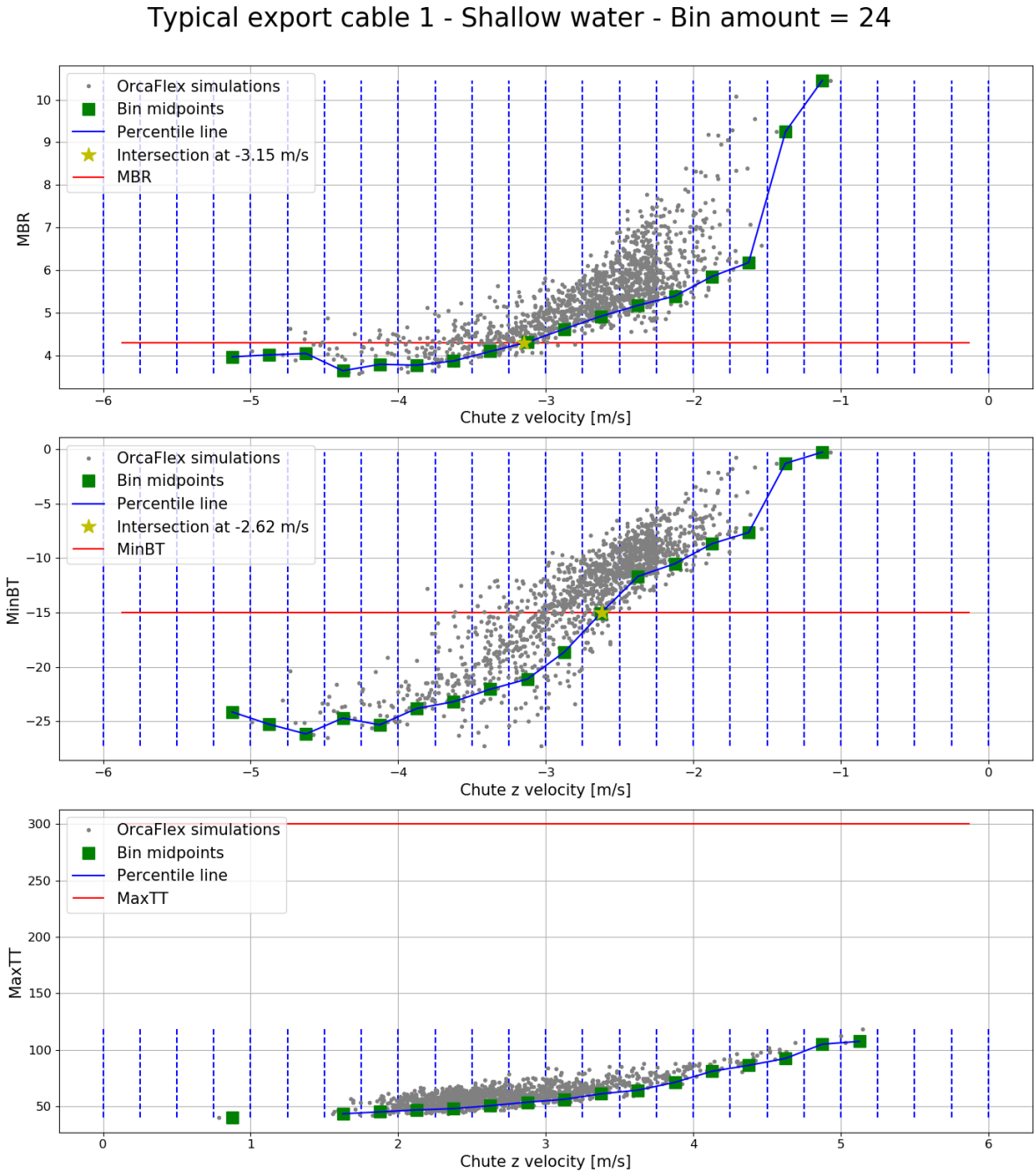

Figure E.15: Quantification graphs typical export cable 1 in shallow water ($30m$), 5 seed numbers, binwidth of $0.25m/s$

E.2.2. Quantification graphs typical export cable 1 in deep water

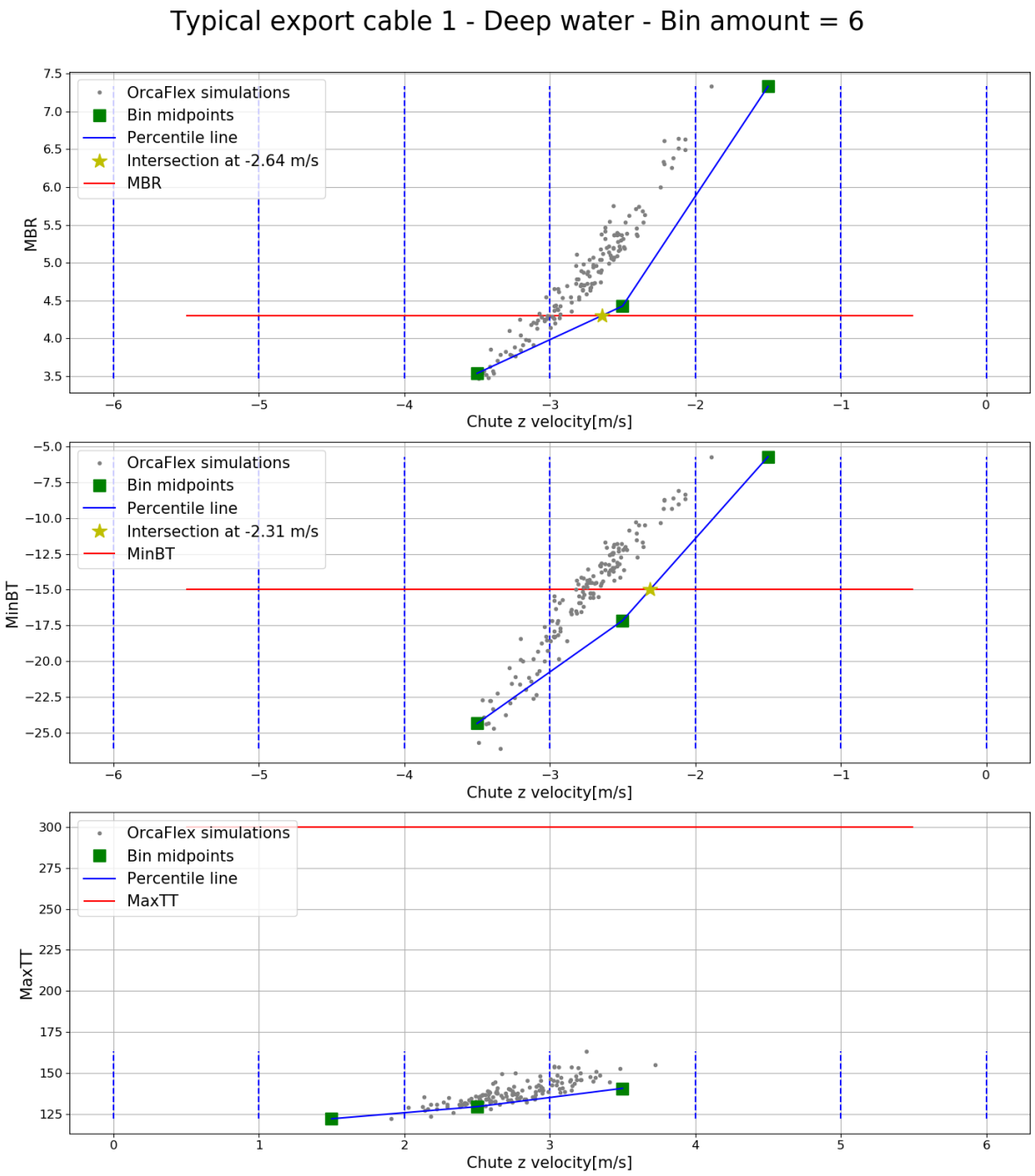

Figure E.16: Quantification graphs typical export cable 1 in deep water ($150m$), 1 seed number, binwidth of $1m/s$

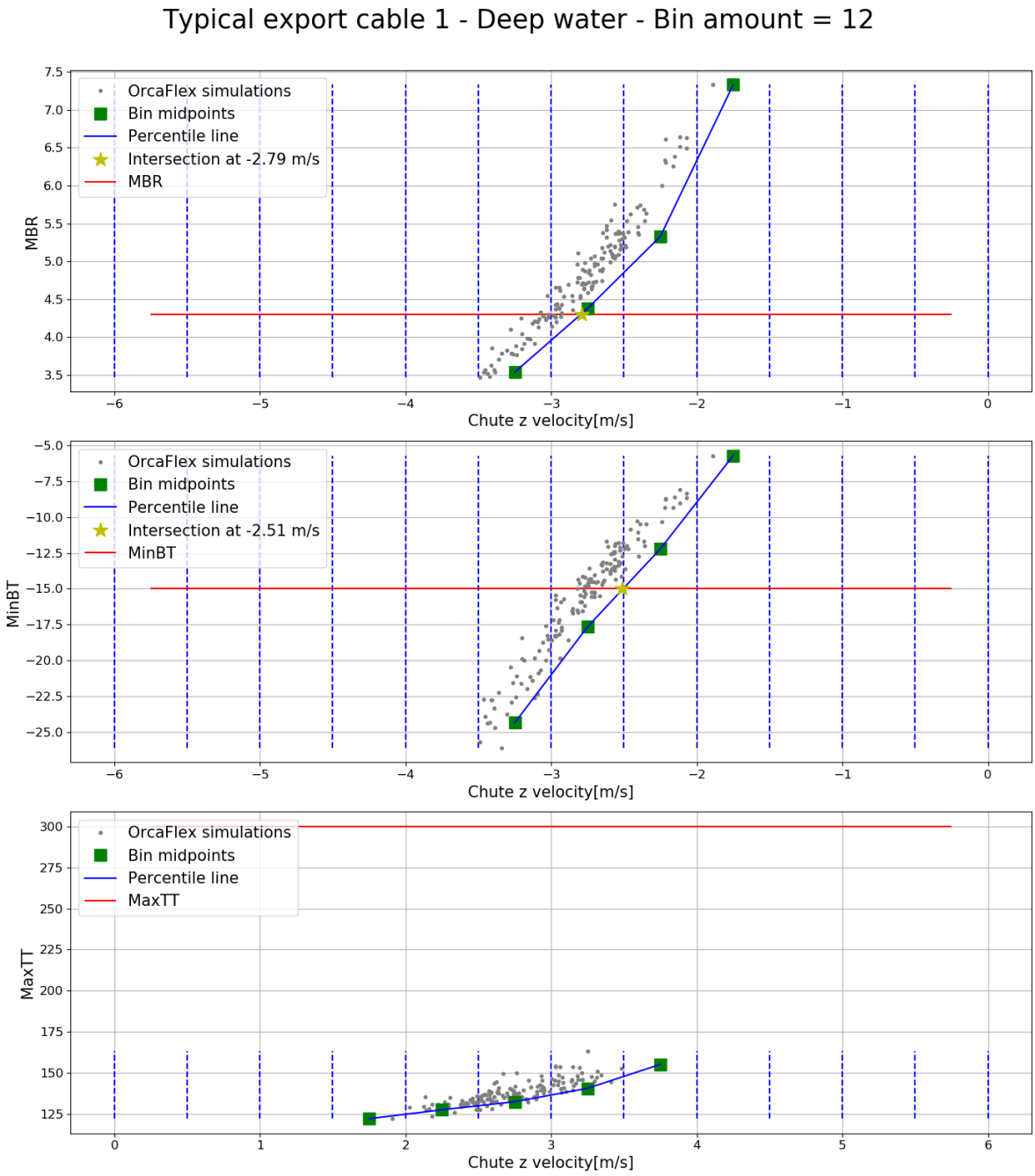

Figure E.17: Quantification graphs typical export cable 1 in deep water ($150m$), 1 seed number, binwidth of $0.5m/s$

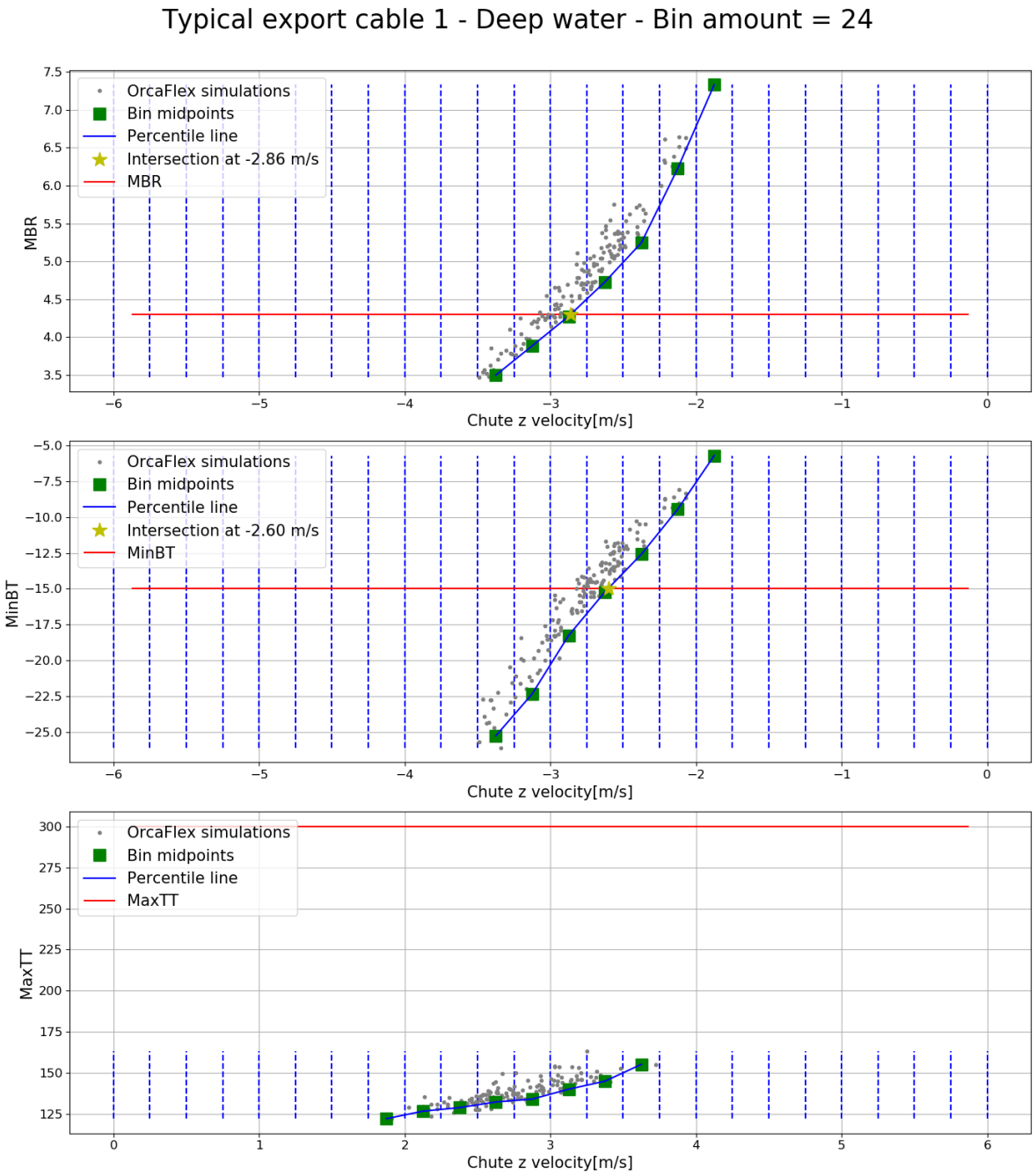

Figure E.18: Quantification graphs typical export cable 1 in deep water ($150m$), 1 seed number, binwidth of $0.25m/s$

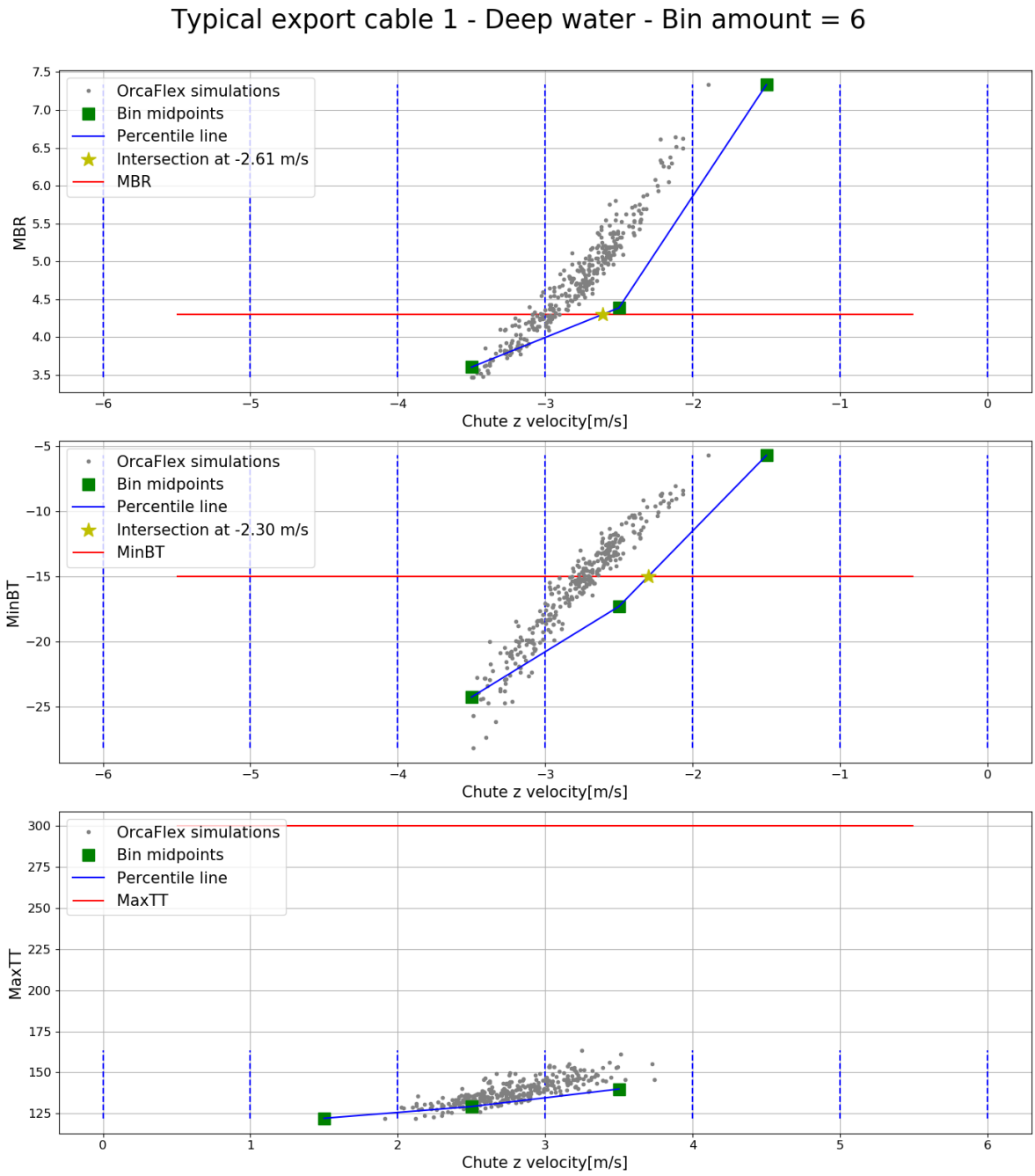

Figure E.19: Quantification graphs typical export cable 1 in deep water ($150m$), 2 seed numbers, binwidth of $1m/s$

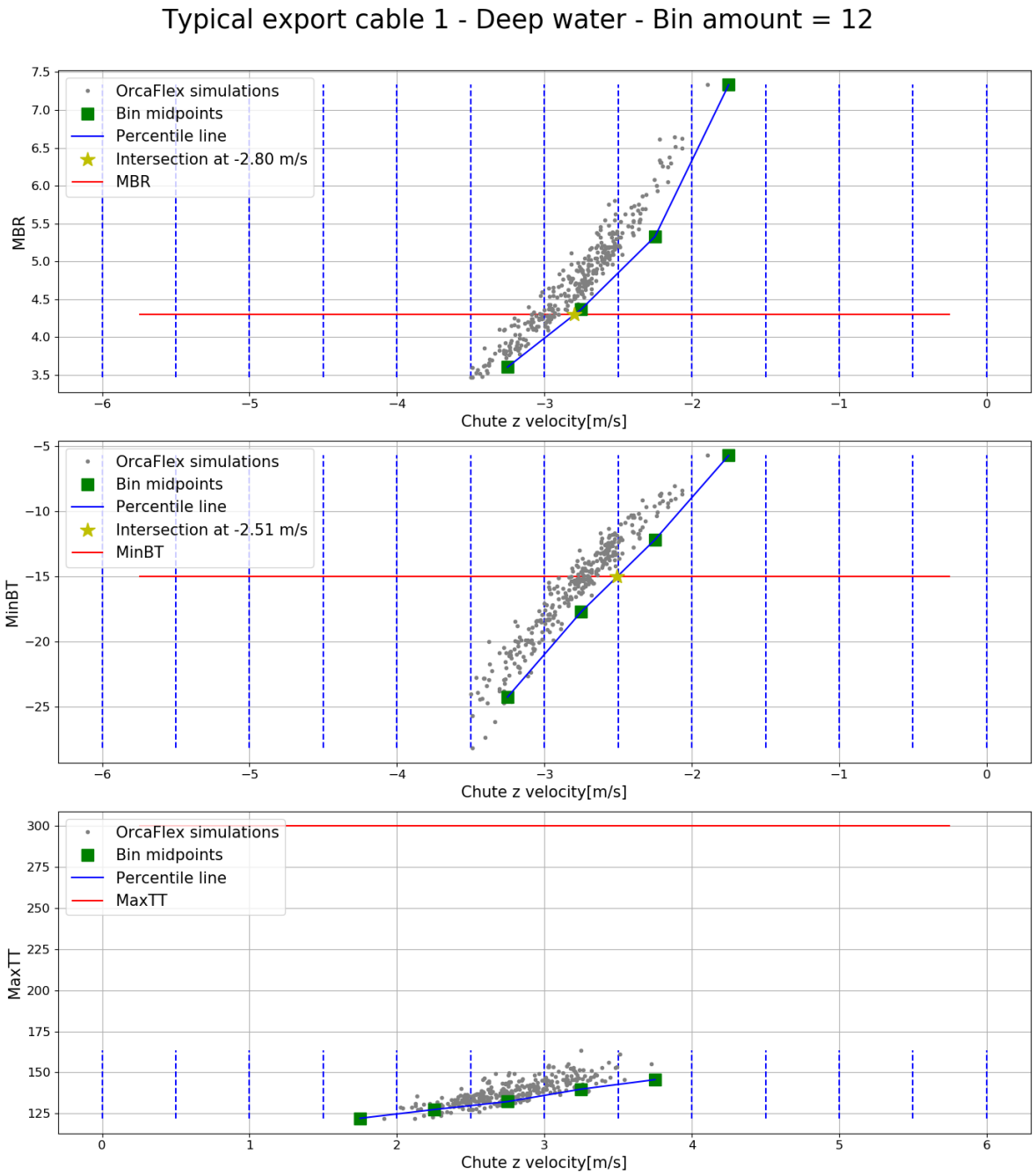

Figure E.20: Quantification graphs typical export cable 1 in deep water ($150m$), 2 seed numbers, binwidth of $0.5m/s$

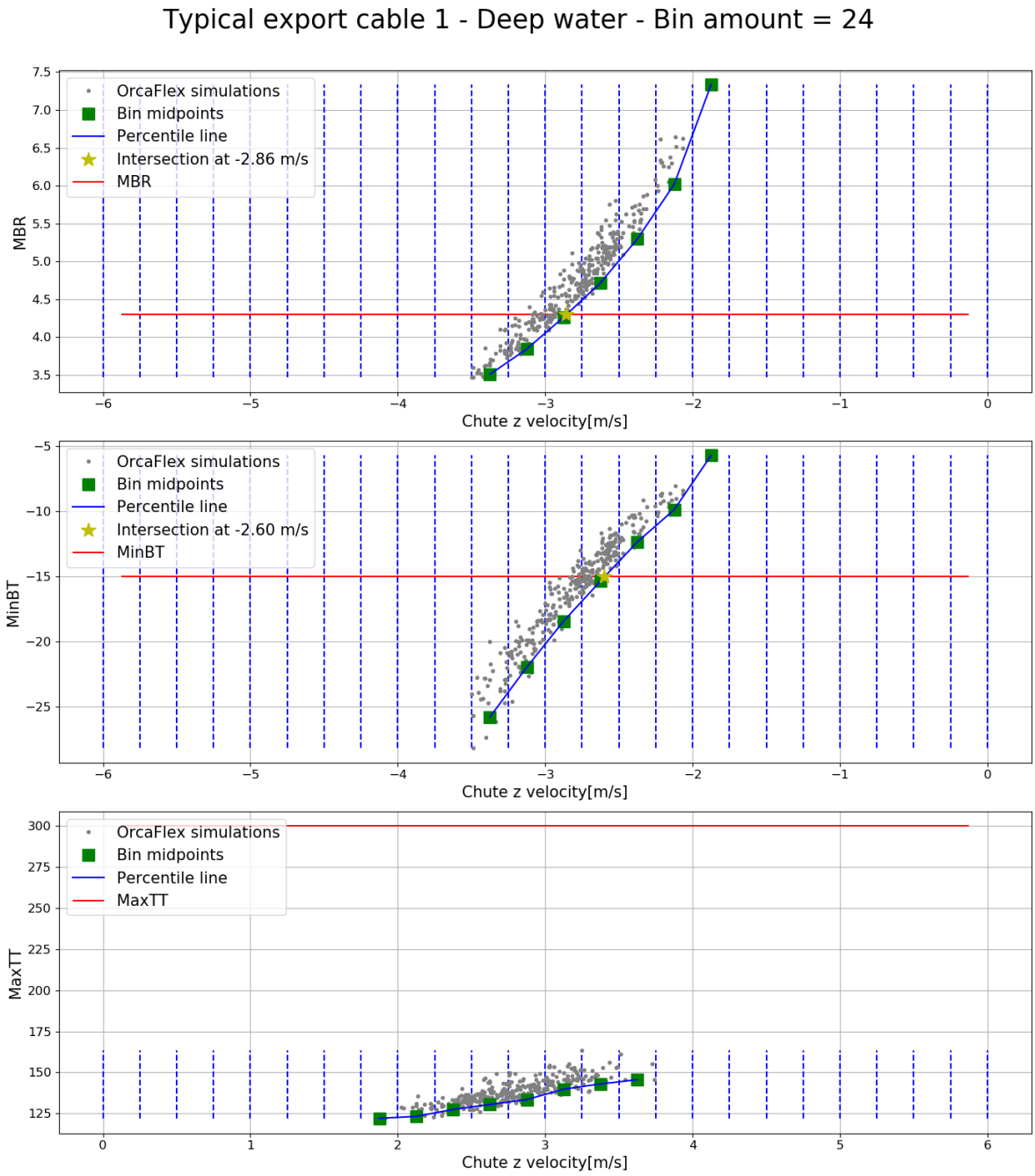

Figure E.21: Quantification graphs typical export cable 1 in deep water ($150m$), 2 seed numbers, binwidth of $0.25m/s$

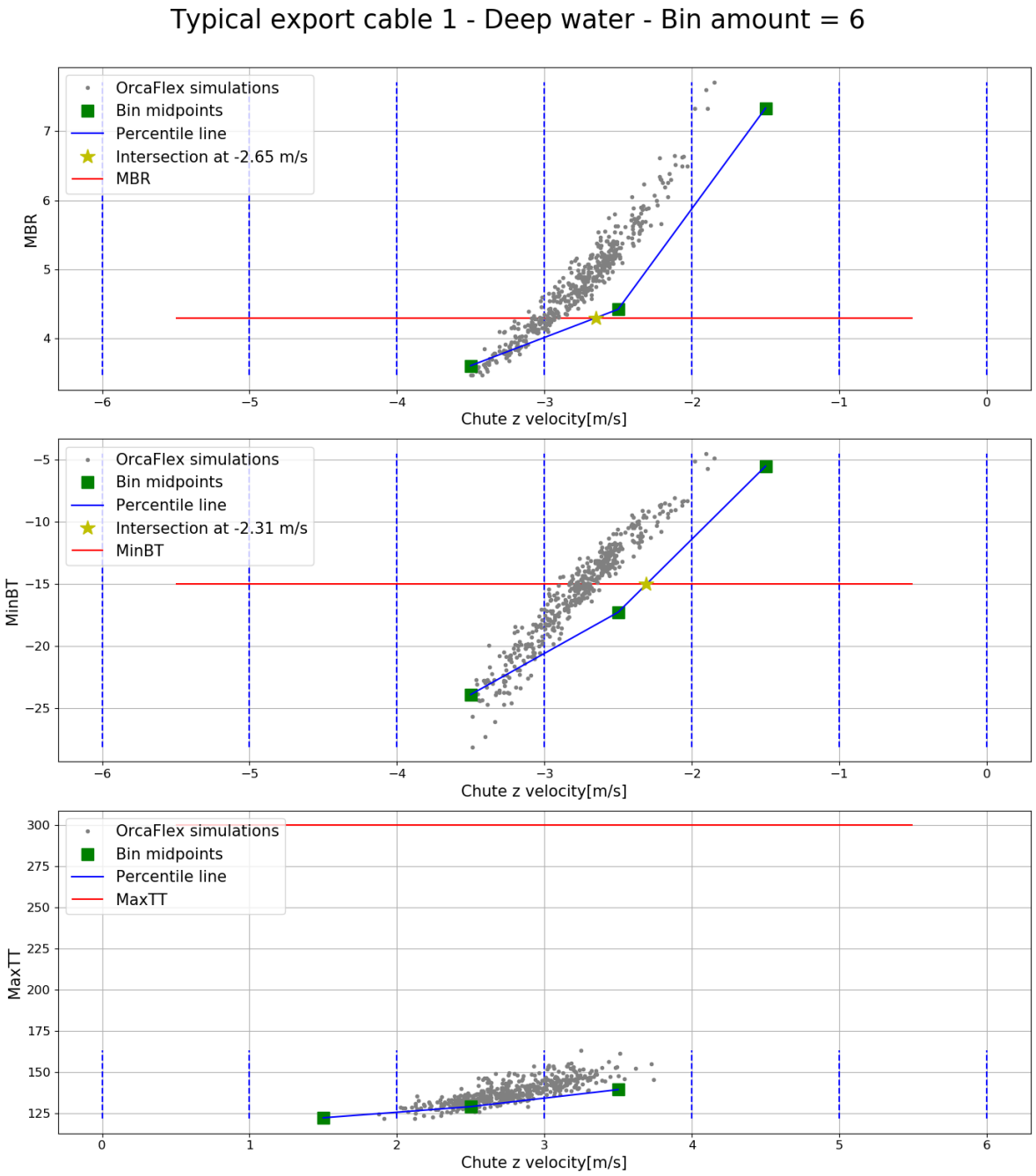

Figure E.22: Quantification graphs typical export cable 1 in deep water ($150m$), 3 seed numbers, binwidth of $1m/s$

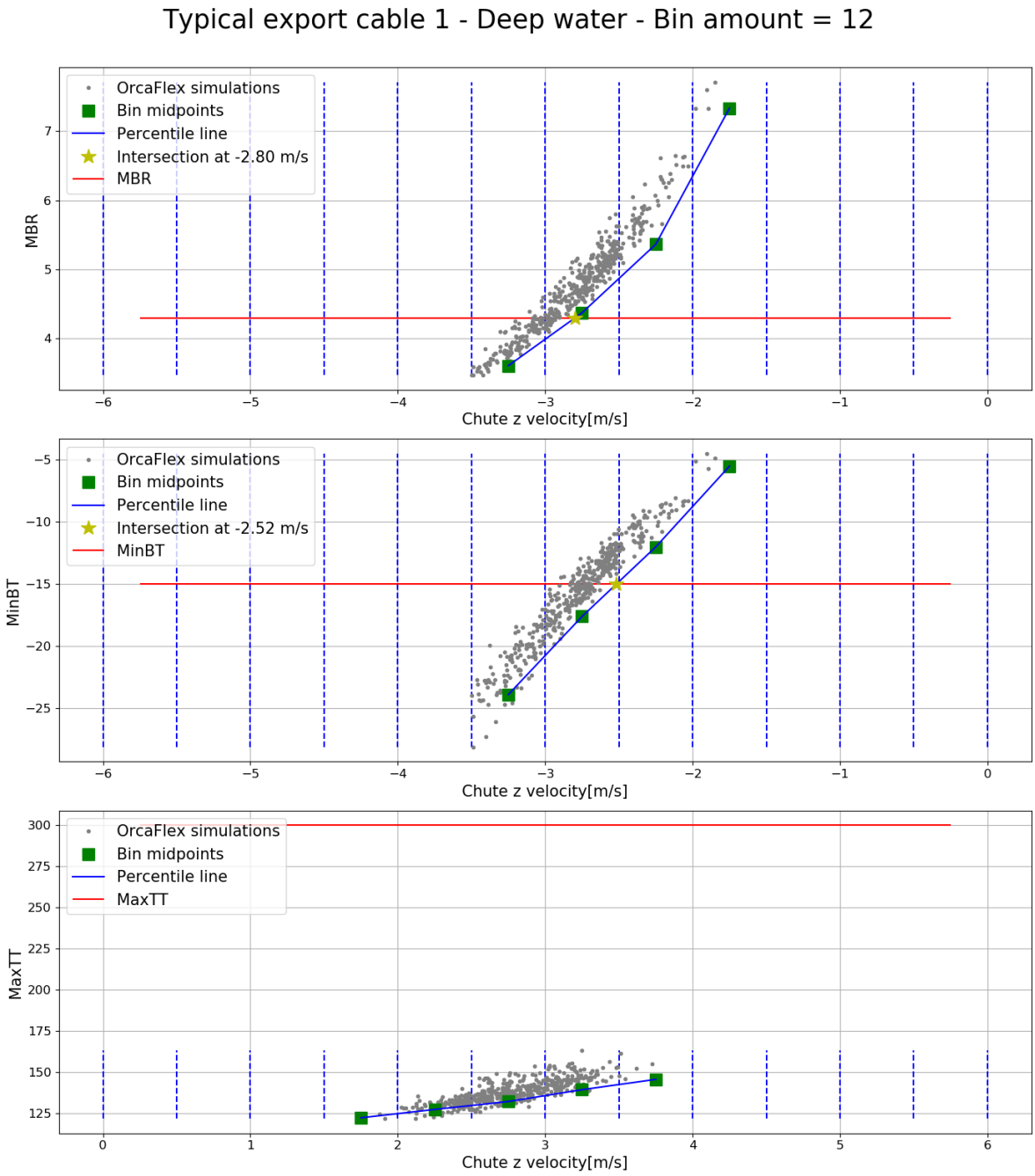

Figure E.23: Quantification graphs typical export cable 1 in deep water ($150m$), 3 seed numbers, binwidth of $0.5m/s$

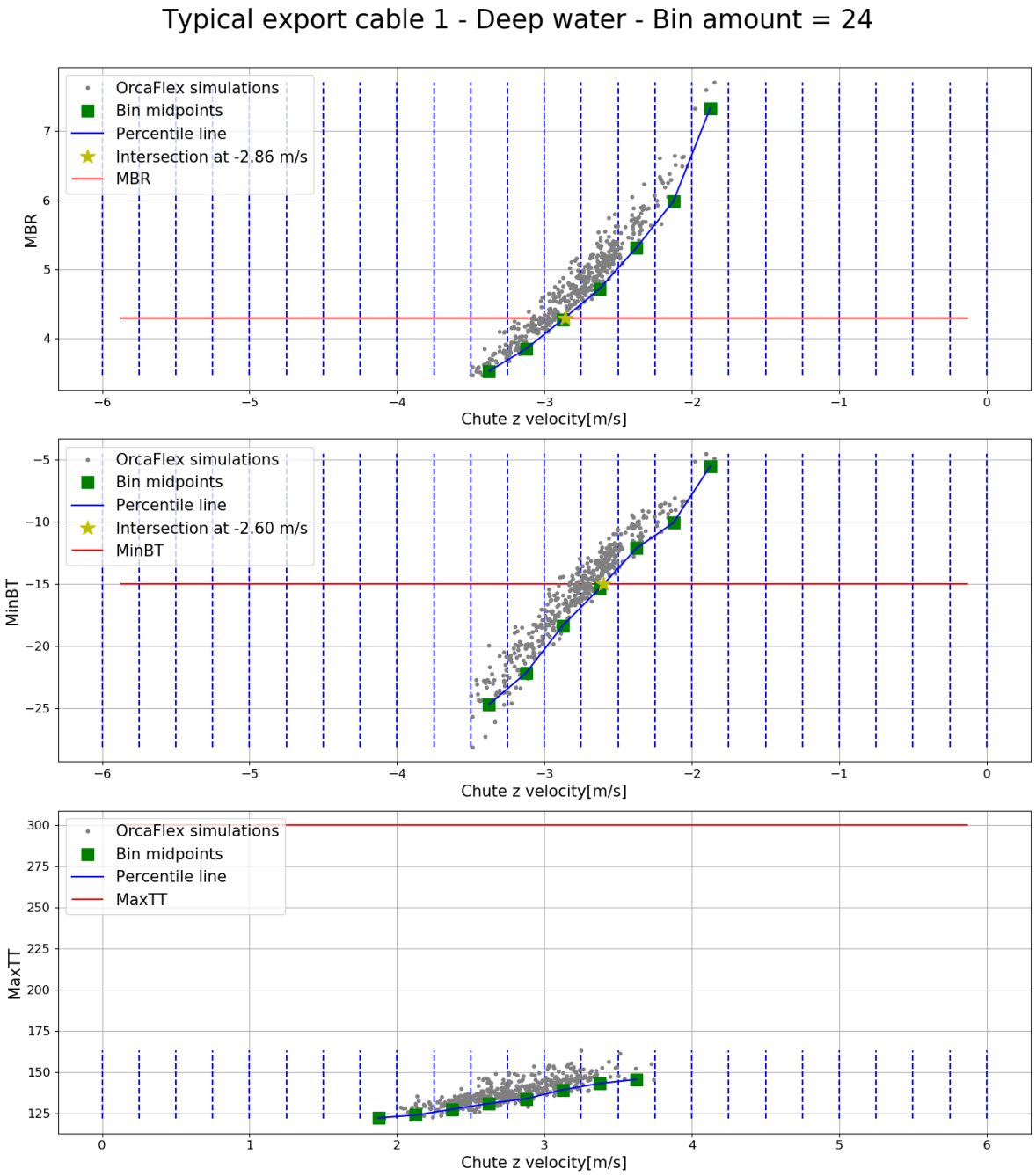

Figure E.24: Quantification graphs typical export cable 1 in deep water ($150m$), 3 seed numbers, binwidth of $0.25m/s$

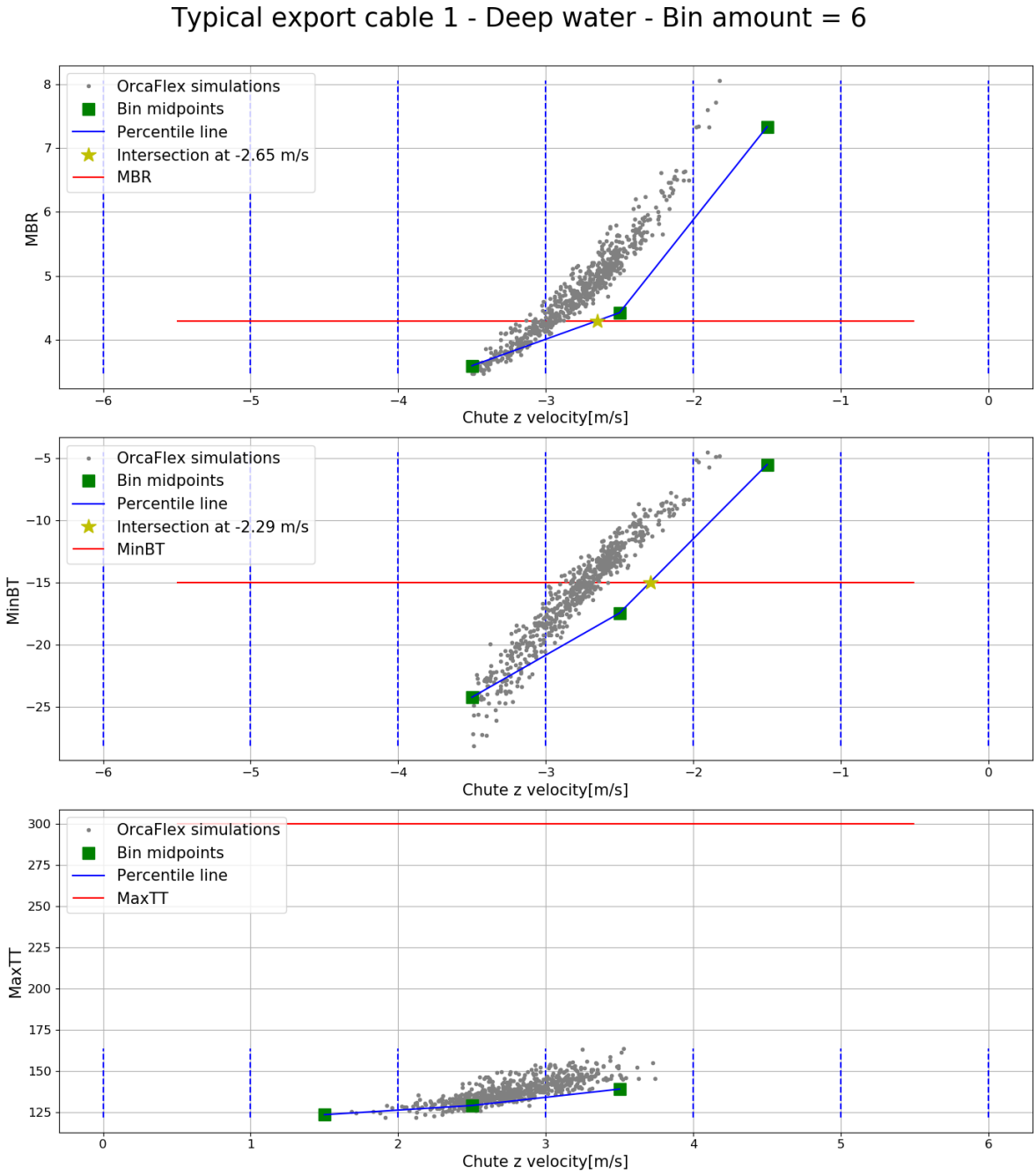

Figure E.25: Quantification graphs typical export cable 1 in deep water ($150m$), 4 seed numbers, binwidth of $1m/s$

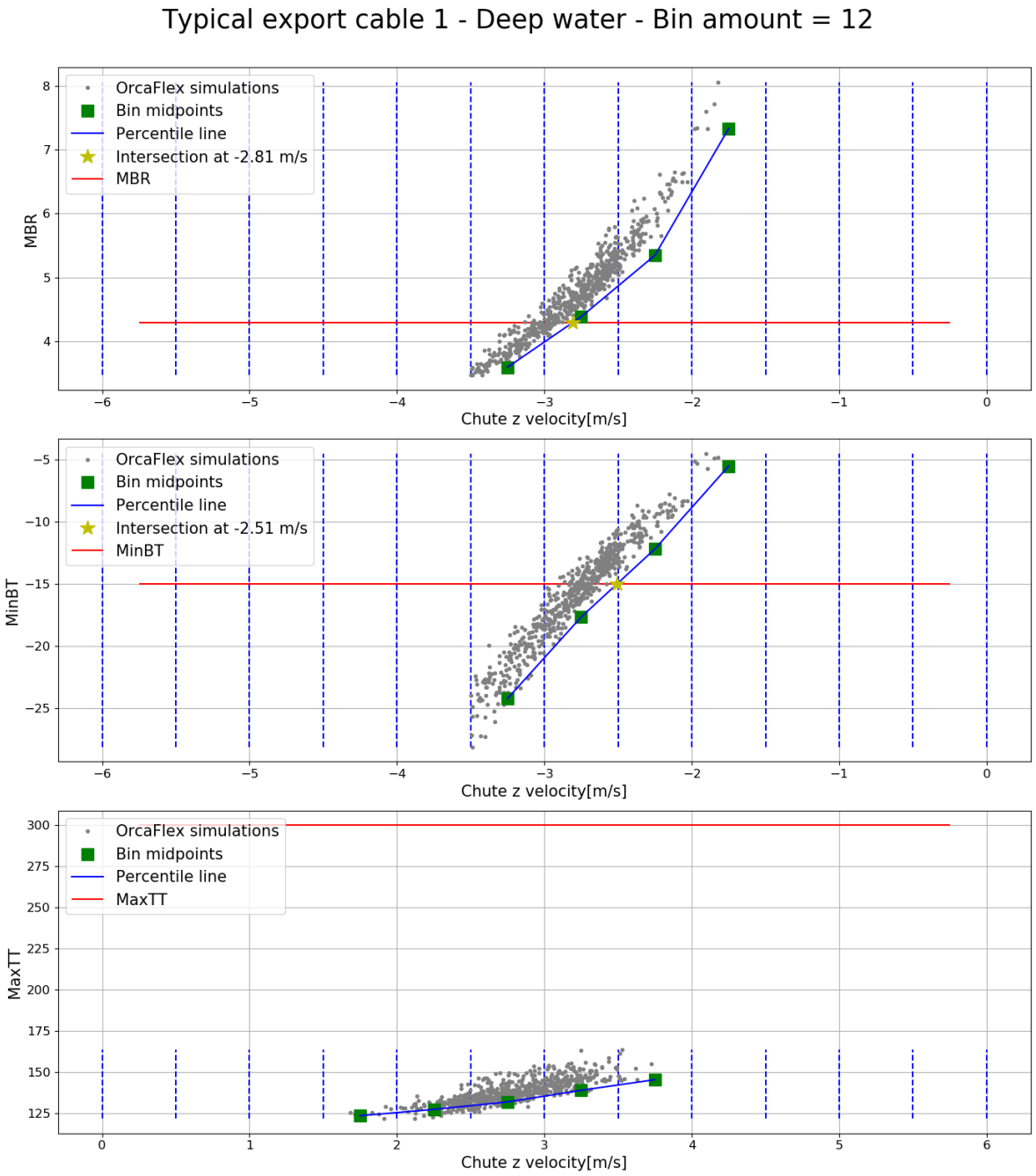

Figure E.26: Quantification graphs typical export cable 1 in deep water ($150m$), 4 seed numbers, binwidth of $0.5m/s$

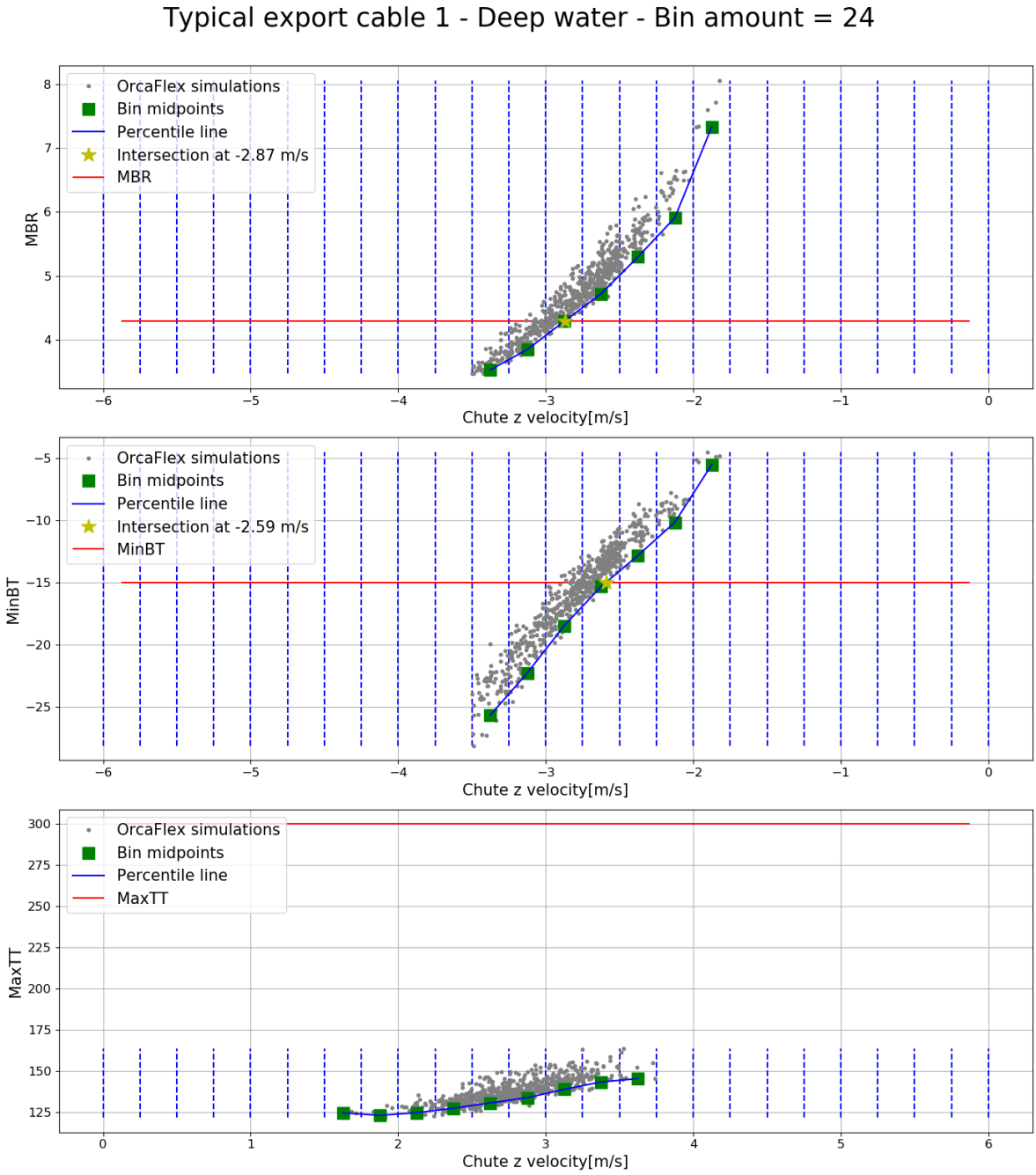

Figure E.27: Quantification graphs typical export cable 1 in deep water ($150m$), 4 seed numbers, binwidth of $0.25m/s$

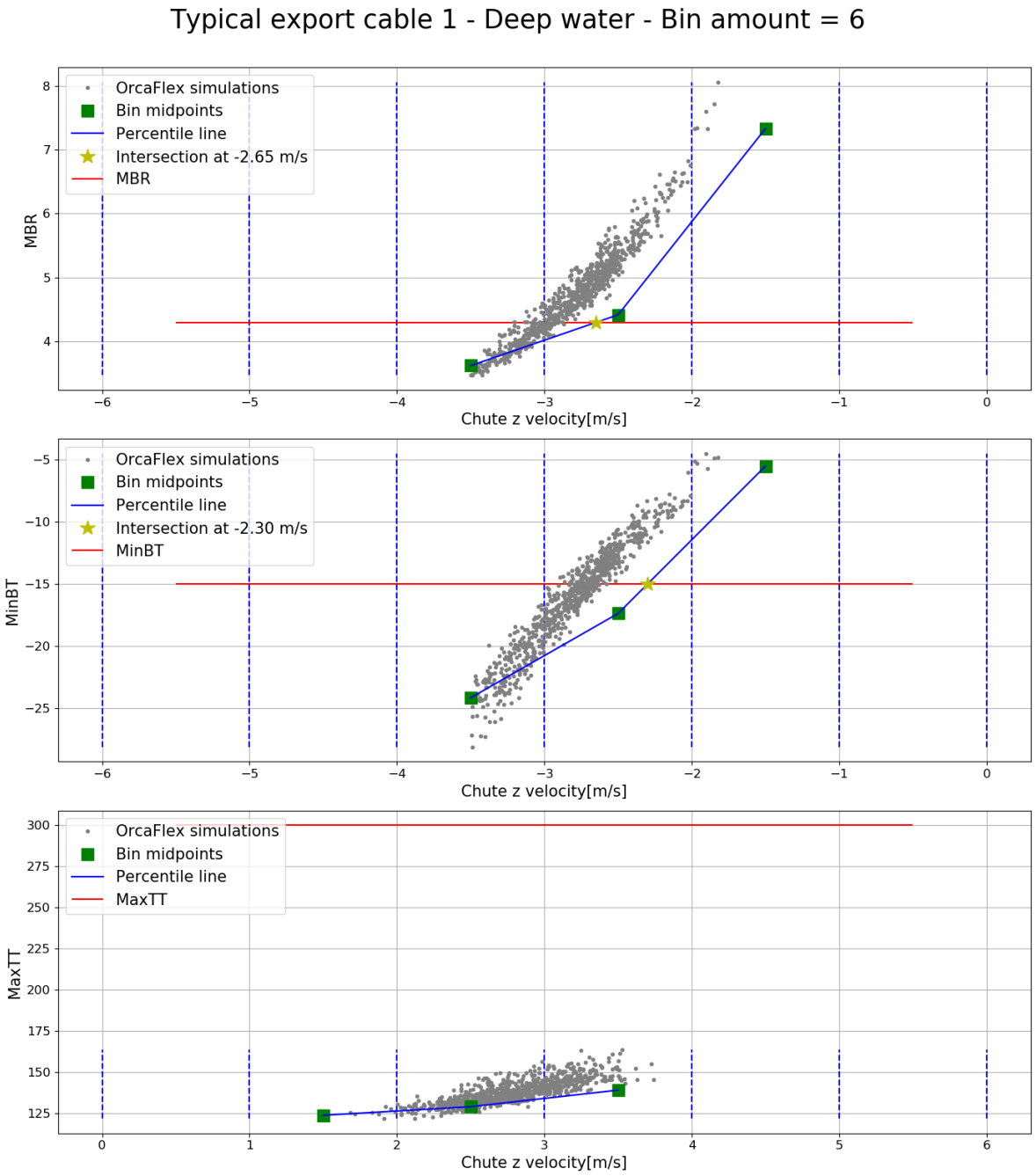

Figure E.28: Quantification graphs typical export cable 1 in deep water ($150m$), 5 seed numbers, binwidth of $1m/s$

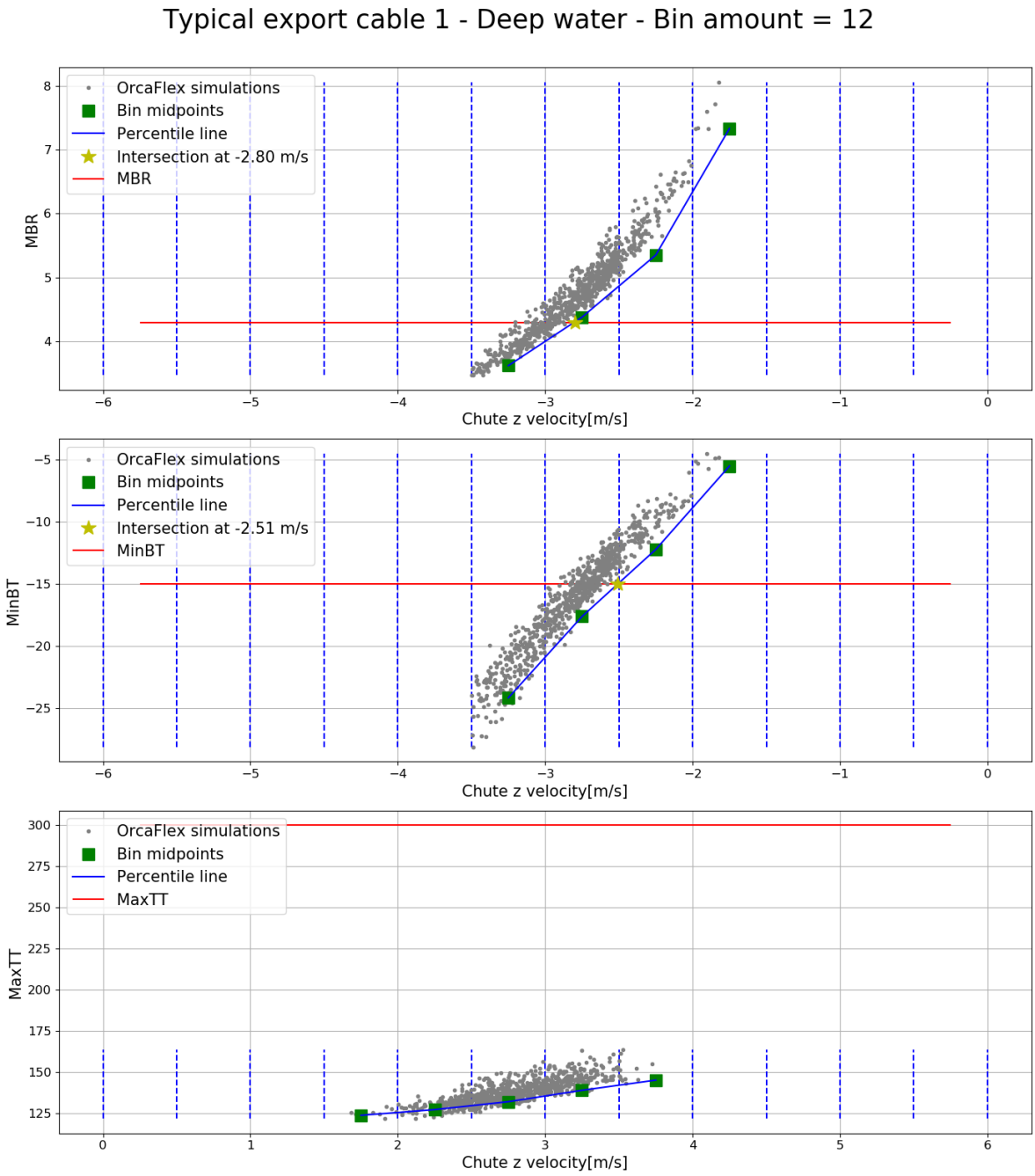

Figure E.29: Quantification graphs typical export cable 1 in deep water ($150m$), 5 seed numbers, binwidth of $0.5m/s$

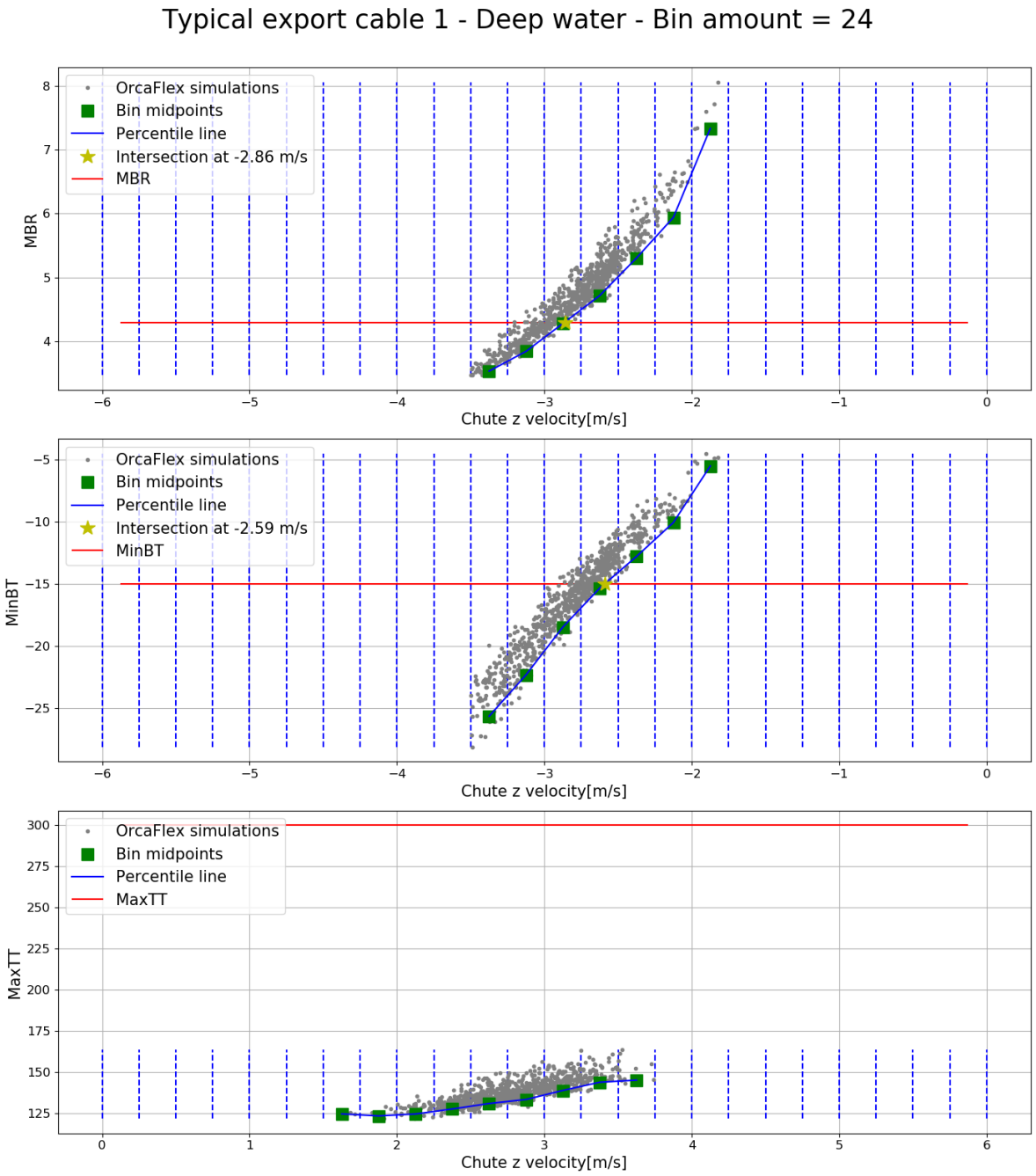

Figure E.30: Quantification graphs typical export cable 1 in deep water ($150m$), 5 seed numbers, binwidth of $0.25m/s$

E.3. Amount of seeds and binwidth sensitivity

E.3.1. Sensitivity shallow water (water depth of 30m)

Typical inter-array cable 1

Typical inter-array cable 1 - Sensitivity analysis					
Binwidth sensitivity		Average chute z velocity (m/s)	Confidence interval (%) Binwidth=1	Confidence interval (%) Binwidth=0.5	Confidence interval (%) Binwidth=0.25
5 Seeds	BR	-2.13	92.0	98.6	93.4
4 Seeds	BR	-2.12	91.8	98.7	93.1
3 Seeds	BR	-2.11	91.8	98.7	93.0
2 Seeds	BR	-2.10	92.7	98.7	94.0
1 Seed	BR	-2.11	89.3	97.0	92.3

Table E.1: Binwidth sensitivity analysis inter-array cable 1, shallow water

Typical inter-array cable 1 - Sensitivity analysis							
Seeds sensitivity		Average chute z velocity (m/s)	Confidence interval (%) 5 Seeds	Confidence interval (%) 4 Seeds	Confidence interval (%) 3 Seeds	Confidence interval (%) 2 Seeds	Confidence interval (%) 1 Seed
Binwidth=1	BR	-2.29	99.7	99.9	99.5	98.2	97.9
Binwidth=0.5	BR	-2.08	98.9	99.4	99.9	99.6	98.7
Binwidth=0.25	BR	-1.97	98.9	99.9	99.6	99.9	99.1

Table E.2: Seeds sensitivity analysis inter-array cable 1, shallow water

Typical inter-array cable 2

Typical inter-array cable 2 - Sensitivity analysis					
Binwidth sensitivity		Average chute z velocity (m/s)	Confidence interval (%) Binwidth=1	Confidence interval (%) Binwidth=0.5	Confidence interval (%) Binwidth=0.25
5 Seeds	BT TT	-2.27 4.91	99.9 98.0	99.9 99.5	99.7 97.5
4 Seeds	BT TT	-2.26 5.00	99.4 99.2	98.8 99.2	99.4 x
3 Seeds	BT TT	-2.28 5.00	99.6 99.2	99.6 99.2	100 x
2 Seeds	BT	-2.24	99.4	99.0	98.4
1 Seed	BT	-2.34	98.7	97.0	98.3

Table E.3: Binwidth sensitivity analysis inter-array cable 2, shallow water

Typical inter-array cable 2 - Sensitivity analysis							
Seeds sensitivity		Average chute z velocity (m/s)	Confidence interval (%) 5 Seeds	Confidence interval (%) 4 Seeds	Confidence interval (%) 3 Seeds	Confidence interval (%) 2 Seeds	Confidence interval (%) 1 Seed
Binwidth=1	BT TT	-2.29 5.03	99.3 99.6	99.3 99.8	99.8 99.8	97.6 x	96.3 x
Binwidth=0.5	BT TT	-2.25 4.95	99.2 99.7	99.0 99.9	99.2 99.9	98.6 x	99.2 x
Binwidth=0.25	BT TT	-2.30 4.79	99.2 100	98.8 x	99.2 x	99.2 x	96.4 x

Table E.4: Seeds sensitivity analysis inter-array cable 2, shallow water

Typical export cable 1

Typical export cable 1 - Sensitivity analysis					
Binwidth sensitivity		Average chute z velocity (m/s)	Confidence interval (%) Binwidth=1	Confidence interval (%) Binwidth=0.5	Confidence interval (%) Binwidth=0.25
5 Seeds	BR BT	-3.16 -2.58	98.8 97.9	99.3 99.4	99.6 98.6
4 Seeds	BR BT	-3.17 -2.59	98.6 98.1	99.2 99.6	99.5 98.5
3 Seeds	BR BT	-3.19 -2.61	98.9 97.8	99.9 99.1	99.0 98.7
2 Seeds	BR BT	-3.17 -2.59	99.5 97.3	99.9 98.5	99.6 98.8
1 Seed	BR BT	-3.22 -2.61	99.6 96.9	99.2 98.5	99.6 98.5

Table E.5: Binwidth sensitivity analysis export cable 1, shallow water

Typical export cable 1 - Sensitivity analysis							
Seeds sensitivity		Average chute z velocity (m/s)	Confidence interval (%) 5 Seeds	Confidence interval (%) 4 Seeds	Confidence interval (%) 3 Seeds	Confidence interval (%) 2 Seeds	Confidence interval (%) 1 Seed
Binwidth=1	BR BT	-3.21 -2.53	99.6 99.8	99.9 99.8	99.4 99.4	99.3 99.4	99.4 99.8
Binwidth=0.5	BR BT	-3.17 -2.62	99.2 99.2	99.2 99.2	99.2 99.7	99.9 99.7	99.2 99.2
Binwidth=0.25	BR BT	-3.17 -2.63	99.4 99.5	99.4 99.9	99.7 99.7	99.7 99.5	98.1 99.3

Table E.6: Seeds sensitivity analysis export cable 1, shallow water

Typical export cable 2

Typical export cable 2 - Sensitivity analysis					
Binwidth sensitivity		Average chute z velocity (m/s)	Confidence interval (%) Binwidth=1	Confidence interval (%) Binwidth=0.5	Confidence interval (%) Binwidth=0.25
5 Seeds	BR BT	-1.56 -1.39	92.1 90.9	97.7 99.0	94.5 91.8
4 Seeds	BR BT	-1.56 -1.38	92.1 90.4	97.7 98.8	94.5 91.6
3 Seeds	BR BT	-1.39 -1.22	66.3 65.4	85.3 87.2	81.0 78.2
2 Seeds	BR BT	-1.43 -1.24	72.2 68.5	88.6 88.7	83.6 79.8
1 Seed	BR BT	-1.47 -1.28	77.6 72.1	90.5 89.6	87.1 82.5

Table E.7: Binwidth sensitivity analysis export cable 2, shallow water

Typical export cable 2 - Sensitivity analysis							
Seeds sensitivity		Average chute z velocity (m/s)	Confidence interval (%) 5 Seeds	Confidence interval (%) 4 Seeds	Confidence interval (%) 3 Seeds	Confidence interval (%) 2 Seeds	Confidence interval (%) 1 Seed
Binwidth=1	BR BT	-1.19 -1.02	79.4 76.0	79.4 77.0	77.1 78.7	86.3 83.7	95.5 90.6
Binwidth=0.5	BR BT	-1.60 -1.39	99.9 99.6	99.9 99.6	99.5 99.0	99.5 99.0	99.2 98.9
Binwidth=0.25	BR BT	-1.65 -1.50	99.8 99.7	99.8 99.7	99.8 99.6	99.6 99.6	98.6 99.7

Table E.8: Seeds sensitivity analysis export cable 2, shallow water

E.3.2. Deep water (water depth of 150m)

Typical inter-array cable 1

Typical inter-array cable 1 - Sensitivity analysis					
Binwidth sensitivity		Average chute z velocity (m/s)	Confidence interval (%) Binwidth=1	Confidence interval (%) Binwidth=0.5	Confidence interval (%) Binwidth=0.25
5 Seeds	BR BT	-1.81 -1.74	93.4 90.6	95.6 97.3	97.8 93.3
4 Seeds	BR BT	-1.86 -1.74	94.8 90.6	94.4 97.3	99.6 93.3
3 Seeds	BR BT	-1.86 -1.74	95.0 90.6	94.3 97.3	99.3 93.3
2 Seeds	BR BT	-1.89 -1.77	93.8 91.9	92.4 97.4	98.6 94.5
1 Seed	BR BT	-1.94 -1.78	92.9 92.0	89.0 97.4	96.0 94.6

Table E.9: Binwidth sensitivity analysis inter-array cable 1, deep water

Typical inter-array cable 1 - Sensitivity analysis							
Seeds sensitivity		Average chute z velocity (m/s)	Confidence interval (%) 5 Seeds	Confidence interval (%) 4 Seeds	Confidence interval (%) 3 Seeds	Confidence interval (%) 2 Seeds	Confidence interval (%) 1 Seed
Binwidth=1	BR	-1.76	96.1	99.9	99.3	99.3	97.6
	BT	-1.60	98.6	98.6	98.6	98.3	97.6
Binwidth=0.5	BR	-2.00	94.5	98.0	98.5	98.5	92.5
	BT	-1.80	99.2	99.2	99.2	99.1	98.6
Binwidth=0.25	BR	-1.85	99.8	99.8	99.8	99.7	99.7
	BT	-1.87	99.7	99.7	99.7	99.8	99.2

Table E.10: Seeds sensitivity analysis inter-array cable 1, deep water

Typical inter-array cable 2

Typical inter-array cable 2 - Sensitivity analysis					
Binwidth sensitivity		Average chute z velocity (m/s)	Confidence interval (%) Binwidth=1	Confidence interval (%) Binwidth=0.5	Confidence interval (%) Binwidth=0.25
5 Seeds	BR	-2.34	94.2	98.6	95.6
	BT	-1.73	89.6	97.1	92.5
	TT	3.92	94.6	99.5	95.1
4 Seeds	BR	-2.38	95.8	99.6	95.4
	BT	-1.73	90.0	97.3	92.7
	TT	3.87	97.4	98.4	99.0
3 Seeds	BR	-2.33	93.4	98.0	95.4
	BT	-1.73	89.8	96.9	92.9
	TT	3.89	98.1	97.8	99.7
2 Seeds	BR	-2.37	95.4	99.2	94.5
	BT	-1.74	90.1	97.3	92.7
	TT	3.75	94.2	98.8	95.4
1 Seed	BR	-2.45	97.6	95.9	93.5
	BT	-1.74	90.1	97.3	92.7
	TT	3.74	94.7	98.6	96.2

Table E.11: Binwidth sensitivity analysis inter-array cable 2, deep water

Typical inter-array cable 2 - Sensitivity analysis							
Seeds sensitivity		Average chute z velocity (m/s)	Confidence interval (%) 5 Seeds	Confidence interval (%) 4 Seeds	Confidence interval (%) 3 Seeds	Confidence interval (%) 2 Seeds	Confidence interval (%) 1 Seed
Binwidth=1	BR	-2.49	99.8	99.8	99.8	99.8	99.0
	BT	-1.56	99.4	100	99.4	99.4	99.4
	TT	3.99	96.6	99.4	99.1	99.4	98.6
Binwidth=0.5	BR	-2.38	96.9	99.7	95.6	99.7	93.0
	BT	-1.78	99.8	99.8	99.8	99.7	99.7
	TT	3.78	96.9	99.3	99.5	98.1	97.6
Binwidth=0.25	BR	-2.25	99.5	99.2	98.6	99.5	98.3
	BT	-1.86	99.9	99.9	99.4	99.6	99.6
	TT	3.73	99.9	97.3	95.4	96.0	96.6

Table E.12: Seeds sensitivity analysis inter-array cable 2, deep water

Typical export cable 1

Typical export cable 1 - Sensitivity analysis					
Binwidth sensitivity		Average chute z velocity (m/s)	Confidence interval (%) Binwidth=1	Confidence interval (%) Binwidth=0.5	Confidence interval (%) Binwidth=0.25
5 Seeds	BR BT	-2.77 -2.47	95.7 93.2	98.9 98.2	96.8 95.0
4 Seeds	BR BT	-2.78 -2.46	95.4 93.0	98.8 98.1	96.6 94.9
3 Seeds	BR BT	-2.77 -2.48	95.7 93.3	98.9 98.3	96.8 95.0
2 Seeds	BR BT	-2.76 -2.47	94.7 93.1	98.4 98.4	96.3 94.7
1 Seed	BR BT	-2.76 -2.47	95.5 93.4	99.0 98.5	96.5 94.9

Table E.13: Binwidth sensitivity analysis export cable 1, deep water

Typical export cable 1 - Sensitivity analysis							
Seeds sensitivity		Average chute z velocity (m/s)	Confidence interval (%) 5 Seeds	Confidence interval (%) 4 Seeds	Confidence interval (%) 3 Seeds	Confidence interval (%) 2 Seeds	Confidence interval (%) 1 Seed
Binwidth=1	BR BT	-2.64 -2.30	99.6 99.9	99.6 99.5	99.6 99.7	98.9 99.9	100 99.7
Binwidth=0.5	BR BT	-2.80 -2.51	100 99.9	99.6 99.9	100 99.7	100 99.9	99.6 99.9
Binwidth=0.25	BR BT	-2.86 -2.60	99.9 99.8	99.7 99.8	99.9 99.8	99.9 99.8	99.9 99.8

Table E.14: Seeds sensitivity analysis export cable 1, deep water

Typical export cable 2

Typical export cable 2 - Sensitivity analysis					
Binwidth sensitivity		Average chute z velocity (m/s)	Confidence interval (%) Binwidth=1	Confidence interval (%) Binwidth=0.5	Confidence interval (%) Binwidth=0.25
5 Seeds	BR BT	-1.54 -1.40	78.4 77.3	91.8 93.3	86.6 84.0
4 Seeds	BR BT	-1.54 -1.40	78.4 77.9	91.8 93.6	86.6 84.3
3 Seeds	BR BT	-1.54 -1.40	77.4 76.6	91.3 92.6	86.1 84.0
2 Seeds	BR BT	-1.56 -1.41	80.0 78.0	92.5 92.9	87.4 85.1
1 Seed	BR BT	-1.58 -1.42	81.8 78.4	93.4 92.7	88.4 85.6

Table E.15: Binwidth sensitivity analysis export cable 2, deep water

Typical export cable 2 - Sensitivity analysis							
Seeds sensitivity		Average chute z velocity (m/s)	Confidence interval (%) 5 Seeds	Confidence interval (%) 4 Seeds	Confidence interval (%) 3 Seeds	Confidence interval (%) 2 Seeds	Confidence interval (%) 1 Seed
Binwidth=1	BR BT	-1.23 -1.09	98.4 99.1	98.4 100	96.7 98.2	98.4 99.1	95.1 98.2
Binwidth=0.5	BR BT	-1.67 -1.50	99.8 99.2	99.8 99.2	99.8 99.9	99.6 99.5	99.6 99.8
Binwidth=0.25	BR BT	-1.75 -1.62	99.8 100	99.8 100	99.8 100	99.7 100	99.7 100

Table E.16: Seeds sensitivity analysis export cable 2, deep water